Author:
Palange, Caterina

Title:
The effects of surface modification of microfibrillated cellulose on its dispersion and reinforcement potential in polyolefin composites.

The effects of surface modification of microfibrillated cellulose on its dispersion and reinforcement potential in polyolefin composites.

Caterina Palange

A dissertation submitted to the University of Bristol in accordance with the requirements for award of the degree of *Doctor of Engineering* in the School of Civil, Aerospace and Mechanical Engineering (CAME).

December 2019

48,390 words

This page is left intentionally blank

Abstract

Microfibrillated cellulose (MFC) is a highly expanded, high surface area networked form of cellulose-based material. It is mainly obtained from wood pulp and thus it is readily available, abundant and cheap. These characteristics alongside with the high modulus and strength of cellulose nanomaterials make it a suitable candidate in the production of nano-scale cellulose based reinforced composites. The idea is to combine the easy processability of nanomaterials with the superior mechanical and impact properties obtained using fibrous reinforcements such as glass or carbon fibres. The main obstacle in the production of performant MFC reinforced polyolefin based composites is the natural incompatibility of the polar cellulose fibrils with the apolar polyolefin macromolecule which lead to filler segregation, phase separation, poor interphase adhesion, reduced filler-matrix interphase, poor stress transfer to the reinforcement fibrils and consequently poor mechanical and impact properties of the composites. The present research work propose the use of a facile water-based chemistry based on the reaction of MFC with tannic acid and subsequent functionalisation with an alkyl amine to render the surface of the MFC fibrils hydrophobic and enhance the dispersion of the cellulose-based filler into an apolar thermoplastic matrix. The successful production of tannic acid-primary amine reacted MFC was evaluate using Fourier-Transform infrared spectroscopy (FTIR), and the effectiveness of the reaction in producing a hydrophobic form of MFC was evaluated using contact angle measurements (water contact angle increate to 93° for the TA-C_{18}-Cellopahne from 21° of the native Cellophane sample) . The most suitable processing for the production of the reinforced nanocomposites was selected considering the effect of temperature and compounding process on the filler dispersion in the matrix. The level of dispersion of the compatibilized MFC reinforced composites was evaluated using a variety of spectroscopic and microscopic techniques, the most efficient of which were found to be the Time of Flight Secondary Ion Mass Spectrometry (ToF-SIMS) and the multi-channel Spectral Confocal Laser Scanning Microscopy (SCLSM). The agglomeration of cellulosic filler within the composites was reduced by functionalising the surface of the MFC fibrils with tannic acid and octadecylamine. The resulting composites exhibited an increase in modulus at a high cellulose content (Modulus up to 1.9 GPa for a 20 wt.% TA-C_{18}-MFC reinforced composite compared to 1 GPa of the neat matrix). Despite a large portion of the functionalised MFC filler roved to be dispersed below 2 µm in diameter, the presence of medium and large aggregate affects the impact properties of the composites produced.

Project Keywords: *Microfibrillated cellulose – Composites – Quasi-static and dynamic characterisation – Aggregates analysis – Spectral Confocal Laser Scanning Microscopy.*

This page is left intentionally blank

Acknowledgements

Firstly, I would like to express my sincere gratitude to Prof Stephen J. Eichhorn and Dr Jonathan S. Phipps for the continuous support of my Doctorate study and related research, for their patience, motivation, and immense knowledge. Their guidance helped me in all the time of research and writing of this thesis. I could not have imagined having better advisors and mentors for my EngD study.

Besides my advisor, I would like to thank the rest of my thesis committee: Prof Ian Hamerton and Prof Valenska Ting, for their insightful comments and encouragement, but also for the hard questions which incented me to widen my research from various perspectives.

My sincere thanks also go to Dr David J. Scurr (University of Nottingham), who gave access to the laboratory and research facilities and supported my research with its specialistic knowledge. Without his precious support, it would not had been possible to conduct this research.

I would like to thank Dr Rinat Nigmatullin and Dr Marcus A. Johns, for their support help and for sharing their knowledge and experience with me.

I thank Dr Daniel J. Hewson and my former fellow labmates in FiberLean for the stimulating discussions -especially Lewis R. Taylor-, and for all the fun we have had in the last four years. Also, I thank Valentina Guerra at Warwick University, for being such a good friend.

Last but not the least, I would like to thank my family: my amazing husband Leonardo Baldassarre for supporting and tolerating me physically mentally and spiritually through this entire process and life in general, and to my brother Nazareno Palange because he is way too funny to be with!

This page is left intentionally blank

Author's declaration

I declare that the work in this dissertation was carried out in accordance with the requirements of the *University's Regulation and Code of Practice for Research Degree Programmes* and that it has not been submitted for any other academic award. Except where indicated by specific reference in the text, the work is the candidate's own work. Work done in collaboration with, or with the assistance of, others, is indicated as such. Any views expressed in the dissertation are those of the author.

Signed:  Date: 13-12-2019

This page is left intentionally blank

Table of Contents

This page is left intentionally blank

List of Figures

List of Tables

This page is left intentionally blank

List of abbreviations

AA	Acetic anhydride
ACC	Aqueous counter collider
AFM	Atomic force microscope
AKD	Alkyl keto dimer
ASA	Alkenyl succinyl anhydride
BC	Bacterial cellulose
BN	Bromonaphthalene
C_{18}	Octadecylamine
C6	Cellulose carboxy group
C_6	Hexylamine
CEs	Cellulose esters
CTE	Coefficient of thermal expansion
DES	Deep eutectic solvent
DMA	Dimethylamine
$\overline{DP}$	Average degree of polymerisation
DS	Degree of substitution
DSC	Differential scanning calorimetry
EBSD	Back-scattered Electron Diffraction
EDX	Energy-dispersive X-ray (spectroscopy)
FTIR	Fourier-Transform infrared (spectroscopy)
GFs	Glass fibres
GMA	Glycidyl methacrylate
HEPES	4-(2-hydroxyethyl)-1-piperazineethanesulfonic acid
MA	Maleic anhydride
MAgPP	Maleic anhydride grafted polypropylene
MAS-NMR	Magic angle spinning-nuclear magnetic resonance (spettroscopy)
MCC	Micro crystalline cellulose
MCl	Myristoyl chloride
MEI	1-methylimidazole
MFC	Microfibrillated cellulose
MW	Molecular weight

PCL	Polycaprolactone
PE	Polyethylene
PEO	Poly(ethylene oxide)
PHB	Poly(hydroxy butyrate)
PLA	Poly(lactic acid)
PP	Polypropylene
PPPE	Polypropylene/polyethylene
PU	Polyurethane
PVOH	Poly(vinyl alcohol)
RH	Relative humidity
ROP	Ring opening polymerisation
SCLSM	(Multi-channel) Spectral Confocal Laser Scanning Microscopy
SEM	Scanning electron microscope
SMPs	Shape memory polymers
TA	Tannic acid
T_c	Crystallization temperature
TCs	Terminal complexes
TEM	Transmission electron microscope
TEMPO	2,2,6,6-tetramethylpiperidine-1-oxyl
T_g	Glass transition temperature
TGA	Thermogravimetric analysis
THF	Tetrahydrofuran
T_m	Melting temperature
ToF-SIMS	Time of flight-Secondary ions mass spectroscopy
TPS	Thermoplastic starch
WRV	Water retention value
XRD	X-Ray diffraction

1. Introduction

The following chapter contains an introduction on the State of Art of the industrial production of MFC reinforced polyolefin-based composites. In the following paragraph the context of the research is clarified alongside with the viewable application for the new water-based chemistry and products investigate. The project aims and objectives are highlighted in the final paragraphs.

1.1 Background and context

The development of nanocomposites based on nanocellulose is a new and fast-growing research area. Cellulose is abundant in nature, biodegradable, sustainable and cheap;[1] thus it is a promising nano-scale reinforcement for polymers. The combination of cellulose and other biodegradable renewable polymers is attractive from an environmental point of view. The application of nanocellulose fillers can enhance neat polymer matrix mechanical properties more efficiently than conventional micro- or macro-inorganic reinforcements.

The automotive industry is one of the areas that could benefit from the advantages deriving from the use of micro cellulose as reinforcement: micro celluloses can, in fact, improve both impact strength and stiffness in composites at low loading levels, thus enabling lighter parts with better properties than the conventional mineral-filled composites.[1] The large number of reactive hydroxyl groups exposed on the surface of nanocelluloses allows the production of a wide range of functionalized materials for advanced applications. Despite the many promising achievements obtained at the laboratory or pilot scale, the industrial production of cellulose reinforced composites remains limited to polar matrices. A major obstacle to the successful production and commercialisation of performant nanocellulose reinforced polyolefin-based composites is the natural incompatibility of the hydrophilic cellulose fillers with the hydrophobic matrix.[2]

A good filler-matrix interaction is essential in achieving efficient filler-matrix stress transfer and obtaining excellent mechanical and impact properties. To incorporate nanocellulose into an apolar polyolefin matrix, a surface chemical modification is essential.

Although several studies have been devoted to chemical modification of nanocelluloses, to date no practical industrially based method using conventional thermoplastic processing equipment to produce cellulose-based nanocomposites with hydrophobic polymers is yet available.[3] However, Elastopoli Acquacomp and the Kyoto processes are good exemples of the industrial production of MFC reinforced thermoplastics achieved using injection moulding equipment adapted to high water content processing.

There is also an important gap in the development of a novel, environmentally friendly methods for the compatibilization of cellulose-based fillers. Finally, there is a lack of understanding of the mechanisms regulating the cellulose-polymer matrix interface. These topics represent the main objectives of the present research work.

This thesis reports research into microfibrillated cellulose, the production methods, morphology, surface chemical compatibilization, mechanical properties, and its potential use as a reinforcement in composites materials. The first part of this chapter includes a general introduction and a summary of the project objectives. The second part presents a brief summary of the thesis structure.

1.2 Relevance of the project

Microfibrillated cellulose (MFC) is an expanded surface area, network type of cellulosic material obtained by the mechanical fibrillation of natural cellulose macro-fibres to yeeld.[1,2] MFC contains cellulose fibrils of typical thicknesses in the range between 5 and 20 nm,[1] and aggregates of cellulose microfibrils in the range between 20-40 nm.[1,3] The FiberLean MFC product is defined by its fibres thickness distribution by *i.e.* 10 % of the fibrils have a thickness < 12nm, 60 % a thickness < 50nm, and 90 % have a thickness < 250 nm. The length of the cellulose microfibrils can vary considerably and is difficult to determine accurately because of the peculiar MFC networked morphology and because of the presence of numerous entanglements which make difficult to identify both ends and the extent of a single fibril.[1]

The term 'microfibrillated cellulose' was first introduced in the late 1970s by Turbak, Snyder, and Sandberg and was used to produce a type of gel material obtained from the homogenization of wood pulps at high temperature and high pressure.[3] The nomenclature remains currently in use, although a large number of synonyms are used in the literature to describe MFC including cellulose microfibrils,[4–8] microfibril aggregates,[9–11] microfibrillar cellulose,[5,12,13] nanofibrils,[14,15] nanofibres,[5,16,17] nanofibrillar cellulose,[5,13,14,18,19] or fibril aggregates.[20–22]

The main proposed applications of MFC currently cover mechanical reinforcement in synthetic and natural polymer matrices,[1,23] as emulsion stabilizers,[24] and in the production of films,[7,14,25,26] aerogels,[27,28] and electronic components.[29,30] Cellulose-based nanocomposites based on hydrophilic matrices and fibrils were the first to be produced, and phenol-formaldehyde resins reinforced with fully fibrillated cellulose,[31] acrylic and epoxy resins reinforced with alkali-treated MFC,[32,33] poly(styrene-*co*-butyl acrylate) MFC reinforced composites,[34,35] polyurethane-MFC composites prepared using the film stacking method,[36] shape memory polyurethanes reinforced with MFC,[37,38] and poly(vinyl alcohol)-MFC

nanocomposites[16,33,39–41] represent some of the most relevant suggested applications of this material as a polymer reinforcement derived by the most recent literature produced.

Other uses of cellulose fibrils involve combining them with native starch and thermoplastic starch (TPS) in films to improve their poor mechanical properties and high water uptake,[42–46] as a reinforcement to brittle amylopectin films,[3,47] and as a reinforcement in chitosan films. The addition of MFC to chitosan films increases the neat film oxygen-gas barrier capacity, hydrophilicity, and insolubility in water.

Furthermore, the deformability of chitosan-acetic-acid-salt films was improved because the MFC fibrils restrict chitosan film deformation associated with moisture.[48] Cellulose fibre-based materials are promising candidates in packaging, meeting the requirement for renewability, biodegradability, light weight, and recyclability.[49,50] However, the poor resistance to moisture and oxygen barrier of the cellulose-based materials requires them to be used in multi-layered structures with other polymers, which significantly decreases their recyclability.[1,51–54] The addition of MFC to cellulosic materials such as paper and cardboard,[54] and as a coating agent to improve their barrier properties[13,25,55,56] and paper printing performance[56,57] were reported as one of the most active research areas and as the major application of MFC in industry.

Among these interesting applications, the main focus of the research described in this thesis is the production of MFC reinforced polyolefins. As mentioned before, the characteristic networked morphology and highly expanded interfacial area,[58] alongside attractive mechanical properties such as a theoretical Young's modulus of ≈ 20 GPa and strength of ≈ 240 MPa,[39,40,59] low production cost, renewability, and wide availability,[1,17,60–62] make MFC an ideal candidate as a reinforcement in composites with enhanced mechanical performance.[63–70]

The concept of dramatically increasing the physical, chemical and mechanical performance of materials by reducing their size to the micro-, and nanoscale was introduced in the early 1960s,[71] marking the beginning of 'nanoscience'. The production of nanocomposites - materials showing enhanced physical, mechanical, thermal, and optical properties - is one of the natural applications of the nanoscience discipline. Nanomaterials are defined as a class of materials having at least one dimension less than 100 nm.[1] Nanofillers, one form of nanomaterials, are generally characterised by an extremely high surface to volume ratio, which generates an extended filler-matrix interfacial area.[1,2] Using an appropriate filler-matrix combination, it is possible to obtain reinforced nanocomposites in which the strong and extended interfacial area increases the mechanical properties of the matrix.[52,58,72]

Following this vision, the application of cellulose fibrils as polymer reinforcements has attracted the attention of both academia and industry in recent years as indicated by the increasing number of publications on the subject.[1]

The reason for the large interest in this area of research is because cellulose nanomaterials have the potential to increase the mechanical performance of composites dramatically, even at extremely low concentrations.[73–77] There is also relatively recent attention given to sustainable, green and environmentally friendly materials for various applications.[78,79] Thermoplastic polyolefins represent a massive portion of the polymers market and have a well-consolidated infrastructure network, from synthesis to the final product. Polyolefins are easily processable, having low melting temperatures and viscosities appropriate for industrial applications. Polyolefin products are durable and chemically stable; however, they are not biodegradable. An interesting alternative is the use of bio-derived polymers as matrices.[80,81]

The development of an easy methodology for the production of MFC reinforced polyolefins is, therefore, an important target to achieve in order to conquer a larger portion of the composite materials market.

The main MFC competitors as thermoplastic reinforcements are currently inorganic fillers such as nanoclays, glass fibres, and talc, to mention but a few.[82] These inorganic fillers are thermally stable and inexpensive, and efficiently improve a composite's stiffness or toughness compared to the neat matrix, but generally not both, the exception being for long glass fibres. They also increase a composite's specific weight. Fibres proved to be an exception: long glass fibres can enhance the material stiffness without impairing its impact resistance, unfortunately, they are extremely difficult to process.[82] MFC fibrils, on the other hand, can exploit the benefits of long fibres and preserve the easy processability of much smaller reinforcements in thermoplastic matrices.[83]

The hydrophilic and polar nature of MFC promotes two agglomeration mechanisms: the first one is caused by the water removal during drying. The water removal causes the irreversible agglomeration of cellulose fibrils also known as hornification.[84–86] The second type of aggregation is due to the dispersion of MFC in an apolar medium. MFC has a natural tendency to agglomerate and reduce the interfacial area exposed to an apolar medium.[79,87–89] This natural tendency is exasperated in polyolefin matrices due to the incompatible nature of the two phases and due to the tendency of the particles to aggregate during polymer processing.[90–92]

In the literature, physical and chemical methods have been used to reduce and prevent the irreversible aggregation of cellulose fibrils'. Fibril surface modification has proven to be efficient in preventing aggregation phenomena by decreasing the fibrils' surface energy.[79,87,88]

Surface treatments include corona or plasma discharge for the compatibilization of the polymers matrices,[93] surface derivatization,[94] graft copolymerization,[95] the application of surfactants,[96,97] silylation,[24] acetylation,[98] carboxymethylation,[99] to name but a few examples. Furthermore, surface modification of cellulose microfibrils improves interfacial adhesion with thermoplastic matrices while preserving their original morphology.[100]

The mechanical performance of a fibre-reinforced plastic composite is dependent on the modulus and the strength of the reinforcement and of the matrix, and the effectiveness of the interfacial adhesion between the matrix and the reinforcement.[101] A good interfacial adhesion is essential in transferring stress across the components of the composite and ensuring superior mechanical performance.[102–108] Fibre-reinforced composite properties are strongly dependent on properties such as fibre length and thickness, volume fraction, and alignment.[109–113] In the case of randomly oriented fibre composites, good interfacial bonding between fibres and the matrix ensure reinforcement takes place even at extremely low filler volume fractions.[113] Impact performance of reinforced composites is, on the other hand, strongly linked to the presence of filler aggregates.

Filler aggregation in polyolefinic composites is reported to affect stiffness only marginally, but strongly influences impact resistance which decreases sharply when the extent of aggregation increases.[114] Failure modes in polymer composites depend on aggregate size: in composites containing large aggregates, debonding is the dominant deformation mechanism, while composites containing small particles are more susceptible to crack initiation and propagation.[90,114] Under the effect of external loading, small particles can induce stress concentrations and impair the impact performance of the specimens.[92]

1.3 Aim of the project

The production of MFC-reinforced polyolefin composites was investigated. The chemical surface reaction methods used to compatibilize the hydrophilic cellulose fibrils were divided into those that were organic solvent-based and water-based. Solvent-based techniques are industrially impractical, due to the use of large amounts of organic solvents. Nevertheless, they have been reported to be efficient in preventing the aggregation of cellulose fibrils and for obtaining a uniform dispersion of cellulose fibrils in composites. Water-based approaches have the advantage of being carried out in water under mild conditions but are found to be inefficient whenever not backed by physical treatments such as freeze drying. An innovative chemical route was developed by Cranston's group that makes use of tannic acid (TA), a representative of the polyphenol family, as an activating agent.[115] In this research work, results obtained from various MFC surface reaction treatments are evaluated, in terms of mechanical and impact properties, against the reference systems selected: composites reinforced with maleic anhydride grafted polypropylene (MAgPP) treated MFC, glass fibres (GFs), and talc.[65] The level of filler dispersion in the composites was also evaluated using spectroscopic and microscopic techniques to correlate their tensile and impact performance with filler dispersion, by determining filler aggregate size distributions. The aim of this research project is the production of MFC reinforced composites showing enhanced quasi-static and dynamic properties at low filler content (≤1 wt. %); the compatibility between the polar MFC filler and the apolar matrices will be enhanced preferentially using water-based cellulose surface chemistry

The present study was sponsored by FiberLean, a multinational company specialised in the production of microfibrillated cellulose (MFC) obtained by an innovative process and commercialised by the tradename FiberLean^{TM}. The company can already vaunt commercial products in the paper industry, which are used to increase the mechanical properties and inorganic filler content of the final products, and they are seeking other applications. The addition of FiberLean^{TM} as reinforcement in polyolefin matrices could enlarge the company's market base.

1.4 Project objectives

To fulfil the aim of thus research project, the following objective were identified as fundamental achievement:

- ✓ The identification of the most suitable water-based microfibrillated cellulose surface chemistry to prevent cellulose fibrils agglomeration during drying, to achieve a sufficient compatibility between the polar and apolar filler and prevent phase segregation during the production of the reinforced composite, and to produce compatibilized MFC fillers stable at the processing temperature (170 °C);
- ✓ The production of MFC reinforced composites using unmodified thermoplastic manufacturing equipment;
- ✓ the quasi-static and dynamic investigation of MFC reinforced composites at different filler loading and the comparison of the collected data with composite reinforced using talc and glass fibres (relevant comparisons) at similar loadings;
- ✓ the analysis of the MFC aggregates dimension and distribution in the analysed composites and the correlation of the aggregate population with the quasi-static and dynamic analysis properties recorded for the samples under analysis;
- ✓ This research work aims to shade light on the potential of MFC as polyolefin matrices reinforcement and replacement for inorganic filler as talc and glass fibres.

1.5 Research novelty

The current research work investigate the potentiality of MFC as polyolefin reinforcement using an innovative approach: the chemistry used in the present study is water-based to allow an easy scalability of the process to the industrial scale; the composites are produced using a conventional compounder to enhance the easy introduction of this research findings in the industrial practice; the filler dispersion and aggregation stare in the composite is investigated using innovative approaches (ToF-SIMS and SCLSM) aimed to simplify the analysis of the cellulose based filler aggregates in the composites analysis; the results of the aggregate analysis are, furthermore, used to investigate and understand the influence of the filler aggregation on the composites dynamic properties.

1.6 Implications of the research

The present research identified a successful water-based chemistry for the surface functionalisation of MFC. The final product is a dry powder that can be conveniently addition to the matrices in an unmodified compounder to obtain MFC reinforced composite. Mani of the potential application of the compatibilized MFC product obtained are highlighted in **Paragraph 1.1**. Among the most relevant application for the MF reinforced composites produce the automotive sector is one of the most relevant. To eliminate the impact of the large filler aggregate presence of the dynamic properties of the composite and render them suitable for the automotive sector, however, further studies are necessary.

The main application for the composite produce and characterised in the present study is the packaging industry; FiberLean industry has already a strong presence in packaging and aim to conquer a larger share of the market introducing innovative MFC-polyolefins based products.

1.7 Thesis structure

The second chapter "**Background information and literature review"** will outline the characteristics of cellulose, microfibrillated cellulose, and polyolefin matrices. The second chapter also contains an introduction to the MFC production methodology and its current applications, and a review of MFC surface modifications with particular attention paid to MFC modification *via* chemical reactions. The final part of the second chapter is dedicated to the understanding of the relationship between filler dispersion and the mechanical properties of the composites.

The third chapter **"Microfibrillated cellulose surface modification"** gives a more detailed description of the MFC chemical surface modifications of MFC used in this research. The chemical approaches suggested are divide in organic solvent based and water based, the advantages in the use of each of the is discussed. The chapter contain a schematic representation of the product obtained from the individual reactions.

The fourth "**FiberLean MFC characterisation, surface reaction and preparation of composites**" contain the description of the chemical recipe used to prepare the compatibilized MFC based products and the description of the necessary preparation steps in the case of the solvent-based and water-based chemistry.

The fifth chapters **"Evaluation of filler dispersion and mechanical properties of the filled composites"** contains the description of the techniques used to produce the composites under analysis and the techniques used to analyse the crystallinity, thermal stability, mechanical and impact performance, and filler distributions of the composites and component materials. The chapter contains the explanation of the mathematical tolls used to divide the aggregates population identified using SCLSM into the four distinctive categories.

The sixth chapter **"Results and discussion"** discusses the findings on the effectiveness of the surface treatment in dispersing the filler in the polymer composites, and on the effect of the filler dispersion on the mechanical properties of the composites.

The seventh chapter **"Conclusions"** contains the conclusions of the present research work along with suggestions for future work.

Research questions:

- ✓ is the production of a hydrophobic and thermostable form of MFC, avoiding the use of organic solvents and energetically demanding processes possible?
- ✓ Is possible to obtain homogeneously dispersed MFC-reinforced composites using conventional polyolefin manufacturing?
- ✓ What is the correlation between tensile modulus, impact energy and MFC filler dispersion in composites?
- ✓ What is most successful MFC-reinforced composite production route (surface chemistry, drying method, filler incorporation and compounding procedure)?

2. Background information and literature review

The following chapter contains an overview on the main characteristics of micro- and nano-cellulose-based reinforcements, their properties, the currently used preparation methods and some of the main applications for those products. The final part of this chapter is devoted to investigation of the MFC theoretical reinforcement potential.

2.1 Cellulose

Native cellulose, the most representative component of pulp and therefore microfibrillated cellulose presents several layers of organisation and a hierarchical structure, held together by physical entanglement, hemicellulose, and lignin. Cellulose was first identified by the French chemist Anselm Payen in 1838. He determined the molecular formula of cellulose to be $(C_6H_{12}O_6)_n$. The first description of a complex cellulosic structure in plants can be dated back to the 1800s by Nägeli who described a complex structural assembly surrounding plant cells formed by microscopic crystalline particles which he named micelles.[116] Nägeli's findings were later confirmed by Meyer and Mark in the early 1900s which also identified the building blocks of the micelles as formed of a polymer type of molecule called cellulose. Cellulose is a high molecular weight homopolysaccharide originating from the polymerisation of β-1,4-anhydro-D-glucopyranose units. It presents a chain conformation in which successive glucose residues are rotated by 180° about the molecular axis and hydroxyl groups are in an equatorial position.[117] Polymer chains possess directional asymmetry: one end presents the hemiacetal group with reducing functionality, and the other has a pendant hydroxyl group non-reducing end.

The degree of polymerization (DP) in cellulose chains varies depending on the origin; DP in natural cellulose is estimated to be between 10000-15000 glucopyranose units. Glucopyranose rings expose on the surface three hydroxyl groups which are able to form hydrogen bonds. The hydrogen bond network plays a major role in the formation of cellulose hierarchical structures and in the packaging of cellulose fibrils.[118]

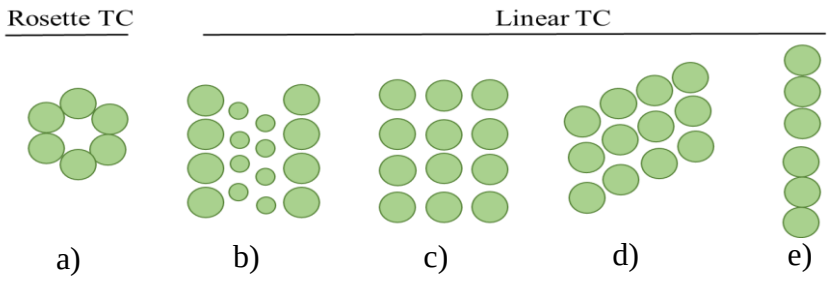

Figure 2.1 Schematics of rosette and linear terminal complexes (TC) for woody plants a), tunicate b), green algae c), yellow-green algae d), and bacteria e).

Cellulose, in fact, is not naturally produced as an isolated individual molecule but is assembled into fibrils. The cellulose fibrils are synthetized by specific enzymatic terminal complexes (TCs) having a diameter of 30 nm and localized in the cell plasma membrane (**Figure 2.1**).[119,120]

In the natural biosynthetic process to produce cellulose, 36-glucan chains are synthetized and packed together by Van der Waals forces and both intra- and inter-molecular hydrogen bonds, forming larger units known as elementary fibrils (protofibrils) of 2-4 nm in diameter and up to several microns in length;[121] several elementary fibrils combine into units called microfibrils, and these are assembled into the familiar cellulose fibres. Celluloses from different natural sources exhibit different structural organisations.[122,123] If the TCs are not perturbed, they generate nanofibrils having a limited number of defects or amorphous regions.[120] Natural fibres, in fact, present characteristics of alternating amorphous and crystalline regions.[124,125] The supramolecular structure of the cellular wall in plants is due to the arrangement of larger cellulose fibres, polysaccharides, and lignin (**Figure 2.2**).

That complex structure is particular to the material source and presents complicated and articulate morphology.[126] Cellulose has no taste nor odour. It is mainly hydrophilic and insoluble in water and in most organic solvents.

Cellulose is a semi-crystalline polymer having several known crystalline structures. Natural cellulose comprises two allomorph structures; Iα and Iβ.[117] The ratio between the two forms depends on the source. In fact, bacteria and algae cellulose are Iα rich, while higher plant celluloses are Iβ rich. Regenerated cellulose's structure is denoted II. The conversion of cellulose crystalline structure from I to II during the regeneration process is irreversible suggesting that the cellulose I structure is metastable while cellulose II is thermodynamically more stable. Other crystalline forms of cellulose are cellulose III and IV which are obtained *via* chemical treatments.[125] Cellulose undergoes thermal degradation at temperatures above 250 °C. This process is known as pyrolysis.[127,128]

Cellulose represents the structural component in higher plants and is contained in the vegetal secondary cell wall. Cellulose can be found in the secondary wall of many algae and in bacteria; some even secrete a highly crystalline form of it to protect themselves, forming a so-called biofilm.[121]

Cellulose represents the structural component in higher plants and is contained in the vegetal secondary cell wall. Cellulose can be found in the secondary wall of many algae and in bacteria; some even secrete a highly crystalline form of it to protect themselves, forming a so-called biofilm.[121]

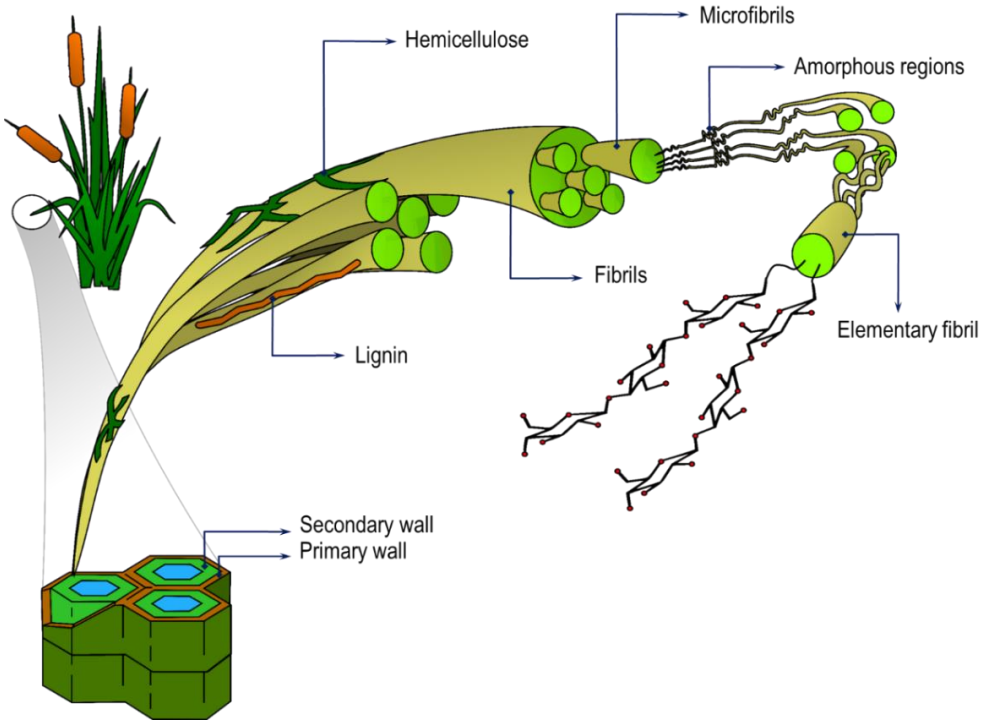

Figure 2.2 Schematic representation of a cellulose fibre's hierarchical and microscopic organization. Author's own work.

Furthermore, cellulose is also produced by a type of sea organisms called a tunicate.[9,11,62] Cellulose is estimated to be the most abundant organic polymer on Earth: its overall annual production is in fact estimated to be 10^{11} tons.[23]

In 1870 the Hyatt Manufacturing Company successfully produced and released the first thermoplastic polymer based on cellulose, which was known by the Celluloid tradename.[87] The 1890s witnessed the production of regenerated cellulose fibres, also known as rayon, while in 1912 cellophane, a regenerated film produced from cellulose, was developed and commercialised.[129] Owing to the increased interest in cellulose, further studies on its structure were conducted and in 1920 Hermann Staudinger finally determined cellulose's polymeric structure.[130]

In 1992 Kobayashi and Shoda[131] successfully chemically synthesized a cellulose macromolecule without the use of any biologically derived enzymes. Currently, cellulose is mainly used in the paper and paperboard industry and in textiles. Only a small proportion of the cellulose industry produces and sells cellulose derivative products such as rayon and cellophane. A larger part of the market is however reserved to the production of cellulose-based drugs or hydrophilic bulking dietary aids agents in the form of microcrystalline cellulose (E460i).

2.2 Nanocellulose

Under the umbrella-name of nanocellulose fall a variety of nano- and micro-sized cellulose structures such as microcrystalline cellulose, cellulose nanocrystals, cellulose nanofibres, microfibrillated cellulose, and bacterial cellulose.[1,51,53,72] The term nanocellulose refers to all the materials composed of or containing nanosized cellulose fibrils.[1] These materials have in common a high aspect ratio, typical fibril diameters in the range 5-20 nm and a huge variability in lengths; from tenths of a nm up to several micrometres.[53,72] Cellulose fibrils are usually isolated from cellulose fibres which are produced either by woody or non-woody plants or algae. Bacteria produce a form of cellulose which is already on the nanoscale.[132] Cellulose nanocrystals, on the other hand, are usually produced from native cellulose fibrils by acid hydrolysis or by TEMPO-oxidation. The type of nanocellulose obtained is a highly crystalline form of nanoparticle with lengths that may vary between 100 and 1000 nm.[133–135]

2.2.1 Nanocellulose sources

The most industrially used cellulose sources are wood, from which pulp is produced by the Kraft process, and cotton, which is the purest vegetable source of cellulose, containing up to the 90 % of the natural polymer. However, those are not the only sources of natural cellulose neither the most convenient. [136]

2.2.1.1 Wood and non-wooden plants

Mechanical extraction of cellulose fibrils from wood dates back to the 1980s when Herrick [60] and Turbak[137] produced MFC using cyclic mechanical treatments in a high pressure homogenizer. The homogenization process consists in the mechanical defibrillation of bleached Kraft pulp into sub-structural microfibrils.[24] MFC gels from homogenisation consist of a networked structure of cellulose nanofibres.[16,133,138–143] Cellulose fibres can be also obtained from alternative sources to wood, such as agricultural by-products and non-woody plants.

These alternative cellulose resources are becoming more and more important especially because of alternative uses of wood to construction, furniture production and the papermaking industry.[144] Non-woody plants' secondary cell walls are generally less rigid than woody plants because they contain less lignin. Owing to the reduced amount of lignin in non-woody starting materials, bleaching and alkali pre-treatments can be less intensive.[33,145]

The literature offers several examples of non-woody sources for the production of microfibrillated cellulose *e.g.* wheat straw and soy hulls,[146] sugar beet pulp,[145,147–151] potato pulp,[152] swede root,[33] bagasse,[153] sisal,[154] algae,[155] stems of cacti,[34,156] and banana rachis.[157]

2.2.1.2 Bacterial cellulose (BC)

Cellulose can also be obtained from bacteria. The bacteria responsible for the production of cellulose are *Acetobacter*, *Agrobacterium*, *Alcaligenes*, *Pseudomonas*, *Rhizobium*, or *Sarcina*.[158] The most efficient cellulose producer is *Acetobacter xylinum* (or *Gluconacetobacter xylinus*), a gram-negative acetic-acid-producing bacteria.[62,159] BC has some typical structural characteristics:

- ✓ it is generally secreted in a ribbon-shaped fibril, less than 100 nm wide, which is composed of nanofibrils of 2-4 nm width;[160,161]
- ✓ it is produced in a highly crystalline Iα form up to 84-89 %;[31,162]
- ✓ it possesses excellent properties: elastic modulus of 78 GPa,[163] higher than that of macro-scale natural fibres, [164] and on the same order as the elastic modulus of glass fibres (70 GPa);[83,165]
- ✓ higher water holding capacity, a degree of polymerization up to 8,000, and a fine web-like structure;[62,166,167]
- ✓ it is produced as a pure cellulose membrane: no chemical treatments are needed to remove impurities.[166,167]

Because of the properties listed above, recent studies indicated that BC is one of the most promising natural reinforcements in nanocomposites.[31,44,171–175,158–160,165,166,168–170]

2.3 Preparation of cellulose microfibrils from pulp

The present research work focus on the production of MFC reiforced compistes using unfodified thermoplastic processing equipments. The industrial fabrication of MFC-reinforced poliolefin based composites has been so far problematic due to the incompatibility of the polar cellulose based filler withnthe polar thermolpastic matrices (PP and PE). Polar MFC tend to aggregate naturally during drying; this behavior is exacerbated when polar MFC is mixed with incompatible apolr pgases, such as the poliolefinc matrices used in this study.

Water based surface chemistry is an efficent and economic method to mitigare the MFC-Matrix incompatibility. The watre based approach used in this study make use of the surface reaction among cellulose fibrils, tannic acid and primary maines.

The reaction prduct is an hydrophobic for of MFC that can be ground at room therperatrure, mixed with the polimeric matrix and processed through compounding and injection moulding to obtain the samples used in the composites charactreisation.

The production of nanocellulose from pulp (**Figure 2.3**) requires intensive mechanical treatments which expose the cellulose macro fibrils to high shear forces in order to efficiently fibrillate them in their micro-components. The mechanical production of nanocellulose can be energetically demanding, up to 70 MWh/tonne in the case of homogenized nanocellulose fibrils.[176] Chemical treatments, such as bleaching or enzymatic pre-treatments, are used prior to mechanical fibrillation to reduce the energy consumption during the initial step of the processing and to purify the obtained nano cellulose.[10,177] The degree of polymerization, morphology and aspect ratio may vary considerably depending on the raw materials and fibrillation techniques.[178] The following sections contain a review of the most commonly used methods for the production of nanocellulose.

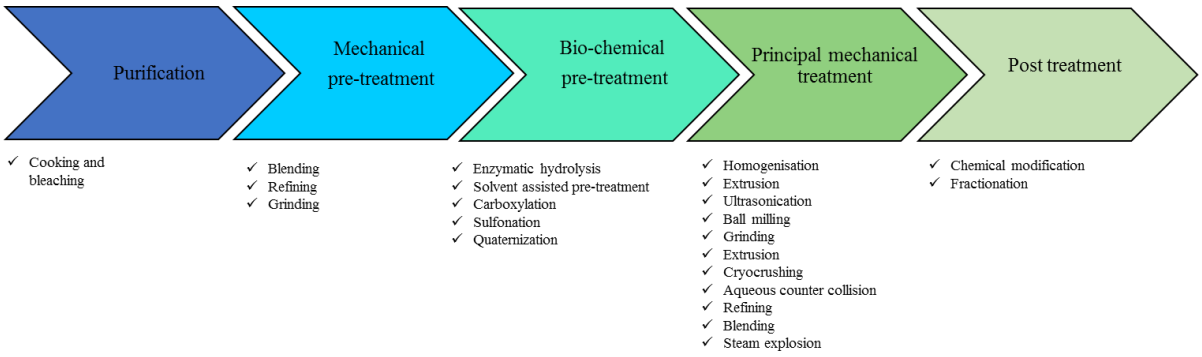

Figure 2.3 Nanocellulose based products schematic production steps from wooden plants.

2.3.1 Pre-treatments

Pre-treatments can be applied to untreated lignocellulosic materials and to Kraft pulp. They represent an efficient alternative to repeated passages in mechanical fibrillating devices[61] and can efficiently reduce the energy consumption even to an astonishingly low 1,000 kWh/ tonne, preserving the final product quality.[72,179] Alkali pre-treatment with NaOH or $NaClO_2$ at 80 °C[23] are used on lignocellulose feeds to purify the raw materials.

The alkali pre-treatment is used to dissolve lignin, pectins and hemicelluloses.[180–183]Owing to the aggressive conditions, the entire procedure has to be strictly controlled to ensure that hydrolysis occurs only at the surface of the fibres,[16,180] preventing extensive damage to the fibrils. Alternatively to the use of strong alkali, natural enzymes can be used.[177] These enzymes belong to the cellulases family and are able to digest cellulose fibres.

The A- and B-type cellulases, termed cellobiohydrolases, attack high-crystalline cellulose regions and the C- and D-type cellulases termed endoglucanases degrade amorphous cellulose regions.[184,185]

Cellobiohydrolases and endoglucanases show strong synergistic effects.[10,186] Cellulases are extracted from fungi like Dutch elm disease, which contains the OS1 complex used for pre-treating cellulosic raw materials.[138] The OS1 fungal complex shows mild activity against cellulose which means that the use of carefully controlled reaction conditions can minimise cellulose fibril degradation, especially when compared to mechanical methods.[10,177] The combination of mechanical and enzymatic treatments is beneficial as mechanical treatments increase the accessibility of the cell wall to the subsequent enzyme treatments. A final passage through high-pressure microfluidizer produces controlled nanofibrillar morphology and a quality final product, minimizing the energy demand.[3,10,187]

The use of strong acids such as sulfuric acid is successfully used in the production of cellulose fibrils; the method goes by the name of sulfonation. Sulfonation introduces negatively charged groups on the cellulose fibre surface, promoting charge repulsion between the fibrils and consequently greatly improving fibrillation.[188,189] Several other reactions are known to introduce sulfonic groups on cellulose fibrils. Bleached Kraft hardwood pulp treated with periodate and bisulfite and passed through a homogenizer five times, produces fibrils of 10-60 nm width and anionic charge densities of 0.18-0.51 meq/g, elastic modulus and tensile strength of 13.5 GPa and 164 MPa, respectively.

The sulfonation pre-treatment based on periodate and sodium bisulfite has great potential as industrial pre-treatment since periodate is efficiently recycled (90-100 % recovery).[188]

As opposed to sulfonation, quaternization pre-treatment introduces positive charges on the cellulose fibrils' surface.[190–192] Positively charged fibrils present electrostatic repulsion which simplifies the fibrillation process.[193] Cationic charge densities between 1.10 and 2.13 meq/g have been achieved, depending on the reaction conditions used.[194] Nanofibrils of 2.6-3.0 nm diameter[195,196] are obtained from purified pulp that was first cationized with (2-3-epoxypropyl) trimethylammonium chloride in the presence of water, isopropanol and sodium hydroxide (**Figure 2.4**).[188] Nanofibrils of 10-50 nm in width are produced from cellulose fibres treated with periodate and then quaternized by reaction with (2-hydrazinyl-2-oxoethyl)-trimethylazanium chloride, followed by mechanical disintegration in a high-pressure homogenizer. Films produced from quaternized microfibrillated cellulose exhibit antimicrobial activity,[197] which is reported to be preserved in quaternized MFC composites.[198]

Regardless of their chemical nature, acidic or basic pre-treatments are used to extract impurities such as hemicellulose and lignin from lignocellulosic starting materials and to releases the pulp fibres.[183,199–201] Cellulose is insoluble in water and in most organic solvents; nevertheless, microemulsions (surfactant-oil-water systems) of urea or ethylenediamine are reported to loosen hydrogen bonds between cellulose fibrils,[202] actively acting as "solvents" for cellulose fibrils, increasing their accessibility in further processing and consequently reducing the energy demand for the production of fibrillated cellulose. Deep eutectic solvents (DES), based on choline chloride and urea at 1:2 molar ratio, have been reported to enhance pulp fibrillation in a micro-fluidization process at 100 °C, producing fibrils of 2-5 nm in diameter and 15-200 nm in length. The original DP of cellulose fibres is preserved during DES treatments.[203]

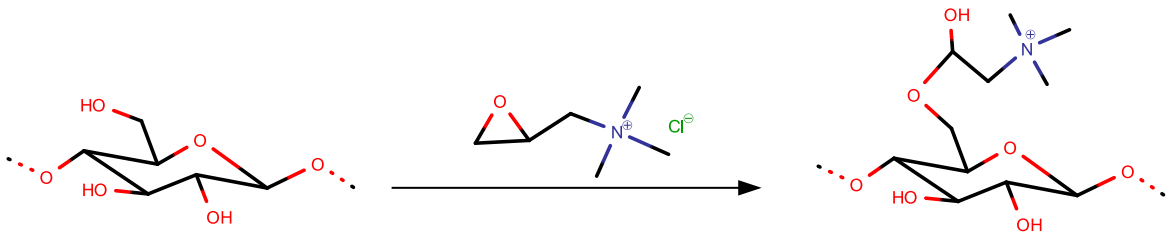

Figure 2.4 Schematic reaction of cellulose quaternization using (2-3-epoxypropyl) trimethylammonium.

2.3.1.1 TEMPO-mediated oxidation: between pre-treatment and nanocellulose production method

TEMPO-mediated oxidation deserves a special mention as it can be considered an efficient pre-treatment prior to mechanical fibrillation and an efficient production method for quality cellulose nanocrystals. 2,2,6,6-tetramethylpiperidine-1-oxyl (TEMPO) mediated oxidation is a surface modification method used for native celluloses. TEMPO-mediated oxidation introduces, under aqueous and mild conditions, carboxylate and aldehyde functional groups on the surface of native cellulose (**Figure 2.5**).[133,139,140,142,151,204–206] The method is highly selective for the modification of C6. Fibrillation is favoured by the negative charge introduced on to cellulose fibrils by their oxidation.[205] NaBr and NaClO are used as a catalyst and primary oxidant respectively in the TEMPO-mediated oxidation reaction. TEMPO-mediated oxidation requires neutral or slightly acidic conditions in order to avoid side reactions triggered by alkaline conditions.[142] The TEMPO/NaClO/$NaClO_2$ oxidation system produces fibrils with an extremely high degree of polymerisation (DP), uniform width distribution around 15 nm and of hundreds of nm in length (**Table 2.1**). The final product obtained is free from superficial aldehyde groups.

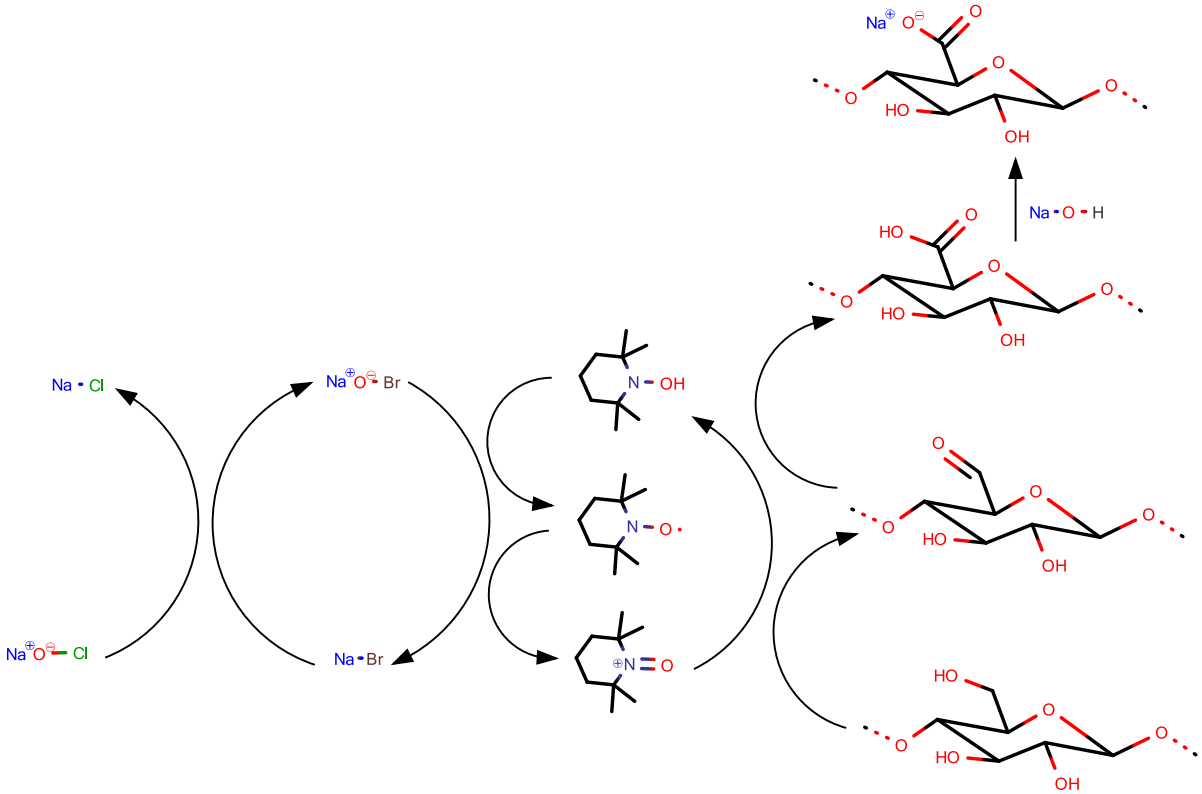

Figure 2.5 Schematic representation of TEMPO mediated oxidation on a cellulose segment.

Films prepared from TEMPO-oxidized cellulose possess high transparency, high toughness and low density.[23] Despite the profound importance of TEMPO-oxidized products in the area of nanocellulose, the present work did not involve any comparison with TEMPO-oxidized cellulosic products because of the peculiar preparation method which offers limited space for process modification.

Table 2.1 Nanocellulose characteristic widths and lengths.[1]

Cellulose structure	Diameter (nm)	Length (nm)	Aspect ratio (l/d)
Elementary fibril	2-10	>10000	>1000
MFC	10-40	>10000	100-150
Cellulose nanocrystals	2-20	100-600	10-100
Microcrystalline cellulose	>1000	>1000	≈1

2.3.2 Mechanical methods

The first examples of the production of cellulose microfibrils involved the application of mechanical shear to a slurry of cellulose pulp in water. The production of individualised cellulose fibrils through high-pressure homogenization was first reported by Herrick[60] and Turbak[137] in the 1980s. Homogenization consists of forcing a dilute pulp-water suspension through a mechanical homogenizer which consists of a spring-loaded valve disk. The impact of the fibres against the valve's surface, and the forced passage through the narrow orifice opened by the high pressure, promoted a high degree of fibrillation in the pulp which is further driven by the pressure drop registered after the homogenizer. Nowadays, homogenisation is used as a refining process for mechanically- or chemically- produced cellulose fibrils. The application of extensive mechanical fibrillation processes damages the cellulose fibrils, reducing their degree of fibrillation and crystallinity. Elevated degrees of mechanical processing of cellulose fibrils results inefficient as some large fibres or aggregates remain in the product even if elevated degrees of processing are used.[9] An initial step of mechanical or chemical treatment is nevertheless applied before the mechanical fibrillation procedure to efficiently peel off the cell wall layers and prepare the fibres for subsequent treatment.[5,31,177,207] Homogenization produces fibrils of 20 to 100 nm in diameter and several tens of μm in length. Efficient homogenization requires a pressure of 1000 bar and up to 15 cycles[40] to obtain a product with an expanded interfacial area and an increased bonding potential.[207] Further increase in the homogenization cycle number does not improve fibrillation,[34,143,152] but increases fibrils damage and the energy consumption which is already reported to be as high as 30,000 kWh/t.[39,207]

Aqueous counter collision (ACC) is a convenient industrial method to produce large amounts of cellulose fibrils. The process is based on the collision of two high-pressure jets of aqueous cellulose suspensions. Because of the high energy of the colliding jets, a high shear force is produced. The shear force effect effectively separates individual fibrils of ≈180 μm in length from the native cellulose macrostructures. Using a homogenized, diluted (≤0.4 wt.% in cellulose) bacterial cellulose slurry it is possible to obtain a suspension of individualized cellulose fibrils of ≈15 nm in diameter and a length of ≈700 nm.[208] The ACC procedure reduces the cellulose crystallinity fraction compared with the initial raw materials (*e.g.* bacterial cellulose whereas the crystallinity fraction is >70 %).[209]

ACC requires homogenized pulp as an initial cellulose material to obtain individualised fibrils; the method can be thus efficiently applied to reduce the number of passages in the homogenizer but cannot substitute the latter.

The application of high shear forces to a cellulose slurry to produce cellulose fibrils can be accomplished using a Masuko 'Supermasscolloider'. The fibrillation of cellulose, in this case, is accomplished forcing the slurry between a static and a rotating grindstone revolving at 1,500 rpm.[61] The plant cell wall is delaminated by the shearing forces generated from the grinding stones which efficiently produces individualized nanofibrils having dimensions of 50 to 100 nm in diameter.[11,143,210] As in the case of the ACC method, an extended cellulose fibril degradation is reported for this production method [11] affecting the product potential as a reinforcement. Furthermore, owing to the complicated multi-layered structure of the cellulose microfibers, and to the interfibrillar hydrogen bonds, the product obtained for untreated pulp contains aggregated nanofibers with a wide variety of sizes.[17]

Uniform individualised cellulose nanofibers of about 15 nm in diameter have been obtained for pre-treated products from which lignin and hemicellulose were first removed and aggregation was prevented by utilising an appropriate number of passages between the grinding stones.[17,20,72] Similar results have been obtained using high-speed blenders.[211] The optimum condition involves the use of a diluted Kraft pulp slurry (0.7 wt.% of fibrils) at 37,000 rpm for 30 min. This blending method, with optimum conditions, produced the same degree of fibrillation and less damage than the grinding in a Supermasscolloider for one pass.[212] High-speed blending can thus increase the process efficiency reducing the time required for fibrillation by half.[201,213]

A relatively recent technique has been developed at FiberLean to produce cellulose microfibrils by transferring shear forces to cellulose fibres *via* wet stirred media milling. This technique involves the use of a diluted cellulose suspension placed in a rotating container partially filled with grinding media (*e.g.* ceramic, zirconia, or metal balls). Cellulose fibres are fibrillated by the high-energy collision between the balls. Using a ball milling technique an average fibril diameter of 100 nm is achievable. Process conditions, such as ball size density and surface finishing, and ball-to-cellulose weight ratio are critical parameters to control in order to prevent the degradation of cellulose fibrils and their fragmentation, thereby preserving the characteristic microfibrillated cellulose networked morphology.[214]

The production of cellulose microfibrils from TEMPO-pre-treated, never-dried, bleached hardwood Kraft pulp at high solid contents (≥50 %) using a ball milling process, has been reported.[215] Individual fibrils of 3.2 nm diameter are produced along with larger aggregates with dimensions in the range 10-150 nm.

The influence of grinding time, moisture content, carboxylic charge and starting material strongly affect the final product quality. Despite the advantages offered by the ball milling technique, the final product quality and homogeneity remains a major challenge. The main advantage is represented by the little energy consumption required for the fibrillation of TEMPO-pre-treated materials.

Along with the more conventional mechanical methods, more exotic approaches have been developed to reduce fibril damage and energy consumption. Ultrasonication is one of these approaches. The technique consists of exposing a fluid to ultrasonic waves (>20 kHz) which creates small unstable vacuum bubbles due to the alternation of low and high-pressure waves.[216,217] The unstable bubbles collapse creating strong hydrodynamic shear forces used to delaminate cellulose fibres. Ultrasonication methods do not usually require pre-treatment,[216,218,219] but can be applied successfully after TEMPO-mediated oxidation.[139,220–222]

Cryocrushing is another exotic fibrillation method usually followed by mechanical refining of the product.[16,146] Cryocrushing consists of freezing a pulp with liquid nitrogen and then applying high shear forces to the frozen product[223] to exert pressure on the cell walls causing them to rupture and thereby liberating the microfibrils.[181] Cryocrushing produces size-controlled fibrils of which 60 % have dimensions of between 30-40 nm microns in length, and widths in the range 50-100 nm.[180,181] Cryocrushed fibrils are dispersible in water;[138] in fact the cryocrushed product is used to produce a diluted feed for homogenisation.

In contrast to the extremely low temperature used in cryocrushing, steam explosion exploits high temperature to produce cellulose fibrils. Steam explosion consists of exposing the pulp to pressurized steam for a short time. This procedure is followed by a rapid release of pressure afterwards. The steam explosion was developed for the extraction of cellulose fibres from lignocellulosic materials, without prior application of bleaching to the lignocellulosic starting fibres. The sharp decrease in pressure causes the rupture of the cell walls and the separation of significant amounts of hemicellulose and lignin, and cleaves macromolecules into water-soluble oligomers.[224,225]

Steam explosion is currently employed in the production of cellulose fibrils from pulp and from agricultural by-products such as pineapple leaves[226], banana fibres[227], *Helicteres isora*[228], and jute.[229] Regardless of the fibre source, the quality of the final produced nowadays remains questionable.

2.3.2.1 Fiberlean™ method

Fiberlean Technology has developed a new cost-effective method to produce MFC based on the principle of wet stirred media milling. This method uses a diluted cellulose pulp slurry and minerals to obtain MFC of higher quality, through an energetically efficient process. The Fiberlean™ method presents two main advantages:

- ✓ the cellulose fibres are co-processed with mineral particles which act as micro-grinding media, thus reducing energetic requirements for the cellulose fibrillation;
- ✓ the process can be accomplished using robust, industrially proven grinding equipment.

The resulting MFC-mineral product is commercialised as FiberLean™. FiberLean™ is currently used in the paper industry to improve both the wet and dry strength of the final products, to enhance printing paper finishing for high-quality print and to improve aesthetics in cardboard packaging. More fascinating applications are currently under development. The improvements in mechanical properties of paper when MFC is added is due to an increased hydrogen bonding mediated by the MFC microfibrils which possess a very high surface area compared to regular fibres. The solid content of FiberLean™ product is limited by the high viscosity of the slurry. The initial material is a dense water-based slurry of ~2.5 wt.% fibre and 12.5 wt.% solids depending on the fibre source. The solid content is regulated by strict cellulose to mineral weight ratio. During the production of FiberLean™ the slurry viscosity increases as a result of fibrillation up to a maximum of energy intake which results in an optimum product characteristic. This increase in viscosity is thought to arise from the development of an increasing hydrophilic surface area and from fibrils entanglements as a consequence of the individualisation of the fibrils.[230]

2.3.2.2 Modified extruder in the production of nanocellulose and reinforced thermoplastic in one step

As in the case of the TEMPO-oxidized product, a special mention is due to the production of nanocellulose using a modified extruder even if, owing to the peculiarity of the method, small space is left for independent studies, therefore the extruder compounding/fibrillation process is described in the next paragraph as it has a special relevance to this project, but no direct

investigation was directly performed in this work. A modified co-rotating twin-screw extruder equipped with extra venting (up to 20 wt.% water contained in the main feed), has been reported for the production of MFC and reinforced thermoplastic nanocomposites in one step.

The modified vented extruder co-process wet pulp (up to 85 wt.% water) and premixed polymer powder. The mixture is heated to the polymer melting temperature while continuously mixed. The shear force transferred to the mixture by the screws causes the fibres fibrillation and the fibrils dispersion into the molten matrix. The water in the feed vaporise as a consequence of the mixture heating and is vented from the mixture through appropriately designed ports.

Where applicable, the extrusion method for the production of MFC, presents several advantages over mechanical fibrillation:

- ✓ the cellulose slurry can have, and actually should be, fed at a high solids content, 25-40 wt.% of cellulose;[231]
- ✓ the cellulose *in-situ* fibrillation is performed together with the melt compounding of the matrix.

Besides the technological advantages of this one-step manufacturing technique, the compounder screw profile and processing conditions optimisation to induce the delamination and fibrillation of the fibres and prevent major fibril degradation is challenging. In addition to this, a special extruder is needed due to the high moisture content of the feed, which needs to be removed during processing in the form of steam. The optimisation of the screw profile can be obtained through a combination of kneading and feeding sections. This setup allows a pulp concentration of up to 28 wt.% and fibrillates the starting material into MFC after 14 passes. A final composite product with 45 wt.% cellulose reinforcement load can be produced.[231] Further processing of the product is not recommended because of the moisture evaporation and the high temperature required to melt the matrix which results in the possible thermal degradation of the nanofiller. The starting materials for *in situ* cellulose fibre fibrillation and extrusion are never-dried bleached Kraft pulp and polypropylene. Maleic anhydride grafted polypropylene is used as compatibilizer.[232]

Composites prepared in a single screw extruder using thermoplastic starch and TEMPO-oxidized cellulose fibres are also reported in the literature.[233] TEMPO-activated cellulose fibres are fibrillated into cellulose fibrils of ≈30 nm in diameter during extrusion. Despite the demanding equipment, the described technique is very promising in the production of cellulose-based nanocomposites, but its application remains strongly related to the use of an appropriately modified extruder.

2.4 Nanocellulose commercial forms

Nanocellulose is produced and commercialized in a number of forms. The most relevant of these for the purpose of this study is the slurry, or aqueous suspension, form. In the next paragraph a short review of the most commonly produced nanocellulose forms are reported, alongside their most relevant feature.

MFC aqueous suspension (slurry) is the type of nanocellulose used in this study. It is produced by the mechanical fibrillation of Kraft pulp, from wood, and has properties that derive from the pulp origin and from the production method. The rheological behaviour of the MFC slurry is characterized by high viscosity which tends to increase during fibrillation. Regardless of the production methods, all the MFC water suspensions show gel-like, shear thinning and thixotropic behaviours at low solid content.[234–236] MFC water suspension represents, in most cases the starting material in the preparation of cellulose hydrogels, aerogels, powders, or films. Nanocellulose films are usually obtained by solvent casting[4,24,141,147] or vacuum filtration.[11,15,31,32,143,237,238] The removal of the majority of the water usually causes the formation of a hornified cellulose network stabilized by hydrogen bonds which cannot be re-dispersed in water.[239] The main challenge in the production of nanocellulose powders is the prevention of the agglomeration of the fibrils, which ensures excellent properties and re-dispersibility of the final dry product. The driving force for the production of nanocellulose dry powders is their ease of storage, transportation and use. Dry nanocellulose powders are produced by oven drying, spray drying, freeze-drying, or supercritical drying of nanocellulose water suspensions.[240,241] Unfortunately, the formation of highly-networked structures (hornified cellulose) and stable agglomerates renders the produced dry fibres of limited utility.

Carboxymethylation of the nanocellulose surface has been shown to prevent cellulose hornification during the drying procedure.[242] Above a critical threshold of 2.3 wt.% of cellulose carboxymethylation, the nanocellulose obtained from the oven-dried procedure is fully re-dispersible in water and shown to possess the same properties as the initial water suspension.[243] The absorption of sodium chloride on the surface of nanocellulose has also proven to enhance the water-redispersibility of nanocellulose dry powders.[243] The method is convenient as it does not involve the use of organic solvents; it is in fact based on the exchange of the cellulose counterion from H^+ to Na^+, a modification that decreases significantly the intermolecular hydrogen bonding, most likely due to the electrostatic repulsion of the sodium counter ions.

Nanocellulose water suspensions at low cellulose concentrations can be converted into hydrogels which are hydrophilic materials with a highly networked structure, able to contain up to 99.9 wt.% of water[244] while maintaining their original shape. The production of hydrogels using mechanically fibrillated cellulose aqueous suspensions with sodium hydroxide followed by a neutralization procedure is reported in the literature. The hydrogels obtained are thought to be formed by the shrinkage and coalescence of the cellulose fibrils. The main suggested mechanism involves swelling, entanglement and aggregation of the fibrils.[245,246] Hydrogels produced by TEMPO-oxidized nanocellulose suspensions, under acidic conditions, are thought to be produced because of the reduction of electrostatic repulsion among nanofibrils led by the protonization of the carboxylate groups at acidic pH.[244] Hydrogels obtained from TEMPO-oxidized water suspensions can also be produced by means of cationic metal crosslinking of the fibrils.[247,248] The nanocellulose hydrogel has potential applications in the field of tissue engineering, drug delivery, sorbents, sensors, contact lenses and water purification,[247] alongside with nanocellulose aerogels.

Aerogels are porous sponge-like materials produced by replacing the liquid phase of the nanocellulose water suspensions with air. They have a density of ≈0.02 g cm^{-3}, a porosity of 98-98.7 % and a specific surface area of 20-70 m^2g^{-1}.[27,249,250] The production process preserves the three-dimensional (3D) networked structure of the nanocellulose water suspension during dehydration and prevents aggregation. Aerogels have a high specific surface area, low density and high porosity.[177] Crosslinkers are not necessary since hydrogen bonding and nanofiber entanglement can provide acceptable stability and mechanical resistance to the dry structure. MFC aerogels were first prepared using freeze-drying techniques.[19] Solvent exchange can present a valid alternative to the production of aerogels from water suspensions; in fact aerogels with a specific surface area of 284 m^2g^{-1} and reduced level of cellulose aggregation have been produced by solvent exchange with organic solvents.[244,251–253] Cellulose aerogels could be used as adsorbents, carriers for catalysts and drug release, thermal and acoustic insulation.[250,251]

2.5 Nanocellulose main applications

Nanocellulose products can provide many technical benefits; in fact, their use in the replacement of expensive additives, the substitution of less "green" products or additives, and in the improvement of the performance of commercial products have been the topic of many recent studies and patent applications.[254] One of the first applications of nanocellulose was as an industrial varnish to improve coating scratch resistance,[255] and as a starting material in the preparation of transparent films.[132,256] Alternative uses of nanocellulose material are as a paper strength enhancer, a food additive, a paper surface modifier, a polymer reinforcement, a film-forming additive, a barrier coating, and an emulsion stabiliser.[255] Further studies on the use of nanocellulose as a coating in the paper industry were performed at the University of Maine[257] and followed by many other organisations.[258,259] The high price of the nanocellulose compared to normal fibres make its industrial development challenging. A well-known form of nanocellulose - microcrystalline cellulose (MCC) - and its derivatives have been used for many years as a rheological modifier in food, cosmetics and for tablet preparation. An innovative application as a thickening or rheology-modifying agent in aircraft de-icing fluids was proposed by Boluk and Zhao.[260]

Various forms of nanocellulose have been investigated as reinforcements and as barrier property enhancers in polymers, in particular in polymers of hydrophilic nature[25,261,262] because of the compatibility between the reinforcing fibre and the suspending polymeric medium. A good compatibility between the matrix and the reinforcement is necessary for chemical wetting (maximum adhesion between the components). Initially, nanocellulose dry powders were shown to be an effective reinforcement for extrusion and injection moulded starch derivatives.[263] Nakagaito and Yano, who worked on this subject, concluded that the degree of fibrillation that we normally associate with well-refined pulp fibres is not sufficient to provide adequate polymer reinforcement. It requires fibrillation at the micro or nano scale to achieve this desired effect.[31] Nanocellulose use as reinforcement was also investigated in natural rubber,[264] in polyurethanes,[264] and in biopolymers such as poly(lacticacid) (PLA)[265–267] as a substitute for the more commonly used inorganic fillers such as carbon black, nanoclay, nanosilica, and nanoalumina. A more detailed review of the application of MFC in polymer reinforcement is provided in **Section 2.9**.

A final and curious application of nanocellulose product refers to the electronic market. For the last 10 years, there has been considerable interest in the use of conventional printing to fully print electronic products at a very low cost. Paper and other cellulose derivatives have themselves been considered as substrates.[29,268,269] In recent research the coefficient of thermal expansion of common polymer films has been noticeably decreased by the addition of nanocellulose.[268,270] New opportunities for plastic films designed for printed electronics may result from the combination of nanocellulose with synthetic polymers. Recent research activities have identified many interesting and exciting potential applications for different forms of nanocellulose products. This attracted significant interest from both academia and industry. However, a strong value proposition and business case based on market size estimation and real industrial uses is not yet fully developed.[254]

2.6 Microfibrillated cellulose structure and properties

The microstructure of MFC has been extensively investigated through electron microscopy (TEM),[239] scanning electron microscopy (SEM),[239,271] field-emission scanning electron microscopy (FE-SEM),[39,219,239,272,273] atomic force microscopy (AFM),[153,274] wide-angle X-ray scattering (WAXS)[275–277], and solid-state ^{13}C cross-polarization magic angle spinning (CPMAS) NMR spectroscopy.[271,278,279] Microscopic techniques and image analysis measure the widths of nanofibres, but usually fail in determining their lengths as the unequivocal identification of both ends of nanofibre is challenging (**Figure 2.6**). MFC morphology is generally not homogeneous because of microscopic fibre fragments, non-fibrillated residues, and cellulose aggregates of various shapes and sizes.[4,24] Agglomeration is considered to be caused by the high density of hydroxyl groups on the surface of the microfibrils, which promotes hydrogen bonding and irreversible agglomeration in concentrated water suspensions and dry cellulose products.[39] When the fibrils are dispersed in water, the hydroxyl groups on their surfaces interact with water molecules through hydrogen bonding because the concentration of water molecules is much higher than the fibrils that inter-fibril hydrogen bonding is probably minimal. When the water is removed, fibrils concentration increases and they start to form hydrogen-bonds with each other. The fibrils are brought into close contact by the surface tension of the last bridges of liquid water as the material approaches dryness. If the material is freeze-dried, the surface tension effects are largely eliminated, so inter-fibril hydrogen-bonding is much reduced. The width distributions of nanofibres depend on the origin of the cellulose fibres and processing: the presence of residual hemicelluloses and pectins is reported to mitigate agglomeration even at high solids content.

The presence of hemicellulose and pectins in Kraft pulp is, however neglectable, reducing the applicability of the described findings to the present study. Reduced aggregation in the presence of hemicellulose and pectin suggests these macromolecules have a fundamental function in limiting fibrils interconnection.[20,22,149,280–284] Further studies on pulp with high hemicellulose content demonstrate that the presence of hemicellulose facilitates the fibrillation and improves the physical properties of the nanocomposites obtained.[283] Studies on MFC produced from highly pure Kraft pulp demonstrated that the removal of hemicellulose and lignin results in an X-ray crystallinity fraction of the product up to 0.35.[146] Pectin content, on the other hand, seems to be correlated with the ability of cellulose fibrils to form coherent films: films obtained from pectin free MFC had an inferior tensile module, compared to the ones containing pectin.[147] It is thought that pectins act as a binder among cellulose fibrils, improving the stress transfer mechanism and forming a tougher network structure.

An AFM evaluation of MFC film morphology indicated that an MFC slurry with a high hemicellulose content tends to form a network structure in films,[14] while an MFC slurry with low hemicellulose content tends to form smoother and denser films.[285] Despite the experimental indication of a strong connection between hemicellulose, pectin and cellulose fibrillation and network formation, a comprehensive model of the interactions among these important fibre components and their relationship with the structure and performance of the microfibrils has not been fully developed yet.

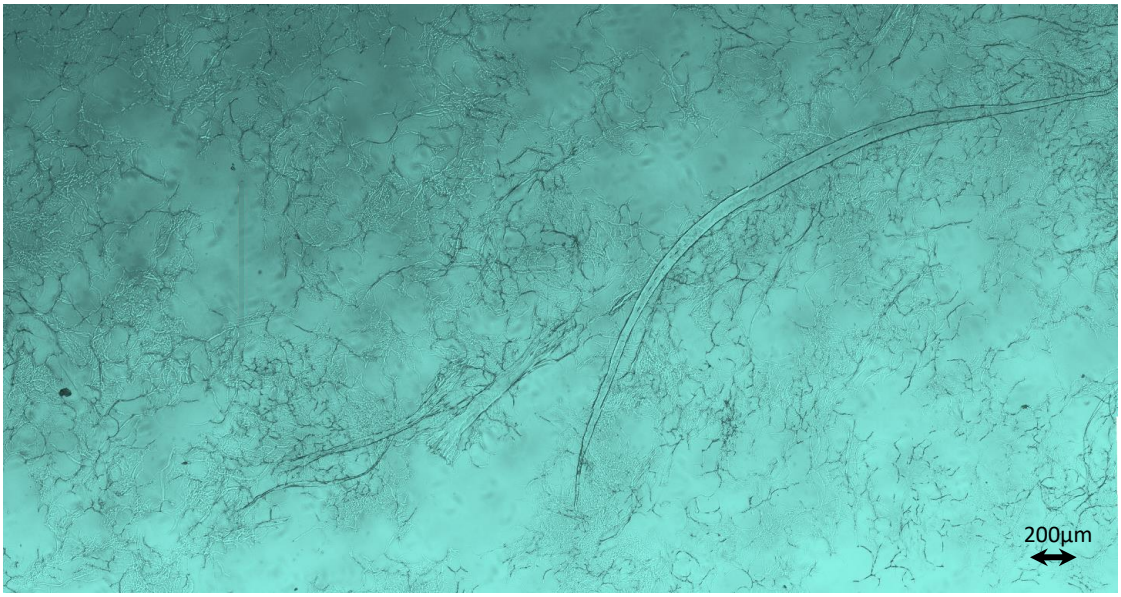

Figure 2.6 FiberLean™ polarized optical microscopy images in water. The characteristic networked structure of FiberLean is visible in the background. Large unfibrillated cellulose fibres are present in the centre of the image.

2.6.1 Degree of polymerisation of nanocellulose

Production methods affect the morphology of the produced MFC. The "degree of polymerisation" (DP) can be used as an estimate of the quality of the produced fibrils. The DP of cellulose is reported to be 1,200–1,400 in native fibres and efficient mechanical fibrillation reduces the DP by 30-50 % (up to 700 units).[10] Unfortunately superior tensile modulus (at least 2 GPa)[286] is obtained only from fibrils with high DP,[10] which indicates an inverse correlation between the DP and tensile modulus of the MFC films. To estimate DP, an indirect measurement such as water retention has been developed and used.[60]

Different methods are reported to evaluate the DP: centrifugation, to determine a water retention value (WRV)[133,202,213,287–289] and viscosity of the slurry are generally used. Fibril suspension viscosity increases dramatically during the fibrillation process because of the increased number of hydroxyl groups exposed to the water medium due to the increase in the exposed surface area.[10,33,143] More reliable in the measurement of DP resulted in the light transmittance or scattering/turbidity of aqueous MFC suspensions.[99,141,213,288,290] The value of DP is correlated to the light scattering of the non-fibrillated fragments in MFC solution dissolved in appropriate solvents. The result is evaluated against the light scattering of a reference solution or MFC films. Ultraviolet-visible (UV) spectroscopy is an excellent optical technique to measure the light transmittance (*T*) of MFC suspensions and films and their transparency as well, which is influenced by the presence of non-fibrillated fragments.[99,139,242,288,290,291]

2.7 Microfibrillated cellulose mechanical properties and reinforcing potential

The development of models aimed to understand the mechanical behaviour of fibre networks dates back to the 1950s (Cox 1952) and invoked the assumption of rather simple geometries and stress transfer mechanisms, implying a uniform strain. Nevertheless, the mechanisms underlying such models produced important results.[292] In fact they are applied to current MFC networks in which the nanosize of the fibrils reduces the impact of the defects and fibre damage on the film performance. The work first of Cox (1952), and later of Kallmes and Corte (1960), correlated the geometric properties of fibres in paper networks, such as the average number of crossings with other fibres, the mean length of the fibres and the fibre density, to the properties of the network.

The reference macroscopic model was a two-dimensional sheet in which the thickness of the fibres was negligible. For the purpose of the model, the fibres were assumed to be randomly distributed over the selected area and to have a uniform orientation distribution. The results of this study formed the basis for the development of the uniform strain model which related the fibre and bond parameters to the mechanical properties of a network.

Under the uniform strain assumption, the strain is equal everywhere in a film and thus equal to the average measured strain. In a network, the homogeneous strain assumption implies that each bond centre is displaced according to the mean strain. The displacement of the fibre ends is then calculated as a function of mean strain. Assuming a linear elastic behaviour for the fibres, the elastic coefficients of the single fibres can be calculated. In Cox's network model (1952)[292] the fibres were assumed to extend from side to side, to carry only the axial load and not interact with each other. The fibre elastic modulus was evaluated using the equation

$$E = \frac{1}{3}\frac{\rho_s}{\rho_f}E_f \qquad \textbf{(1)}$$

where E indicates the modulus of the network, ρ_s is the network density, and ρ_f is the fibre density. The stiffness values predicted by Cox's model are not reached in real networks because of defects, limited lengths of the fibres, and real fibre behaviour under stress, but they could be viewed as an upper limit. To account for the finite length of the fibres in a real network, the fibre modulus is reduced by an amount corresponding to the average stress in a short fibre compared with the stress in an infinite fibre.

More correction was introduced in Cox's equation in later years to account for deviation from ideal behaviour of the real networks: Kallmes and Perez[82] introduced a theory dependent on three factors; the fibre orientation, the number of fibre interconnections, and the probability that a fibre interconnection carries a load. Failure is assumed to result from either the fibre strength being exceeded or from progressive bond failure. In 1969, Page derived the following equation for paper strength, T, under uniaxial tension[293]

$$\frac{1}{T} = \frac{9}{8Z} + \frac{12A_f\,\rho_f\,9.81}{bPl_f RBA} \qquad \textbf{(2)}$$

where Z denotes zero-span tensile strength, ρ_f fibre density, b shear bond strength per unit area, A is the fibre cross sectional area, P the perimeter of the fibre cross-section, l_f is the mean fibre length, and RBA the relative bonded area of the sheet.

The Page equation emphasizes the importance of fibre and bond properties in the failure of real networks. In a further review of the equation by Page and Seth, the elastic modulus of the network was found to be correlated with the fibre modulus, load transfer between the fibres and defects in the fibres such as micro compressions, curl and kinks. For networks of long, straight, well-bonded fibres the modulus is derived by Cox's equation, which is the one used as a reference in this work.

Despite the excellent theoretical performance calculated for perfect cellulose networks (Young's modulus of ≈20 GPa and strength of ≈240 MPa),[53] MFC cellulose films consistently underperform the estimated modulus and strength values for a random network of infinite length fibres, in which the maximum theoretical E-modulus has been evaluated to be one-third of that of the one of the individual fibres.[13] The discrepancy between the theoretical and empirical values is due to the imperfect nature of the fibrils constituting the real network in MFC films, and due to the reduced crystallinity fraction of MFC caused by mechanical production methods. Nevertheless, excellent results were obtained from Kraft pulp MFC and tunicin MFC films of 3-100 μm thickness, whose tensile strength exceeds that of print paper by 2.5 times, and of polyethylene (PE) films of the same thickness by 2.7 times.[210] The tensile strength of pure MFC films approaches the strength of clear wood (80-100 MPa), and their modulus of elasticity is ≈9.6 GPa.[33,39,40,59] An analysis of different MFC films containing cellulose fibrils of different molar mass related the molar mass distribution of the microfibrils with the macroscopic mechanical properties of the samples.[15]

Lateral dimensions of nanofibres determined by SEM were found to be in the range 10-40 nm suggesting the presence of aggregates rather than individual microfibrils, which in turn reduces the stress transfer in the network.

An important parameter for the mechanical performance of a fibrous network is the film porosity; in fact, the mechanical properties of porous MFC films decrease significantly when the porosity is increased. The porosity of MFC films is dependent on the solvent used during the film preparation, among other parameters more related to the fibre type and size. MFC films with porosity, up to 28 %, were reported to have Young's modulus of 13.2 GPa and tensile strength up to 214 MPa, which are remarkably high in MFC films.[15] The superior performance of MFC films, despite high porosity, a high level of defects introduced by mechanical fibrillation, and the decreased length of the fibrils caused by the mechanical fracture introduced during the possessing, are ascribed to the decrease in the fibril size.

This decrease mitigates the effect of defects, increasing the fibril density and the network crossing points (bonding) which respectively increases the stress transfer in the resulting network. **Table 2.2** presents a comparison of the reinforcement potential of industrially commonly used and cellulose-based fillers. Cellulose is five times lighter than steel wires and has a theoretical modulus of the same magnitude, characteristics that alone present potential in the area of composites fillers.

Table 2.2 Property of cellulose and several reinforcement materials. [53]

Material	**ρ** **(gcm^{-3})**	**σ_f** **(GPa)**	**E_A** **(GPa)**	**E_R** **(GPa)**
Kevlar-49 fibre	1.4	3.5	124-130	2.5
Carbon fibre	1.8	1.5-5.5	150-500	-
Steel wire	7.8	4.1	210	-
Clay nanoplatelets	1.3		170	-
Carbon nanotubes	1.6	11-63	270-950	0.8-30
Boron nanowhiskers	2.7	2-8	250-360	-
Crystalline cellulose	1.6	7.5-7.7	110-220	10-50

Key: ρ=density, σ_f=tensile strength, E_A=elastic modulus in the axial direction, E_R= elastic modulus in transverse direction.

Besides the influence of mechanical and geometrical parameters of the fibrils and the network, the mechanical properties of MFC films are reported to be strongly affected by the moisture content.[9]

2.8 Other relevant microfibrillated cellulose properties

The mechanical properties of MFC fibrils are undoubtedly their most relevant property for this study. However, this fascinating type of cellulose possesses other important properties. One of the relevant properties of nanoscale cellulose is its optical transparency.

Optical opacity is caused by light scattering from particles whose dimensions are larger than the incident light wavelength. Because of the dimension of MFC fibrils (5-10 nm) the incident light is not scattered, and so films of this material and composites, therefore, retain their transparency.[170] MFC transparency is, however, compromised when significant agglomeration occurs. The light transmittance of orange light (600 nm) is reported to be 78 % - 90 % for a 20 μm-thick TEMPO-oxidized MFC film.[294] In contrast with TEMPO-oxidized nanocellulose, which has a narrow width and length distribution, in the range of tens of nm, the carboxymethylated MFC films containing small quantities of hemicellulose are reported to form large aggregates and have shown a great decrease in film transparency under the same conditions. The optical transparency of MFC films is improved through homogenization because large aggregates are broken down. The light transmittance of orange light (600 nm) for a 20 μm-thick homogenized carboxymethylated MFC films improved from 61 to 82 %. Refractive index contrast is a critical parameter in film transparency;[295] in fact, MFC film optical transparency is greatly improved (up to ~90 %) when the film is impregnated with optically transparent polymers of similar refractive index.[296]

Another important property of MFC films is their barrier property: small diffusing molecules penetrate highly crystalline nanocellulose networks only with difficulty.[13] The high crystallinity of the nanocellulose film[41,285] and the ability of nanosized cellulose fibrils to form a dense network results in an oxygen permeability of 21 μm-thick MFC films of 17.75 ml m^{-2} day^{-1} at 23 °C[13,294]: comparable with common polyolefins. The addition of MFC to polylactide (PLA) composites decreases the oxygen permeability by about 700-fold. Unfortunately, MFC films are extremely sensitive to moisture and their vapour barrier properties are less remarkable because of the less dense packing of the amorphous sections. The hydrophilicity of MFC films is strongly correlated to the DP of the fibrils and to the mesostructure of the films itself.[285] Unfortunately, only a small number of studies have been conducted on the reduction of vapour permeability in MFC films: the addition of amylopectin seems to decrease the water uptake in MFC films,[47,152] while film porosity, geometry and orientation of the nanofibrils in the films were correlated to the vapour permeability of both neat films and MFC, reinforced composites.[3,9,15]

2.9 Nanocellulose reinforced composites

Nanocomposites are two-phase materials in which the dimensions of one of the phases is in the nanometre range (1-100 nm). Cellulosic nanocomposites, compared to conventional ones, possess superior thermal, mechanical and barrier properties at low reinforcement levels (*e.g.* 1-5 wt.%); they are recyclable, the addition of biodegradable fillers can generate a fully biodegradable nanocomposite,[297–301] they are transparent and can have a low density. The use of cellulose fibres in composites is a well-established practice (**Figure 2.7**) in industry[65,79,83,88,302,303]. It is known that the properties of fibre-reinforced composites depend on fibre size, fibre/matrix adhesion, volume fraction, aspect ratio and orientation of the fibres, as well as stress transfer efficiency through the interface.[304] The dependence of the composites upon these parameters will be described in more details in a separate paragraph.

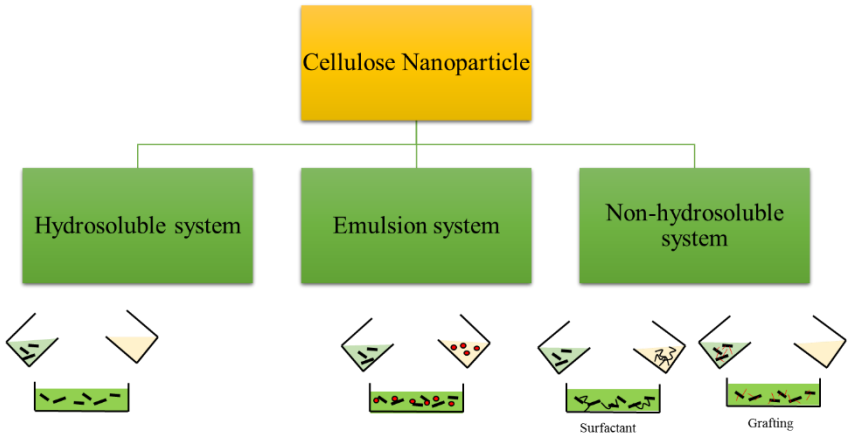

Figure 2.7 General strategies used in the preparation of cellulose-based nanocomposites for polar and apolar matrices. The cellulose reinforcement is represented as black segments. In the hydrosoluble system, a water suspension of nanocellulose is mixed with a water soluble polymer solution. In the emulsion system, a water suspension of nanocellulose is mixed with a latex emulsion. In the non-hydrosoluble system, the cellulose is hydropobised either by the addition of surfactant or by surface compatibilization of the cellulose fibrils.

The properties of cellulose nanocomposites are dependent on the same parameters; in fact, the content of fibrils is a critical factor in cellulose nanocomposites because higher filler loadings can lead to aggregation,[305,306] which compromise the properties of the nanocomposites.

Poorly performing cellulose-reinforced nanocomposites have been produced from cellulose nanowhiskers and BC in polyethylene (PE), and polypropylene (PP) matrices, while nanocomposites with superior properties have been obtained from biodegradable polar polymers (*e.g.* PLA, poly(vinyl alcohol) (PVOH), starch, polycaprolactone (PCL) and polyhydroxybutyrate (PHB)). The difference in performance and dispersion in polar and apolar matrices is attributed to poor compatibility, which makes surface chemical modification mandatory as a first step in the production of nanocellulose reinforced polyolefins.[1]

2.9.1 Nanocomposites with hydrophilic matrices

As already mentioned, MFC is an excellent reinforcement in hydrophilic polymers. The following paragraph contains examples of the characteristics and preparation methods of polar matrix-MFC nanocomposites.

Nanocomposites based on hydrophilic matrices and cellulose were the first types to be produced. Phenol-formaldehyde resins impregnated MFC composites are a good example of them: they have shown Young's modulus of 19 GPa and bending strength of 370 MPa respectively,[31] however the authors did not report the properties of the unfilled resins. Typical values for the phenol-formaldehyde are Young's modulus in the range of 2-4 GPa and bending strength in the range of 100-400 MPa. The filler was a fibrillated cellulose form produced by the passage of a pulp suspension through a fibre disintegrator 16-30 fold, and refined in a high-pressure homogenizer.[31,207] Acrylic and epoxy resins reinforced with 20 wt.% alkali-treated MFC had strain at fracture twice as high as those reinforced with unreacted MFC, based on the same resin.[9,32,33] MFC-reinforced acrylic resin retains the matrix optical transparency up to a 70 wt.% fibrils content,[11,143] mainly because of the similarity in refractive index between the polymer and the fibres. Cellulose nanofibres have a thermal expansion coefficient (CTE) as low as 0.1 ppm K^{-1}, comparable with the CTE of quartz glass,[307] which along with their high strength and modulus make them suitable as reinforcement in the roll-to-roll technology. A transparent acrylic coated MFC film with a CTE of 8.5–14.9 ppm K^{-1} and modulus of 7.2-13 GPa, which has characteristics suitable for the production of foldable electronic devices, has been reported[295,296]. The production of flexible electronics by roll-to-roll technology represents a major industrial goal.

Aqueous suspensions of cellulose microfibrils and a latex of poly(styrene-co-butyl acrylate) have been solvent cast to obtain reinforced nanocomposites,[34] the tensile modulus of the reinforced nanocomposites increased from 0.6 MPa to 34.5 MPa and values of tensile strength as high as 14.5 MPa have been reported in nanocomposites containing 10 wt.% MFC. Unfortunately, the addition of MFC decreased the matrix ductility, as indicated by the decrease of the elongation at break at increasing reinforcement loads, which is a disadvantage in ductile matrices-based composites. The thermal stability of the matrix has been reported to be significantly increased, while the swelling behaviour of the composite in organic solvents decreased remarkably even at low filler loadings. The preparation method of the nanocomposite strongly affects its properties: solvent casting results in the formation of a rigid network of nanofibrils, which enhances the filler reinforcement effect and also the thermomechanical stability of the composite. Freeze-dried MFC based reinforcements have shown only a limited reinforcement effect in the same matrix,[35] probably due to the incomplete wetting of the fibrils by the viscous matrix.

Polyurethanes (PU) are relatively polar polymers, which may be why they represent good matrices for MFC reinforced composites. PU-MFC composites, prepared by the film stacking method have demonstrated enhanced thermal stability and mechanical properties, due to the good interfacial adhesion between the cellulose fibrils and the matrix. Film stacking method is a technique based on the composites lay-up method: layers of PU were alternated to dry MFC films. The sandwich structure is then hot pressed to obtain the laminated composite. The number of layers and the stacking sequence can be tailored to obtain optimum performances.

Nanocomposites reinforced with a 16.5 wt.% fibril content have achieved tensile strength and elastic modulus values five and thirty times respectively higher than the pure PU.[36] Shape memory polymers (SMPs) are based on PU matrices; they can fix a transient shape, which can be converted back to their original shape by external stimuli.[37,38] Shape memory PUs reinforced with 1 wt.% MFC were reported to achieve a 53 % increase in modulus and retained shape memory properties of the neat matrix.[37]

Poly(vinyl alcohol) (PVOH) represents an ideal candidate for the production of cellulose reinforced composites for biomedical applications.[308,309] Long chain PVOHs can be suspended in cold water and once fully dried and crosslinked by hydrogen bonds, have excellent polar solvent resistance, biocompatibility, mechanical properties similar to soft biological tissues, and biodegradability.

PVOH's major flaw is its limited durability,[310] as in the long term this biopolymer can degrade, especially in wet environments. 20 wt.% PVOH-MFC nanocomposites have been reported to have elastic moduli and tensile strengths three- and five- times higher than the neat matrix,[39] while for reinforcement up to 50 wt.%, the Young's modulus increased up to five times. The tensile strength of the nanocomposites increased linearly as a function of filler content up to an increase of the 44 % at a filler content of 5 wt.%, suggesting that cellulose content is the major determinant in the increase of strength in the composites.[40] At 10 wt.% reinforcement, a plateau in mechanical properties was reached,[16,33,41] suggesting a PVOH matrix saturation. The plateau is registered when the percolation network is formed in the composite. In this case, a well-bonded network of fibres is formed, and the strength of the network is determined by the strength of the fibres. Any further filler addition does not result in enhanced tensile properties of the product. The strong interfacial bonding between cellulose and PVOH hydroxyl groups is believed to be responsible for the superior mechanical properties of the PVOH-MFC reinforced nanocomposites.[40]

Starch is a natural source of a biodegradable polymer, which can potentially be obtained at low cost compared to petroleum-based materials.[43] Starch is formed by a linear (amylose) and branched (amylopectin) (1-6)-linked polymers.[304] In its glassy state, it is brittle and very sensitive to moisture, flaws that can be mitigated by converting it into thermoplastic starch (TPS)[152] through thermomechanical processes,[42] or plasticizing native starch with glycols, urea[43,311], or formamide.[312,313] Native starch and TPS have poor mechanical properties and high water uptake which can be improved adding MFC to them.[42–46]

Starch reinforced with MFC up to a 50 wt.% loading demonstrated a linear increase in tensile modulus as a function of filler content: a tensile modulus of 7 GPa was reported for a cellulose content of 50 wt.%, compared to 2 GPa for unreinforced samples (0 % MFC). Furthermore, the biodegradability of the original starch matrix was left unaltered,[152,304] while water uptake at equilibrium and water diffusion coefficient in the composites were strongly decreased. Conditioning the samples at a high relative humidity (75 % RH), resulted in a decreased MFC reinforcement efficiency. Nanocomposites prepared by solution casting from wheat straw nanofibres and thermoplastic starch showed superior thermal and mechanical properties: modulus of 271 MPa at 10 wt.% reinforcement, compared to the 111 MPa of the neat matrix, and significantly higher glass transition temperature (T_g).[314]

Using the melt mixing method to produce MFC-reinforced nanocomposites of up to 2 wt.% MFC content, a maximum of 20 % increase in tensile strength and a 100 % increase in stiffness is achieved, compared to the original starch matrix.[223]

Amylopectin represents another interesting bio-based matrix for the production of MFC reinforced composites. Gelatinized films of amylopectin and MFC were prepared by the cast film technique; the final product was a stiff and strong film.[187] Adding 70 wt.% of MFC, a tensile strength of 160 MPa, a tensile modulus of 6.2 GPa, and a work of fracture of 9.4 MJm^{-3} are achieved,[3] all impressive properties when compared to the poor mechanical and impact properties of the unreinforced film. Amylopectin films are, in fact, brittle, and as such they are impossible to handle without the addition of glycerol as a plasticizer at a threshold concentration of 38 wt.%. The addition of MFC not only makes it possible to handle the composite product without adding a plasticizer, it also decreases the moisture diffusivity and uptake of the matrix.[47] MFC reinforcement is believed to act as an indirect plasticizer for the neat matrix. This hypothesis is also supported by the great level of dispersion of the reinforcement in the matrix revealed by microscopy techniques. This technique revealed a layered nanocomposite structure and good filler dispersion.

Poly(ethylene oxide) (PEO) is a highly biocompatible, biodegradable, hydrophilic and flexible polymer,[161,315] with a great potential as cellulose-based nanocomposite matrix and as a surface modifier of the fibrils. The ether oxygen of the PEO has the potential to connect to the cellulose hydroxyl groups and even form hydrogen bonds, a condition that can even alter the crystallinity of the native cellulose. This alteration of crystallinity results in the fine-tuning of their physical, thermal and mechanical properties.[161]

Chitosan is a natural polymer produced from the partial de-acetylation of chitin. It is a polysaccharide composed of glucosamine and N-acetyl glucosamine.[316] Its hydrophilicity makes it possible to dissolve it in water, mix it with MFC, and solution-cast the suspension into composite films.[48,317,318] Biodegradable chitosan-reinforced MFC (up to 40 wt.% chitosan in MFC) composite films with high oxygen-gas barrier capacity, hydrophilicity and insolubility in water,[319,320] and a maximum wet strength of 60 MPa at 10-20 wt.% chitosan to cellulose were produced. The dry tensile strength of the same sample was 100 MPa. When chitosan is not used as filler, but as a matrix, as in the case of flexible acetic-acid-protonated chitosan (chitosan A), the main advantage of the addition of the MFC is to increase the deformability of the material in the wet state.[321] Protonated chitosan (chitosan A) can be formed in various shapes in its wet state at room temperature and acquire rigidity during drying.

Water-plasticized films possess very low strength, thus shaping cannot be achieved by the application of large strain to the net material.[48] Deformability of chitosan-acetic-acid-salt films was improved by the addition of 5 wt.% of MFC. SEM analysis of the nanocomposites suggested that cellulose fibrils were evenly distributed in the matrix. MFC fibrils restrict the chitosan film deformation associated with moisture. The composite wet strength increases from 12 to 25 % compared to the neat matrix, and the wet modulus increases from 0.4 to 3 % compared to the pure chitosan (A) films.[48]

2.9.2 Microfibrillated cellulose in hydrophobic polymers

Industrial production of nanocomposites with superior performance based on cellulose nanofillers and polyolefins have been the target of much recent research.[63–66] Polyolefins are easily processable, having low melting temperatures and viscosities appropriate for most industrial applications. The products obtained from polyolefins are durable and chemically stable. Furthermore, polyolefins represent a massive portion of the polymers market and have a well-consolidated infrastructure network, from synthesis to the final product.

MFC-reinforced polyolefin is, consequently, an important target to achieve to enter a larger portion of the market. As stated above, MFC represents a sustainable and renewable filler that has the potential to replace inorganic nanofillers (*e.g.* clay, glass fibres, talc) currently used in polyolefin nanocomposite production.[65] Unfortunately, MFC is not as cheap as inorganic fillers, therefore its use as a thermoplastic reinforcement must provide important improvements to the net matrix to be economically and industrially advantageous.

The filler aggregation is less relevant in composites reinforced with macroscopic cellulose fibres than in those reinforced with MFC. Composites reinforced with cellulose fibres at up to 5 wt.% were produced by melt-mixing followed by compression moulding into PE and PP matrices.[180,182] These and a few more studies on the reinforcement of polyolefins with cellulosic fibres can be easily transposed on MFC giving an ideal starting point for the production of MFC reinforced polyolefins.

Despite their potential, to date an efficient, industrially facile, environmentally friendly and scalable methodology for the production of nanocellulose-reinforced polyolefins using conventional thermoplastics equipment is not available, despite the significant amount of research on this topic.

Research into the production of nanocellulose-reinforced polyolefins has concentrated mostly on the use of TEMPO-oxidized nanofibers, cellulose nanowhiskers, and BC,[65,66] due to the less complex morphology and better characterisation of those cellulose fillers compared with mechanically-produced MFC. Little research effort has been reserved for the production of MFC-reinforced polyolefins nanocomposites.[63,64]

The aim of the research work described in this thesis is to develop a facile method to produce MFC-reinforced composites industrially based on polyolefinic matrices, using typical equipment for processing thermoplastics.

Even though the main focus of the present work is polyolefinic matrices, it is worthwhile mentioning some industrially relevant thermoplastics such as polylactide and poly(ε-caprolactone). Polylactide (PLA) is a relevant matrix as it is produced from 100 % renewable resources and presents useful physical and mechanical characteristics[322] similar to those of fossil fuel-based plastics.[323,324] PLA is, however, brittle,[325–327] has low thermal stability,[328] a relatively high price[329] and poor water vapour barrier properties.[330–332] All these negative characteristics prevent it from substituting polyolefins in most base applications. Reinforcement of PLA with a nanocellulose filler is considered to be a promising method to improve its thermal, mechanical, and barrier properties.[299,306,333,334] MFC has been dispersed in a water-based emulsion of PLA, using a customised twin-screw mixer. The resulting dry mixture has been hot pressed at 190 °C, and the resulting nanocomposite showed a uniform filler dispersion, as proven by microscopy analysis. Fabrication of MFC/PLA nanocomposites based on a papermaking-like process is also reported in the literature and has good industrially practical applications. In this procedure, the PLA is mixed with an MFC slurry, and an aqueous emulsion is obtained and passed through a metal sieve. The obtained MFC/PLA sheets were dried at 105 °C and, subsequently, eight layers were sandwiched and hot pressed,[266] producing composites with enhanced mechanical performance compared to the neat matrix. PLA and PHB based cellulose nanocomposites obtained from the addition of 5 wt.% of chemically modified cellulose fibrils were prepared by melt blending and injection moulding.[182] TEM analysis revealed major agglomerates and poor fibril dispersion in the nanocomposites, which strongly affected the mechanical properties of the composites. Poly(ε-caprolactone) (PCL) is an oil-derived, biodegradable and semi-crystalline polyester presenting good water, oil, solvent, and chlorine resistance, a low melting point, low viscosity, and easy processability through conventional melt blending technologies.[335,336] PCL has low tensile strength (23 MPa) but an extremely high elongation at break (700 %),[337] which makes it a suitable matrix for the

production of MFC-reinforced thermoplastics. Polymer grafting on the surface of MFC fibrils is reported as a promising route in the production of well dispersed MFC-reinforced PCL based nanocomposites. PCL reinforced PCL-grafted MFC composites were produced by alternating layers of PCL and PCL-grafted-MFC and hot-pressing them together. The final product is a laminate structure with improved interfacial adhesion, compared to the laminates obtained with non-grafted MFC films.[1] In fact, PCL-grafted-MFC reinforced PCL composites had a higher modulus and lower elongation at break, compared to the neat PLC matrix.[338] N-octadecyl isocyanate proved to be an excellent grafting agent for cellulose nanofillers and an excellent compatibilizer for PCL matrix.

2.10 Theoretical evaluation of microfibrillated cellulose reinforcement potential.

Classical short-fibre models fail to explain the unusually high reinforcing effect observed in cellulose-reinforced nanocomposites. This has driven research on the development of more accurate models that can predict and explain the nanocellulose reinforced composites extreme mechanical properties.[339] Classical modelling also fails to explain the tensile properties of cellulose networks because, as mentioned in **Section 2.7**, while the modulus and the geometry of the fibrils are taken into account, the interaction and stress transfer within the network are not.[340] More holistic modelling for composites takes into consideration the strong interactions between fibrils and the formation of a percolation interconnected network of the filler which efficiently transfers the stress to the filler network. The formation of a continuous cellulosic network happens when the percolation threshold is reached. The percolated network is probably responsible for the unusually high mechanical performance of nanocellulose reinforced composites. The stiffness and strength of the cellulosic network are due to the strong interactions that interconnect the cellulose fibrils.[339] Using the classical series-parallel model,[23,341] combined with the percolation theory, the mechanical behaviour of cellulose nanocomposites has become better understood and more reliable models have been developed. To fully understand the properties of the cellulose-based reinforcement composites produced in this research work, two approaches can be used: in the first one, the reinforcement effect is attributed to the presence of rigid inclusions in a soft matrix. This approach only accounts for the increased stiffness of the composites, which, according to this model, also became more brittle, showing decreased impact properties at increasing filler contents. This approach is a simplified vision of the filler and matrix as it does not account for any filler/filler or filler/matrix

interactions,[340] but takes into account the filler particle anisotropy and its effect as a stress concentrator in the matrix. In the case of unevenly dispersed composites, or in the case of poor interaction between the filler and the matrix and filler agglomeration, this model can give a good enough approximation of the mechanical properties of the final product.[342] The second approach takes into consideration the filler/filler interactions and the effect of the development of a percolated network.[339] Percolation is a statistical concept that can be applied to any system involving a great number of species likely to be interconnected. The interactions among the fibrils in a cellulose network, for example, induce the so-called mechanical percolation phenomena in which the interconnected fibrils have a synergistic effect with one another.
The mechanical properties of such systems are efficiently predicted by the method of Ouali.[342] The concept of percolation is used and implemented in Takayanagi's classical series-parallel model,[343] which also accounts for the impressive mechanical properties of the nanocellulose reinforced composites, when a percolation threshold is reached and surpassed. Typical reinforcement loadings to obtain the development of a percolation network are between the 15-25 wt.% for tunicin reinforced plasticised starch composites.[344] The percolation threshold was proven to be dependent on the aspect ratio and the orientation distribution of the filler particles. Owing to the complexity of such a theory, the modelling and the theoretical prediction of the model will not be investigated further in this thesis. Furthermore, such a model is applicable when the filler is evenly dispersed in the matrix and can develop an interconnected filler network.

For a non-percolated network, the potential of MFC as reinforcement in a matrix can be evaluated using a basic 'Rule of Mixtures' model, expressed by the equation

$$E_{\text{composite}} = \eta_0 \eta_1 E_{\text{fibril}} V_{\text{fibril}} + (1 - V_{\text{fibril}}) E_{\text{matrix}} \quad \textbf{(3)}$$

where $E_{\text{composite}}$ is the modulus of the composite, V_f is the volume fraction of the fibres (or fibrils) in the composite and E_{matrix} is the modulus of the matrix; η_l and η_0 are the fibre length and orientation efficiency factors: η_l is equal to 1 for long fibres, and η_0 is equal to 3/8 for an in-plane random orientated system. The mechanical properties of a single cellulose fibril can be evaluated using the Cox equation for an in-plane random percolated network of fibres. The measurement of the mechanical properties for the in-plane random percolated network of fibres is obtained from a cellulose film in which the fibrils are assumed to be strongly bonded together, so deformation of the network is attributed entirely to stretching of the fibres and not

bond slippage or breakage. The modulus for a single cellulose fibre or fibril is calculated using the equation

$$\mathrm{E_{fibril}} = \frac{8}{3} \times \mathrm{E_{MFC\ network}} \quad \textbf{(4)}$$

The impact properties of the composite can be evaluated using the Jäger-Fratzl model combined with the Griffith equation.[345] According to this model, the reinforcement carries the tensile load while the matrix transfers the load between the reinforcement particles.[346]

To ensure the integrity of the composite structure, the reinforcement should be able to withstand large tensile stresses without fracture, while the matrix bares large shear stress without failure.

The filler particles are treated as a brittle inclusion in a soft matrix. The fracture resistance of the reinforcement particle is influenced by the flaw size according to the Griffith criterion

$$\sigma_r^f = \alpha E_r \Psi \quad \textbf{(5)}$$

$$\Psi = \sqrt{\frac{\gamma}{E_r h}} \quad \textbf{(6)}$$

where σ_r^f is fracture strength of the filler, E_r is the theoretical modulus of a reinforcing particle, γ is the surface energy and h is the thickness of the reinforcement. The parameter α depends on the crack geometry and can be considered approximately equal to $\sqrt{\pi}$.

Below a defined reinforcement thickness (h^*) the fracture strength of a cracked reinforcement particle becomes identical to the one of a flawless structure.[346] It is possible the estimate of the critical aggregate length scale as

$$h^* \approx \alpha^2 \frac{\gamma E_r}{\sigma_{th}^2} \quad \textbf{(7)}$$

where σ_{th} represents the theoretical tensile strength of cellulose fibrils.

Having discussed the main characteristics of the main cellulose-based filler reinforcement forms, and their theoretical filler potential in the present chapter, it is natural to introduce the chemical properties of cellulose fibrils and the main surface compatibilization strategies currently used, alongside same of the more exotic ones in the next chapter.

This page is left intentionally blank

3. Microfibrillated cellulose surface modification

In the following chapter the most relevant solvent-based and water-based chemical surface modification of cellulose fibrils are presented and critically evaluated. The final part of the chapter is dedicated to the description of the chemical route used at FiberLean technologies to prepare the compatibilism MFC fillers used in the present study.

The reinforcement effect in composites relies on two important parameters: the uniform dispersion of the filler in the matrix and the compatibility of the composite components, characteristics that both enable efficient stress transfer between the matrix and a reinforcement. Natural cellulose fibrils are mainly hydrophilic, and are therefore incompatible with apolar, hydrophobic polyolefins. As with any cellulose-based nanofiller, MFC in a water environment exposes the cellulose hydroxyl groups on its surface. When water is removed cellulose fibrils undergo an irreversible process called "hornification". The aggregates formed *via* hornification are stable and difficult to re-disperse in water or polar solvents, even under extreme mechanical mixing, and essentially impossible to disperse in any other solvents. Nanocellulose aggregation is caused by the substitution of a polar environment (*e.g.* water) by a less suitable apolar environment (*e.g.* air or apolar polyolefin matrices). When cellulose is removed from its polar environment, a more energetic surface is created such as the cellulose/polyolefin one. This interface has higher energy than a cellulose/cellulose one because the apolar nature of the polyolefin is less able to accommodate the polar hydroxyl groups of cellulose. These groups prefer to interact with homologous hydroxyl groups on adjacent cellulose chains in order to minimize the surface exposed to the unfavourable apolar environment and consequently form cellulose aggregates. MFC nanoscale cellulose structures, with highly developed specific surface (S), possess an increased thermodynamic potential (G).

To achieve a stable state, nano-objects dispersed in incompatible phases must decrease their specific energy as indicated by the equation:

$$\Delta G = \sigma A - T\Delta S < 0 \quad \textbf{(8)}$$

where ΔG is Gibbs' Free Energy, σ is the change in specific surface energy that occurs when a particle is wetted by the matrix, A is the surface area of the particles and ΔS is the change in entropy associated with dispersing the particles in the matrix. The first term of the equation (σA) is positive when unmodified MFC is dispersed in an incompatible phase -such as apolar thermoplastic- because of the poor capability of polyolefins to accommodate the cellulose

hydroxyl groups, which cause the cellulose/polymer interphase energy to assume higher values. The second term of the equation ($T\Delta S$) is only relevant if the particles are free to aggregate or disperse under thermal motion.[89]

In order to decrease its thermodynamic potential, MFC tends to form larger structures *via* aggregation and agglomeration, if the nanophase possesses adequate mobility.[89]

Considering the characteristics of the system under analysis, only two approaches are possible to produce dispersed MFC reinforced polyolefin-based composites: the first involves the physical prevention of aggregation of the cellulose fibrils. This can be obtained using physical production methods such as freeze-drying. Unfortunately, this method does not enhance the cellulose/polymer compatibility, leaving a weak interface between the filler and the matrix, which results in a poor matrix-filler stress transfer and in poorly performing composites. It also do not prevent agglomeration of the fibrils during compounding, although this is much less likely to occur than it is during drying from water. The second method is the core of this research project and is based on the surface modification of the cellulose fibrils. The concept is to modify MFC surfaces to prevent the hornification of cellulose fibrils, and to decrease the surface energy of the fibrils to a level comparable with the matrix surface energy, in order to obtain a type of cellulose fibrils which can efficiently interact with apolar polyolefins.[79,87,88] This should also improve interfacial adhesion and stress transfer between the matrix and the filler, while preserving the original networked morphology of the MFC.[100] Surface modification of MFC can be achieved by optimizing the general surface modification procedure developed for cellulose macro and micro fillers such as cellulose fibres and cellulose nanocrystals, nanowhiskers or bacterial cellulose. A variety of physical and chemical cellulose filler surface modification methods are available in the literature[79,88] including corona or plasma discharges[93] surface derivatization,[94] graft copolymerization,[95] and applications of surfactants.[96,97]

Among the various available surface modification methods, chemical functionalization is one of the most promising for industrial applications. Chemical surface modification of cellulose fibrils can achieve full compatibilization of MFC with polyolefins while preserving MFC original morphology, thus avoiding polymorphic conversion.[100] A short review of the chemical surface modification methods applied to cellulose nanomaterials, with special attention to industrially suitable methods is now presented in **Section 3.1**.

3.1 General reactivity of cellulose macromolecules: a review of the literature

Cellulose surface chemistry is based on the reactivity of the hydroxyl groups pendant from cellulose macromolecules (**Figure 3.1**). Cellulose is a condensed form of β-1,4-anhydro-D-glucopyranose units. Each glucopyranose ring in the macromolecule exposes three hydroxyl groups which are all able to form hydrogen bonds.[118] Some potential functionalisation reactions of cellulose are displayed below. The most relevant chemical reactions of cellulose are reviewed in the following paragraphs.

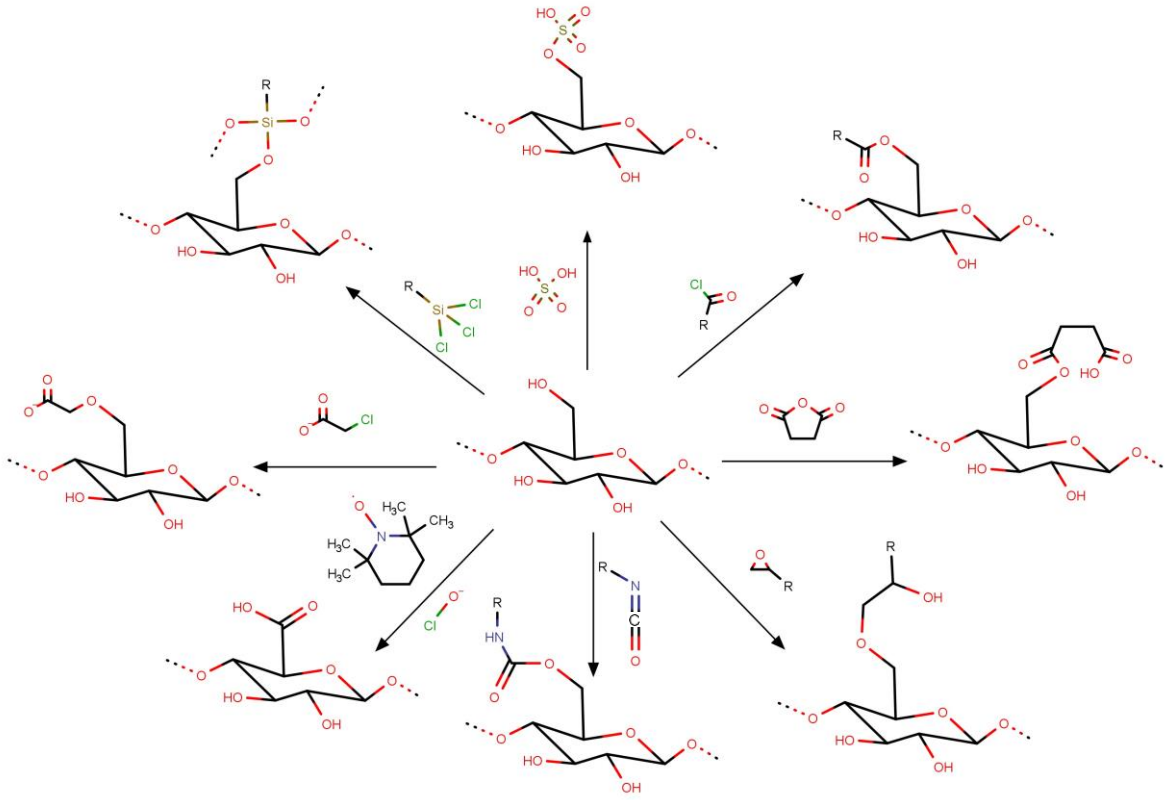

Figure 3.1 Surface chemical modification of MFC: (clockwise from top-right) sulfuric acid treatment provides sulfate esters, carboxylic acid halides and acid anhydrides create ester linkages, epoxides create ether linkages, isocyanates create urethane linkages, TEMPO mediated hypochlorite oxidation creates carboxylic acids, halogenated acetic acids create carboxymethyl surfaces, and chlorosilanes create an oligomeric silylated layer.

Acylation is a well-known and commonly-used cellulose chemical modification. Acetylation reactions involve the substitution of the cellulose hydroxyl groups with less hydrophilic acetyl groups; from this point reactions with various type of anhydrides and fatty acids are undertaken.[347–349] Acylation is a well-established procedure in papermaking sizing: alkenylsuccinic anhydrides (ASA), acetic anhydride (AA)[350] and stearic acid, are all hydrophobic coupling agents used in papermaking. More recently they have been used as compatibilizers in the production of polyolefin-cellulose reinforced composites.[351] Acetylated cellulose, a subclass of acylated cellulose, is a hydrophobic form of cellulose produced by the "acetic acid process": the cellulose macromolecules are reacted with acetic anhydride in the presence of sulphuric/perchloric acid as a catalyst. The technique represents an efficient cellulose hydrophobisation method and is still in use despite major degradation registered during the reaction, and the hydrolysis of the produced cellulose acetate during the final quenching step with water. Because of these flaws in the process, the acetic acid process is sometimes substituted with an ASA treatment (**Figure 3.2**).

ASA reacted cellulose products have strong water repellency, like the acetylated ones, and the hydrophobicity of the final product can be carefully tuned depending on the ASAs dosage, to achieve the requested hydrophobicity of the final cellulose based product.[352,353] ASA reactions are reported to require aqueous alkaline conditions (pH 8.5-9.0) and an optimum temperature of 23 °C. In the ASA reaction with a cellulose product, the reaction condition is of extreme importance as it takes place in a heterogeneous phase, due to the water insolubility of most ASAs reagents, conditions that require constant vigorous agitation of the reacting suspension to allow good contact between the reacting phases. Cellulose microfibres concentration in the mixture can be increased by up to 65 wt.% without compromising the reaction efficiency, while the required concentration for fibrillated cellulose must be lower due to the issues with viscosity. On the other hand, acylation reagent concentrations can be as low as 5 wt.% with respect to the suspension. The ASA hydrophobic chain length is another important parameter as their alkyl chain length regulates the reagent solubility in the water based reaction media; an increase from 8 (water soluble ASA) to 18 (water insoluble ASA) carbons reduces the reaction efficiency dramatically.[354]

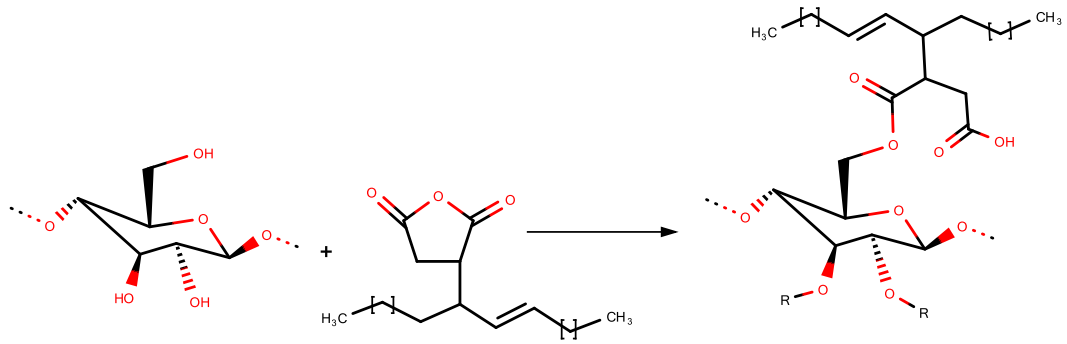

Figure 3.2 General reaction scheme for cellulose acetylation with ASA. The product contains an ester linkage and long alkyl chains.

Cellulose reactions with alkyl ketene dimers (AKDs) have been typically used for sizing in the papermaking industry. Cellulose AKD reactions are heterogeneous reactions as AKDs are solid compatibilizing agents having two long alkyl pendant chains and one hetero four-membered ring. AKD reactions with cellulose are not, strictly speaking, an acylation as they form a β-ketoester bond with cellulose (**Figure 3.3**). The heterogeneous reaction requires, besides vigorous mixing of the phases, a catalytic amount of 1-methylimidazole (MEI). AKD wax does not require dispersion in an organic phase, as the reaction is more efficient than ASAs towards cellulose. The reaction can be thus conducted without the use of organic solvents. AKD treated cellulose has thermoplastic properties and can be converted into transparent films by hot pressing at 160-180 °C.[355] The long alkyl chains introduced onto cellulose fibrils increases the product's solubility in organic solvents and its compatibility with apolar polymers.[356,357] Depside both ASAs and ADK are used industrially they usually react slowly and after drying, condition unsuitable for the production of hydrophobic powder form of MFC to be used as polymer filler.

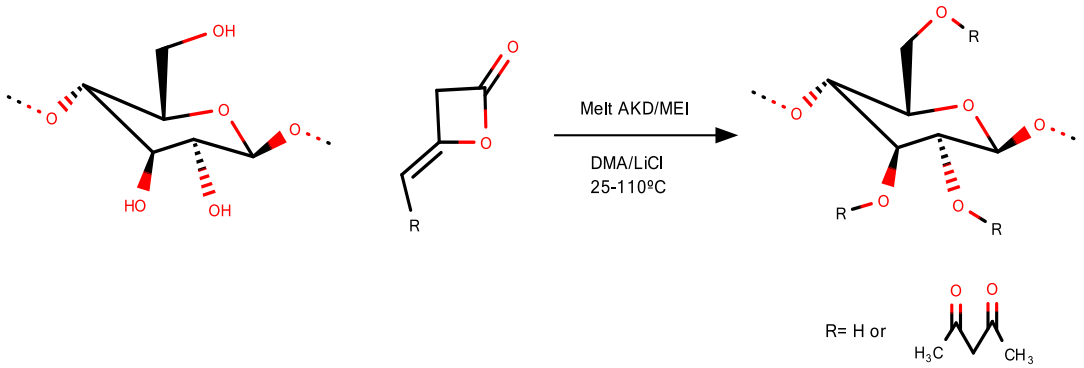

Figure 3.3 A general reaction scheme for cellulose acetylation with AKD in the presence of MEI. The product contains a β-ketoester linkage.[358]

Silane-coupling is another commonly-used method in the production of hydrophobic cellulose. Organosilane reagents are sensitive to water and moisture; in fact, they easily undergo hydrolysis in the presence of water.[293] Hydrolysed, or activated organosilanes can react through a condensation reaction with cellulose hydroxyl groups forming polysiloxanes on the cellulose polymeric backbone (**Figure 3.4**).[359–361] Organosilanes bear different types of hydrophobic hydrocarbon chains which are efficiently introduced on the cellulose surface, restraining cellulose hydrophilicity, agglomeration and swelling tendency, and forming a hydrophobic cellulose based product. Commonly used silylating agents are alkyldimethylchlorosilanes, whose alkyl chains lengths vary from isopropyl (C_3) to n-octyl (C_8), and dodecyl (C_{18}). The sylilation reaction requires organic solvent media as the sylanes are extremely reactive toward water and thus unsuitable in water environment. Efficient hydrophobisation of cellulose products is obtained for a degree of substitution (DS) of the cellulose hydroxyl groups between 0.6 and 1, a condition under which the native cellulose also retains its initial morphology. At a DS greater than 1, cellulose fibrils' core chains silylate, resulting in the disintegration of the original fibril structure.[100]

As already mentioned, organosilanes are extremely sensitive to moisture which cause hydrolysis and condensation. For that reason, the vast majority of silylation is based on organic solvent media such as THF and other low polarity solvents. Examples of water/alcohol base silylation reactions are reported in the literature.[362,363] Regardless of the potential of this approach, a more sustainable method has been adopted in the present study.

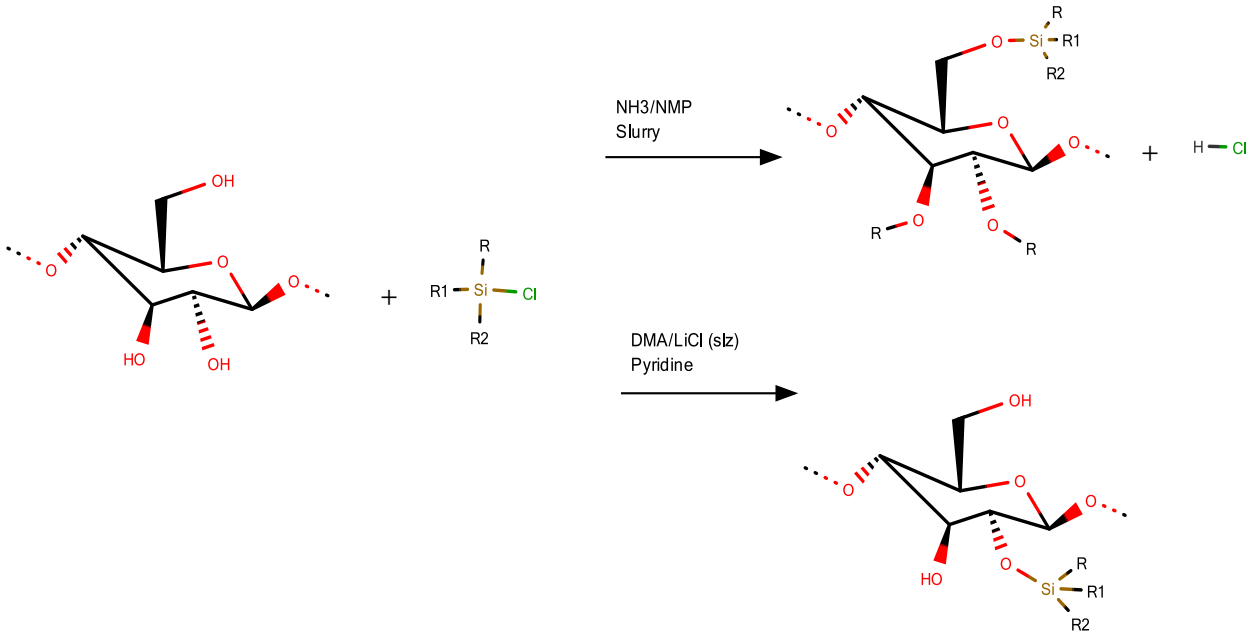

Figure 3.4 General reaction scheme for cellulose silylation with an alkylsilane. Two different solvents are used: NH_3 and DMA/LiCl.

Polymer grafting represents a convenient method to attach hydrophobic groups to cellulose macromolecules. Based on the general grafting technique used to grow polymer chains directly on the surface of organic and inorganic supports, the reaction with nanocellulose can be performed using two different approaches the "*grafting-onto*" and "*grafting-from*". *Grafting onto* method involves the substitution of hydroxyl groups with pre-synthesized polymer chains, while the *grafting from* procedure involves the *in-situ* polymerisation directly on the cellulose surface using polymerisation initiators immobilized on the surface.[100]

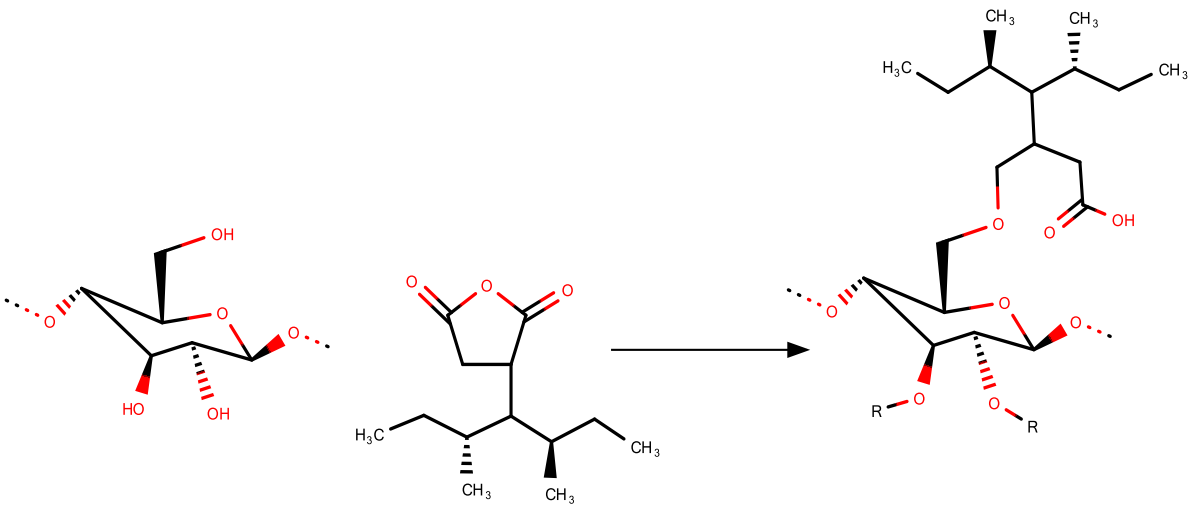

Figure 3.5 General reaction scheme for cellulose acetylation with MAgPP.

The grafting onto procedure is based on the reaction with maleated polypropylene (MAgPP) as grafting agent (**Figure 3.5**).[364] MAgPP modified nanocellulose products present good compatibility and high adhesion with an atactic polypropylene matrix. The grafting from approach is still mainly a research concept and makes use of polycaprolactone (PCL) as a grafting agent and monomeric unit for the development of polymeric chains directly from the cellulose surface. The PCL polymerisation mechanism involves the ring-opening polymerization (ROP) of the monomeric units catalysed by tin(II) 2-ethylhexanoate ($Sn(Oct)_2$).[151] Both grafting onto and from methods are based on organic solvent suspensions and require either nanocellulose in a dry dispersible form or a series of solvent swap steps to suspend cellulose nanomaterials in an appropriate organic solvent.

Water/oil interface nanocellulose surface reactions are possible and are mainly represented by functionalization with epoxy groups catalysed by cerium (IV) followed by grafting with glycidylmethacrylate, and grafting of hexamethylene diisocyanate on cellulose fibrils followed by reaction with amines (**Figure 3.6**).[1] These heterogeneous methodologies are separately analysed below.

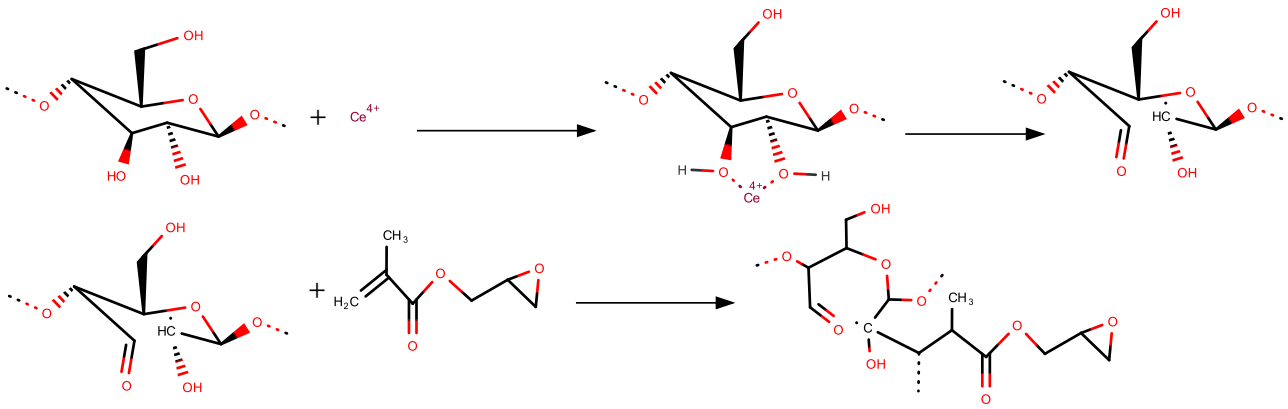

Figure 3.6: General reaction scheme for oxidation of 1,2-glycol groups followed by grafting of glycidyl methacrylate.

Cerium(IV) ions are powerful oxidation agents for 1,2-glycol group polyalcohols. Cerium reaction mechanisms involve the formation of a chelate complex with cellulose hydroxyls which result in the development of radicals on the cellulose backbone. The radicals produced on the cellulose surface react in the presence of glycidylmethacrylate (GMA) monomers attaching the GMA units *via* radical polymerisation to the surface. Crystalline and amorphous cellulose regions have different reactivity towards Cerium(IV) ions; the amorphous regions are more keen to produce complexes with the ions also because of their increased accessibility.[365] Cellulose surface reactions with Cerium(IV) ions retain the cellulose native morphology as

well as their mechanical properties and water dispersibility because only a small amount of the glucose rings is reacted. Cerium(IV) ion surface reactions efficiently introduce a layer of medium hydrophobic polymers on the surface of cellulose which can either be used directly or can be further reacted to increase the hydrophilicity of the final product to meet special requirements. Cerium(IV) surface reactions are conducted in aqueous media, avoiding solvent exchange, and thus present the potential for industrial scalability.[5]

Another example of an efficient heterogeneous cellulose surface reaction is represented by di-isocyanate grafting. Di-isocyanate groups can react readily with cellulose hydroxyl groups forming urethane bonds under strictly water-free conditions. As in the case of organosilane, water and moisture exposure cause hydrolysis of the di-isocyanate reagent. As a final result of the reaction between the di-isocyanate group and the hydroxyls, an amino group is introduced onto the cellulose fibrils,[366] which can be confirmed by FTIR spectroscopy. Di-isocyanate grafting reactions are strictly restricted to anhydrous apolar solvents which limit their industrial application. Nevertheless, the reaction is an extremely efficient hydrophobisation method as the final product is hydrophobic. That combined with the necessary solvent exchange procedure prior to reaction, which leaves the amorphous areas of the fibrils more accessible to derivatization, leads to partial detachment of the cellulose fibrils from the native structure allowing them to migrate in the reaction medium. This causes a partial loss of the initial microfibrillar structure[24,150,367] with important consequences on the mechanical properties of the product obtained; cellulose nanofillers coated with a highly hydrophobic isocyanate layer have been used in polymer nanocomposites.[368]

3.1.1 TEMPO-oxidation in nanocellulose chemical surface reactions

TEMPO-mediated oxidation can be considered as a pre-treatment and a production method for nanocellulose-based products. In the TEMPO-oxidation reaction the hydroxylmethyl groups on cellulose surface, *i.e.* the cellulose hydroxyl groups attached to the C6, are converted into their carboxylic form by oxidation with (2,2,6,6-tetramethylpiperidine-1-oxyl) (TEMPO) mediated reagent. The reaction is highly selective for primary hydroxyl groups. The reaction mechanism involves the formation of a stable nitroxyl radical produced by TEMPO in the presence of NaBr and NaOCl. TEMPO-mediated oxidation is topologically confined by the morphology of cellulose chains: only half of the accessible hydroxymethyl groups can react, whereas the rest of them are bent within the crystalline structure. After TEMPO-mediated oxidation, the fibrils maintain their native morphology and form a homogeneous suspension in water.[369] TEMPO-mediated oxidation is an intermediate step to promote grafting of polymeric chains which can be efficiently and more easily reacted with the more reactive carboxylic groups generated with TEMPO oxidation.

3.2- FiberLean™ surface reactions: the production of functionalised MFC for composites

The final objective of this research work is to obtain FiberLean™ MFC reinforced polyolefin composites using typical thermoplastic processing equipment. To achieve this ambitious objective, it is necessary first to identify a cellulose surface chemical modification reaction able to prevent the aggregation of cellulose fibrils and promote a uniform filler dispersion during the processing of the composites.

Furthermore, the selected cellulose surface modification method should be easily implementable in an industrial setting, and in general and should possess sustainable characteristics, which strongly limit the use of organic solvents as reaction media for the production of hydrophobic forms of MFC. The hydrophobic MFC product obtained must also be thermally stable up to polyolefin processing temperatures (≈200 °C) and should preserve the MFC network structure in order to fully exploit its potential as a composite reinforcement. Among the cellulose surface reactions reported in the literature, a few are selected and applied to FiberLean™. The surface reactions were divided into organic solvent-based and water-based ones and are separately presented in the following paragraphs.

3.2.1 Surface modification of FiberLean™ in organic solvents

Among the possible organic solvent compatibilization routes, esterification reactions with maleic anhydride-grafted-polypropylene (MAgPP) and esterification reactions with myristoyl chloride ($C_{14}H_{27}OCl$) were used in this research work. Esterification reaction mechanism is based on the substitution of the cellulose hydroxyl groups, responsible for the cellulose fibrils hydrophilicity, with more hydrophobic ester groups.[350,370–372] Anhydride esterification, a type of reaction that refers to the use of anhydrides to substitute cellulose hydroxyl groups, is currently considered the effective method for the surface modification of nanocellulose to be used as reinforcement in apolar thermoplastics,[373–376] and is used in this study as a reference. The general reaction mechanism for the esterification of cellulose fibrils with MAgPP is shown in **Figure 3.7**.

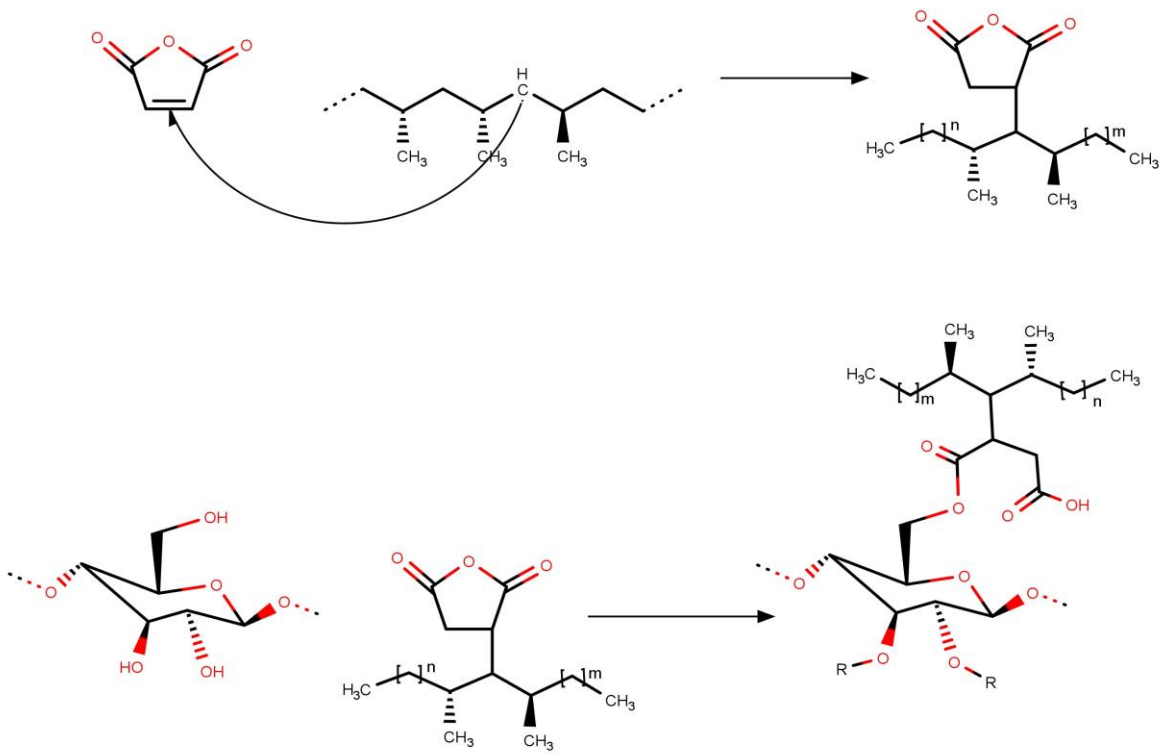

Figure 3.7 Preparation of MAgPP from MA monomers and PP chains showing the radical scheme (top), and esterification reaction scheme of the MAgPP with the cellulose (bottom).

Organic cellulose esters (CEs) are industrially produced[377] in the fibres sector because of the superior properties and processability of the final products.[378,379] The final product of the esterification reactions is an acylated form of cellulose, but the reagents used are alkyl halide rather than anhydrides. Cellulose esterification with linear saturated acyl substituents requires the addition of pyridine as an activator.[380] The esterification of fibrillated cellulose with myristoyl chloride requires the dispersion of cellulose fibrils in toluene[381] to prevent their chemical degradation *via* dispersion in a diluted acid solution.[380]

The cellulose esterification reaction mechanism is shown in **Figure 3.8**.

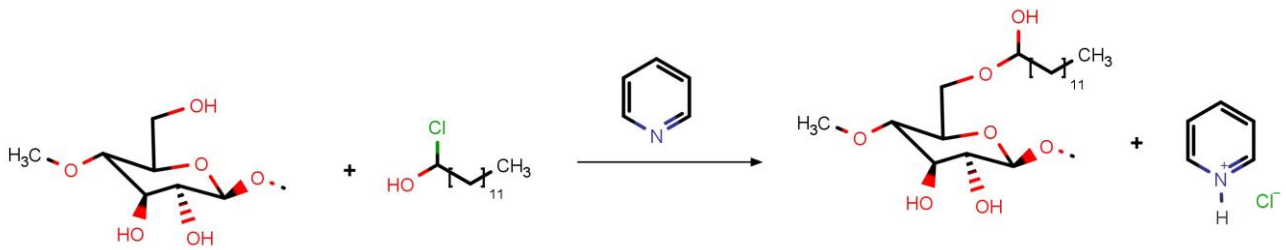

Figure 3.8 Esterification reaction of myristoyl chloride with cellulose, promoted by pyridine.

The esterification reactions require cellulose fibrils to be suspended in a solvent of an apolar nature. In this study the selected solvent was toluene. In order to achieve a good suspension of cellulose fibrils in toluene a series of solvent exchanges in solvents of increased apolarity is applied to the MFC water-based slurry. The solvent exchange procedure is called a 'solvent swap' and is further explained in the next chapter.

3.2.2 Surface modification of FiberLean™ in water

Water based methods were tested in this study to limit the use of the organic solvents during MFC surface reactions, and to develop a sustainable compatibilization method. The water-based methods made use of two different approaches; the first one made use of the steric stabilizing effect of biodegradable and biocompatible polymers such as poly(vinyl alcohol) (PVOH) and poly(ethylene oxide) (PEO) on cellulose nanosuspensions (**Figure 3.9**).[41,369,382]

Poly(vinyl alcohol) (PVOH) is a thermoplastic, biocompatible, and biodegradable carbon-carbon single bond backbone polymer.[383] PVOH is strongly hydrophilic and soluble in water.[383] The hydroxyl groups of PVOH can develop strong hydrogen bonds and acetal linkages with the hydroxyl groups of cellulose fibrils,[384,385] reducing cellulose microfibril hydrophobicity. It is thought that because of the development of hydrogen bonds between cellulose and PVOH macromolecules, the hydrophobic aliphatic carbon backbone of the PVOH can be exposed to the polyolefin matrix. The development of apolar interactions between the PVOH covered cellulose filler and the matrix is then possible.[41,382]

Figure 3.9 PVOH polymeric structure and the interaction of PVOH hydroxyl groups with cellulose (left). PEO polymer structure and interaction of PEO with cellulose (right).

A similar approach is used in the development of the method based on the use of PEO which is a biodegradable and biocompatible polymer synthesized by suspension polymerization of ethylene oxide in water. In recent years, it was used for the steric stabilization of cellulose microcrystal suspensions in a two-step process[369,381] The method used in this study is based on the stabilisation effect of PEO on cellulose nanocrystal suspensions.[369] As in the case of PVOH, the cellulose-PEO interaction is mediated by the development of a hydrogen bond network.

As a consequence of this, the PEO can mitigate the hydrophilic character of cellulose fibrils and develop hydrophobic interactions with the polyolefin matrix.

The second water-based approach takes inspiration from the protection system developed by higher plants. In this protection system the cellulosic structure is 'protected' by a class of naturally occurring products called polyphenols which mitigate the cellulose's tendency to adsorb humidity.[115,386] Polyphenols are naturally produced in plants for biological, defensive, and structural functions.[386] A representative of the polyphenols family is tannic acid (TA, **Figure 3.10**), which can polymerise on the surface cellulose fibres under alkaline conditions.[387–389]

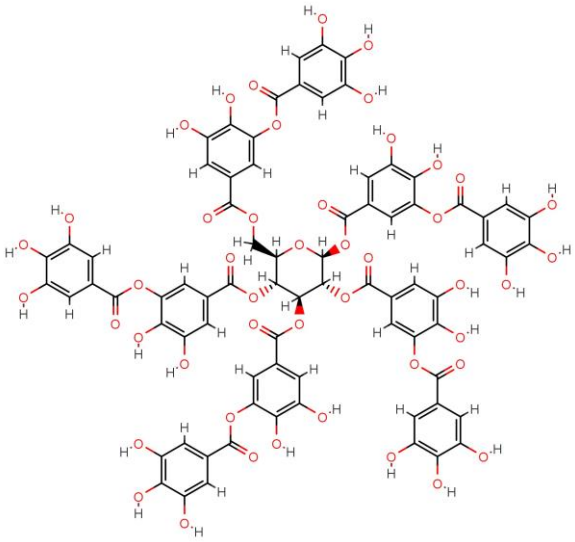

Figure 3.10 Tannic acid chemical structure. ( )

The hydrophilic product obtained derive from the oxidation of TA catechol groups to quinones, able to further react with primary amines[115,386–390] such as the hydrophilic hexylamine ($C_6H_{13}NH_2$) and the hydrophobic octadecylamine ($C_{18}H_{73}NH_2$). The material obtained from the reaction of the TA-activated MFC with the short chain hexylamine and the long chain octadecylamine was filtered and oven dried to obtain a dry material. This dry MFC form obtained by the reaction with the hydrophobic octadecylamine was easy to grind at room temperature to obtain a powder that can be processed alongside polyolefins in an industrial compounder to obtain nanocomposites. The TA-primary amines-based chemistry presents the important advantage of being carried out in an aqueous environment at room temperature and under mild conditions which would favour potential industrial applications.

The tannic acid activated cellulose-amine reaction mechanism is not yet fully clarified.[387,389,391] The supposed mechanism involves the development of a Schiff base and a Michael-type addition. The elucidation of the reaction mechanism is beyond the purpose of this study. Nevertheless, it results in the covalent attachment of primary amines onto the TA activated fibre system (**Figure 3.11**).[386,389]

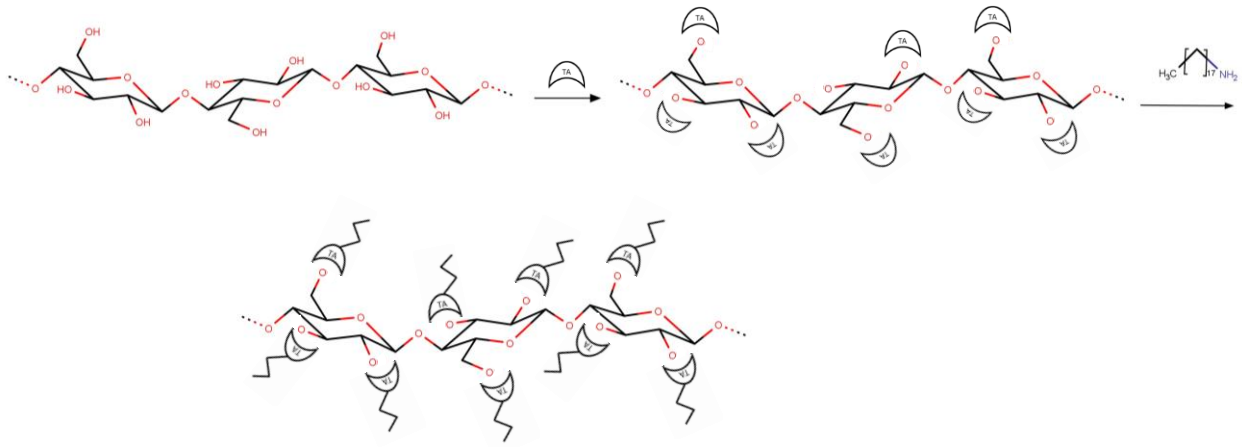

Figure 3.11 Representation of the activation reaction between tannic acid and cellulose hydroxyl groups (top) and between TA-activated MFC and octadecylamine (below).

The present chapter discussed some of the most relevant compatibilization strategies applicable to cellulose based fillers. The next chapter contain an overview pd the surface chemistry used in the present study.

This page is left intentionally blank

4. FiberLean MFC characterisation, surface reaction and preparation of composites

The following chapter introduces the methodologies used to prepare the compatibilized MFC fillers and to characterise the various types of modified and unmodified MFC fillers obtained by chemical surface treatments in both organic solvents and water. This chapter also contains the methodologies used to prepare the MFC-reinforced composites and the techniques used to determine their morphological and thermal properties, alongside the mechanical and impact properties of the reinforced composites.

4.1 FiberLean^{TM} surface modification in organic solvents: materials

An MFC slurry with a water content of 95 wt.% was produced by FiberLean by the mechanical grinding of softwood bleached pine Kraft pulp. A PPPE matrix material (with a melting temperature of 170 °C and average particle size ≈ 350 μm) was purchased from Lyondellbasell. The following chemicals and reagents were purchased from Sigma Aldrich (Dorset, UK): polypropylene-graft-maleic anhydride average (MAgPP) $\overline{M}_w$ ~9,100 by GPC, average $\overline{M}_n$ ~3,900 by GPC, maleic anhydride 8-10 wt.%; acetone ≥99.9 % (ρ = 0.79 g cm^{-3}); myristoyl chloride (MCl) 97 % (ρ = 0.91 g cm^{-3}); anhydrous toluene 99.8 % (ρ = 0.87 g cm^{-3}). Xylene 99% (ρ = 0.88 g cm^{-3}) was supplied by Fisher Scientific (Leicestershire, UK).

4.2 Solvent swap method

MFC slurry (40 g) in water (5 wt.% in cellulose), containing cellulose fibrils (2 g), was solvent exchanged with 100 ml of acetone. The suspension was magnetically stirred for 10 min at 500 rpm and then filtered under vacuum on a glass filter before re-suspending in acetone; this procedure was repeated 3 times. The filtered material was then re-suspended in toluene (100 ml). The washing procedure was repeated 3 times with toluene. The solvent-exchanged material was recovered and further processed.

4.2.1 Anhydride esterification of cellulose microfibrils with maleic anhydride-grafted polypropylene

The solvent-swapped MFC sample (2 g of MFC) was re-suspended in xylene (100 ml) and washed, as previously described, 2 times; the precipitate was filtered and re-suspended in xylene (160 ml) in a round-bottomed, three-necked flask and heated up to 160 °C.

The suspension was kept at 160 °C (boiling point of xylene) and refluxed under magnetic stirring at 500 rpm for 10 min to eliminate residual water. MAgPP (0.2 g) was added through a separate funnel and the system was refluxed under magnetic stirring at 500 rpm for 1 h. The final solid product was filtered on a glass filter with a Venturi vacuum system, weighed and kept in a vacuum oven at 60 °C overnight.

4.2.2 Esterification of cellulose microfibrils with myristoyl chloride

The solvent swapped MFC sample (2 g of MFC) was re-suspended in xylene (100 mL) and washed, as previously described, 2 times; the precipitate was filtered and re-suspended in xylene (160 mL) in a round-bottomed, three-necked flask, heated up to 80 °C and magnetically stirred at 500 rpm for 10 min to eliminate water residues. Myristoyl chloride (2.75 g) and pyridine (2.08 ml) was then added through a separate funnel and the system was kept at 80 °C under magnetic stirring at 500 rpm for 1h. The product suspension was filtered on a glass filter with a Venturi vacuum system. The filtered sample was resuspended in toluene to eliminate reagents excess and filtered again on a glass filter with a Venturi vacuum system. The precipitate was then recovered, weighed and kept in a vacuum oven at 60 °C overnight.

4.3 FiberLean™ surface modification in water: materials

MFC slurry having a water content of 95 wt.% was produced by FiberLean by the mechanical grinding of softwood bleached pine Kraft pulp. The following chemicals and reagents were purchased from Sigma Aldrich (Dorset, UK): Poly (vinyl alcohol) (PVOH) average M_w = 130,000, 99 % hydrolysed; poly(ethylene oxide) (PEO) average M_w = 5,000,000; tannic acid (TA) powder; octadecylamine ($C_{18}H_{37}NH_2$) powder technical grade 90 %; hexylamine ($C_6H_{13}NH_2$) 99 %; HEPES powder >99.5 %; acetone ≥99.9 % (ρ = 0.79 g cm^{-3}); alizarin (dye content 97 %). Sodium hydroxide (reagent grade) was supplied by Fisher Scientific (Leicestershire, UK).

4.3.1 Surface hydrophobization of cellulose microfibrils using polyvinyl alcohol

MFC slurry (5 wt.%, 40 g) was added to distilled water containing(300 mL) pre-dissolved PVOH (1g). The suspension was heated at 80 °C and kept under magnetic stirring at 1000 rpm for 1h. The suspension was left to cool at room temperature, and a portion was frozen in a laboratory freezer at -70°C overnight and then freeze-dried for 24 hours in a Labobanc freeze dryer system. The freeze-dried sample was recovered, weighed and kept in a vacuum oven at 60 °C overnight. The sample was then cooled in liquid nitrogen and ground using a laboratory grinder. Liquid nitrogen was used as cooling agent to refrigerate the PVOH-MFC mixture below its glass transition temperature and provide good quality grinding (particle average size =200 μm). The powder was then kept in a vacuum oven at 60 °C for 24 hours to eliminate the residual humidity. The residual portion of the PVOH-compatibilized MFC slurry not used in the freeze-dry procedure was left to dry in a vacuum oven at 60 °C. The obtained material was ground using liquid nitrogen as a cooling agent, but unfortunately, it was impossible to obtain a powder from the vacuum-dried PVOH-compatibilized MFC samples. The latter observation highlighted the importance of the freeze-drying procedure in producing compatibilized MFC samples that can be used as reinforcements for polyolefins.

4.3.2 Surface hydrophobization of cellulose microfibrils using polyethylene oxide

PEO (2 g) was mixed with distilled water (160 ml) and kept under magnetic stirring at 500 rpm for 24 hours. The suspension was then heated up to 65 °C (PEO melting temperature T_m) and magnetically stirred at 1000 rpm for 2 h to completely dissolve the PEO. When a clear solution was obtained, MFC slurry (5 wt.%, 40 g) was added and the suspension was kept at 65 °C under magnetic stirring at 1000 rpm for 1h.

The suspension was left to cool at room temperature, and a portion was frozen in a laboratory freezer at -70°C overnight and then freeze-dried for 24 hours in a Labobanc freeze dryer system. The freeze-dried sample was recovered, weighed and kept in a vacuum oven at 60 °C overnight. The sample was then cooled in liquid nitrogen and ground using a laboratory grinder. Liquid nitrogen was used as cooling agent to refrigerate the PEO-MFC mixture below its glass transition temperature and provide good quality grinding (particle average size =200 µm). The powder was then kept in a vacuum oven at 60 °C for 24 hours to eliminate the residual humidity. The residual portion of the PEO-compatibilized MFC slurry not used in the freeze-dry procedure was left to dry in a vacuum oven at 60 °C. The obtained material was ground using the liquid nitrogen as a cooling agent, but unfortunately, it was impossible to obtain a powder from the vacuum dried PEO compatibilized MFC samples. The latter observation highlighted the importance of the freeze-drying procedure in producing compatibilized MFC samples that can be used as a reinforcement for polyolefins.

4.3.3 Surface reaction with tannic acid, octadecylamine and hexylamine

MFC slurry (100 g) at 1 wt.% of cellulose was diluted to a final volume of 500 mL with distilled water; HEPES (2.5 g) was added to the suspension and the pH was adjusted to 8 with sodium hydroxide. Tannic acid (TA) (0.5 g) was added to the suspension and kept under magnetic agitation at 500 rpm overnight at room temperature. Octadecylamine (T_m 50 °C) (0.5 g) was suspended in water (50 mL) at 70 °C. The suspension was added to the MFC-TA reacted suspension and kept under magnetic stirring at 200 rpm for 3 h. A fast stirring speed was chosen to ensure the octadecylamine was broken down into small droplets and thoroughly mixed throughout the sample. The product was filtered on a paper filter (Whatman^{TM}541-hardened ashless) under vacuum. The recovered material was resuspended in acetone (100 mL), filtered under vacuum, recovered and kept in a fume cupboard to dry. The dried product was weighed and then passed through a laboratory grinder. The same procedure was followed to produce MFC samples functionalised with hexylamine in place of octadecylamine, replacing octadecylamine (0.5 g, 0.002 mol) with hexylamine (0.2 g, 0.002 mol).

4.3.4 Optimisation of the molar ratio of tannic acid and octadecylamine

In Cranston's original work with tannic acid and nanocellulose,[115] a large excess of primary amine was used to ensure complete coverage of the TA-nanocellulose reactive sites. In a preliminary study, a similar molar ratio of tannic acid to octadecylamine of 1:250 was used after reacting the tannic acid with the MFC. Unfortunately, the large excess of hydrophobic primary amine was difficult to remove by washing because of the characteristic networked structure of the MFC. The presence of large octadecylamine aggregates was confirmed by an optical microscopy investigation of the reacted MFC samples (**Figure 4.1**).

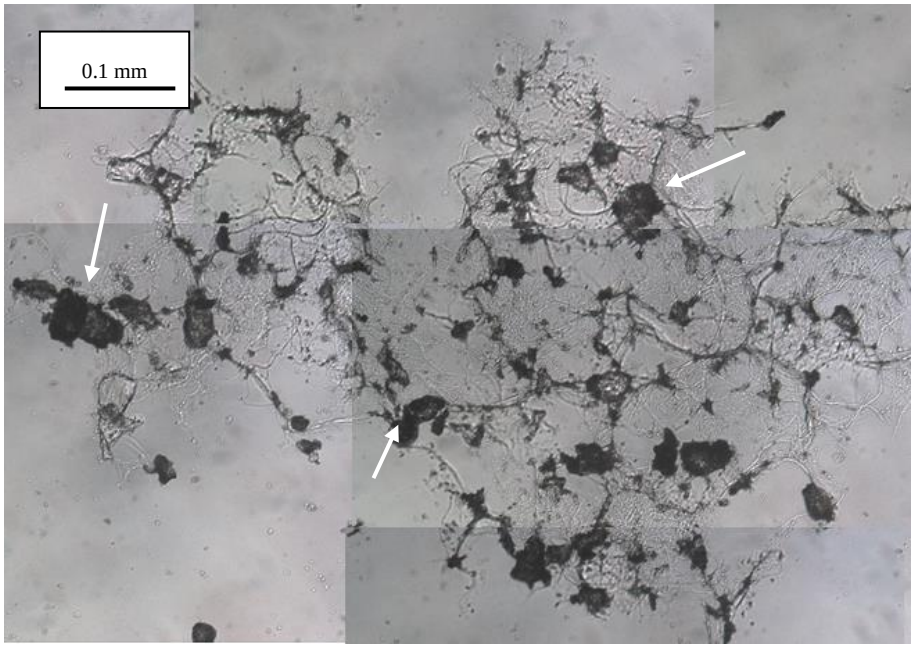

Figure 4.1 Compatibilised FiberLean™ polarized optical microscopy images. Large amine-based aggregates are visible in between the FiberLean™ network (white arrows).

The excess of amine in the filler preparation also compromised the subsequent processing of the filler-polyolefin mixture, decreasing the thermal stability of the filler and of the resultant nanocomposites. To mitigate the problems caused by a large excess of the water-insoluble octadecylamine, its excess after the reaction with TA-MFC was titrated using a spectrophotometric method. The excess amine was washed out of the sample using a large excess of acetone (880 mL), and the collected solution was titrated using alizarin as an indicator.[392] 1 g of cellulose has $\approx 1.53 \times 10^{-5}$ moles of superficial reactive hydroxyl groups.[393] Given this assumption, it is possible to evaluate the molar ratio between MFC-OH and TA (M_w = 1701.20 g mol^{-1}) in the preparation described above. The MFC-OH-TA ratio is 1:2.

Similarly, it is possible to calculate the molar ratio between TA and octadecylamine (M_w = 269.51 g mol^{-1}); this is found to be 1:250. The large excess of octadecylamine can be removed from the final product with repeated washing with acetone. To calibrate the absorbance, alizarin solution (0.4685 mmol dm^{-3}) in acetone (1 mL) was added to a series of standard amine solutions in acetone (0 up to 20 mg ml^{-1}) (2 ml). The absorbances of the reference samples were registered at 529 nm to obtain the calibration curve for the system. The sample containing the excess amine from the amine/TA reaction absorbance was determined after dilution 1:4 using the Beer-Lambert equation:

$$A = (\varepsilon \times b) \times c \quad \textbf{(9)}$$

where A is the sample absorption, ε is the characteristic system extinction coefficient, b is the thickness of the optical path, and c is the concentration of the solution. The total amount of excess amine after reaction with TA/MFC was determined from the concentration of the amine in the test solution. This was then subtracted from the amount of amine added to determine the amount reacted and thus the optimum ratio between TA and octadecylamine.

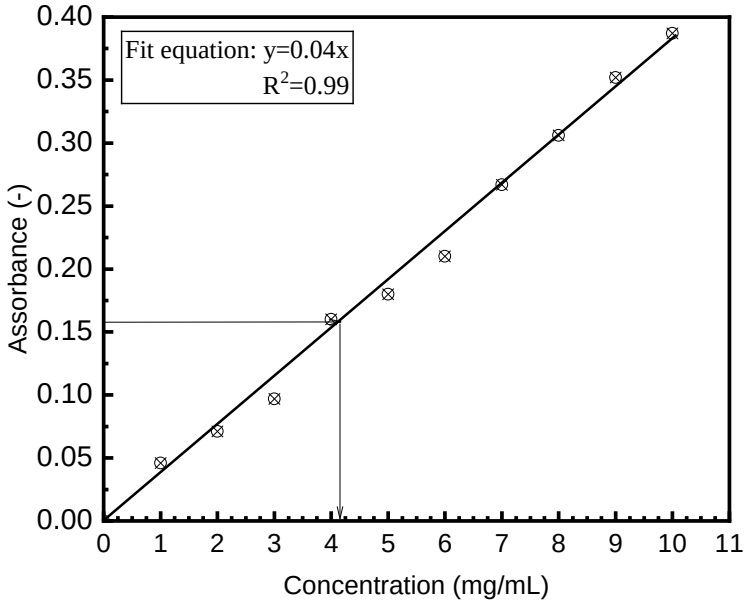

Figure 4.2 Typical calibration curve for the system acetone-alizarin-octadecylamine. The horizontal and vertical lines indicate the A/4 registered for the diluted test solution system and the corresponding c/4 value respectively.

The calibration line determined for the octadecylamine-alizarin-acetone system (**Figure 4.2**) indicates an extinction coefficient (ε) of 0.04 mL mg^{-1} mm^{-1}, and a value of R^2 of 0.99.

The value of the absorbance registered for a 1:4 diluted washing solution was $A_{c/4} = 0.16$. The concentration for the diluted solution was obtained from the Beer-Lambert equation and was found to be equal to c/4 = 4.3 mg mL^{-1}. The concentration of the original solution was thus equal to c = 17.2 mg mL^{-1}. The total volume of washing solution collected is 880 ml, and the weight of octadecylamine in the solution was 15 g. From the difference between the initial amount of octadecylamine added to the reaction (20g) and the excess of amine washed out by the acetone and titrated (15g) it was possible to evaluate the amount of amine reacted with the initial dry MFC (10g) and TA added (5g).

The optimised mass ratio of the system results as following dry MFC (10g):TA (5g):octadecylamine (5g). The optimised ratio proved effective in producing a type of hydrophobic MFC filler with enhanced thermal properties, which is easy to compound with normal polyolefins and able to produce good composite materials. The optimum MFC:TA:octadecylamine ratio determined was used in this research work.

4.5 Size distribution of aqueous MFC suspension

An MFC suspension of 5 wt.% was produced at FiberLean by the mechanical grinding of softwood bleached Kraft pine pulp. The size distribution of the fibres in the slurry is an important marker for the quality of the reinforcement that will be produced by the surface chemical reactions presented in Chapter 3. The particle size distribution of the produced slurry was determined at FiberLean using a static light scattering system (Malvern 2000).

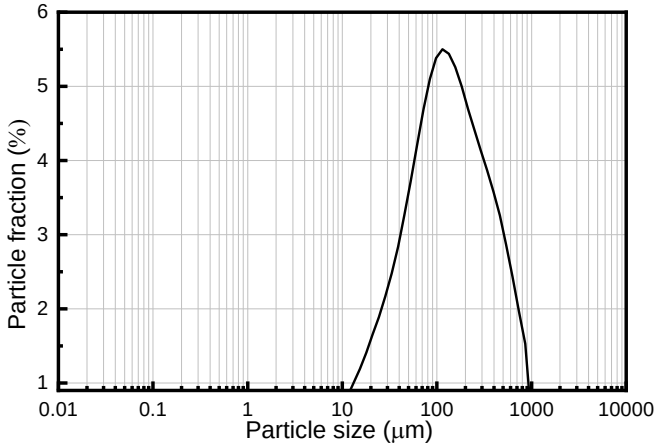

Figure 4.3 Typical particle size distribution for a diluted MFC slurry. Particle size is plotted on a log scale.

The typical particle size distribution for the slurry analysed is reported in **Figure 4.3**. The fibrils' median size is estimated to be ~100 μm.

It is important to note that the Laser Obscuration system does not provide reliable information on the aspect ratio of the cellulose fibrils in the suspension under analysis as the system measures the intensity of scattered light as a function of scattering angle, and then converts this into a size distribution using a theory (Mie) which assumes the particles are spherical. Because fibrils are far from spherical, the calculated size values do not correspond to any particular dimension of the fibrils. Nevertheless, the apparent size decreases with processing energy and so is a useful indicator of the degree of fibrillation achieved.

4.6 Fourier-transform infrared spectroscopy (FTIR) of surface-treated films

FTIR spectroscopy was used to establish the formation of the TA-MFC and TA-cellophane active intermediates and of the MFC/Cellophane-tannic acid-octadecylamine products along with the characteristic spectra of MAgPP reacted Cellophane and MFC films. The characteristic spectra of the reacted films were compared against the pure MAgPP, TA, and octadecylamine spectra. The FTIR spectra of the pure materials and of the reacted films were recorded using a Nicolet iS50 spectrometer using a detector at 4 cm^{-1} resolution and 64 scans per sample. All the reacted samples were washed with acetone before the analysis to remove the unattached amine. The FTIR spectra were collected within a wavenumber range between 4000 and 500 cm^{-1}. The region of interest incorporated peaks in the range between 3000 and 3500 cm^{-1}, characteristic of hydroxyl residues, the characteristic amine region, between 2800 and 3000 cm^{-1}, and the region between 1400 and 1500 cm^{-1} characteristic of compounds containing α,β-unsaturated ketone-groups.

The spectra of the TA reacted cellophane and MFC films were collected every hour during the reaction with octadecylamine, to record the evolution of the ammine characteristic peak (between 2800 and 3000 cm^{-1}) over time.

4.7 Contact angle and free surface energy

Liquid contact angles of pure cellophane and TA-octadecylamine reacted cellophane films were measured using a Fibrodat 68-96 Dynamic Absorption Tester (DAT) (Testing Machines, Inc.). Sheets of MFC for contact angle measurements were made by filtration (using a standard handsheet former), followed by pressing of the filtercake into a sheet and drying according to TAPPI procedure T205. Sheets were made from the unreacted MFC, MFC reacted with tannic acid-hexylamine, and MFC reacted with tannic acid-octadecylamine, and their contact angles were measured using the same DAT instrument. De-ionized water was used as a probe liquid. The free surface energies of the two cellophane films and the three MFC films were evaluated from contact angle measurements, using water and bromonaphthalene (BN) as the polar and apolar probe liquids respectively. To minimize experimental errors, the values were measured at five random locations for each sample, and an average reported. The free surface energy was calculated from the contact angles of the two liquids using the Owens, Wendt, Rabel and Kaelble method[394] according to Equation 10:

$$\sigma_{sl} = \sigma_s + \sigma_l - 2[(\sigma_{sw}\sigma_{lw})^{\frac{1}{2}} + (\sigma_{sd}\sigma_{ld})^{\frac{1}{2}}] \quad \textbf{(10)}$$

combined with Young's equation:

$$\sigma_s = \sigma_{sl} + \sigma_l \cos\theta \quad \textbf{(11)}$$

where σ_{sl} is the solid-liquid interfacial tension, σ_s is the solid-air surface tension, σ_l is the liquid-air surface tension, σ_{sw} is the polar component of the solid-air surface tension, σ_{sw} is the polar component of the liquid-air surface tension, σ_{sd} is the dispersed component of the solid-air surface tension, σ_{ld} is the dispersed component of the liquid-air surface tension, and θ is the measured contact angle. The Owens, Wendt, Rabel and Kaelble method relies on the data collected for at least two liquids, one polar and one apolar. From the two sets of contact angle data it is possible to write a system of two equations which can be solved by the geometrical mean method giving a value for the solid-air surface tension ($\sigma_{s)}$. σ_{sw} and σ_{sw} are known for each liquid, and σ_{sd} and σ_{ld} are the incognita.

4.8 Preparation of the reinforced composites

The reinforced composites were prepared using different manufacturing approaches. A series of small batches were prepared using the Haake MiniLab 3 micro-compounder (Thermo Scientific) equipped with a set of counter-rotating screws. The mini compounder was used to process batches up to 5 g of materials with a filler concentration up to 20 wt.%. The premixed matrix and filler powders were processed for 10 min at 210 °C at a maximum speed of 50 rpm. The composites obtained were recovered for further processing.

To improve the filler dispersion in the composites, a series of batches with a filler concentration of up to 20 wt.% were prepared in a ZSK Mc^{18} counter rotating twin screw extruder (Coperion) with a specific torque of 18 $Nm{\cdot}cm^{-3}$, maximum screw speed of 1200 min^{-1}, and screw inner diameter ratio (D_o/D_i) of 1.55 (8.2 mm screw diameter). The samples were compounded at 210 °C at a 2 kg h^{-1} feed rate and 200 rpm. Pellets of the composites obtained in this way were recovered for further processing.

To investigate the influence of the filler preparation and the manufacturing process of the composites on the filler aggregate size and its distribution within the PPPE matrix, a series of composites reinforced at 1 and 20 wt.% tannic acid-octadecylamine-MFC were prepared using three different filler preparation methods; namely never-dried, oven-dried and freeze-dried, and two different mixing methods, namely direct mix and solvent assisted mixing.

In the never-dried filler production method, the MFC slurry was reacted first with tannic acid and then with either hexylamine or octadecylamine, filtered to obtain a wet concentrate cake and resuspended in 50:50 vol.% water: acetone to wash out the excess reagents. The cake was premixed with the neat PPPE powder and the mixture was compounded in a Brabender torque rheometer, increasing the temperature gradually from 100 up to 210 °C to prevent the build-up pressure in the torque rheometer caused by the evaporation of residual moisture contained in the samples. In the oven-dried filer preparation method, the reacted MFC slurry was filtered and washed with acetone and dried at 60 °C in a vacuum oven until dry. In the freeze-dried method, the reacted MFC slurry was filtered and washed with a 50:50 vol.% water acetone solution, filtered, washed with water to eliminate the acetone residues and freeze-dried at a 3 wt.% solid in water concentration.

The composites were prepared using two different approaches. For direct mixing, the MFC based filler was premixed into the polymer matrix and fed to the compounder. For solvent-assisted mixing, the PPPE matrix (100 g) was pre-suspended in toluene (200 ml) at 100 °C under magnetic agitation until a clear toluene-polymer suspension of vegetable oil consistency was obtained, and the filler was added to the suspension and mixed for 1 h. The mixture was then cast in an aluminium tray. The obtained dry mixture was then compounded. The solvent assisted mix method is based on the observation that compatibilized oven-dried MFC fibrils appear, in an optical microscopy analysis, to be clustered (**Figure 4.4 a**). The same batch of compatibilized fibrils, however, appears less entangled when dispersed in toluene (**Figure 4.4 b**). The idea is that an organic solvent can assist the dispersion of the filler in the matrix reducing the viscosity of the melt polymer. This, in turn, disaggregates the filler bundles resulting in more intimate contact between the polymer and the cellulose fibrils.

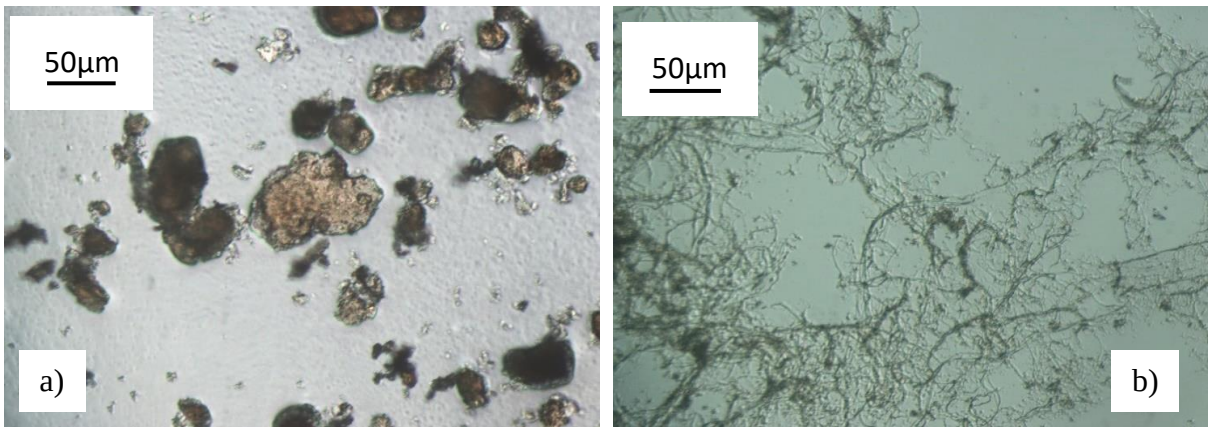

Figure 4.4 Typical polarized optical microscope images of a) the dry-ground TA-C_{18}-MFC powder and b) a dry-ground TA-C_{18}-MFC powder re-dispersed in toluene by magnetic agitation at 50 rpm and dried on a microscope slide (both images are taken at ×25 magnification).

The tannic acid-octadecylamine reinforced composites prepared using the different filler and composite manufacturing methods were compared against materials prepared using untreated MFC and tannic acid hexylamine reacted MFC. The comparison was central to determining the importance of the correct MFC surface treatment to enhance filler dispersion and obtain composites with good mechanical and impact properties. **Figure 4.5** contains a list of the composites prepared, the filler type, filler preparation method, composites preparation method and reinforcement loading used.

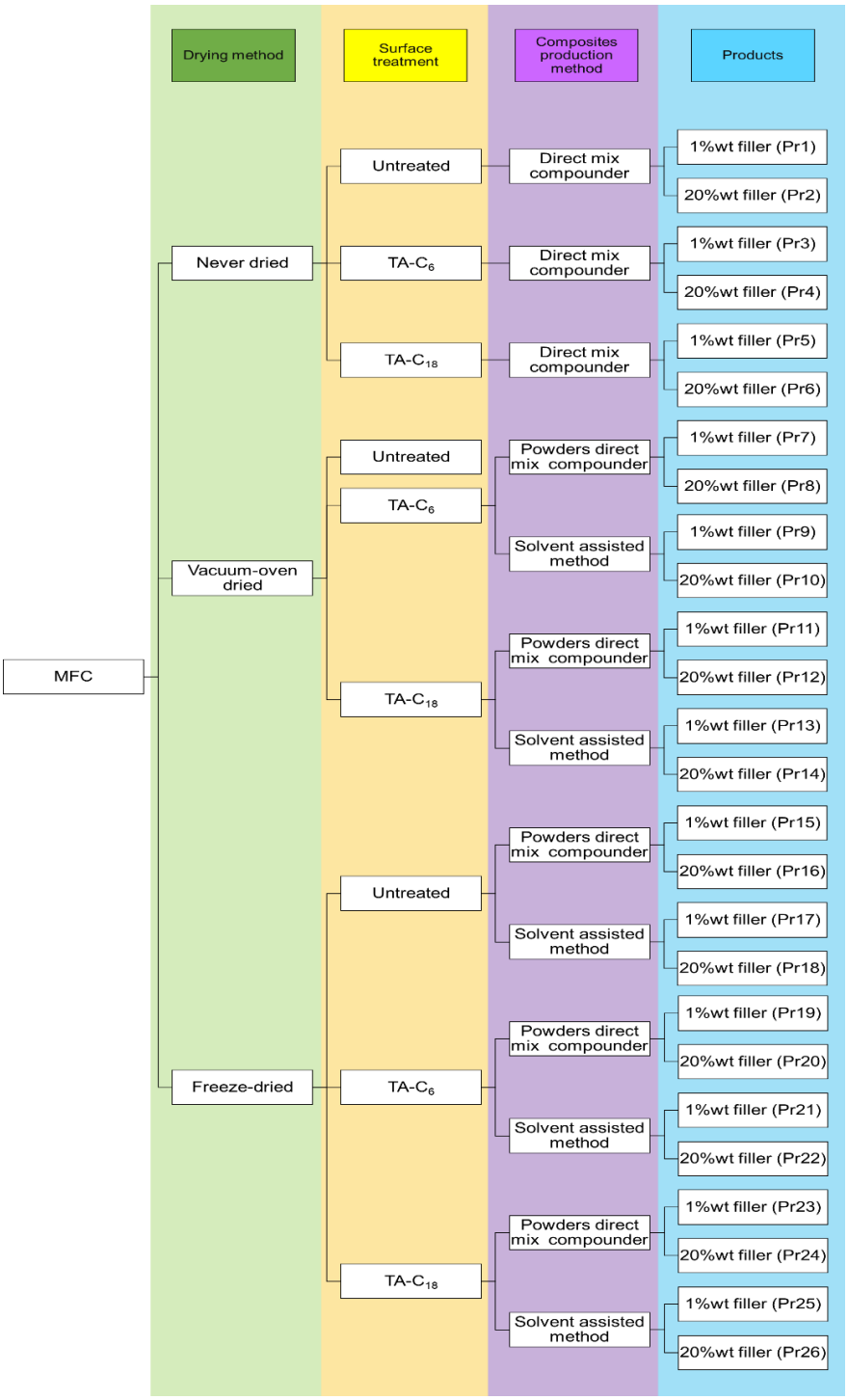

Figure 4.5 Summary of the composites produced. Each product is identified by a number that accounts for the MFC surface treatment used, the filler preparation method, the composites preparation method, and the filler loading. The vacuum-oven dried MFC produced a hard solid that cannot be ground to produce a powder to be used as reinforcement. For that reason, the composites produced using untreated oven dried MFC are not listed.

4.8.1 Preparation of specimens for tensile and impact measurements

The specimens for tensile and impact tests were prepared using two different methods:

-the small batches prepared using the Haake MiniLab 3 mini compounder were hot pressed at a temperature of 170 °C and a hydraulic pressure of the press of 60 bar in a stainless-steel mould of 1 mm of thickness. The films obtained were cut into a dumbbell shapes using a preformed puncher of the dimensions of the Type V specimen according to ASTM D 882.

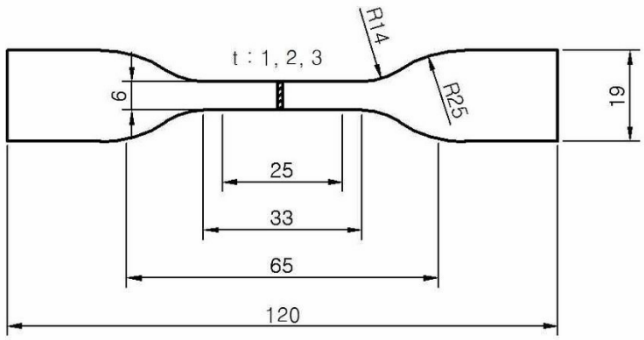

Figure 4.6 Dimension of Type V tensile specimen used. The diagram was taken from ASTM D 4761-13.

-the large batches obtained from the ZSK Mc[18] counter-rotating twin screw extruder was injection moulded using an Arburg 221 M machine, in accordance with ASTM D4761-13 and ASTM D 882. The specimens produced were Type I of the ASTM D 882.

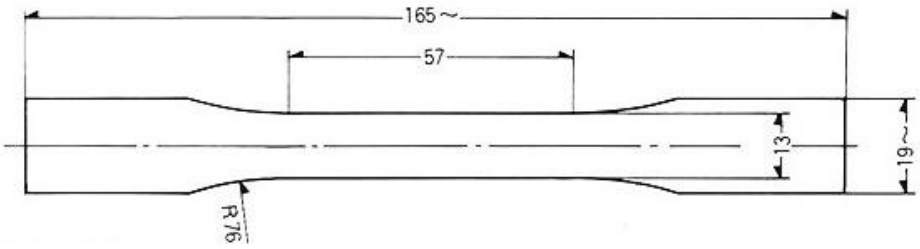

Figure 4.7 Dimensions of Type I tensile specimen used. The diagram was taken from ASTM D 4761-13

The measurements were registered only for the samples in which the fracture occurred in the gauge length.

4.9 X-ray Diffraction (XRD)

X-ray diffraction patterns of the pure matrix, unreacted MFC samples, surface treated MFC samples, and the corresponding composites were obtained using an X-ray powder diffractometer (Bruker D8 Advanced) having a 1.35 Å wavelength copper Kα X-ray source. Measurements were taken in the range 2θ = 10° to 50° using a step size of 0.5°. The collected diffraction patterns were used to investigate the crystallinity of the unreacted MFC samples and to evaluate the effect of the filler on the crystallinity of the composites prepared. The crystallinity fraction of the samples (χ_{cr}) was evaluated using Equation **12**:

$$\chi cr = \frac{A_{cr}}{A_{cr}+A_{am}} \quad \textbf{(12)}$$

where A_{cr} is the total area of the integrated peaks and A_{am} is the area of the amorphous background. The amorphous baseline was evaluated using a mathematical fitting program.

4.10 Differential scanning calorimetry (DSC)

The melting behaviour of pure PP samples, and the nanocomposites produced by adding 1 wt.% of surface treated MFC species were investigated using differential scanning calorimetry (Metteler Toledo DSC1), using aluminium pans. The samples (approximately 10 mg) were heated from 25 to 240 °C and then cooled back down to 25 °C at a heating/cooling rate of 10 °C min^{-1} under a nitrogen gas flow rate of 50 mL min^{-1}.

4.11 Thermogravimetric analysis (TGA)

TGA was used to determine the thermal stability of the pure materials along with the thermal stability of the obtained composite. the thermal degradation behaviour of all of the components of the composites, including compounds used for surface treatment, was investigated using thermogravimetric analysis (Mettler Toledo TGA/DSC1). The samples (approximately 5 mg) were heated from 30 to 300 °C at a heating rate of 10 °C min^{-1} under a flow of 20 mL min^{-1} pure nitrogen gas. The onset and degradation temperatures were obtained from the first derivative of the weight loss as a function of temperature. The data obtained from the TGA analysis were used to determine the upper operational temperature for the different materials.

The present chapter contain an overview of the filler compatibilization strategies used in this research alongside the specimens' production and characterisation methods. The next chapter introduce elevant filler dispersion and aggregate analysis technique to further evaluate the filler compatibilization effectiveness.

5. Evaluation of filler dispersion and mechanical properties of the filled composites

In the following chapter a series of microscopic and spectroscopic techniques that were used to determine the level of filler dispersion in the composites is presented. The dimension, morphology and distribution of the reinforcement in the matrix have a profound effect on the mechanical and impact performance of the composites produced. For that reason, one of the main goals of the work was the evaluation of the filler dispersion within the polyolefin matrix used. The techniques and methodologies used in this study are presented in the following sections.

5.1 Scanning electron microscope (SEM) and Energy-dispersive X-ray spectroscopy (EDX) imaging

SEM is an excellent technique for the investigation of the pure MFC, compatibilized fillers and the morphology of the fracture surfaces of composites. SEM images were obtained from dried MFC and compatibilized MFC samples and from slices of reinforced composites prepared using a microtome. SEM images of the fracture surfaces of composites after tensile testing were also obtained.

EDX imaging was used to investigate the dispersion of the cellulose filler in the composites. The focus of this analysis is the identification of the spatial positioning of the oxygen signal in a 2D EDX map of the analysed specimens, along with the carbon signal. The cellulose-based reinforcement contains a number of oxygen atoms, but unfortunately, the oxygen signal can be related also to external contaminants, to some of the compatibilizers that were used, and to impurities present in the original matrix. For this reason, EDX imaging was used merely as an initial scanning technique to understand the filler dispersion in the composites.

A JEOL IT300 Scanning Electron Microscopy (SEM), operated at 2 keV, was used to image the filler powders and the reinforced composites. The samples were coated with graphite using a vacuum sputter-coater to improve the conductivity of the samples, and thus the quality of the SEM images and the Energy-dispersive X-ray spectroscopy (EDX) mapping.

5.2 Transmission electron microscopy (TEM) imaging

TEM is a powerful technique for the analysis of the filler dispersion in composites. In the system under analysis, however, TEM is a demanding and challenging technique: since the X-ray scattering power of atoms is proportional to their atomic number, little contrast between the matrix and the filler can be obtained because they are all made of atoms of similar atomic number, which renders the unequivocal identification of the filler difficult. The contrast between the matrix and the cellulose-based filler can be enhanced using staining agents such as uranyl-acetate. However, the introduction of this contrast agent in the materials proved impractical. When microtomed slices of the composites were stained with uranyl acetate, the stain did not penetrate the cellulose agglomerates, and as a result, the staining was not effective.[395] For this reason, the TEM data were used as comparisons to the dispersion analysis developed using mapping with Time of flight-Secondary Ions Mass Spectroscopy (ToF-SIMS) and Multi-channel Spectral Confocal Laser Scanning Microscopy (SCLSM).[395] TEM images of TA-octadecylamine-MFC reinforced composites were collected with a JEOL 2100^{+} TEM instrument operating at a 100-kV acceleration voltage. The images were obtained from unstained thin layers of composites, cut using a cryo-microtome, containing either a low (0.5 wt.%) or a high (15 wt.%) concentration of filler.

5.3 Time of flight-Secondary Ions Mass Spectroscopy (ToF-SIMS) mapping

ToF-SIMS data were acquired under the guidance of Dr D. J. Scurr at Nottingham University using a ToF-SIMS IV instrument (ION-TOF GmbH., Münster, Germany) equipped with a bismuth liquid metal ion gun and a single-stage reflectron analyser. Operating conditions utilised Bi_3^{+} with a primary ion energy of 25 kV and a pulsed target current of approximately 1.0 pA. Low-energy electrons (20 eV) were used to compensate for surface charging caused by the positively charged primary ion beam on the insulating surfaces. Individual spots were analysed using rastering areas of 500 × 500 μm^2 at a resolution of 256 × 256 pixels. The total primary ion beam dose for each analysed area was kept below 1×10^{12} ions cm^{-2}, ensuring static conditions.

5.4 Multi-channel Spectral Confocal Laser Scanning Microscopy (SCLSM) mapping

Composite samples were cryo-microtomed into slices of 20 μm thickness cut from the central part of a dumbbell having dimensions of 10 × 4 mm (length × width). Slices were placed between a glass slide and coverslip to flatten the surface. Spectral *z*-stack images (800 × 800 μm^2) were generated using a Zeiss LSM 880 confocal microscope (405 nm diode laser, 5.0 % power, Plan-Apochromat 10×/0.45 M27 objective, MBS-405 filter, 32 channels: λ = 411-695 nm). The maximum distance between stack slices was 2 μm.

5.4.1 Image processing

Image stacks generated using spectral confocal microscopy were processed in Fiji software. The *z*-projection function (projection type: standard deviation) was used to flatten image stacks into single images. After thresholding, images were analysed to determine the observed aggregate areas. Aggregates at the edge of the images were excluded, as were aggregates less than 11 μm^2, *i.e.* less than four pixels, as these could not be visually identified.

5.4.2 Aggregate analysis

Aggregate distribution was subdivided into four categories: small, medium, large, and outliers. Rather than set these categories between fixed area values, the maximum and minimum values for each category were determined using the box plots themselves. A box plot was constructed using the entire data set, and the values for which data would be classified as an upper, or lower, outlier determined. The box plot was then regenerated using the outlier values as the maximum and minimum for the data range and new outlier values calculated. This process was repeated until the range of values fell between the upper and lower outlier values. This determined the aggregates that fell into the small category for each sample. To determine the medium category range, the process was repeated excluding all values in the small category. The process was repeated excluding values in the small and medium categories to define the large category range. All values that fell out of these ranges were classified as outliers. Owing to the skew present in the data sets, the calculated lower outlier values were always less than the initial lower data values for all samples. To compare the aggregate populations, the boundaries for the four size categories were set as the boundaries determined for the 1 wt.% TA-C_{18}-MFC composite sample using the above technique.

5.4.3 Statistical analysis

For the comparison of the composite mean aggregate areas and aggregate population analysis, a one-way analysis of variance (ANOVA) test was used to determine the statistical differences between two or more samples, assuming equal variance, with Tukey HSD posthoc correction, defining n as the sample size per group. The number of images captured for each sample at different depth in the sample was equal to 3 (N). A confidence interval of 0.95 was used (p). The standard error (SE) is calculated from the sample standard deviation.

5.5 Quasi-static and Dynamic characterization

Tensile tests were conducted using a tensile testing machine (Instron 3367). The full-scale load and the crosshead speed used were 30 kN and 10 mm min^{-1}. The tests were performed in accordance with ASTM D4761-13 and ASTM D 882. The impact tests were conducted using an impact testing machine Drop Tower Impact System (Instron CEA5 9340) conveying impact energy of 22.67 J and having an impact velocity of 3.80 ms^{-1}. The analysis was performed at room temperature with unnotched specimens of 80 mm× 10 mm× 4. The tests were performed according to ISO-179 2.

6. Results and discussion

In this chapter the results the characterisation of raw materials, intermediate and final reaction products, untreated and compatibilized MFC fillers and composites containing different reinforcements at different filler loadings are presented and discussed. The findings are used to develop a plan to produce and investigate a set of preformat compatibilized MFC reinforced composite which were compared against similar inorganic reinforced composites. In the final part of the present chapter two spectroscopic techniques are presented and evaluated in the analysis of the filler dispersion in MFC reinforced composite. The results of the SCLMS mapping aggregate analysis were used to explain the poor impact performances of the produced samples.

6.1 Tannic acid octadecylamine surface reaction efficiency evaluation

The organic solvent base MAgPP and the water based tannic acid-octadecylamine surface reaction for the production of hydrophobic MFC product to be dispersed in polyolefin-based matrices was investigated. A review of the relevant results and findings is presented in the following paragraphs.

6.1.1 Fourier-transform infrared spectroscopy (FTIR) of pure and compatibilized MFC films

Fourier-transform infrared spectroscopy (FTIR) was used to evaluate the efficiency of the reaction between TA-activated MFC and octadecylamine. The spectra of the pure reagents and of the pure MFC film were recorded as references.

In **Figure 6.1** the typical spectra of MFC, cellophane, tannic acid, and octadecylamine are presented and compared with compatibilized MFC and cellophane films.
The tannic acid and the MFC have similar FTIR peaks: a distinctive broad peak between 3000 and 3500 cm^{-1}, characteristic of hydroxyl-rich compounds. The octadecylamine spectrum is characterized by an intense set of peaks between 2800 and 3000 cm^{-1}. The tannic acid octadecylamine-MFC spectra present a strong peak between 2800 and 3000 cm^{-1}, which indicates the presence of the primary amine. The amine peak of the compatibilized MFC films did not disappear after washing the samples with acetone, indicating that these groups are covalently attached to the activated cellulose fibrils. The covalent bond between tannic acid

activated MFC fibrils and the octadecylamine is further confirmed by the development of the small peak between 1400 and 1500 cm^{-1} in the compatibilized MFC sample, which indicates the formation of an α,β-unsaturated ketone-group, which is most likely due to a Schiff base reaction.

To investigate the influence of the porosity of the MFC films, the same tannic acid-octadecylamine surface compatibilization was used on non-porous cellulose films (Cellophane). The untreated cellophane films had a similar spectrum to the MFC films with a broad peak between 3000 and 3500 cm^{-1}. The tannic acid-octadecylamine compatibilized cellophane films presented the same characteristic peaks of the reacted MFC: a small peak between 2800 and 3000 cm^{-1}, characteristic of the amino group and the development of a small peak between 1400 and 1500 cm^{-1}, attributed to the development of a Schiff base between the tannic acid activated cellophane surface and the octadecylamine. The intensities of the characteristic peaks are lower than for the compatibilized MFC films; this is due to the different structures of the MFC and cellophane samples. The cellophane films, being non-porous can expose only a smaller surface to the reaction.

FTIR spectra of compatibilized MFC and cellophane films were captured during the reaction every hour; typical spectra are shown in **Figure 6.2**.

The evolution of the peak characteristic of an amine group (between 2800 and 3000 cm^{-1}) in the compatibilized MFC films and in the surface treated cellophane is a strong indicator of the reaction has taken place.

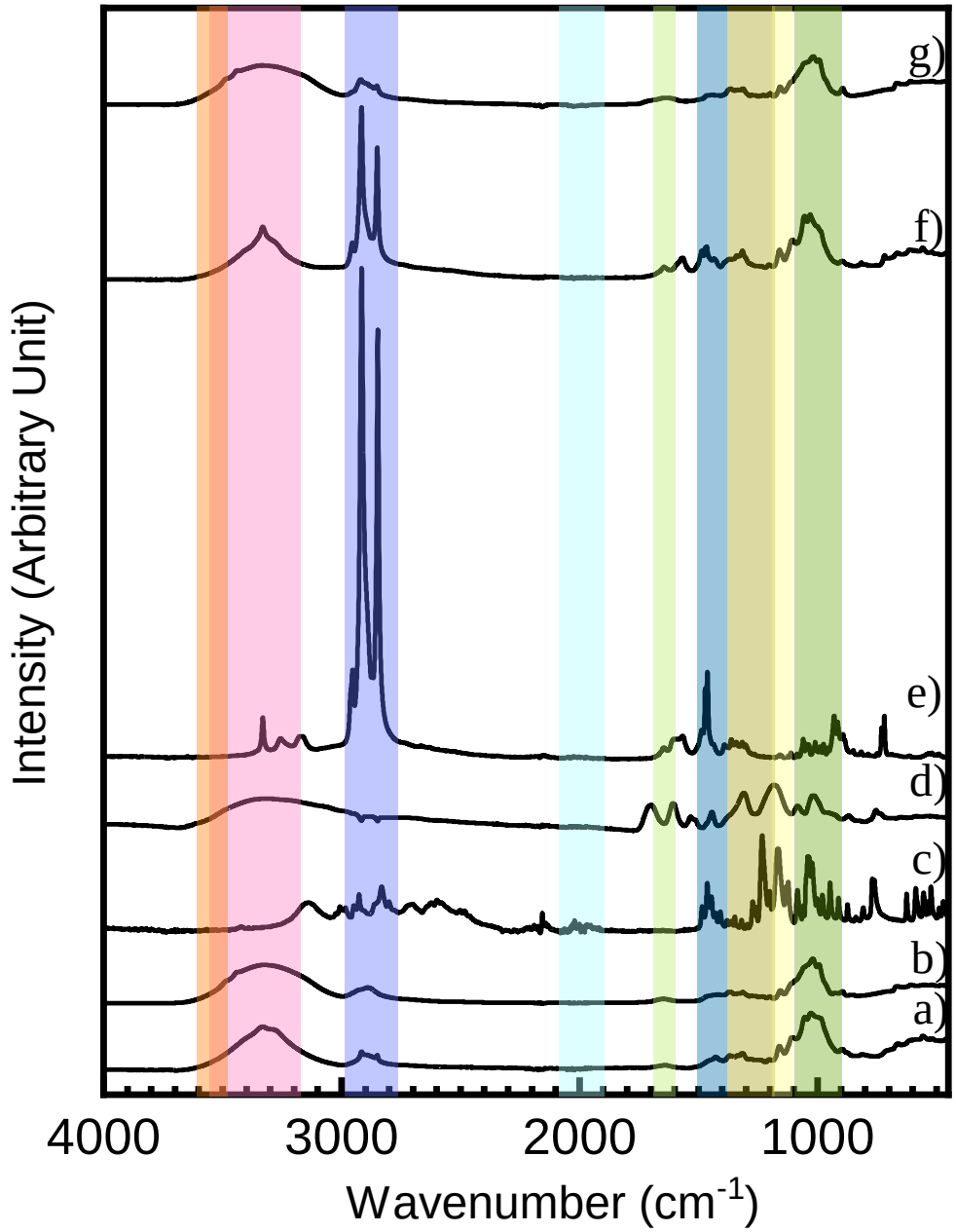

Figure 6.1 Typical FTIR spectra of untreated MFC film a), untreated cellophane film b), HEPES c), tannic acid d), octadecylamine e) TA-octadecylamine compatibilized MFC f), and TA-octadecylamine compatibilized cellophane f). The reference bands highlighted in the diagram are free hydroxyl groups (3500-3600 cm^{-1}) - orange, hydroxyl groups (3200-3500 cm^{-1}) - red, carbonyl and amino groups (2800-3000 cm^{-1}) - violet, C-H bending used as reference peak (1900-2100 cm^{-1}) - light blue, imino group (1600-1700 cm^{-1}) - light green, α,β-unsatured keto-groups (1400-1500 cm^{-1}) - blue, carboxyl groups (1200-1400 cm^{-1}) - olive, ester groups (1100-1200 cm^{-1}) - yellow, and alcohol, carboxyl groups (900-1100 cm^{-1}) - dark green.

The increase in intensity is an indication of the success of the reaction, suggesting that the acetone wash is effective in removing the unreacted octadecylamine, in both the porous MFC films and in non-porous cellophane materials. The development of a small peak between 1400 and 1500 cm^{-1} (α,β-unsatured keto-groups) over time indicates the formation of the Schiff base as a result of the reaction and further confirms the hypothesis that only covalently attached amines are registered in the FTIR analysis.

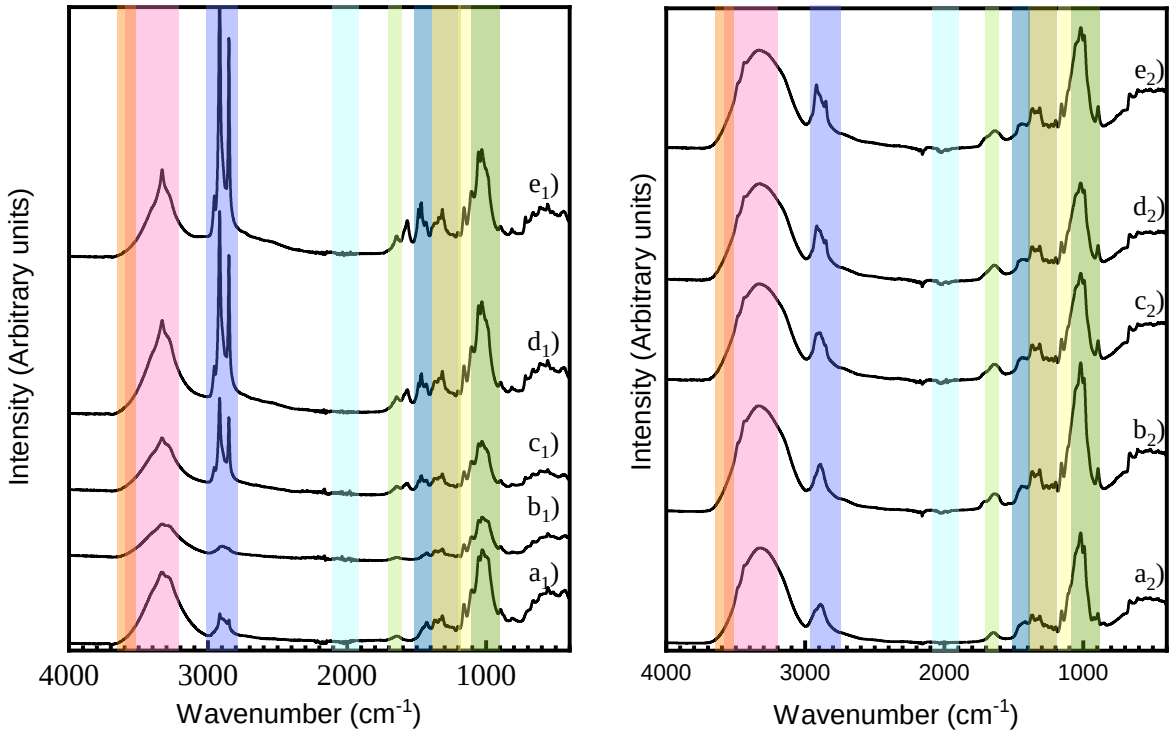

Figure 6.2 Left: typical FTIR spectra of untreated MFC a_1), tannic acid activated MFC b_1), TA-octadecylamine-MFC reacted for 1h c_1), TA-octadecylamine-MFC reacted for 2h d_1), TA-octadecylamine-MFC reacted for 3h e_1). Right: typical FTIR spectra of untreated cellophane a_2), tannic acid activated cellophane b_2), TA-octadecylamine- cellophane reacted for 1h c_2), TA-octadecylamine- cellophane reacted for 2h d_2), TA-octadecylamine-cellophane reacted for 3h e_2). The reference bands highlighted in the diagram are free hydroxyl groups (3500-3600 cm^{-1}) - orange, bounded hydroxyl groups (3200-3500 cm^{-1}) – red, carbonyl and amino groups (2800-3000 cm^{-1}) - violet, C-H bending used as reference peak (1900-2100 cm^{-1}) - light blue, imino group (1600-1700 cm^{-1}) - light green, α,β-unsatured keto-groups (1400-1500 cm^{-1}) - blue, carboxyl groups (1200-1400 cm^{-1}) - olive, ester groups (1100-1200 cm^{-1}) - yellow, and alcohol, carboxyl groups (900-1100 cm^{-1}) - dark green.

6.1.2 Contact angle and free surface energy of porous MFC films and non-porous cellophane films

The contact angle and free surface measurements of the untreated and tannic acid primary amines reacted MFC and cellophane was recorded to determine the efficiency of the tannic acid-octadecyl amine surface treatment in hydrophobising the cellulose-based films and reducing the filler surface energy to a level more suitable for mixing with the apolar polymeric matrix. The results were compared with the organic solvent-based method in which MAgPP was reacted with cellophane and MFC films respectively.

Owing to the porous nature of the MFC films, it would be impossible to apply Owens, Wendt, Rabel and Kaelble method on the MFC films, however, Cellophane films have a similar chemical structure to the MFC films, without being porous. Cellophane films were used to obtain reliable values for the contact angles and free surface energy for the unreacted and tannic acid-primary amine compatibilized films.

The contact angles and the free surface energies of the pure matrix (PPPE), untreated and TA-C_{18} reacted cellulose films (Cellophane) and MFC films are provided in **Table 6.1.** The values were calculated from five different sampling points on the same specimen to minimize errors. The free surface energy was evaluated using water and bromonaphthalene (BN) and applying the Owens, Wendt, Rabel and Kaelble method.

Table 6.1 Free surface energy, polar and apolar contribution, water and BN contact angle of PPPE, untreated cellophane, MAgPP, TA-C_6 reacted, and TA-C_{18} reacted cellophane and water and BN contact angle of MFC and reacted MFC films.

Sample ID	Free surface energy (mNm^{-1})	Polar contribution (mNm^{-1})	Dispersive contribution (mNm^{-1})	Contact angle (^{0})	
				Water	BN
PPPE	37.6±0.2	3.6±0.1	33.9±0.1	83±1.7	41.4±0.9
Cellophane	70.1±0.1	36.1±0.1	34.6±0.1	21±0.9	45.1±0.7
CellophaneMAgPP	41.1±0.1	8.7±0.1	32.3±0.1	45±0.3	72±0.6
CellophaneTAC_6	39.5±0.1	8.19±0.1	31.25±0.1	47±0.5	74±0.7
CellophaneTAC_{18}	33.9±0.1	1.2±0.1	32.8±0.1	93±1.2	44.1±0.5
MFC	N/A			44.2±0.7	80.2±0.7
MFCMAgPP	N/A			110±2	49±1.3
MFCTAC_6	N/A			56.6±0.5	47.5±1.1
MFCTAC_{18}	N/A			121.1±2	62.5±0.7

Untreated Cellophane and MFC films were reported to be hydrophilic, having water contact angles of ~21°, and ~44° respectively. The initial water contact angle values are significantly increased when the fibrils were reacted with both MAgPP and TA and octadecylamine. The tannic acid-octadecylamine proved to be efficient in hydropobizing the cellulose fibrils in cellophane and MFC films. Only the cellophane films measurement, however, were used in the critical aggregate size analysis. The tannic acid hexylamine treatment, on the other hand, proved to be less efficient in hydrophobising the cellulose fibrils in both cellophane and MFC films, highlighting the importance of the primary amine alkyl tail length in mitigating the cellulose fibrils' hydrophilicity.

The water contact angles of both cellophane and MFC films were registered over a time range of one minute to determine the effect of capillary force and porosity on the measurement (**Figure 6.3**).

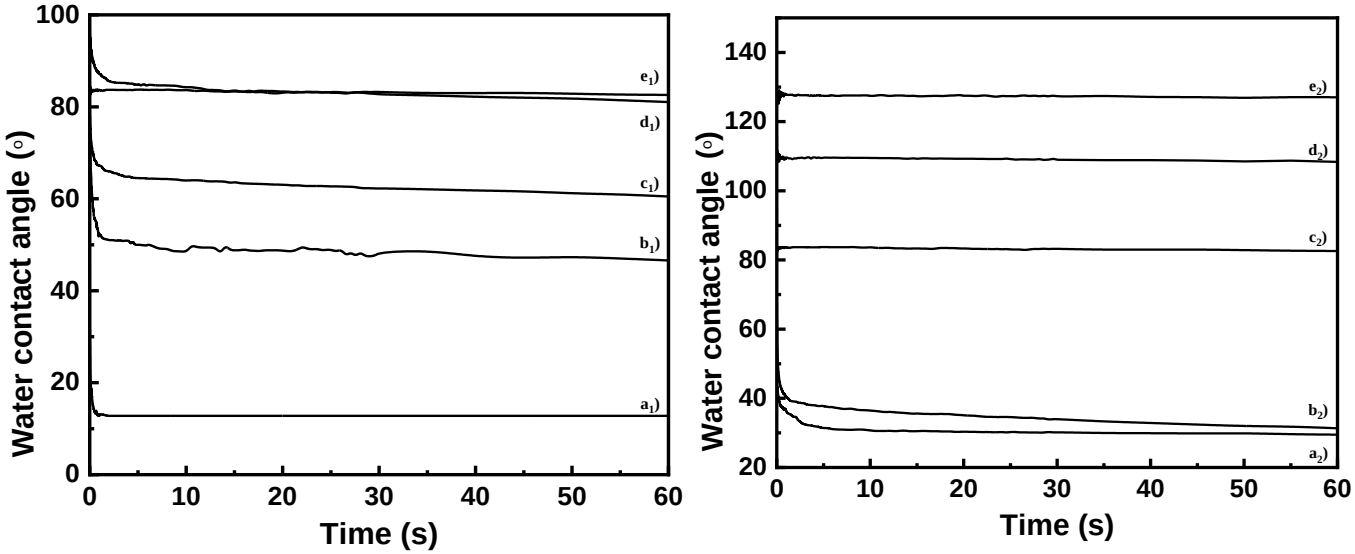

Figure 6.3 Evolution of the water contact angles of Left: Cellophane untreated film a_1), MAgPP-Cellophane film b_1), TA-C_6-Cellophane film c_1), TA-C_{18}-Cellophane film d_1), and neat PPPE film e_1); Right: MFC untreated film a_2), TA-C_6-MFC film b_2), neat PPPE film c_2), MAgPP-MFC film d_2), and TA-C_{18}-MFC film e_2).

The tannic acid- octadecylamine surface treatment of the non-porous cellulose film decreases the free surface energy of the samples from 70.1 mNm^{-1} to 33.9 mNm^{-1}. The surface modification of cellulose with TA and octadecylamine decreases the surface energy of the cellulose substantially and thus should improve its dispersibility in apolar polymers. The free surface energy evaluated for the cellophane reference system is shown in **Figure 6.4**, where the total free surface energy and the polar and dispersive components are presented for the various substrates.

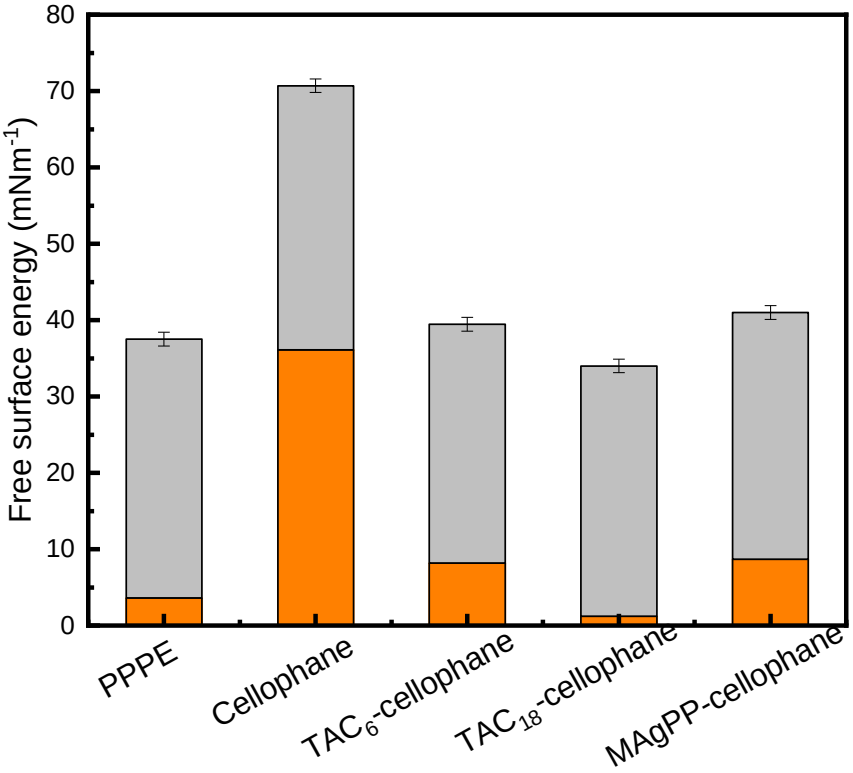

Figure 6.4 Free surface energy polar (orange) and apolar (grey) contributions and total free surface energy (solid line) of PPPE film, untreated cellophane film, TA-hexylamine reacted cellophane film, TA-octadecylamine reacted cellophane film, and MAgPP reacted cellophane film.

The surface treatment of cellulosic films with TA and octadecylamine is clearly efficient in decreasing the surface energy of the materials. This characteristic can be helpful in efficiently dispersing the compatibilized MFC fibrils in polar matrices especially considering the small difference in the free surface energy of the neat PPPE matrix and the tannic acid octadecylamine reacted samples.

6.2 Crystallinity fraction and thermal stability of pure materials and composites

The crystallinity fraction (χ_{cr}) of both neat matrix and filler can have a massive impact on the performances of the composites. Furthermore, the addition of a filler to a polypropylene dominated matrix can cause changes in the crystallinity fraction *via* nucleation and/or trans-crystallization of the matrix on the surface of the cellulose fibrils.[396–398] Crystallinity was evaluated using the X-ray diffraction (XRD) and Differential Scanning Calorimetry (DSC) approaches.

The crystallinity fraction of the reinforced composites obtained using the XRD technique considers the crystallinity of both cellulose reinforcement and matrix. Owing to the superposition of some cellulose and matrix peaks, it was necessary to assume that during compounding and injection moulding no change in the crystallinity fraction of the cellulose reinforcement occurred. The results obtained from each technique were compared. The crystallinity fraction calculated using DSC curves considers only the matrix crystallinity fraction since cellulose does not melt.

6.2.1 X-ray Diffraction (XRD) of the neat and compatibilized fillers and of the reinforced composites

XRD was used in the present study to calculate the crystallinity of the neat matrix and pure MFC filler and to investigate the influence of the untreated and compatibilized fillers on the crystallinity of the composites obtained. The diffraction patterns of the pure samples (**Figure 6.5**) and the nanocomposites (**Figure 6.6**) were recorded using an X-ray powder diffractometer. The samples' crystallinity fraction (χ_{cr}) were calculated using Equation **12**.

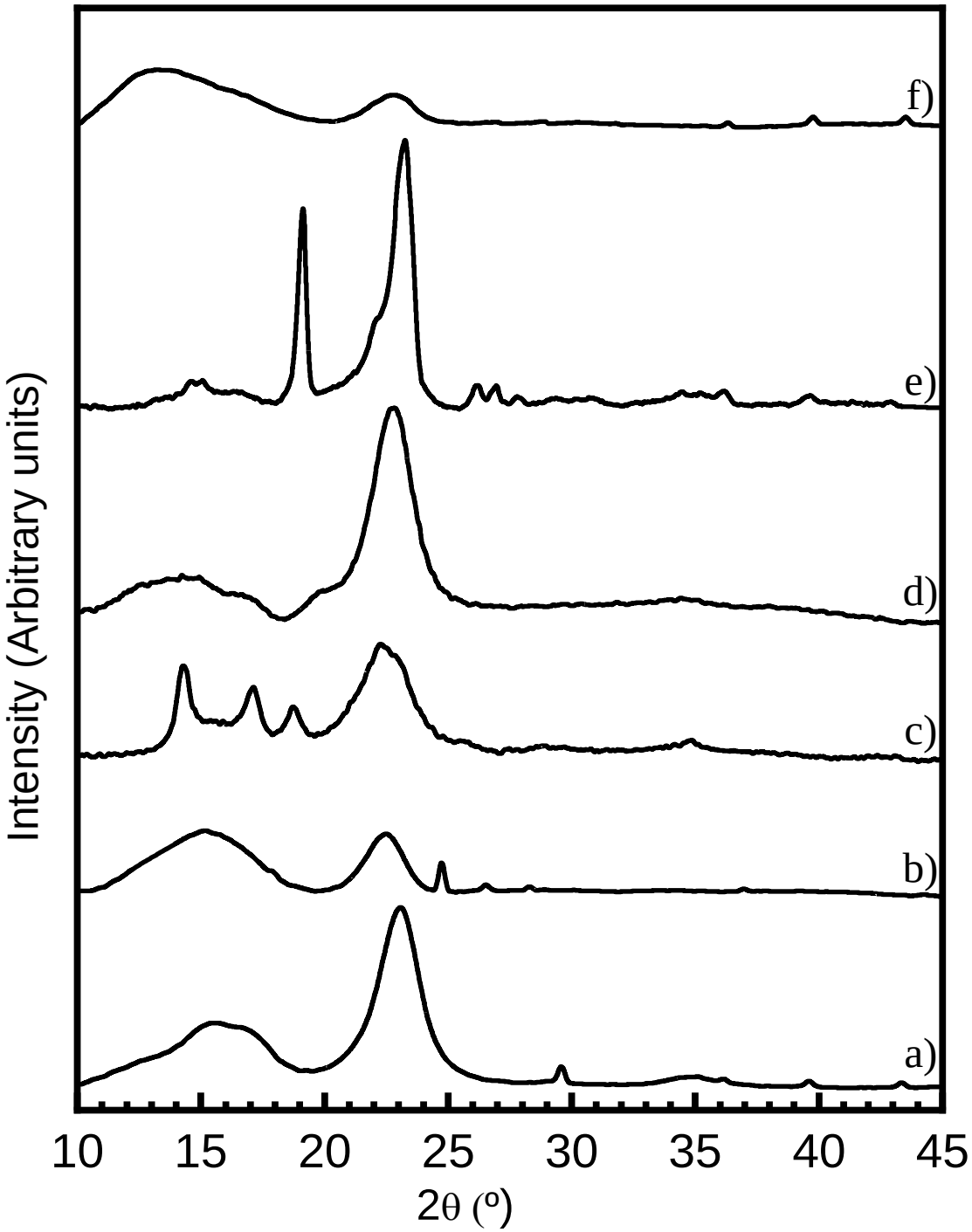

Figure 6.5 Typical XRD diffraction patterns for native cellulose χ_{cr}=0.4 a), untreated MFC sheets χ_{cr}=0.2 b), MAgPP reacted MFC χ_{cr}=0.3 c), PVOH reacted MFC χ_{cr}=0.4 d), PEO reacted MFC χ_{cr}=0.5 e), and TA-octadecylamine reacted MFC χ_{cr}=0.2 f).

The crystallinity fraction of the pure and compatibilized cellulose materials are compared in **Figure 6.5**. Native cellulose I has characteristic Bragg peaks at 15°, indexed as (1-10), at 16°, indexed as (110), and at 23°, indexed as (200).[399] The diffraction pattern of the softwood bleached Kraft pine pulp (**Figure 6.5 a**) has a broad halo at 15° originated from the degradation of native cellulose peaks indexed to (1-10) and (110) and a broad peak at 23° originating from the broadening of the cellulose crystalline peak indexed (200).[400] The characteristic halos at 15° and 23° are present for all compatibilized fillers. The mechanical fibrillation of the softwood bleached Kraft pine pulp reduces the crystallinity fraction of the material from 0.4 to 0.2. The surface compatibilization of the obtained cellulose microfibrils has a different effect on the final product. The reaction of the MFC with MAgPP does not affect the initial crystallinity fraction of the MFC, the difference in the crystallinity fraction registered for the MAgPP reacted MFC filler were attributed to the crystallisation of the PP chains on the surface of the fibrils, in fact in the MAgPP compatibilized filler has new peaks present at 14°, 16°, and 18° (**Figure 6.5 c**). These peaks correlate with characteristic PP diffraction patterns and are indexed (110), (020), and (040).[401] The esterification of cellulose microfibrils with myristoyl chloride resulted in the complete degradation of the cellulose crystalline structure.

The surface compatibilization of the MFC with PVOH and PEO (**Figure 6.5 d** and **e**) resulted in the crystallisation of the water-soluble polymer on the surface of the cellulose fibrils. This effectively increases the filler crystallinity from 0.2 of the untreated MFC to 0.4 and 0.5 in the case of PVOH and PEO reacted samples respectively. The MFC surface reaction with TA-octadecylamine, on the other hand, left the crystallinity fraction of the untreated MFC unaltered (**Figure 6.5 f**), indicating that no crystallisation of the octadecylamine occurred on the surface of the fibrils.

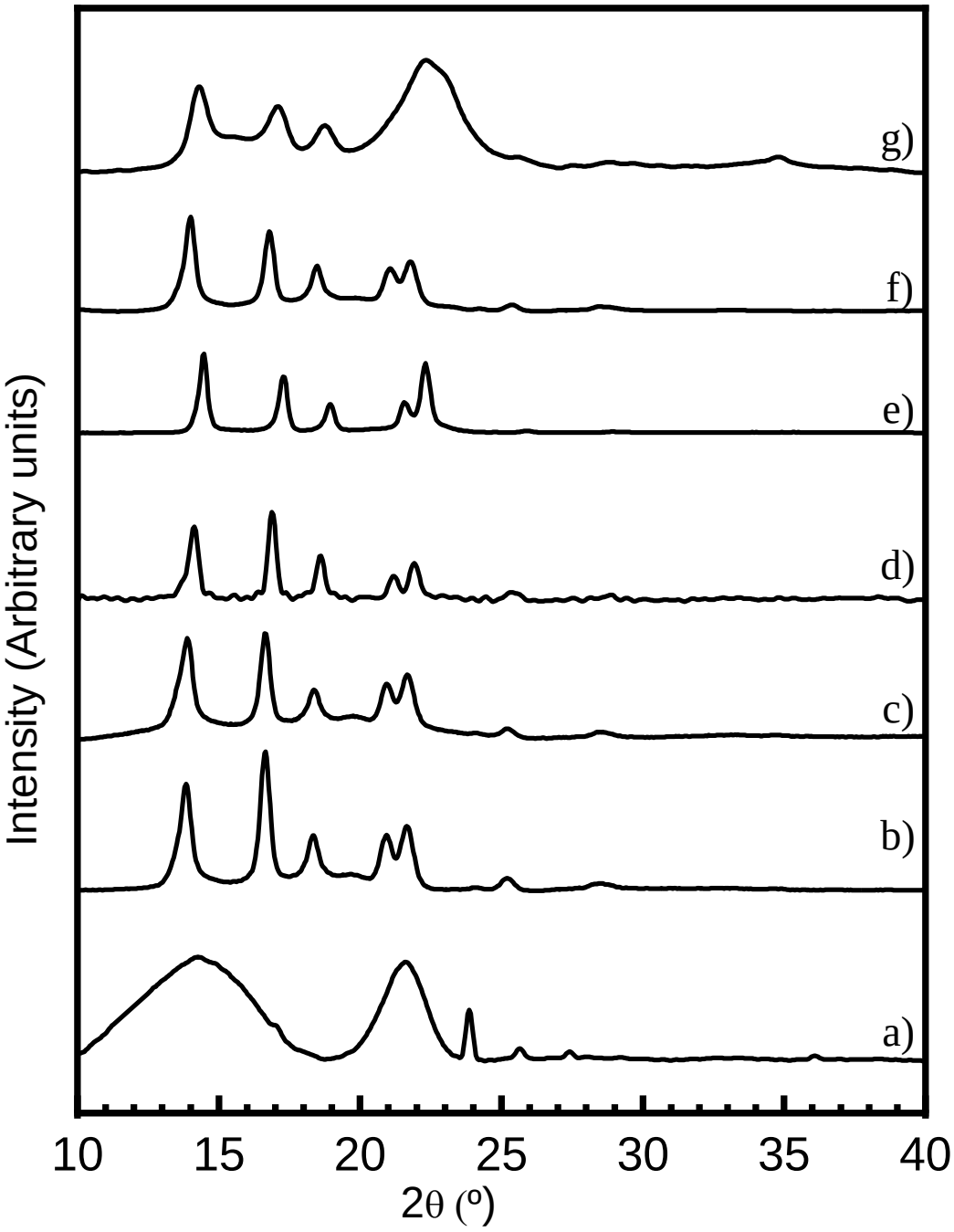

Figure 6.6 Typical diffraction patters of dry pure MFC χ_{cr}=0.2 a), neat PPPE matrix χ_{cr}=0.4 b), 1 wt.% MAgPP compatibilized MFC nanocomposite χ_{cr}=0.5 c), 1 wt.% myristoyl chloride compatibilized MFC nanocomposite χ_{cr}=0.2 d), 1 wt.% PVOH compatibilized MFC nanocomposite χ_{cr}=0.4 e), 1 wt.% PEO compatibilized MFC nanocomposite χ_{cr}=0.4 f), 1 wt.% TA-C_{18} compatibilized MFC nanocomposite χ_{cr}=0.3 g).

In **Figure 6.6** the diffraction patterns of the pure MFC, neat matrix and 1 wt.% reinforced composites with different fillers are compared. The neat PPPE matrix (**Figure 6.6 b**) shows the characteristic Bragg peaks of PP at 14, 16, 18, 21, and 22°, indexed to (110), (020), (040), (111), and (041) respectively and for PE at 21, and 24° indexed to (110) and (200) respectively;[401] the crystallinity for PPPE matrix is found to be ~0.4. The untreated dry MFC has characteristic Bragg peaks of native cellulose at 15, 16 and 23° indexed to (1-10), (110), and (200); the crystallinity (χ_{cr}) value for the fillers was evaluated in a separate set of experiments and was found not to vary during the manufacturing processes.

The MAgPP compatibilized MFC reinforced composite (**Figure 6.6 c**) has a crystallinity fraction (χ_{cr}) of 0.5; characteristic PP Bragg peaks are present at 14, 16 ,18° and characteristic PE peaks at 21 and 24°; the broadening of these peaks is attributed to the influence of the characteristic broad peak at 22° due to cellulose. The increased crystallinity in the samples containing MAgPP compatibilized polypropylene was suspected to be caused by the development of a trans crystalline structure in the surface of the compatibilized fibrils. However, an investigation of this phenomenon using a hot stage microscope revealed that no relevant changes in the crystallization of the MAgPP-MFC reinforced composites occurred. The increased crystallization is therefore attributed to the separate contributions of the filler and the matrix separately.

The 1 wt.% myristoyl chloride-MFC reinforced composites (**Figure 6.6 d**) had a χ_{cr} of 0.2, lower than the neat matrix. The myristoyl chloride treatment is thought to be unstable under the processing conditions. The decomposition of the reacted and partially reacted chemicals can degrade the polymeric matrix itself, producing unusable composites.

Composites filled with PVOH compatibilized MFC and PEO compatibilized MFC (**Figure 6.6 e, f**) had a crystallinity value of 0.4, entirely attributed to the PPPE matrix. The 1 wt.% tannic acid-octadecylamine-MFC reinforced composites (**Figure 6.6 g**) had a χ_{cr} of 0.3. The composite exhibited characteristic PP Bragg peaks at 14, 16, 18° while the large cellulose halo at 23° completely masked the characteristic PE peaks at 21 and 24°. The objective of the XRD analysis is to investigate the influence of the various compatibilized MFC fillers on the crystallinity of the polymeric matrix. The data collected indicate that the addition of the compatibilized cellulose filler affects the crystallinity of the composites in a not trivial way. The addition of myristoyl chloride reacted with MFC, however, it appears to severely damage the polymeric matrix as well.

Table 6.2 summarises the crystallinity fractions, the characteristic Bragg peak positions of the reinforced composites.

Table 6.2 XRD analysis report for the dry native cellulose, the pure dry MFC, the PPPE matrix and the1 wt.% filled nanocomposites.

Sample ID	**χ_{Cr} (-) Cell**	**χ_{Cr} (-) Total**	**2θ (^{0})**
Native cellulose	0.4	0.4	15, 16, 23
MFC	0.2	0.2	23
PPPE	N/A	0.4	14, 16, 18, 21, 22
1 wt.% MAgPP-MFC composite	0.3	0.5	14, 16, 18, 21, 22
1 wt.% myristoyl chloride-MFC composite	0	0.2	14, 16, 18, 21, 22
1 wt.% PVOH-MFC composite	0.4	0.4	14, 16, 18, 21, 22
1 wt.% PEO-MFC composite	0.5	0.4	14, 16, 18, 21, 22
1 wt.% TA-C_{18}-MFC composite	0.2	0.3	14, 16, 18

6.2.1.1 Tannic acid octadecylamine compatibilized MFC crystallinity

Owing to the potential influence of the filler crystallinity on the mechanical properties of the composites obtained, the influence of the grinding process on the tannic acid-octadecylamine-MFC filler was investigated using XRD.

The diffraction pattern of the unreacted MFC and of two forms of TA-octadecylamine compatibilized MFC (film and powder) were compared. The crystallinity (χ_{cr}) of the cellulose filler was calculated using Equation **12**, and the results were used to assess the level of damage caused by the surface treatment, drying and grinding process to the compatibilized MFC filler.

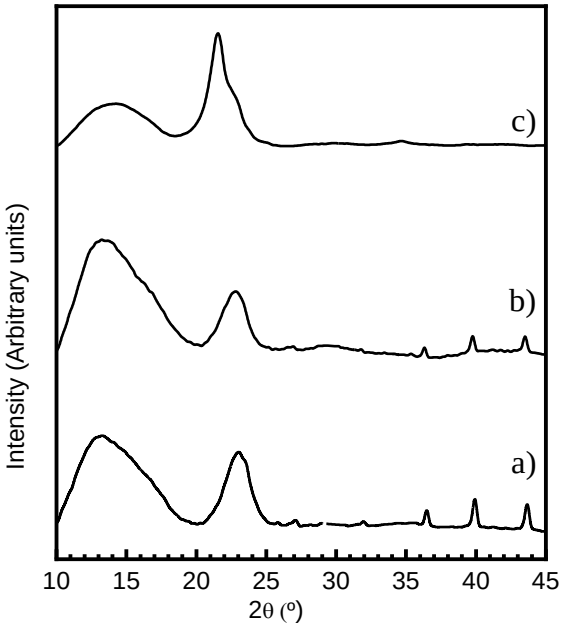

Figure 6.7 Typical XRD diffraction patterns for untreated MFC sheets χ_{cr}=0.2 a), TA-octadecylamine-MFC sheets χcr=0.2 b), and TA-octadecylamine-MFC powder χ_{cr}=0.2 c).

Native cellulose had a χ_{cr} equal to 0.4, as previously evaluated. The χ_{cr} value of the MFC decreased sharply due to the mechanical fibrillation of the Kraft pulp; untreated MFC sheets had a χ_{cr} equal to 0.2. The mechanical fibrillation of native cellulose microfibres decreased the overall crystallinity of the native cellulose by 50 % but increased the surface area of the material. The TA-octadecylamine chemical surface treatment did not decrease the sample's crystallinity any further as demonstrated by the χ_{cr} value of the tannic acid-octadecylamine reacted MFC sheet (**Figure 6.7 b**). The powder sample obtained by grinding the dried tannic acid-octadecylamine-MFC material had a χ_{cr} of 0.2, indicating that neither the surface reaction of the tannic acid-octadecylamine, nor the grinding process further decreases the crystallinity of the MFC filler.

6.2.2 Differential scanning calorimetry (DSC) of the reinforced composites

DSC analysis was used to evaluate the melting and crystallization behaviour of the neat polymeric matrix and of the reinforced composites. The first heating curve obtained for each sample was used to determine the melting temperature of the materials and thus determine the optimum compounding and injection moulding temperatures. The first heating curves of the specimens were also used to evaluate the matrix's crystallinity fraction using Equation **13**:

$$\chi_{Cr\ DSC} = \frac{\Delta H}{\Delta H^{o}} \qquad \textbf{(13)}$$

where ΔH is the melting enthalpy calculated from the first heating curve of each specimen, and $\Delta H°$ is the melting enthalpy of a 100 % crystalline PP matrix, and is equal to 207.1 Jg^{-1}.[402] This value is used a best approximation of the PPPE based matrix as no accurate data are available for the system.

The analysis of the melting curves of the neat matrix and of the sample indicate a melting temperature of about 160 °C for the neat matrix and the reinforced composites, regardless of the reinforcement used. The melting temperature (T_m) of the individual samples are presented in **Table 6.3**. The overlapping peaks obtained for the neat PPPE matrix (**Figure 6.8 a**) are attributed to the possible segregation of the PP (T_m= 155 °C) and PE (T_m= 162 °C) in the original matrix. The addition of the fillers affects the crystallization process of the composite causing the complete overlap of the PP and PE melting peaks. The melting curves of the specimen were used to determine the optimum processing temperatures. All the samples were completely melted at temperatures above 180 °C; for that reason, the processing temperature used was above 180 °C. The optimum temperature was determined considering the viscosity of the melt and the degradation temperature of the individual samples.

The crystallinity of the neat matrix and the reinforced nanocomposites was calculated in order to investigate the influence of the fillers on the crystallinity of the composites obtained. The crystallinity of the sample $\chi_{Cr\ DSC}$ was estimated from the first heating curves of the individual samples (**Figure 6.8**). The results were compared with pure PPPE matrix to investigate the melting behaviour of the filled nanocomposites during the melting processes.

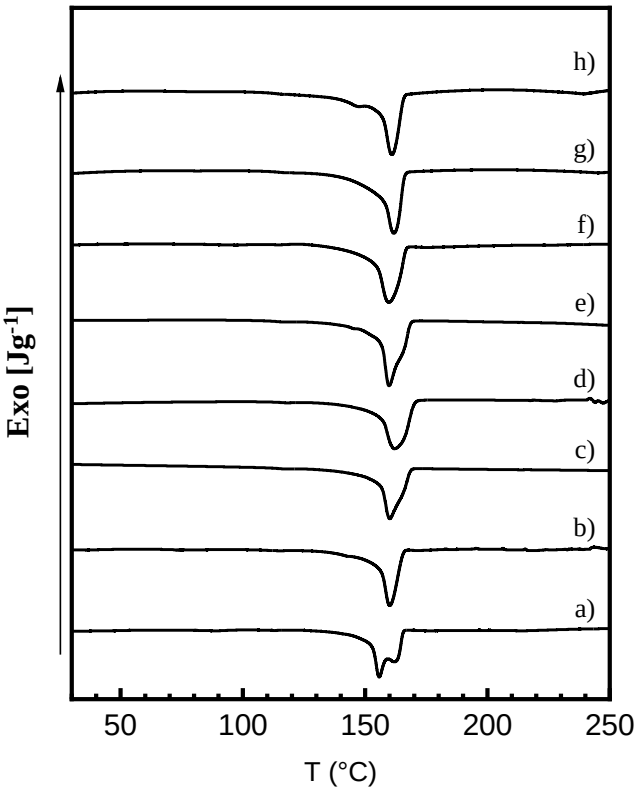

Figure 6.8 Typical DSC 1st heating thermograms of neat PPPE matrix a) 1 wt.% MAgPP-MFC reinforced composite b) 1 wt.% myristoyl chloride-MFC reinforced composite c) 1 wt.% PVOH-MFC reinforced composite d) 1 wt.% PEO-MFC reinforced composite e) 1 wt.% TA-octadecylamine-MFC reinforced composite f) 1 wt.% talc reinforced composite g) 1 wt.% glass fibres reinforced composite h).

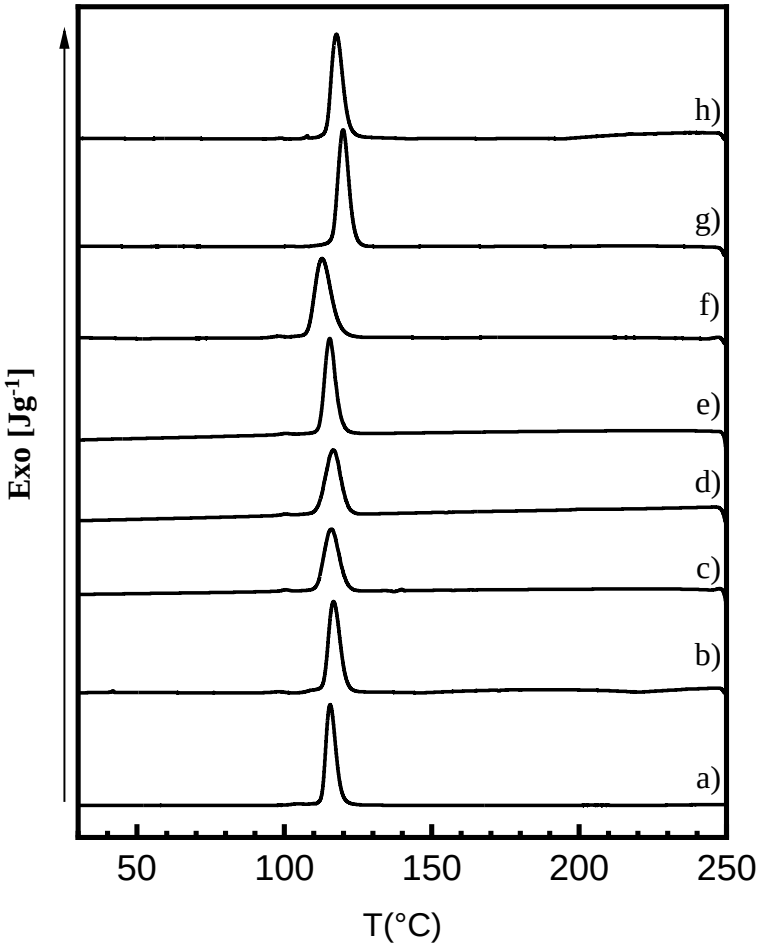

Figure 6.9 Typical DSC 1st cooling thermograms of neat PPPE matrix a) 1 wt.% MAgPP-MFC reinforced composite b) 1 wt.% myristoyl chloride-MFC reinforced composite c) 1 wt.% PVOH-MFC reinforced composite d) 1 wt.% PEO-MFC reinforced composite e) 1 wt.% TA-octadecylamine-MFC reinforced composite f) 1 wt.% talc reinforced composite g) 1 wt.% glass fibres reinforced composite h).

The PPPE matrix had a crystallinity fraction of $\chi_{Cr\,DSC} = 0.39$; the crystallinity calculated from the DSC thermogram is in good accordance with values calculated from XRD analysis. The crystallization peak occurs at 116 °C (**Figure 6.9**) and the melting temperature on the first heating scan occurs at 160 °C, therefore the PPPE neat matrix had a T_m of 160 °C and a T_c of 116 °C.

The crystallinity index of the 1 wt.% reinforced composites was determined to be affected only marginally by the different types of surface chemistry used to compatibilize the cellulose fibrils. The values of crystallinity fraction for the 1 wt.% reinforced composites are reported in **Table 6.3**.

The myristoyl chloride surface treatment was confirmed to interfere with the matrix crystallization process; in fact, the 1 wt.% myristoyl chloride-MFC reinforced composites had an overall crystallinity index calculated from DSC thermogram of 0.3, lower than the crystallinity index of the neat matrix and confirming the unsuitability of the myristoyl chloride surface treatment in the production of stable compatibilized MFC based filler.

The DSC crystallinity analysis was also conducted on composites containing inorganic fillers (talc and glass fibres) to compare the melting and crystallization behaviour of the MFC reinforced nanocomposites with their inorganic counterparts. The talc-reinforced sample shows a higher crystallinity index that the neat matrix $\chi_{Cr\ DSC}$=0.45, due to a nucleating effect of the filler. The glass fibre reinforced sample, on the other hand, exhibited a crystallinity index of 0.3, lower than the one of the neat matrix. This is thought to be due to the presence of the long glass fibres within the matrix which increase the melt viscosity at the operational temperature and consequently strongly limit the polymer chain mobility during the crystallisation process.

The crystallinity values calculated from XRD diffraction patterns and DSC thermograms of the reinforced samples differ considerably in some cases. The DSC crystallinity indices are considered more reliable in this case because of the overlapping of some of the cellulose and matrix peaks in the XRD analysis and because the dataset obtained from DSC only consider the matrix melting behaviour as neither of the fillers melt.

Table 6.3 Crystallinity index, crystallization and melting temperatures of pure PPPE matrix and 1 wt.% reinforced nanocomposites.

Sample ID	**$\chi_{Cr\ DSC}$ (-)**	**Tc (°C)**	**Tm (°C)**
PPPE	0.39	116	160
1 wt.% MAgPP-MFC composite	0.38	116	160
1 wt.% myristoyl chloride-MFC composite	0.34	116	160
1 wt.% PVOH-MFC composite	0.37	116	162
1 wt.% PEO-MFC composite	0.37	116	160
1 wt.% TA-C_{18}-MFC composite	0.38	116	162
1 wt.% talc composite	0.45	122	162
1 wt.% glass fibres composite	0.30	121	162

6.2.2.1 Crystallinity fraction of tannic acid/octadecylamine compatibilized MFC reinforced composites at different loadings

The tannic acid octadecylamine surface reaction proved to be an efficient and practical method to produce hydrophobic MFC fibrils. Therefore, a series of nanocomposites at different loadings were produced, and their DSC crystallinity indices were calculated to investigate the effect of increasing filler loadings on the crystallization behaviour of the composites. The tannic acid-octadecylamine-MFC reinforced composites all show similar DSC thermograms (**Figure 6.10**). Regardless of the filler loading, the tannic acid-octadecylamine reinforced sample had a Tc, calculated from the cooling scan, of 116 °C and a Tm, calculated from the second heating scan, of 162 °C.

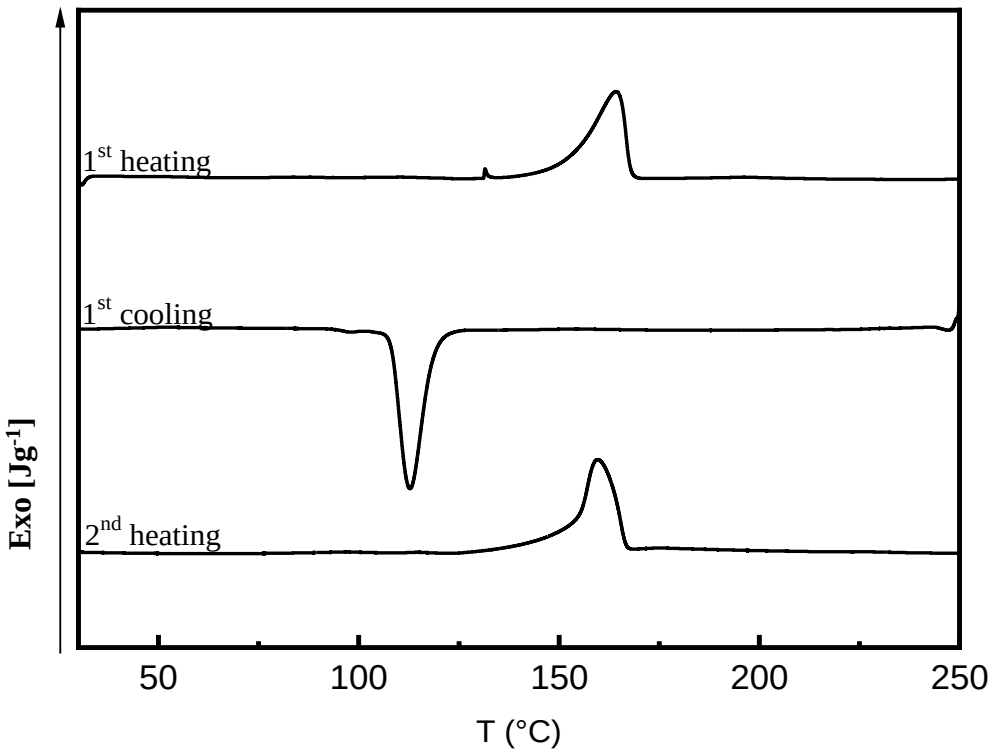

Figure 6.10 Typical DSC thermograms of tannic acid-octadecylamine-MFC reinforced composites.

The addition of tannic acid octadecylamine compatibilized MFC was found to marginally affect the crystallinity of the composites produced. These samples exhibited crystallinity indices (**Figure 6.11**) in the range 0.37 (15 wt.% tannic acid-octadecylamine-MFC reinforced composite) to 0.50 (0.5 wt.% tannic acid-octadecylamine-MFC reinforced composite). The results recorded suggests that the increase the filler content affect the crystallinity of the samples in a complex way. From the crystallinity data, a trend relating the filler load to the crystallinity index cannot be extrapolated. Due to the complex nature of the system under analysis, the modification of the canonical method for the DSC crystallinity fraction evaluand would be advisable.

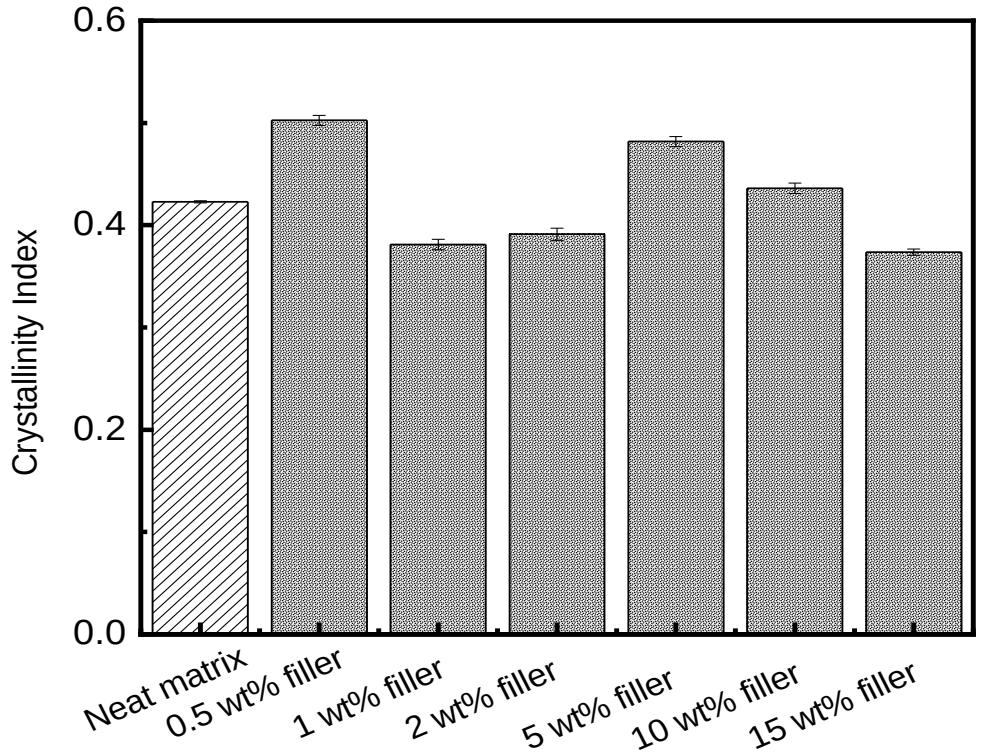

Figure 6.11 DSC crystallinity fraction calculated for the neat PPPE sample, and the reinforced composites. The crystallinity index for the 0.5 wt.% TA-C_{18}-MFC reinforced composite is 0.50±0.01, for the 1 wt.% TA-C_{18}-MFC reinforced composite is 0.38±0.05, for the 2 wt.% TA-C_{18}-MFC reinforced composite is 0.39±0.06, for the 5 wt.% TA-C_{18}-MFC reinforced composite is 0.48±0.05, for the 10 wt.% TA-C_{18}-MFC reinforced composite is 0.43±0.05, and for the 15 wt.% TA-C_{18}-MFC reinforced composite is 0.37±0.03.

6.2.3 Thermogravimetric analysis (TGA) of cellulose fillers

Thermogravimetric analysis was used to determine the water content of the MFC slurry (**Figure 6.12**) and to determine the thermal stability of the neat polymer matrix, the untreated dry MFC, and of the surface reacted MFC filler. The degradation temperatures of the compatibilized fillers were used to determine the maximum operating temperature to be used to process the composites. The cellulose-based reinforced composites were all prepared at temperatures below the filler's degradation temperature.

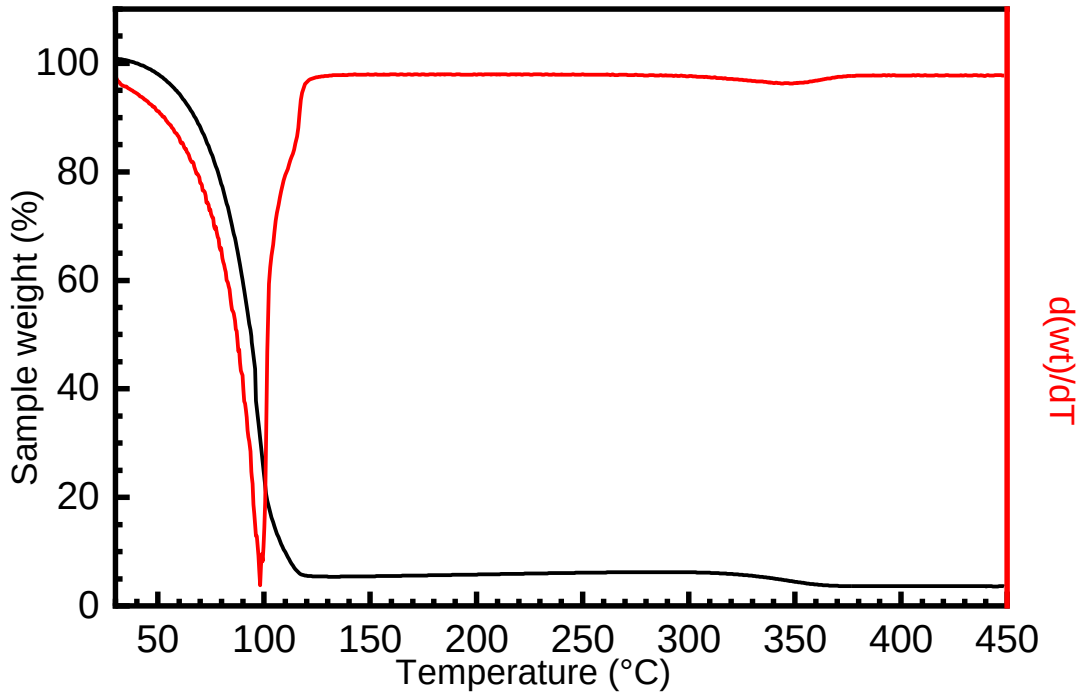

Figure 6.12 General thermogravimetric diagram of the unreacted MFC slurry showing weight loss (black) and differentiated weight loss with respect to temperature (red). The onset degradation temperature was 99 °C, the water content was estimated to be 95 wt.% and the residue at 450 °C was 3 wt.%.

Thermogravimetric analysis data for untreated MFC slurry is shown in **Figure 6.12**. The data confirmed solid contents in the MFC slurry of 5 wt.% (95 wt.% water). The degradation temperature of the unreacted MFC dried films was obtained from an independent thermogravimetric analysis presented in **Figure 6.13**; found to be ≈310 °C

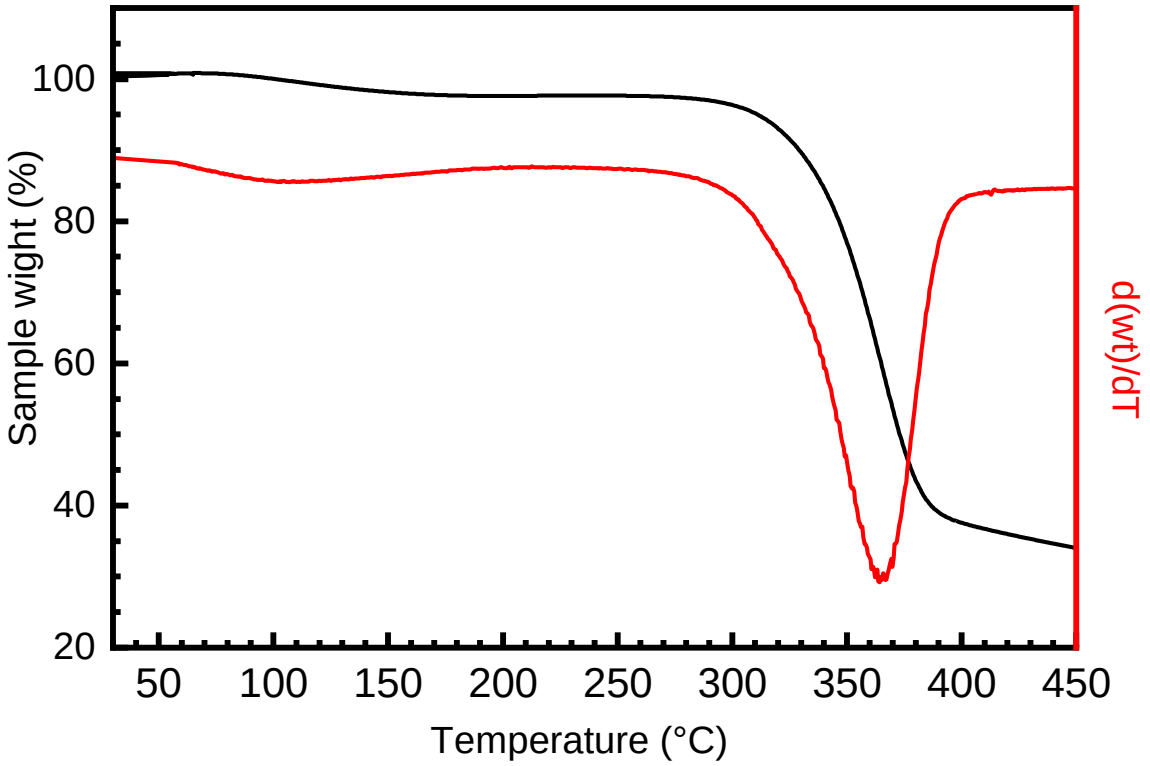

Figure 6.13 General thermogravimetric diagram of the dried unreacted MFC showing weight loss (black) and differentiated weight loss with respect to temperature (red). The onset degradation temperature was between 250 and 300 °C and the residue at 450 °C was 30 wt.%.

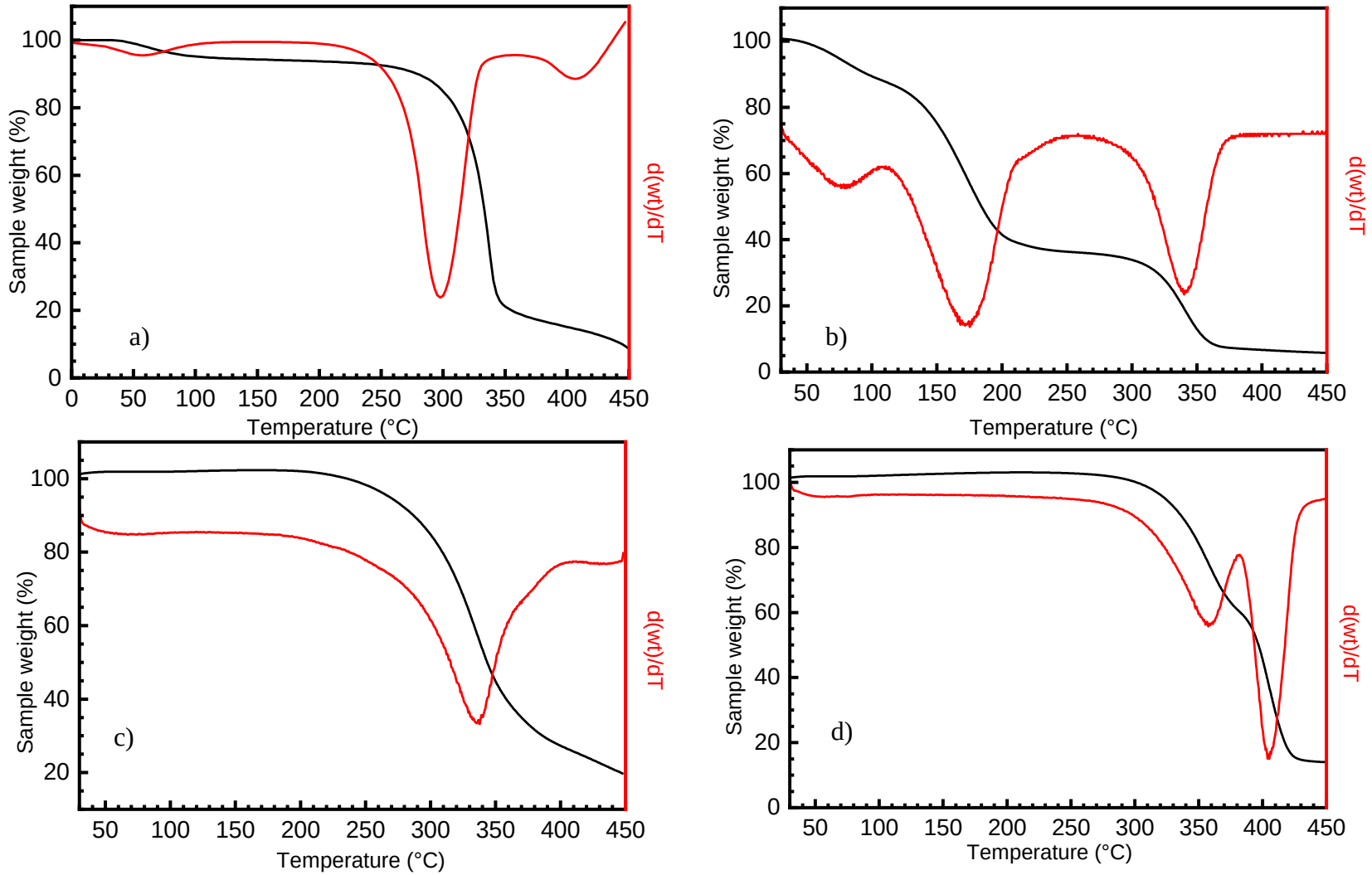

Figure 6.14 Typical thermogravimetric diagrams of MAgPP-MFC onset degradation temperature 240 °C a), myristoyl chloride-MFC onset degradation temperature <100 °C b), PVOH-MFC onset degradation temperature 210 °C c), PEO-MFC onset degradation temperature 280 °C d), showing weight loss (black) and differentiated weight loss with respect to temperature (red).

MAgPP compatibilized MFC filler exhibited an onset degradation temperature of 240 °C (**Figure 6.14 a**), which is lower than the unreacted MFC. The decrease in the onset degradation temperature of the MAgPP reacted filler is possibly due to the instability of the ester linkage formed between the C6 hydroxyl of cellulose and the MAgPP. The thermal instability of the compatibilized filler represents one of the major disadvantages of the use of MAgPP as a compatibilizing agent, along with the necessity of using organic solvents during the compatibilization procedure.

The myristoyl chloride compatibilized MFC has low thermal stability compared to unreacted MFC; the myristoyl chloride compatibilized MFC (**Figure 6.14 b**) exhibited two separate degradation peaks. The first suggested an onset degradation temperature <100 °C and an estimated weight loss of about 60 %. The second degradation peak occurred at 290 °C and accounted for ~ 30 % weight loss.

The thermal instability of the myristoyl chloride compatibilized MFC samples was partially attributed to the degradation of the ester linkages formed during the compatibilization procedure between the C6 hydroxyl group of cellulose and myristoyl chloride. It may be also partially attributed to an early cellulose degradation caused by the residues of pyridinium chloride trapped in the networked structure of the MFC. The higher degradation temperature, recorded at 290 °C, is thought to be attributed to the degradation of the unreacted cellulosic structure. The myristoyl chloride compatibilized MFC samples' low degradation temperature is not compatible with melt processing procedures used in the present study. Therefore, the myristoyl chloride based MFC surface reaction was dismissed early on in this study as unsuitable. The onset degradation temperature of PVOH compatibilized MFC (**Figure 6.14 c**) was found to be ≈210 °C, and the onset degradation temperature of the PEO reacted MFC (**Figure 6.14 d**) was ≈280 °C. All the surface treatments appear to affect the thermal stability of the MFC, however, the MAgPP, the PVOH, and the PEO surface treatment did not compromise the thermal stability of the produced fillers.

6.2.3.1 Tannic acid octadecylamine compatibilized MFC thermal stability

The thermogravimetric diagrams of the pure TA, octadecylamine, and tannic acid octadecylamine compatibilized MFC film were recorded to investigate the samples' thermal stability. The pure tannic acid powder and the octadecylamine exhibited onset degradation temperatures of 220 °C and 170 °C respectively, as shown in **Figure 6.15 a** and **6.15 b**. The PPPE neat matrix exhibited an onset degradation temperature of 250 °C (**Figure 6.16**).

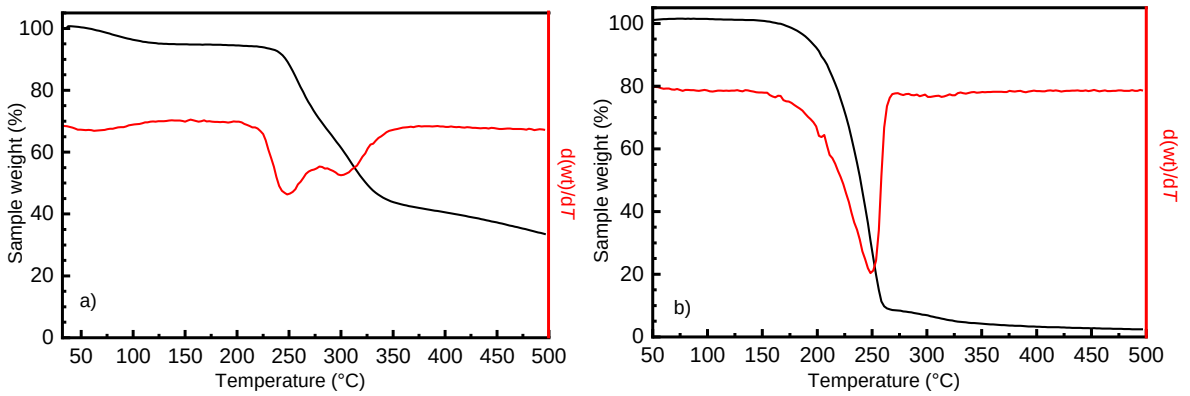

Figure 6.15 Thermogravimetric analysis of the pure tannic acid (TA) a) and pure octadecylamine ($C_{18}H_{37}NH_2$) b) showing weight loss (black) and differentiated weight loss with respect to temperature (red).

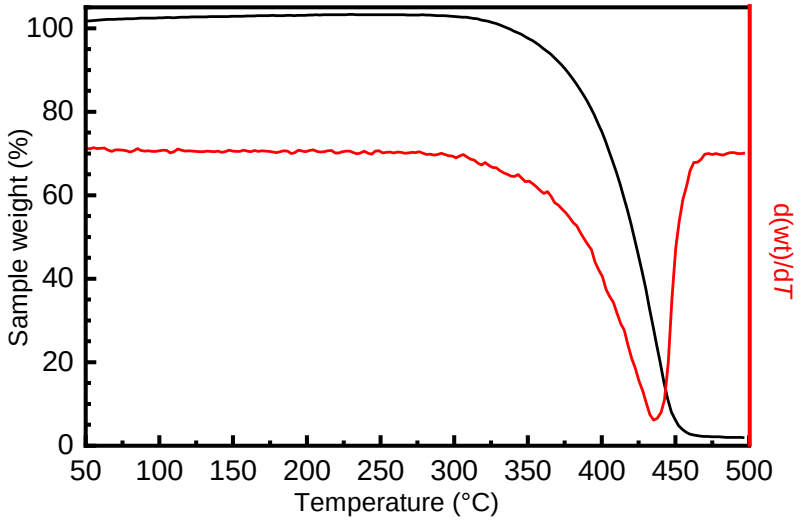

Figure 6.16 Thermogravimetric analysis of the neat PPPE matrix onset degradation temperature 250 °C showing weight loss (black) and differentiated weight loss with respect to temperature (red).

The tannic acid-octadecylamine reacted MFC thermogram showed an initial weight loss of the sample between 50 and 100 °C of about 5 % attributed to the residual moisture content in the sample. A further decrease in the sample weight was registered between 100 and 250 °C, attributed to the degradation of the residual unreacted octadecylamine and tannic trapped in the network structure of the MFC, and a further thermal degradation around 200 °C. The main degradation process in the tannic acid-octadecylamine reacted MFC sample had an onset degradation temperature of 260 °C (**Figure 6.17**). The overall thermal stability of the tannic acid-octadecylamine reacted MFC filler was suitable for thermoplastic manufacturing processes. In fact, the filler did not undergo major thermal degradation at the selected operational temperature (210 °C).

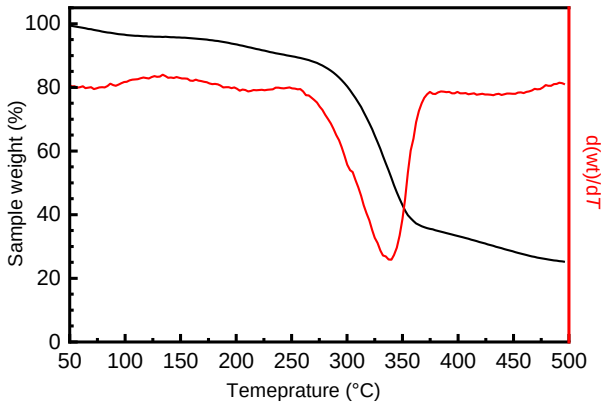

Figure 6.17 Thermogravimetric analysis of the tannic acid-octadecylamine-MFC filler onset degradation temperature 260 °C showing weight loss (black) and differentiated weight loss with respect to temperature (red).

Compounding tannic acid-octadecylamine treated MFC powder with PPPE further increased the thermal stability of the final composite. The thermograms in **Figure 6.18** compare the thermal stability of the melted filler-matrix powder mixture with the thermal stability of the composites obtained from the compounder. When the compatibilized filler was mixed with the matrix the two components showed the thermal behaviour of two separate materials with a first onset degradation temperature of ≈250 °C (**Figure 6.18 a**). When the reinforcement and the matrix are compounded, a different behaviour is recorded: the characteristic thermogram of a unique material shown in **Figure 6.18 b**. The reason for the change remains unclear, however, it is possible to speculate that the cellulose fibrils forms structure around the polymer lumps and that said structure trap the gas formed during the polymer thermal degradation initial phase.

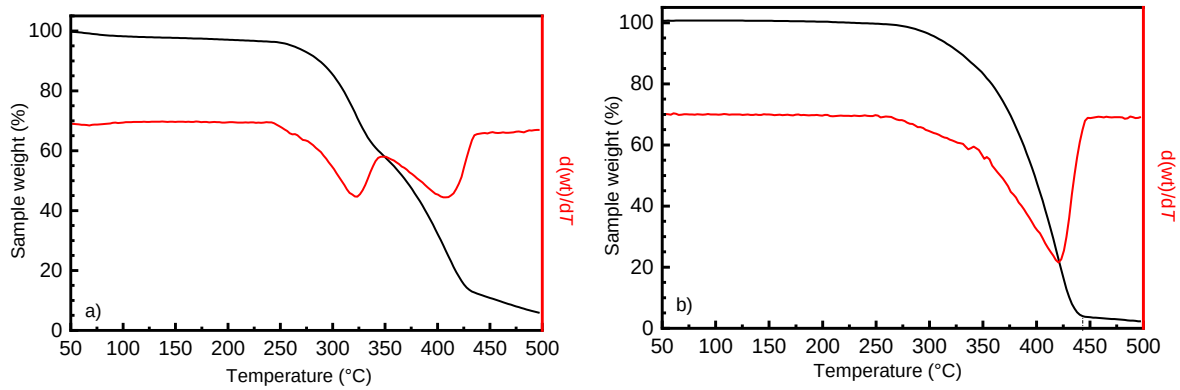

Figure 6.18 Thermogravimetric analysis of the melted matrix-filler mixture for the tannic acid-octadecylamine-MFC and PPPE powder a) and compounded tannic acid octadecylamine-MFC composite b) showing weight loss (black) and differentiated weight loss with respect to temperature (red).

In summary: A series of organic solvents and water-based surface reaction methods were selected from the relevant literature on cellulose reinforced composites to investigate the production of hydrophobic thermostable forms of compatibilized MFC. Organic solvent methods first transferred the MFC from water into the solvent *via* a series of filtration, washing and resuspensions steps, then conducted a surface reaction with myristoyl chloride (MCl) or MAgPP. The reaction with myristoyl chloride proved to be detrimental to the structure of the cellulose fibrils and to the thermal stability of the MFC. The compatibilized filler must be able to withstand the temperature range used in the manufacture of the composites, which could be up to 210 °C. Myristoyl chloride compatibilized MFC was found to have an onset degradation temperature of <100°C, a value related to the instability of the ester bonds formed between cellulose and MCl and to the incipient degradation of both the cellulose and the polymer matrix induced by the chemistry used. The MCl treated MFC was thus found to be incompatible with further polyolefin processing. The thermal instability of the MCl reacted MFC also caused major matrix degradation in the composites and resulted in poor mechanical performance. The esterification reaction requires the addition of a base, in this case pyridine, to neutralise the HCl reaction product. The main cause of the reduced thermal stability of MCl-MFC was attributed to the residual presence of the pyridinium chloride salt, formed during the surface reaction between cellulose and myristoyl chloride. The pyridinium chloride salt was mainly insoluble in the reaction medium and difficult to remove with organic solvents.

The MAgPP based MFC compatibilization was successful in producing a hydrophobic and thermally stable form of MFC filler. The MAgPP compatibilization method was also indicated in the literature as a suitable method to prepare a hydrophobic, dispersible form of nanocellulose.[364] For this reason, this approach was used to determine the dispersion of the reference filler, and the mechanical properties of a compatibilized MFC reinforced composite. The MAgPP esterification reaction of the MFC fibrils was carried out in organic solvents and requires a set of solvent swap steps, and thus was not considered applicable as a production method in this study. Nevertheless, the MFC compatibilized with MAgPP had an onset degradation temperature of 240 °C which was slightly lower than for the unreacted MFC of 250 °C, but compatible with the polymer matrix processing temperatures.

Both PVOH and PEO compatibilized MFC fillers retained the original thermal stability of the untreated MFC, presenting degradation temperatures above the polymer processing temperature.

The PVOH compatibilized MFC filler had a degradation temperature onset of 210 °C, compatible with the selected conditions for processing the composites.

The SEM images of the PVOH-MFC filler revealed a well-preserved networked structure of the freeze-dried compatibilized filler, a structure that can enhance the filler dispersion in the matrix. The PVOH compatibilizer has pendant hydroxyl groups from its aliphatic backbone which can create a hydrogen-bonded network with cellulose hydroxyl groups, while the aliphatic backbone provides a hydrophobic surface that can interact favourably with the polyolefin matrix. However, the PVOH-MFC reinforced composites proved to perform poorly in terms of composite stiffness; in fact, a net decrease in modulus compared to the neat matrix was registered for the reinforced composites; this decrease was attributed to the poor compatibility between PVOH compatibilized MFC fibrils and the matrix. Due to the necessary use of the freeze-drying technique to obtain a processible PVOH-MFC filler, and due to the poor mechanical performance of the reinforced composites, no further studies were scheduled for the PVOH compatibilizer.

PEO reacted MFC filler had an onset degradation temperature of 280 °C, which is comparable with the onset degradation temperature of unreacted MFC films. As in the case of PVOH reacted MFC filler, a freeze-drying step was necessary to obtain a processible material. SEM imaging of the PEO-MFC reinforced composites showed what appeared to be well-dispersed PEO-MFC fibrils in the polymeric matrix. The diffraction pattern and differential scanning calorimetry (DSC) of PEO compatibilized MFC reinforced composites at a 1 wt.% filler loading showed these samples had a crystallinity fraction of 0.37, close to that of the pure PPPE matrix (of 0.4).

The PEO-MFC reinforcement did not affect the melting or crystallization behaviour of the PPPE matrix, but neither did it affect the tensile properties of the composites. This is believed to be due to the poor surface interaction between filler and matrix which prevented any stress transfer to the fibres.

Due to the necessary freeze-drying preparation step, and also the unsatisfactory tensile performance of the PEO-MFC reinforced composites, no further studies were conducted on this compatibilized filler.

The water-based reaction of tannic acid (TA) and primary aliphatic amines (water-soluble hexylamine and water insoluble octadecylamine) with never-dried MFC slurry was selected as the most effective and industrially applicable methodology to modify the hydrophilicity of the cellulose fibrils and enhance their dispersibility in the apolar polyolefin matrix.

The tannic acid surface reaction was based on previous work on polyphenols, and it proved to be an efficient method to modify the surface of cellulose fibrils to make them a suitable substrate to covalently attach aliphatic primary amines by a Schiff base reaction or a Michael addition.

The methodologies developed in the literature used a large excess of the primary amine to ensure the complete reaction of the cellulose-tannic acid-activated site.

However, the large excess of primary amine (TA amine molar ratio = 1:250) was difficult to remove from the compatibilized filler due to the networked structure of the final product. This was found to have a detrimental effect on the preparation of the reinforced composites. Therefore, a first step in the production of these materials was the optimisation of the MFC:tannic acid:primary amine ratio. The amines used in this study were the short-chain hexylamine, which is water-soluble, and the longer-chain octadecylamine. The hexylamine was shown to be unsuitable for assisting the dispersion of compatibilized MFC fillers. The octadecylamine, in contrast, was found to efficiently decrease the surface energy of the final product to a level more suitable for dispersing it in the PPPE matrix.

The MFC:tannic acid:primary amine ratio optimization was calculated for the octadecylamine reagent by washing the unreacted amine from the product with acetone and calculating the concentration of the excess amine in the solution using a spectrophotometric method. The optimum MFC-tannic acid-octadecylamine ratio was found to be 10g-MFC dry fibrils:5g-tannic acid:5g-octadecylamine.

This ratio was then used to prepare the TA-octadecylamine based MFC fillers. The details of the reaction between the tannic acid activated MFC fibrils and the octadecylamine are not fully understood and are beyond the scope of the present study. Nevertheless, the reaction probably involves the formation of a Schiff base as a final product. FTIR spectroscopy was used to verify the formation of the Schiff base in the compatibilized MFC products. FTIR spectra of the tannic acid-octadecylamine reacted MFC indicated the presence of a strong absorption between 2800 and 3000 cm^{-1} possibly related to the presence of covalently attached amines. The formation of a small peak between 1400 and 1500 cm^{-1} in the reacted MFC samples suggests the formation of the Schiff base and thus the successful covalent attachment of the primary amine to the tannic acid-MFC activated reagent.

The compatibility between filler and matrix remains one of the main problems in the production of reinforced composites. An indication of the filler-matrix compatibility was given by the hydrophilicity-hydrophobicity character of the components. The water and bromonaphthalene (BN) contact angles of tannic acid-octadecylamine-MFC films and PPPE polymer, were recorded and used to determine the compatibility of the reacted MFC based filler with the selected matrix (PPPE). The compatibilized MFC films were found to be hydrophobic, a favourable condition for efficient interaction with the apolar PPPE matrix. The MFC cellulose films were, however, reported to be porous, a condition that does not fully comply with rigorous contact angle and free surface energy evaluations.

For that reason, a more reliable model was used to investigate the water and BN contact angle and free surface energy of the compatibilized nonporous cellulose-based films. The selected substrate was a non-porous cellophane film, which was also reacted with tannic acid and octadecylamine and washed with acetone, to mimic the MFC processing. The contact angles values obtained from reacted MFC and cellulose films were comparable indicating a hydrophobic behaviour, a and low free surface energy was reported for the reacted cellophane system. Only the data obtained from the cellophane model system were used in further theoretical evaluations of the filler-matrix behaviour in the produced composites.

Another relevant requirement to produce homogeneously-dispersed composites is to prevent the components from separating before compounding. To obtain that result the matrix and the filler were both powdered and mixed together. The compatibilized MFC powder was obtained by grinding the dried samples at room temperature using a JK-mill.

The crystallinity fraction was calculated for the native cellulose, untreated MFC dry pellets, tannic acid-octadecylamine-MFC films and mechanically produced tannic acid-octadecylamine-MFC powder.

Thermal stability of the cellulose filler is another relevant parameter to be taken into consideration when choosing the operating conditions for the production of the composites.

The thermogravimetric analysis of the compatibilized MFC sample was used to determine the maximum operational temperature to be used during the compounding. The tannic acid-octadecylamine-MFC sample had a degradation temperature onset of 260°C and thus it is suitable for further processing alongside the PPPE matrix selected.

The crystallinity of the reinforced composites can affect both tensile and impact properties significantly. For that reason, the melting and crystallization behaviour of the pure matrix, inorganic and treated MFC filled nanocomposites have been investigated. The modest addition of talc to the matrix does not affect its crystallinity ($\chi_{Cr} = 0.4$) while in the case of the GFs reinforced composite the crystallinity decreased to 0.3. The addition of MAgPP-MFC and tannic-octadecylamine-MFC only marginally changed the crystallinity of the pure matrix at the different concentrations. Higher additions of tannic acid-octadecylamine-MFC filler to the matrix had a much greater impact on the crystallinity of the composite, which reached a maximum value of 0.5 at a 0.5-5 wt.% tannic acid-octadecylamine-MFC filler addition. Nevertheless, the variation of the crystallinity fraction registered for the reinforced composites was only large enough to marginally affect the performance of the composites.

6.3 Characterisation of the filler and its dispersion in the composites

In the next paragraph, a series of analytical tools are presented to investigate the dispersion of the MFC fillers in the composites. The level of filler dispersion is then correlated with the mechanical and impact properties of the samples produced.

6.3.1 Scanning electron microscope (SEM) and Energy-dispersive X-ray spectroscopy (EDX) imaging of cellulose fillers and composites

SEM images of the untreated, of films of a) untreated MFC, b) MFC treated with tannic acid and c) MFC treated with tannic acid and octadecylamine were captured to identify the morphological differences among the samples. All the samples had in common the characteristic networked morphology typical of MFC (**Figure 6.19**). The MFC treatment with both tannic acid first and octadecylamine later appeared to mitigate the ability of the MFC to form densely packed networks when manufactured in films. Because the samples were washed with acetone it would be unlikely the lumps are formed from octadecylamine residues. It is more likely the aggregates are formed by bundles of cellulose fibrils.

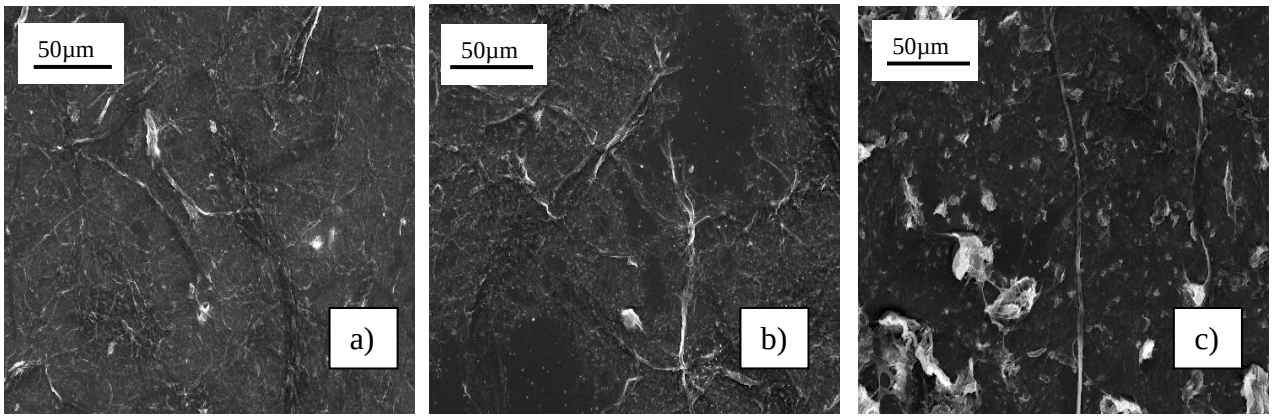

Figure 6.19 SEM images of the film surfaces of untreated MFC a), tannic acid activated MFC b), and tannic acid-octadecylamine reacted MFC c) films.

EDX imaging was used to establish the filler dispersion in the composites produced. The concept is to create a 2D map of the composites with only two contributions: the carbon and the oxygen signals. The carbon contribution was mainly attributed to the polymeric matrix, while the oxygen contribution was attributed to the cellulose-based reinforcement.

Unfortunately, neither the carbon or the oxygen signal can be completely attributed to the matrix, or to the cellulose. However, EDX imaging technique can be used for a general idea of the filler dispersions of the MAgPP- and tannic acid octadecylamine-MFC reinforced composites.

The EDX images of the transverse surfaces of MAgPP-MFC and tannic acid-octadecylamine-MFC reinforced composites were collected to investigate the MFC dispersion in the matrix and evaluate the size of the visible MFC aggregates.

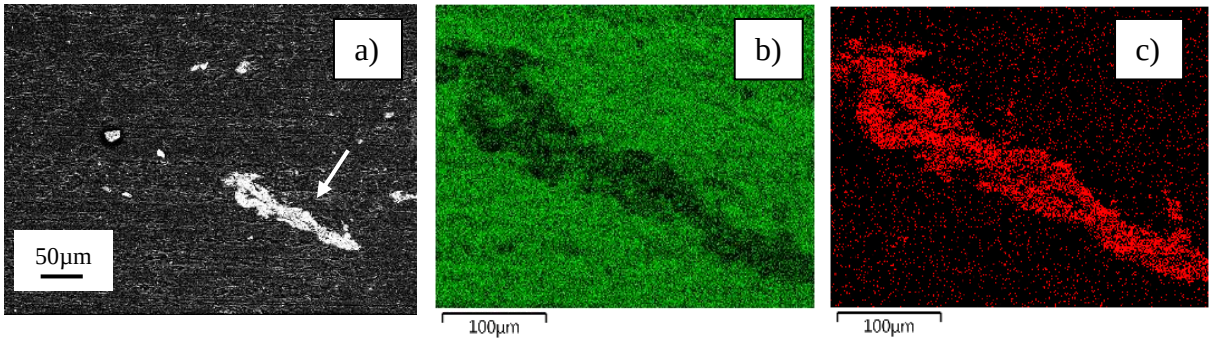

Figure 6.20 Typical Back-scattered Electron Diffraction (BED) and energy-dispersive X-ray spectroscopy (EDX) images of 1 wt.% MAgPP-MFC reinforced composites. From left to right: (a) greyscale image of a large agglomerate (identified with an arrow); (b) back-scattered image of the large agglomerate where carbon is identified with green colour; (c) back-scattered image of the agglomerate, where oxygen is identified in red.

In **Figure 6.20** a typical back-scattered electron diffraction image and the energy-dispersive elements contribution image for a 1 wt.% MAgPP-MFC reinforced composite are presented. The aggregate size was found to be of the order of 100 µm. In **Figure 6.21** a back-scattered electron diffraction image and the energy-dispersive elements contribution image for a 1 wt.% tannic acid-octadecylamine-MFC reinforced composite are presented. The aggregate size of the tannic acid-octadecylamine-MFC reinforced composites was evaluated to be in the range of 25 - 100 µm. The oxygen signal is greater in the tannic acid-octadecylamine-MFC sample, potentially indicating the presence of smaller well-dispersed fibrils. Owing to the lack of specificity of the oxygen signal which can be derived from cellulose, but also from external or internal contaminants (*e.g.* presumed minerals or tannic acid), no conclusions can be drawn on the filler dispersion, based on the EDX imaging.

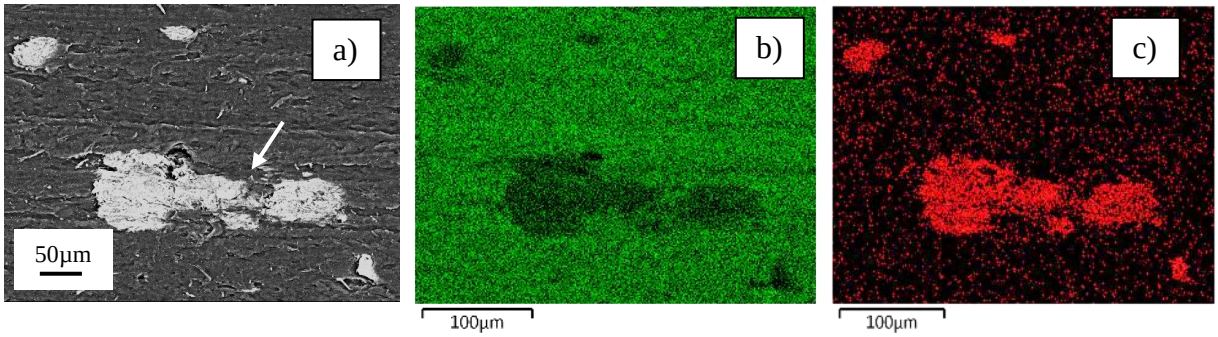

Figure 6.21 Typical Back-scattered Electron Diffraction (BED) and energy-dispersive X-ray spectroscopy (EDX) image of 1 % MFC-TA-C_{18} reinforced composites. From left to right: (a) greyscale image of a large agglomerate (identified with an arrow); (b) back-scattered image of the large agglomerate where carbon is identified with green colour; (c) back-scattered image of the agglomerate, where oxygen is identified in red.

6.3.2 Transmission electron microscopy (TEM) imaging of reinforced composites

EDX analysis showed that the tannic acid-octadecylamine-MFC filler was not uniformly dispersed in the composites, having identified large aggregates (100 µm in size) and a semi-continuous background characterised by the presence of the oxygen signal. The oxygen signal in the background could be caused by a variety of factors, one of which could be the dispersion of smaller fibrils in the composites. For that reason, the tannic acid-octadecylamine-MFC reinforced composites were investigated using TEM imaging at high magnification. **Figure 6.23** shows typical high magnification TEM images of cross-sections of the 0.5 wt.% tannic acid-octadecylamine-MFC reinforced composites. In the images dark lumps smaller than 10 µm are visible (white arrows).

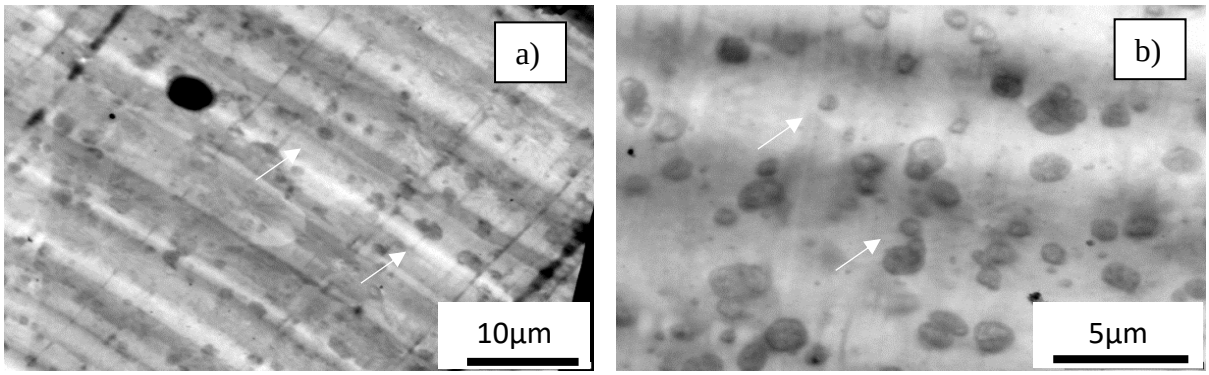

Figure 6.22 TEM images at 1700X low magnification a) and 4200X high magnification b) thin layer of 0.5 wt.% tannic acid-octadecylamine-MFC reinforced composite.

Figure 6.23 present the high magnification TEM images of cross-sections of the 15 wt.% tannic acid-octadecylamine-MFC reinforced composites. Also, in this case, dark lumps smaller than 10 μm are visible. The nature of the visible lumps in the composites remain unclear. It is possible to assume they are formed by cellulose fibrils, however the regularity of their shape and the absence of any other fibril like feature in the picture suggest otherwise. Further investigation to clarify the level of dispersion of the compatibilized MFC filler became mandatory.

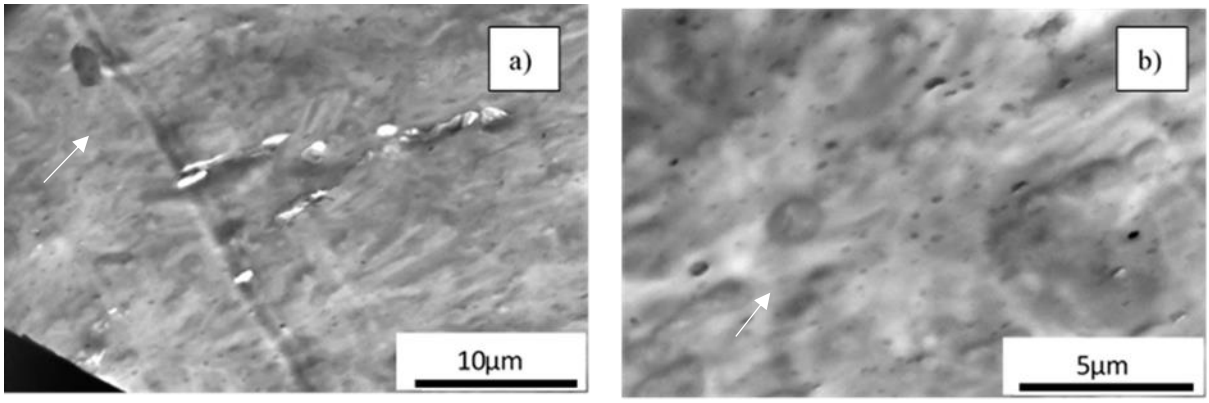

Figure 6.23 TEM images at 2550X low magnification a) and 4200X high magnification b) a thin layer of 15 wt.% tannic acid-octadecylamine-MFC reinforced composite.

TEM analysis on the MFC reinforced composites were impractical due to the necessity to obtain thin layers of composites and the poor difference in density and elemental composition between the filler and the matrix which made difficult to obtain a good contrast between the phases. For that reason, TEM was used only as a comparative technique in this research.

6.3.3 Time of flight-Secondary Ions Mass Spectroscopy (ToF-SIMS) mapping

ToF-SIMS is a mass spectroscopy-based technique that is widely applied to the medical and pharmaceutical field among others. It can be proficiently applied to composites to produce 2D maps of the distribution of cellulose within the composites. In the analysis, characteristic peaks were assigned to the matrix (fragment $C_5H_9^+$ at 69.1 m/z) and to the cellulose (fragment $C_{14}H_{23}O_5^+$ at 270.3 m/z) (see **Figure 6.24**). A magnified section of **Figure 6.24** is shown in **Figure 6.25** and **6.26** indicating the relative positions and intensities of the characteristic peaks selected as references for the matrix and the filler.

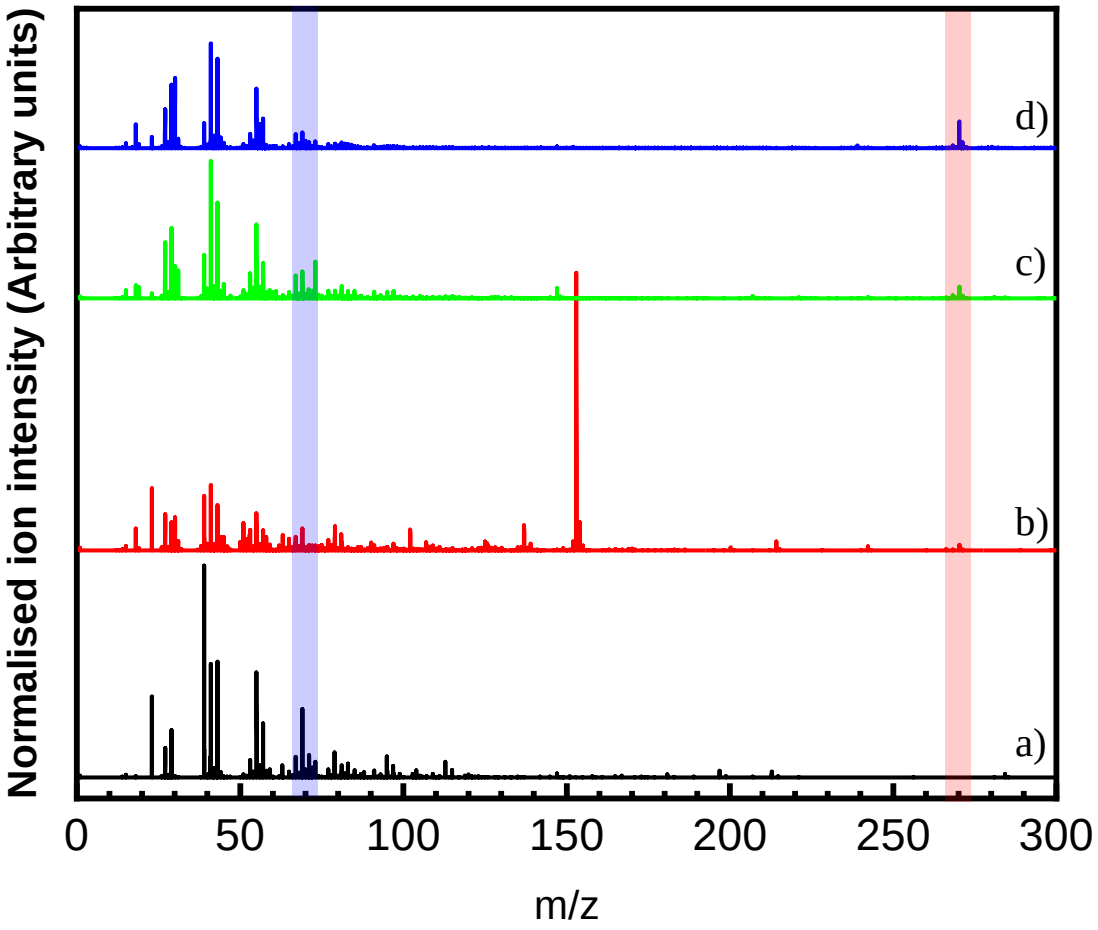

Figure 6.24ToF-SIMS mass spectra of polymeric matrix a), pure tannic acid b), untreated MFC c), tannic acid-octadecylamine-MFC film d). The section highlighted in blue represents the matrix peak region (fragment $C_5H_9^+$ at 69.1 m/z) while the section highlighted in red represents the filler peak region (fragment $C_{14}H_{23}O_5^+$ at 270.3 m/z).

Aggregates in the composites containing 5 wt.% of tannic acid-hexylamine-MFC were large and easy to identify, and so were assumed to be comprised mostly of cellulose and used to verify the peak assignment (**Figure 6.27**). Hexylamine is a water-soluble amine which should react with tannic acid in the same way as octadecylamine; however, its chain length was insufficient to reduce the cellulose fibrils' free surface energy and enhance their dispersion in the polymer matrix.

Large tannic acid-hexylamine-MFC aggregates were observed in the prepared composites (**Figure 6.27**). In the 2D reconstruction of the reference system, the cellulose signal located at 270 m/z, identified by a blue colour, is very distinctive from the signal from the matrix (in red; **Figure 6.27 b**). This shows that the ToF-SIMS mapping has the potential to resolve the cellulose filler from the matrix. ToF-SIMS 2D analysis was used to obtain a map for a 5 wt.% tannic acid-octadecylamine-MFC reinforced composites sample. The area selected for the analysis did not contain visible aggregates (**Figure 6.29**). The 2D reconstructed map (**Figure 6.30**) indicated a more homogeneous dispersion of the hydrophobic filler.

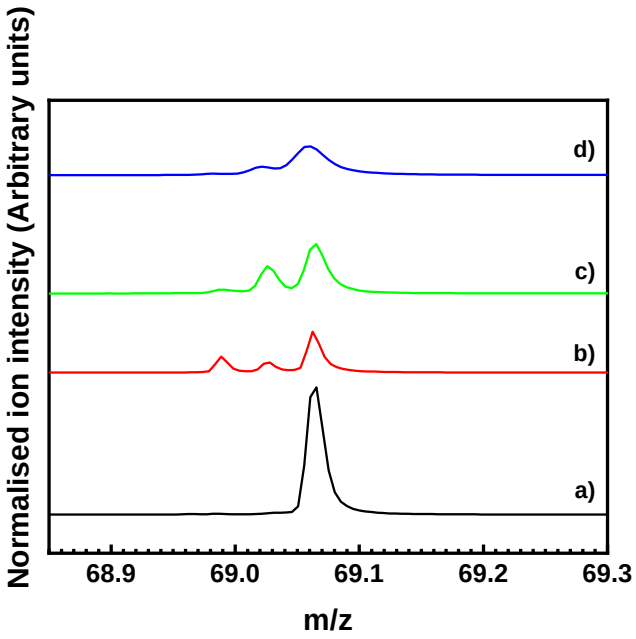

Figure 6.25 Typical ToF-SIMS mass spectra from the region containing the peak assigned to the polymer matrix (fragment $C_5H_9^+$ at 69.1 m/z). Pure matrix a), pure tannic acid b), untreated MFC c), tannic acid-octadecylamine-MFC film d).

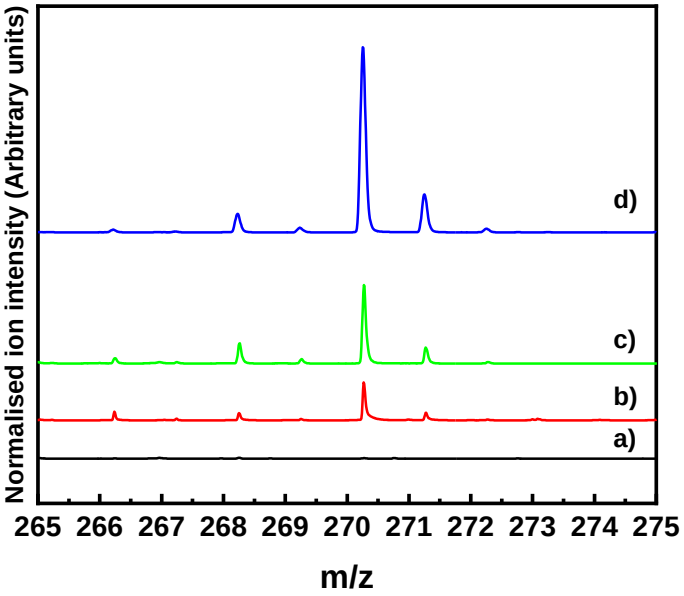

Figure 6.26 Typical ToF-SIMS mass spectra from the region containing the peak assigned to the cellulose (fragment $C_{14}H_{23}O_5^+$ at 270.3 m/z). Polymer matrix a), pure tannic acid b), untreated MFC c), tannic acid-octadecylamine-MFC film d).

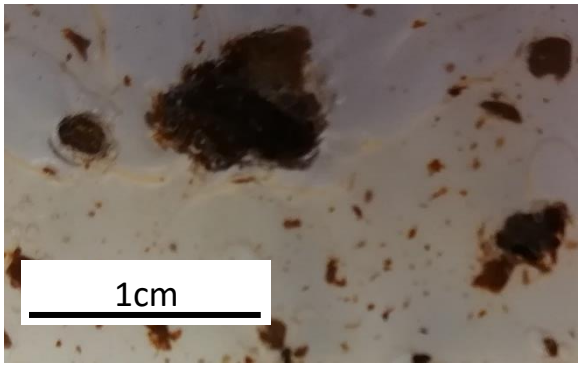

Figure 6.27 Picture of the TA-hexylamine-MFC reinforced matrix reference system; the short chain amine (hexylamine) is not efficient in promoting MFC dispersion in the apolar matrix.

The reference sample selected for ToF-SIMS analysis had a large agglomerate, which was used as a target for analysis. In the 2D reconstruction of the tannic acid-hexylamine-MFC reinforced composite images, the cellulose peak is indicated by a blue colour, while the red colour is representative of the matrix.

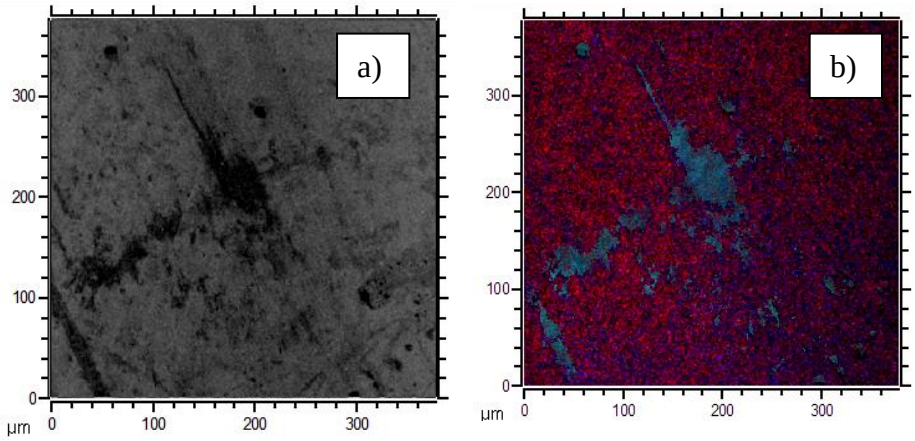

Figure 6.28 ToF-SIMS imaging of the tannic-hexylamine- reinforced composite used to verify the peak assignment. a) Optical image of the sample (greyscale), with a large agglomerate of cellulose reinforcement visible in the centre of the sample and b) a 2D reconstruction of the composite system using the assigned peaks: the red colour indicates the matrix and the blue colour indicates the presence of cellulose.

In **Figure 6.28 a,** a large tannic-acid-hexylamine-MFC agglomerate was identified. The 2D reconstruction confirmed the aggregate as cellulose, as identified by the blue signal. The cellulose signal is hardly identifiable in the matrix (in red), verifying the peak assignment for the filler and the matrix respectively.

The ToF-SIMS imaging of the 5wt.% tannic acid-octadecylamine-MFC composites was captured in an area containing a low concentration of large aggregates, as shown in the optical image in **Figure 6.29**.

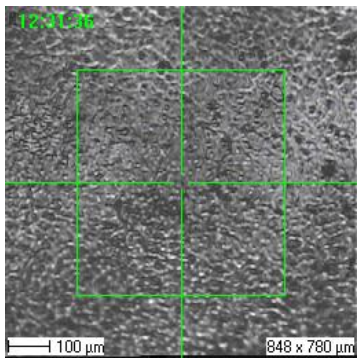

Figure 6.29 Optical image of the tannic-octadecylamine-MFC reinforced composite no large cellulose agglomerates are visible in the sample.

In the 2D reconstruction of the tannic acid-octadecylamine-MFC reinforced composite sample, the MFC filler appears well dispersed in the matrix at low magnification (blue signal **Figure 6.30 a**). At higher magnifications (**Figure 6.29 b** and **c**) a networked structure of the filler (blue) is visible, indicating the presence of small dispersed cellulose in the composite area between the large aggregates.

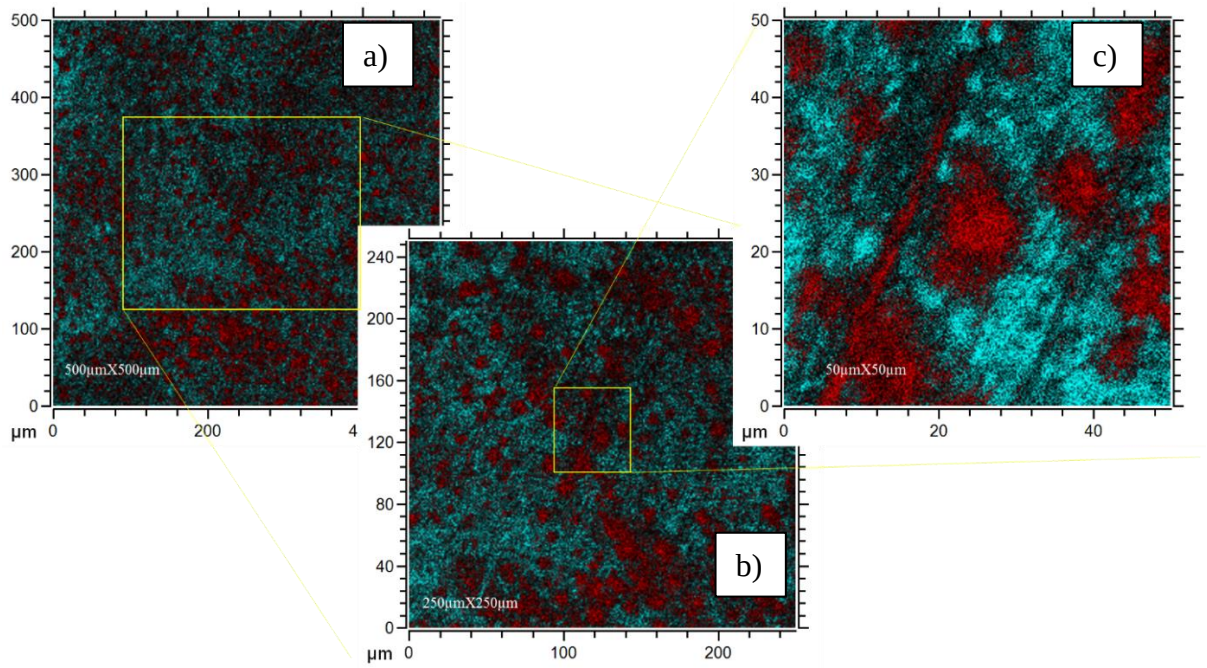

Figure 6.30 ToF-SIMS 2D reconstruction of the tannic acid-octadecylamine-MFC reinforced composite. The red colour indicates the matrix and the blue colour indicates the cellulose. The images are obtained at increasing magnification 500 × 500µm a), 250 × 250 µm b), and 50 × 50 µm c).

The effects on the size of the cellulose aggregates and their distribution in the PPPE matrix of the surface treatment, drying method and the process used to make the composites were investigated using ToF-SIMS imaging.

The MFC used was either never dried, vacuum oven dried or freeze dried and each of these was subsequently treated to introduce a different surface chemistry. The MFC preparations were then used to investigate MFC aggregate size and distribution within the PPPE-matrix. The three surface treatments were untreated MFC, tannic acid-hexylamine-MFC, and tannic acid-octadecylamine-MFC. Each of these was prepared in the final composite material in low and high concentrations of 1 wt.% and 20 wt.%. **Figure 4.5** can be used as an interpretation of the product's (P1-P26) filler content, preparation, and composite manufacturing methods.

In **Figure 6.31** the effect of the surface treatment on the filler dispersion in the composites obtained from never dried MFC based fillers is compared. The untreated MFC reinforced composite (P1-**Figure 6.31 a_1** and **b_1**) and the tannic acid-hexylamine-MFC reinforced composite (P2-**Figure 6.31 a_2** and **b_2**) contain large cellulose aggregates (blue).

There is little to no sign of cellulose in the matrix (red) confirming the incompatibility of the untreated cellulose with the PPPE. The tannic acid-octadecylamine-MFC reinforced composite (P5-**Figure 6.31 a_3** and **b_3**) contains visibly smaller and much more dispersed cellulose aggregates (blue). The comparison between the composites reinforced with the short-tailed hexylamine (P3) and the long-tailed octadecylamine (P5) highlighted the importance of the selecting an appropriate minimum length of the aliphatic amine tail to ensure good compatibility and thus a good dispersibility of the filler in the matrix.

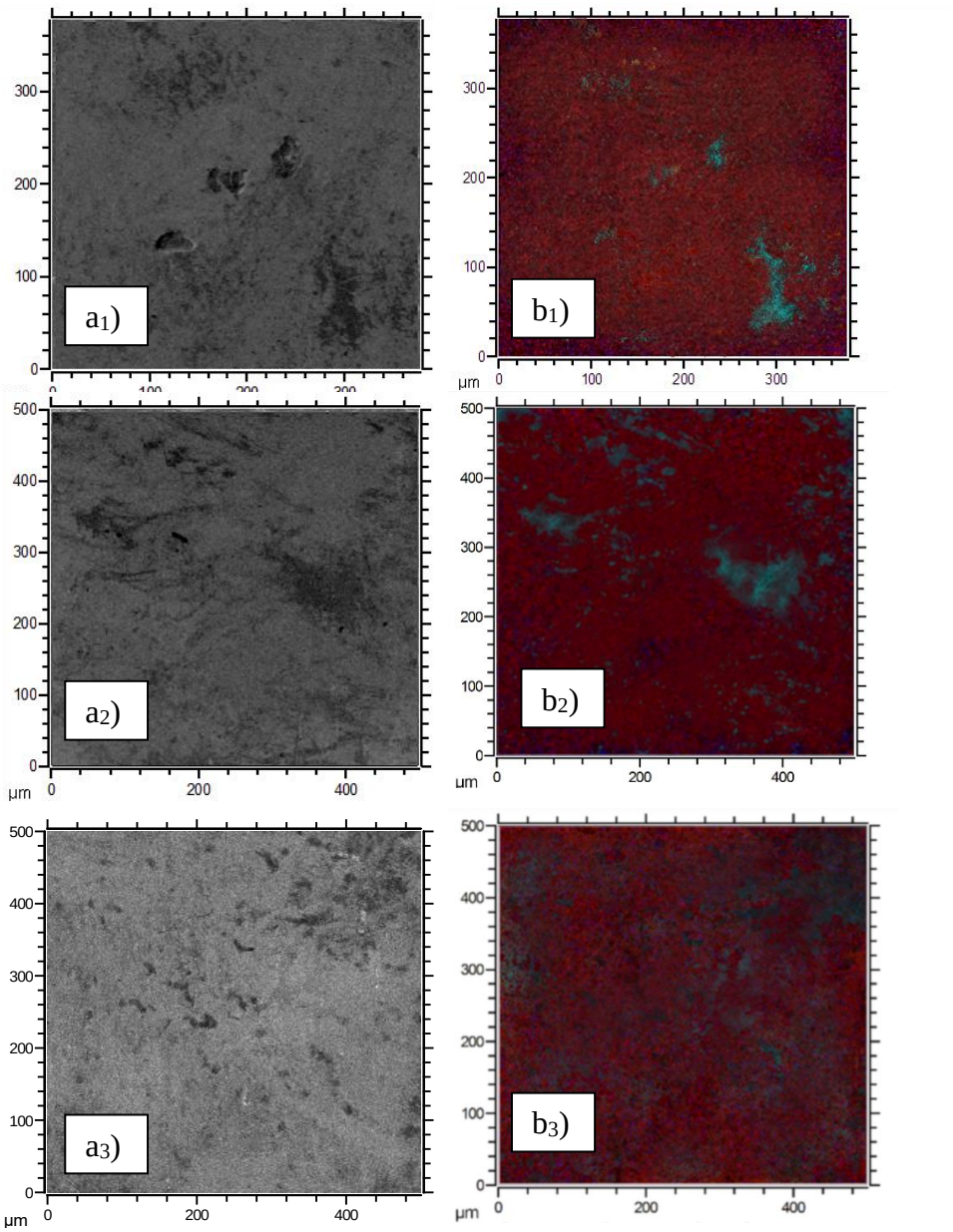

Figure 6.31 1 wt.% never dried untreated MFC reinforced composite prepared by direct mix (P1) optical image of the sample (greyscale) a_1) with a large agglomerate of cellulose visible in the right corner and a 2D reconstruction of the composite system using the assigned peaks b_1) the red colour indicates the matrix and the blue colour indicates the presence of cellulose. 1 wt.% never dried tannic acid-hexylamine-MFC reinforced composite prepared by direct mix (P3) optical image of the sample (greyscale) a_2) and a 2D reconstruction of the composite system using the assigned peaks b_2), and 1 wt.% never dried tannic acid-octadecylamine-MFC reinforced composite prepared by direct mix (P5) optical image of the sample (greyscale) a_3) and a 2D reconstruction of the composite system using the assigned peaks b_3).

Figure 6.32 compares the effect of the filler drying method on dispersibility. The composite in **Figure 6.32** was prepared using a freeze-dried tannic acid-hexylamine-MFC filler reinforcement. The freeze-drying procedure is a well-established method to prevent agglomeration and maintain the high surface area, characteristic of many micro and nano cellulose products. In **Figure 6.32 b**, in fact, smaller cellulose-based aggregates (blue) were visible, compared to **Figure 6.31b2** (never dried filler).

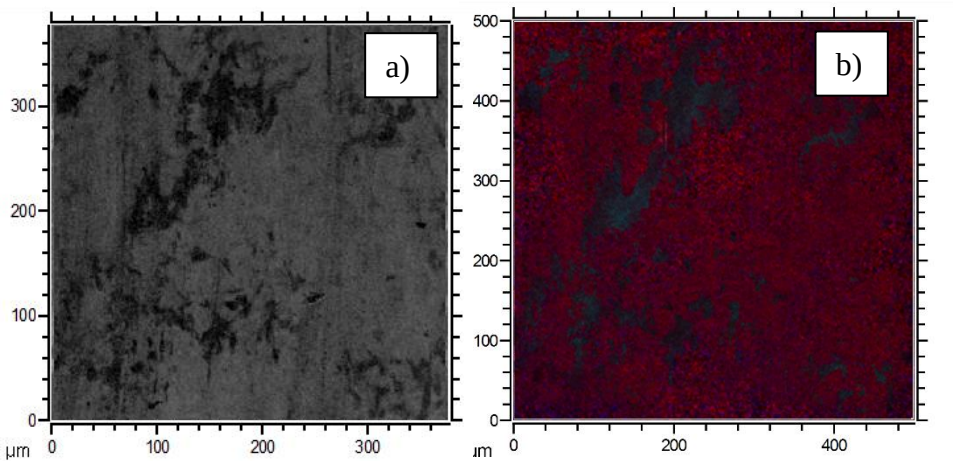

Figure 6.32 1 wt.% freeze-dried tannic acid-hexylamine-MFC reinforced composite prepared by direct mix (P19) optical image of the sample (greyscale) a) with a large agglomerate of cellulose visible in the centre of the image and a 2D reconstruction of the composite system using the assigned peaks b) the red colour indicates the matrix and the blue colour indicates the presence of cellulose.

Despite being an excellent method for the production of dry, non-aggregated, expanded surface area MFC, the freeze-drying technique was not sufficient to obtain uniformly dispersed composites. **Figure 6.33 b1** and **b2** show the ToF-SIMS reconstructed images of the 1 and 20 wt.% freeze dried tannic acid-octadecylamine-MFC reinforced composite. The comparison with **Figure 6.32** indicates that react the surface of the MFC fibrils with long-tailed amines increased their dispersibility in the polyolefin matrix. Comparison between the 1 wt.% (P23-**Figure 6.34 b1**) and 20 wt.% (P24-**Figure 6.33 b2**) tannic acid-octadecylamine-MFC samples did not show any noticeable increase in the filler aggregate size dimension. This indicates that at a filler loading of 20 wt.% or less, the composites were not saturated, indicating a low probability of aggregates coalescing during compounding.

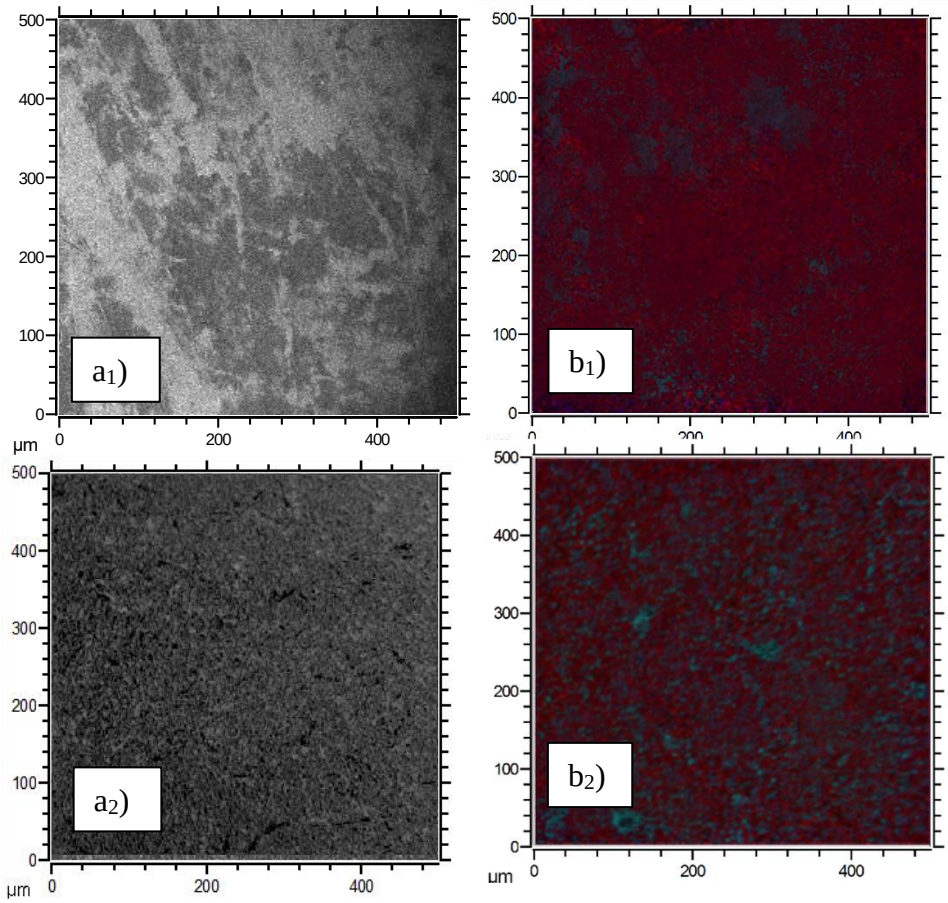

Figure 6.33 1 wt.% freeze-dried tannic acid-octadecylamine-MFC reinforced composite prepared by direct mix (P23) optical image of the sample (greyscale) a_1) and a 2D reconstruction of the composite system using the assigned peaks b_1) the red colour indicates the matrix and the blue colour indicates the presence of cellulose. 20 wt.% freeze dried tannic acid-octadecylamine-MFC reinforced composite prepared by direct mix (P23) optical image of the sample (greyscale) a_2) and a 2D reconstruction of the composite system using the assigned peaks b_2) the red colour indicates the matrix and the blue colour indicates the presence of cellulose.

Figure 6.33 and **Figure 6.34** compared the effect of mixing method on the filler dispersion in the composites obtained from freeze-dried MFC based fillers. The composites in **Figure 6.34 a_1** and **b_1** were obtained by direct mixing, while the composites in **Figure 6.34 a_2** and **b_2** were obtained by so-called solvent assisted mixing. The idea was to improve both polymer and cellulose fibrils mobility by introducing a solvent in which small molecules can efficiently mediate and facilitate the dispersion of the cellulose nanofibrils in the matrix.

In this case, the cellulose filler was represented by the freeze-dried, tannic acid-octadecylamine-MFC reinforcement powder that had a highly expanded, hydrophobic surface area due to the chemical surface treatment and to the drying method. Despite the promise, a comparison between **Figure 6.33** and **Figure 6.34** indicates that the solvent assisted mixing did not significantly enhance the filler dispersibility in the apolar matrix.

As already remarked, ToF-SIMS imaging is used in this research as a qualitative and supportive visual technique. A quantitative analysis of the filler dispersion and aggregate dimensions and distribution was carried out using a Multi-channel Spectral Confocal Laser Scanning Microscopy (SCLSM) technique, the findings of which are reported in **Section 6.3.4**.

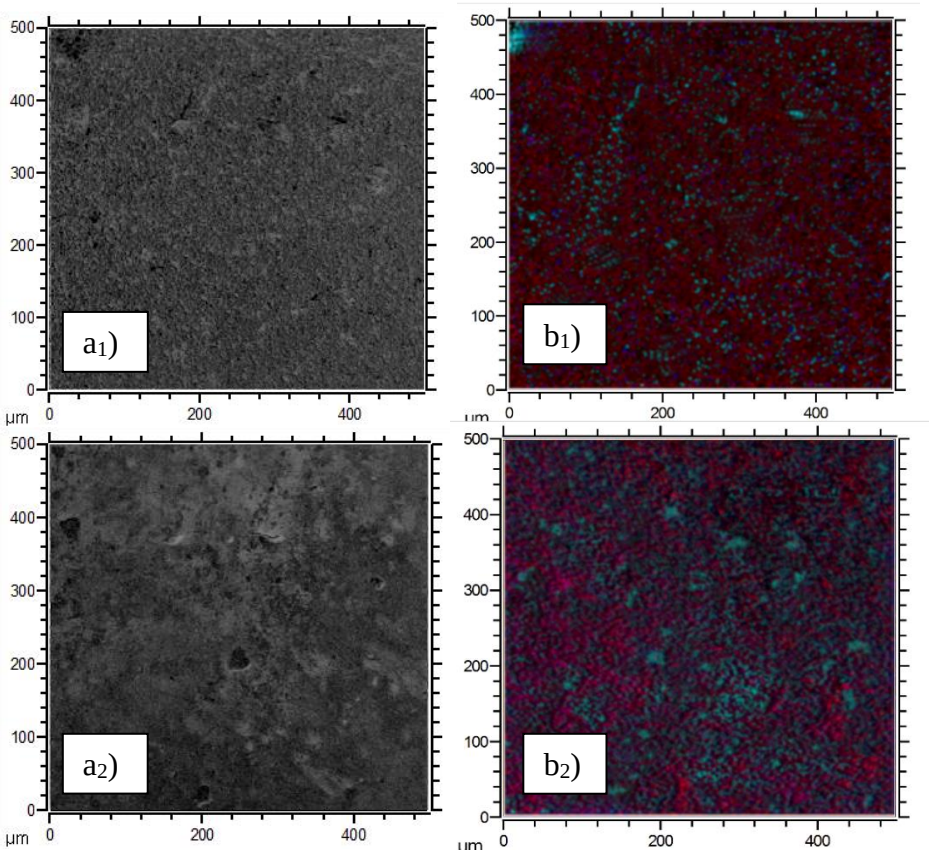

Figure 6.34 1 wt.% freeze-dried tannic acid-octadecylamine-MFC reinforced composite prepared by solvent-assisted mix (P25) optical image of the sample (greyscale) a$_1$) and a 2D reconstruction of the composite system using the assigned peaks b$_1$) the red colour indicates the matrix and the blue colour indicates the presence of cellulose. 20 wt.% freeze dried tannic acid-octadecylamine-MFC reinforced composite prepared by solvent-assisted mix (P26) optical image of the sample (greyscale) a$_2$) and a 2D reconstruction of the composite system using the assigned peaks b$_2$) the red colour indicates the matrix and the blue colour indicates the presence of cellulose.

6.3.4 Multi-channel Spectral Confocal Laser Scanning Microscopy (SCLSM) mapping

6.3.4.1 SCLSM spectra

SCLSM has been previously used to identify cellulose aggregates in composite materials without the need for a fluorescent dye.[403] The SCLSM and SCLSM mapping were used in this research to evaluate the level of cellulose-based filler dispersion in composites and determine the aggregate size. The autofluorescence of microfibrillated cellulose (MFC), tannic acid (TA) and the tannic acid-octadecylamine- MFC filler in composites was used, rendering the use of a dye unnecessary. The fluorescence of the cellulose aggregates ensured the identification of the filler in all the CLSM images of the composites (**Figure 6.35**).

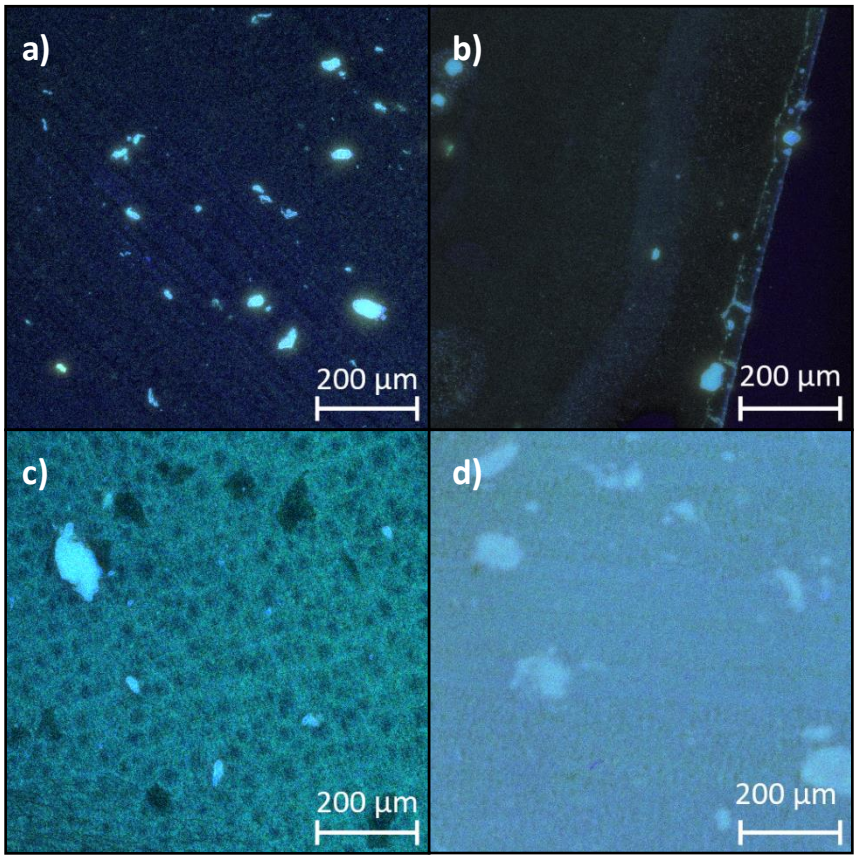

Figure 6.35 Typical images of composites containing a) 1 wt.% MFC, b) 1 wt.% tannic acid, (the visible fibre-like structure is a cutting mark) c) 1 wt. % tannic acid-octadecylamine-MFC, and d) 15 wt.% tannic acid-octadecylamine-MFC composites. The images are flattened from 3D stacks using the standard deviation z-project function in Fiji software.

The CLSM spectra of aggregates observed in the 1 wt.% untreated MFC and 1 wt.% tannic acid-octadecylamine-MFC composites were similar. The 1 wt.% tannic acid aggregates had less intense spectra (**Figure 6.36 a**), in line with those from the raw materials (**Figure 6.36 b**).

All the background spectra for the composites contain the characteristic polypropylene peak and a contribution from the reinforcement material (**Figure 6.36 b**). The 1 wt.% tannic acid-octadecylamine-MFC composite sample background appears to have a honeycomb-like structure (**Figure 6.35 c**). The origin of this structure is unclear and requires further investigation. It is presumed that the 15 wt.% tannic acid-octadecylamine-MFC composite has a similar structure, but the increase in intensity obscures it.

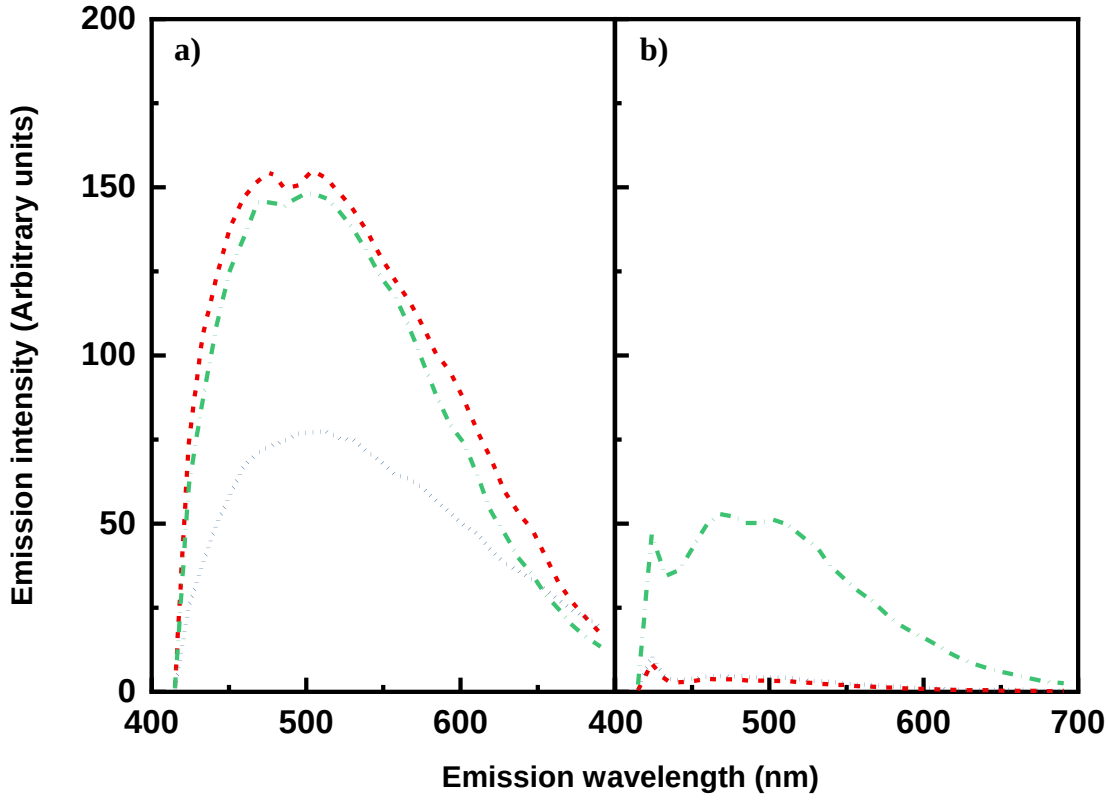

Figure 6.36 Typical emission spectra of a) aggregates and b) the background for 1 wt.% MFC (dashed red line), 1 wt.% tannic acid (dotted blue line), and 1 wt.% tannic acid-octadecylamine-MFC (dash-dot green line). Note that the aggregates for 1 wt.% MFC and 1 wt.% tannic acid-octadecylamine-MFC have similar intensities, whilst 1 wt.% tannic acid is less intense. Note also that the 1 wt.% tannic acid-octadecylamine-MFC background spectrum is more intense than the other two spectra and consists of signals from both the polypropylene and tannic acid-octadecylamine-MFC.

6.3.4.2 Aggregate size and distribution obtained by SCLSM

Tannic acid-octadecylamine-MFC surface treatment resulted in a significant increase in the number of observed aggregates, and a decrease in the mean area of the observed aggregates compared with those in the 1 wt.% untreated MFC and 1 wt.% tannic acid reinforced composites (**Figure 6.37)**. This suggests that the chemical surface modification of the MFC improves the distribution of the material in the produced composites. As expected, an increase in the tannic acid-octadecylamine-MFC loading results in an increase in the number of aggregates observed but has no effect on the mean aggregate area observed.

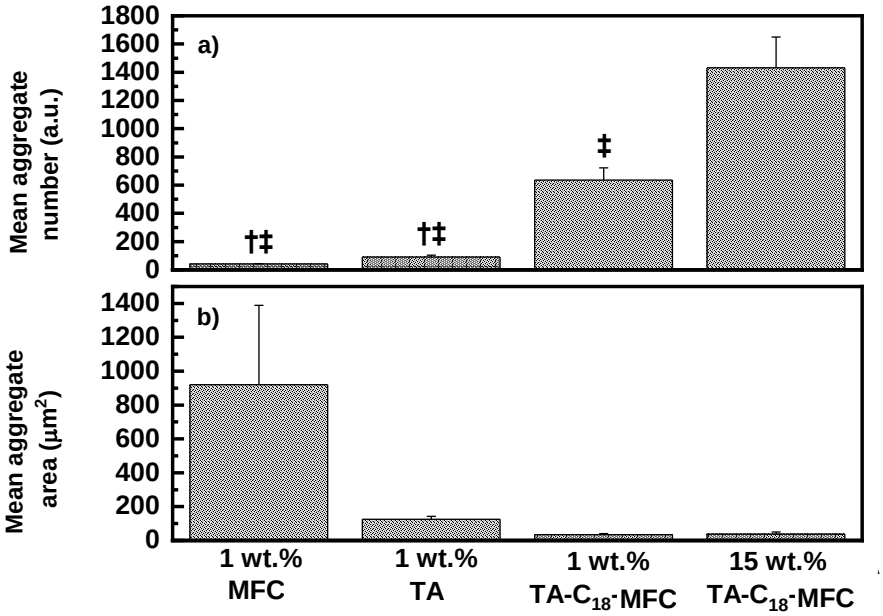

Figure 6.37 a) Mean number of aggregates for each composite sample. N = 3. † $p < 0.05$ compared to 1 wt.% tannic acid-octadecylamine-MFC (TA-C_{18}-MFC); ‡ $p < 0.05$ compared to 15 wt.% tannic acid-octadecylamine-MFC (TA-C_{18}-MFC). Error ± SE; b) Mean aggregate area for each composite sample. No statistical difference was observed between samples. N = 3, n ≥ 35. Error ± SE. a.u.= arbitrary units.

The aggregates were divided into three categories: small, medium and large to investigate the difference in cellulose distribution between the various compositions of the composites. The result of the aggregate size analysis is shown in **Figure 6.38**. The composites reinforced with tannic acid-octadecylamine-MFC had a similar aggregate size distribution regardless of the filler loading (1 or 15 wt.%) while the composites reinforced with 1 wt.% untreated MFC had an average aggregate size on at least one magnitude larger than that of the compatibilized MFC reinforced materials.

It is worth noting that neither the 1 nor the 15 wt.% tannic acid-octadecylamine-MFC composites had a lower bound for the small category, which suggests that a portion of the aggregates are smaller than the minimum viewable area (~11 μm^2). It is also worth noting that, whilst there appear to be many outliers in the 15 wt.% tannic acid-octadecylamine-MFC reinforced composite sample, they consist of less than 1 % of the total number of aggregates observed, and they fall within the same range as the untreated MFC aggregates.

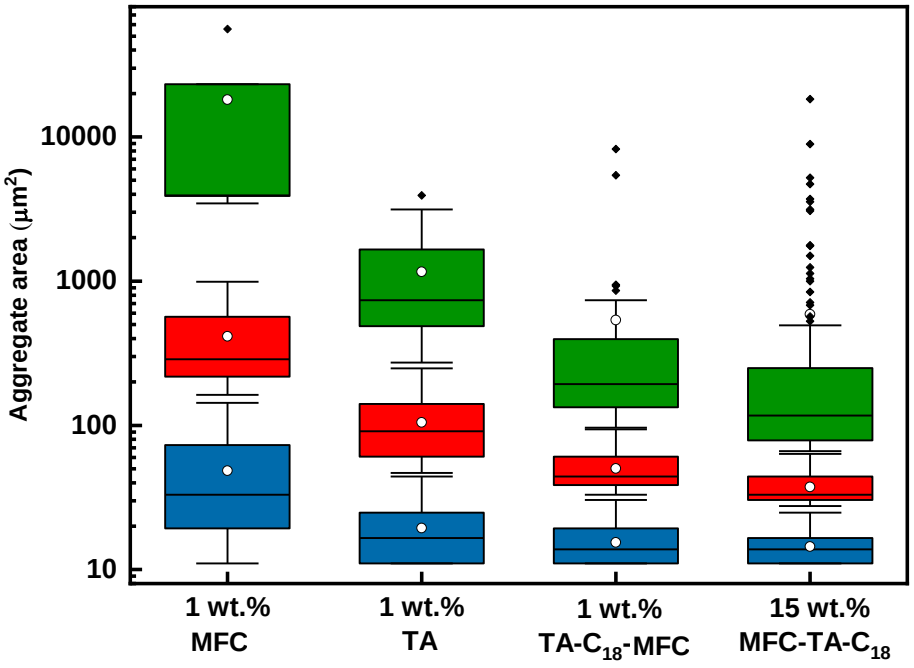

Figure 6.38 Box plot comparing the distribution of aggregates between samples obtained using spectral confocal microscopy. Aggregates are divided into four categories: small (blue boxes), medium (red boxes), large (green boxes), and outliers (black diamonds). The mean values for each category are represented by white circles. Aggregates < 11 μm^2 ignored for analysis. n > 120.

By setting the 1 wt.% tannic acid-octadecylamine-MFC reinforced composite as the control for defining the aggregate area categories, it is possible to compare the population distribution across the samples (**Figure 6.39**). Under these boundary conditions, the distribution of aggregates for the 1 wt.% untreated MFC composite is quite even; 31 ± 4 % of aggregates fall into the small category, whilst 17 ± 5 % are classified as outliers.

The TA-MFC aggregates are significantly skewed towards the small category; 61 % of aggregates fall into this category. There is, however, no significant difference between the untreated MFC and TA-MFC-C_6/C_{18} aggregates for the other three categories.

This analysis confirms that the modification of MFC with tannic acid and octadecylamine significantly improves the filler distribution within the matrix. Over 85 % of the aggregates fall into the small category for both 1 and 15 wt.% TA-C_{18}-MFC composites, with less than 3 % of the aggregates falling into the large and outlier categories combined. The tannic acid-octadecylamine-MFC composites were significantly different from the 1 wt.% untreated MFC reinforced sample in term of aggregate size across all categories and were also significantly different from the 1 wt.% tannic acid reinforced composite in the small and medium categories. Importantly, no significant difference is observed in the aggregate size distribution between the 1 wt.% and 15 wt.% tannic acid-octadecylamine-MFC composites, indicating that the increased loading does not result in aggregation of the compatibilized filler particles.

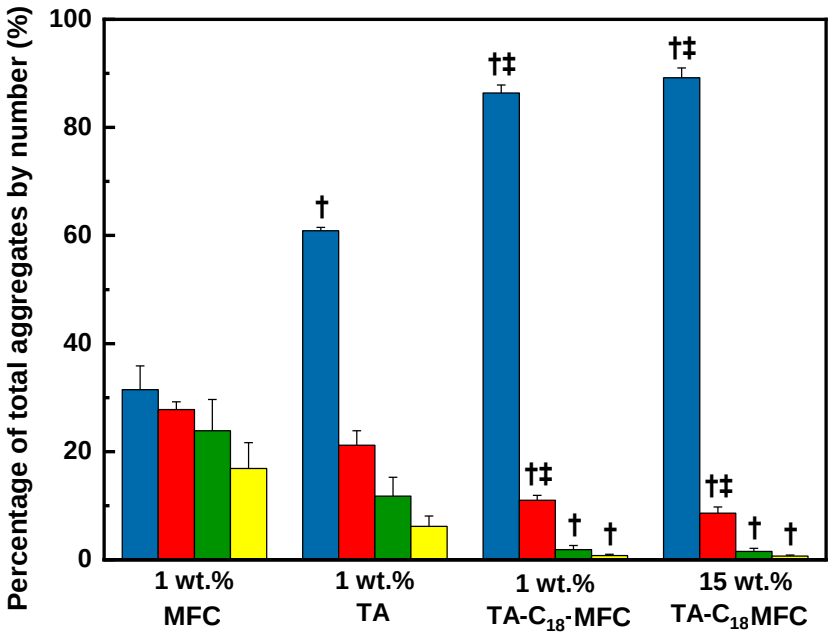

Figure 6.39 Aggregate populations for various composites obtained via SCLSM. Aggregate categories, as defined by ranges determined for 1 wt.% tannic acid-octadecylamine-MFC (TA-C_{18}-MFC): small (blue bars, 11.0 ≥ X ≤ 30.3 µm^2), medium (red bars, 30.3 > X ≤ 93.8 µm^2), large (green bars, 93.8 > X ≤ 385.3 µm^2), and outliers (yellow bars, X > 385.3 µm^2). For all categories N = 3. † p < 0.05 compared to 1 wt.% untretaed MFC in the respective category; ‡ p < 0.05 compared to 1 wt.% tannic acid in the respective category. Error ± SE.

The effect of the filler drying procedure and compounding process on the filler aggregate size and distribution in the reinforced composites were also investigated using SCLSM mapping and data analysis.

The aggregate size and distribution were calculated using the same methodology described for the previous set of samples to analyse the composites prepared from a never dried MFC reinforced composite P1 (1 wt.% untreated MFC), P3 (1 wt.% tannic acid-hexylamine-MFC), and P5 (1 wt.% tannic acid-octadecylamine-MFC), and for the freeze-dried MFC reinforced composites P15 and P16 (1 wt.% and 20 wt.% untreated MFC prepared by direct mix), P17 and P18 (1 wt.% and 20 wt.% untreated MFC prepared by solved assisted mix), P19 and P20 (1 wt.% and 20 wt.% tannic acid-hexylamine-MFC prepared by direct mix), P21 and P22 (1 wt.% and 20 wt.% tannic acid-hexylamine-MFC prepared by solvent assisted mix) P23 and P24 (1 wt.% and 20 wt.% tannic acid-octadecylamine-MFC prepared by direct mix), and P25 and P26 (1 wt.% and 20 wt.% tannic acid-octadecylamine-MFC prepared by solved assisted mix) were compared to evaluate the impact of the filler production method, surface chemistry, and the composite manufacturing method on the filler aggregation. **Figure 4.5** contains the characteristic of the product (P1-P26) in term of filler content, filler preparation method and composite manufacture method. **Figure 6.40** compares the filler dispersion of the unreacted, tannic acid-hexylamine and octadecylamine-MFC reinforced composites for the different samples.

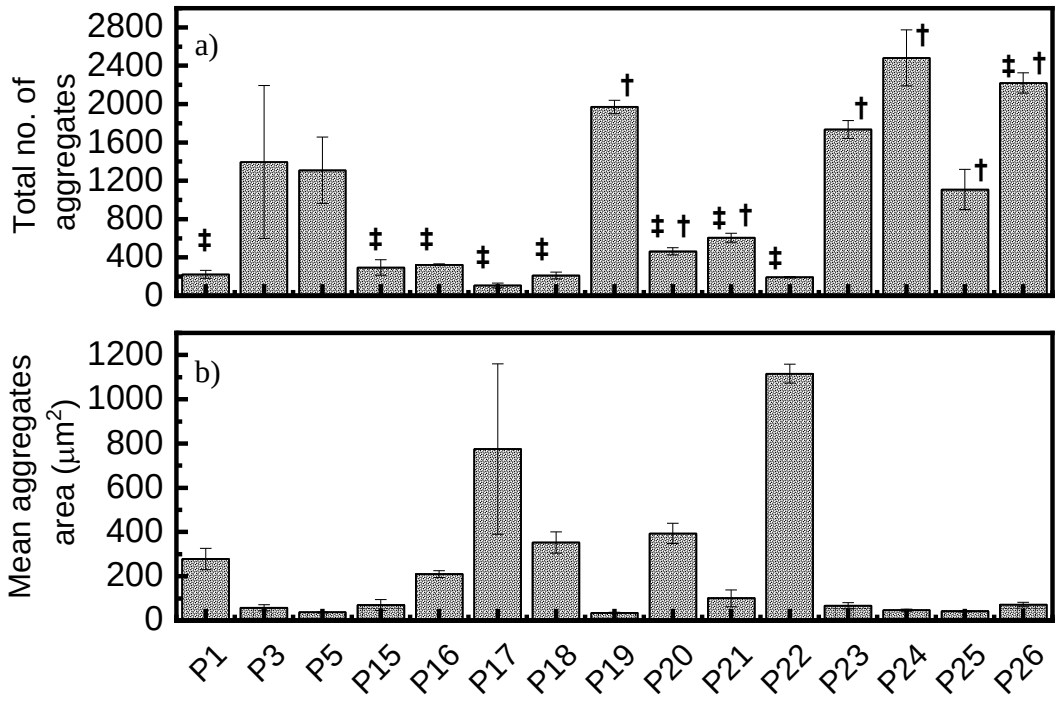

Figure 6.40 a) Mean number of aggregates for each composite sample. N = 3. † p < 0.05 compared to P1 (1 wt.% untreated MFC); ‡ p < 0.05 compared to P 23 (1 wt.% tannic acid-octadecylamine-MFC prepared by direct mix). Error ± SE; b) Mean aggregate area for each composite sample. Error ± SE. a.u.= arbitrary units.

The result of the aggregate size analysis is shown in **Figure 6.40 b**. The overall analysis indicates that decreasing the number of aggregates results in increased average aggregate size, regardless of the filler or composites preparation method. For the composites reinforced using never dried P1 (1 wt.% untreated MFC), P3 (1 wt.% tannic acid-hexylamine-MFC), and P5 (1 wt.% tannic acid-octadecylamine-MFC) a decrease in the aggregate area was registered when the MFC fibrils were reacted with tannic acid and different length primary amines. A similar trend was followed by the freeze-dried MFC reinforced composites P15 and P16 (1 wt.% and 20 wt.% untreated MFC prepared by direct mix), P17 and P18 (1 wt.% and 20 wt.% untreated MFC prepared by solved assisted mix), P19 and P20 (1 wt.% and 20 wt.% tannic acid-hexylamine-MFC prepared by direct mix), P21 and P22 (1 wt.% and 20 wt.% tannic acid-hexylamine-MFC prepared by solvent-assisted mix) P23 and P24 (1 wt.% and 20 wt.% tannic acid-octadecylamine-MFC prepared by direct mix), and P25 and P26 (1 wt.% and 20 wt.% tannic acid-octadecylamine-MFC prepared by solved assisted mix). **Figure 6.41** reports SCLSM images of the analysed composites. From the images, the differences in the morphology of the aggregates of fillers and their size become more clear.

It is worth noting that for composites reinforced using untreated MFC P 1, 15, 16, 17, 18 , the cellulose filler (light blue) was clearly visible against the dark background (polymeric matrix). The reaction of the MFC fibrils with tannic acid and the primary amines enhanced the filler dispersion as proved by the lightening of the background. The tannic acid-octacecylamine-MFC reinforced composites (P5, 23, 24, 25, 26) exhibited a uniform light blue background indicating the presence of dispersed, and small aggregates of cellulose fibrils.

It is worth noting that in all the tannic acid-octadecylamine-MFC reinforced composites all of the aggregates are close to each other and appear evenly distributed across the image; this is most visible for the 1 wt.% reinforced sample (P5, 23, 25). It is assumed the same structure was present in the heavily reinforced composites as well, but the increased cellulose signal masked it.

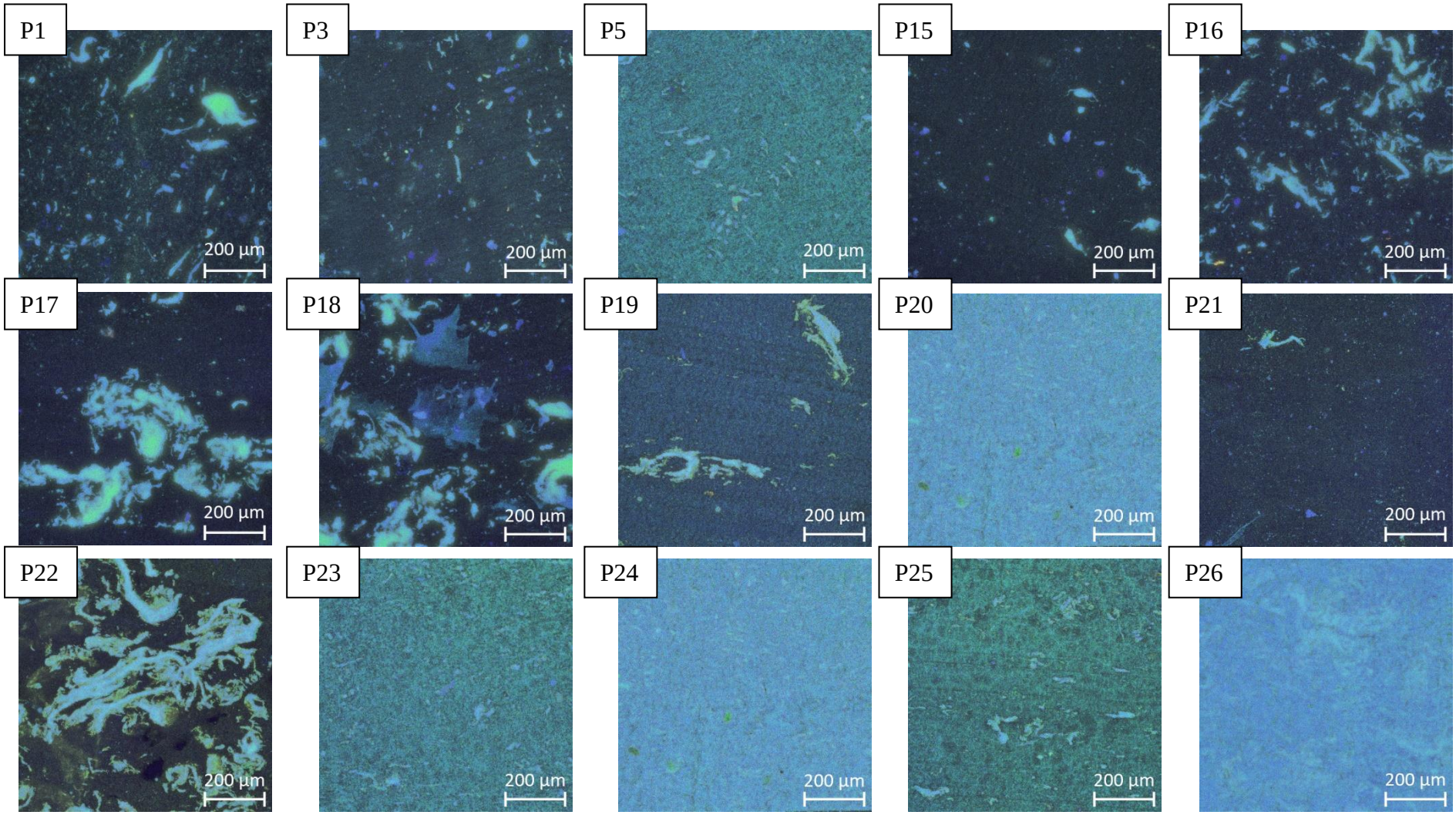

Figure 6.41 SCLSM images of composites prepared never dried MFC P1 (1 wt.% untreated MFC), P3 (1 wt.% tannic acid-hexylamine-MFC), and P5 (1 wt.% tannic acid-octadecylamine-MFC), and for the freeze-dried MFC P15 and P16 (1 wt.% and 20 wt.% untreated MFC prepared by direct mix), P17 and P18 (1 wt.% and 20 wt.% untreated MFC prepared by solved assisted mix), P19 and P20 (1 wt. % and 20 wt.% tannic acid-hexylamine-MFC prepared by direct mix), P21 and P22 (1 wt.% and 20 wt.% tannic acid-hexylamine-MFC prepared by solvent assisted mix) P23 and P24 (1 wt.% and 20 wt.% tannic acid-octadecylamine-MFC prepared by direct mix), and P25 and P26 (1 wt.% and 20 wt.% tannic acid-octadecylamine-MFC prepared by solved assisted mix).

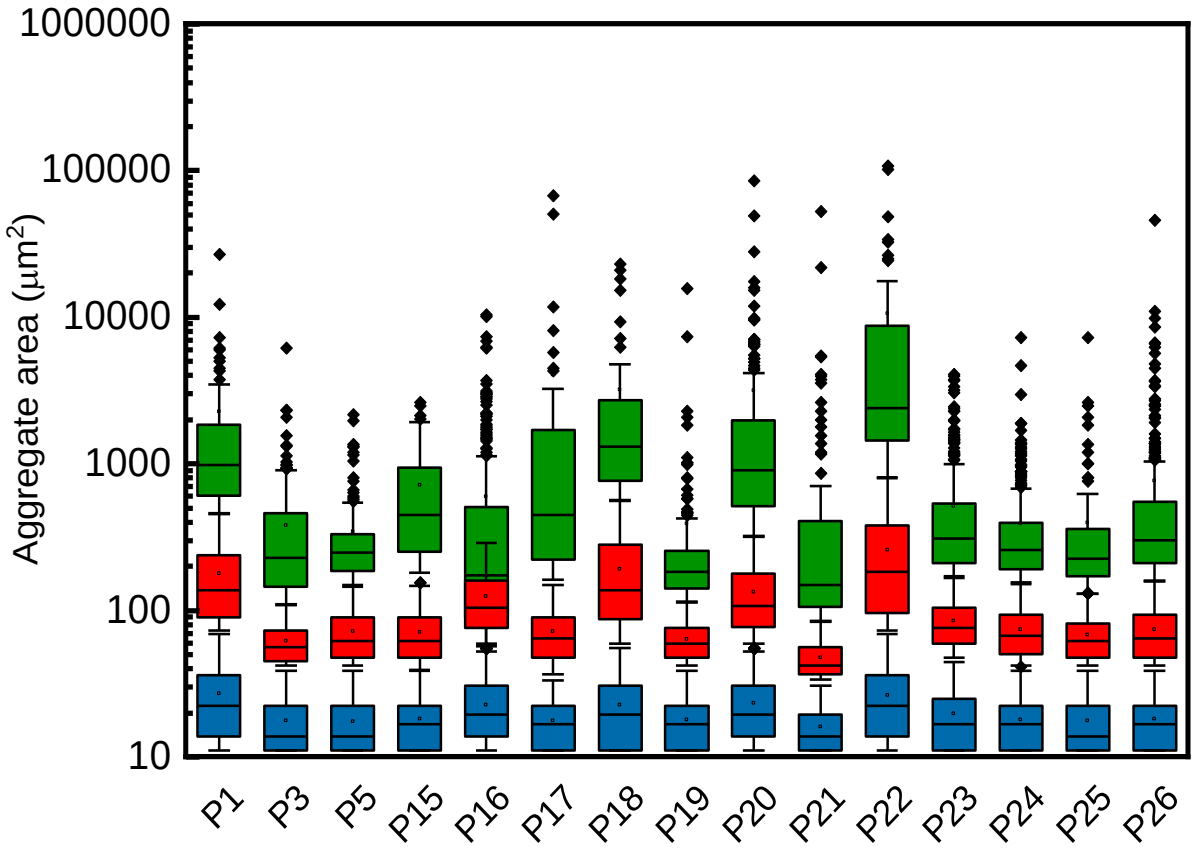

Figure 6.42 Box plot comparing the distribution of aggregates between samples obtained using spectral confocal microscopy. Aggregates are divided into four categories: small (blue boxes), medium (red boxes), large (green boxes), and outliers (black diamonds). The mean values for each category are represented by white circles. Aggregates < 11 µm^2 ignored for analysis. n > 120.

The aggregates were divided into three categories (small, medium and large) as for the previous samples, and the result of the aggregate size analysis is shown in **Figure 6.42**. All the composites reinforced with tannic acid-octadecylamine-MFC (P5, 23, 24, 25, 26) had a similar aggregate size distribution regardless of the filler loading (1 or 20 wt.%). Composites reinforced with unreacted MFC (P1, 15, 16, 17, 18) had an average aggregate size of at least one magnitude larger than that of the compatibilized MFC reinforced samples. The composites reinforced with tannic acid-hexylamine-MFC (P3, 19, 20, 21, 22) had aggregate size distributions strongly affected by the filler loading and the filler and composites preparation methods.

It is worth noting that most of the samples analysed had no lower bound for the small aggregate category, which suggests that a portion of the aggregates are smaller than the minimum viewable area (~11 μm^2). It is also worth noting that, whilst there appear to be many outliers in the analysed composites, they consist of a percent of the total number of aggregates observed that vary in the range up to a maximum of 5 %.

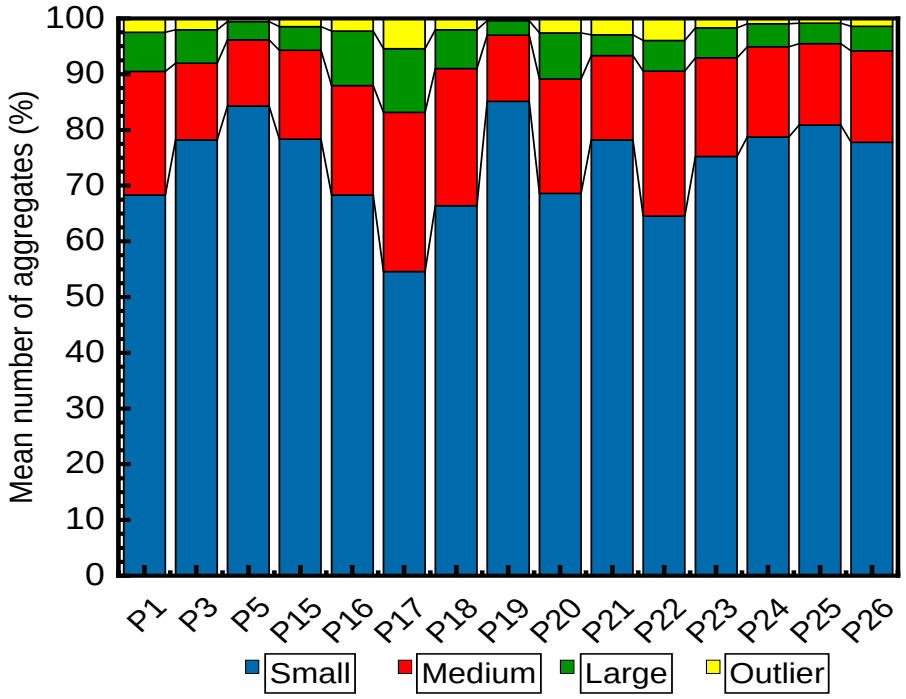

Figure 6.43 Aggregate populations for various composites obtained via SCLSM. Aggregate categories, as defined by ranges determined for 1 wt.% tannic acid-octadecylamine-MFC (TA-C_{18}-MFC): small (blue bars, 11.0 ≥ X ≤ 30.3 μm^2), medium (red bars, 30.3 > X ≤ 93.8 μm^2), large (green bars, 93.8 > X ≤ 385.3 μm^2), and outliers (yellow bars, X > 385.3 μm^2). P1 (1 wt.% untreated never dried MFC), P3 (1 wt.% tannic acid-hexylamine-never dried MFC), and P5 (1 wt.% tannic acid-octadecylamine-never dried MFC), P15 and P16 (1 wt.% and 20 wt.% untreated freeze-dried MFC prepared by direct mix), P17 and P18 (1 wt.% and 20 wt.% untreated freeze-dried MFC prepared by solved assisted mix), P19 and P20 (1 wt.% and 20 wt.% tannic acid-hexylamine-freeze-dried MFC prepared by direct mix), P21 and P22 (1 wt.% and 20 wt.% tannic acid-hexylamine freeze-dried MFC prepared by solvent-assisted mix) P23 and P24 (1 wt.% and 20 wt.% tannic acid-octadecylamine-freeze-dried MFC prepared by direct mix), and P25 and P26 (1 wt.% and 20 wt.% tannic acid-octadecylamine-freeze-dried MFC prepared by solved assisted mix).

By setting the 1 wt.% tannic acid-octadecylamine-MFC reinforced composite in the previous set of experiments as the control for defining the aggregate area categories, it is possible to compare the population distributions across the samples (**Figure 6.43**).

Under these boundary conditions, the distribution of aggregates resulted as follows: the small category represented most of the aggregates accounting for a minimum of 55 % to a maximum of 84 %. The medium aggregate represented a less consistent part of the population accounting for a minimum of 12 % up to a maximum of 29 %. The large aggregates accounted for a minimum of 3 % up to a maximum of 11 % of the population, while the outliers were represented by less than the 5 % of the population of the aggregates.

The different filler preparation and drying method, the compounding process and the filler loading had a profound effect on the size and distribution of the aggregates; a more comprehensive analysis of the influence of the individual parameters on the filler distribution is presented in the next paragraphs.

6.3.4.3 Effect of the MFC surface chemistry

The surface reaction of the MFC with tannic acid and the short water soluble hexylamine did not significantly improve the filler dispersion or affect the filler aggregate population. On the other hand, the reaction of the MFC filler with the tannic acid and the hydrophobic octadecylamine caused a significant decrease in the medium, large and outlier aggregate size, while the average size of the small aggregates remains invariant (**Figure 6.44**). The tannic acid octadecylamine treatment also enhanced the filler dispersion as proven by the increase of the small aggregate population when compared to the unreacted MFC. The amount of medium, large and outlier aggregates was reduced accordingly to account for the increased small aggregate population.

The tannic acid-octadecylamine MFC surface reaction, therefore, proved to be an effective method to disperse the MFC in the PPPE matrix.

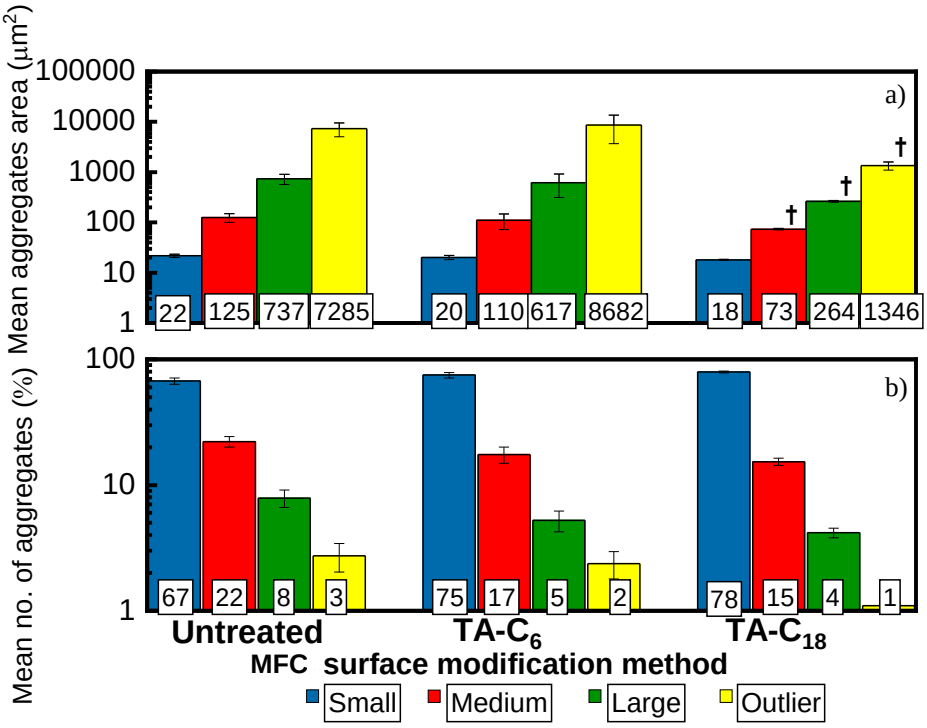

Figure 6.44 Comparison among a) the mean aggregate area for the composites containing untreated MFC, tannic acid-hexylamine reacted MFC (TA-C_6),and tannic acid-octadecylamine reacted MFC (TA-C_{18}). Error ± SE, and b) the mean number of aggregates for each composite sample. N = 3. † $p < 0.05$ compared to untreated MFC reinforced composite samples population of the same category. Error ± SE.

6.3.4.4 Effect of the fillers drying method

The freeze-drying method had a beneficial effect on the dispersion of the filler in the matrix, regardless of the surface chemistry or the loading. All the aggregate categories (small, medium, large and outlier) both the number of aggregates and the total aggregate area were lower in all size categories, compared with those from the never-dried samples (**Figure 6.45**). The freeze-drying method, however, did not affect the distribution of the aggregates between the different size groups (**Figure 6.45**).

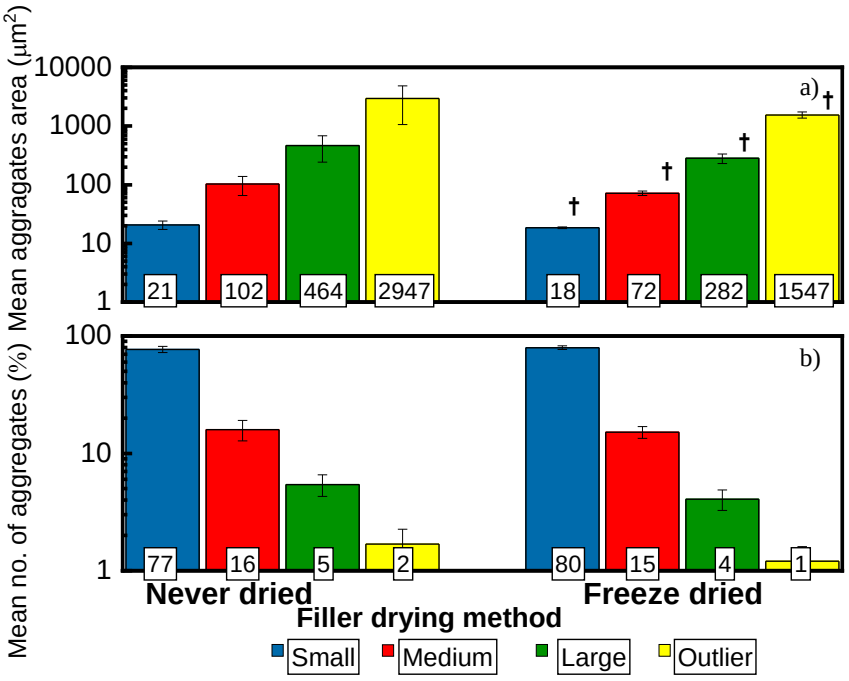

Figure 6.45 Comparison between a) the mean aggregate area for the composites containing never dried and freeze dried MFC based fillers. Error ± SE, and b) the mean number of aggregates for each composite sample. N = 3. † $p < 0.05$ compared to untreated MFC reinforced composite samples population of the same category. Error ± SE.

6.3.4.5 Effect of the preparation method of the composites

The solvent assisted method was introduced to facilitate the mobility of the cellulose fibrils and to enhance their dispersion in the composites. The idea was to use an organic solvent (toluene) to dissolve the polymer matrix, decreasing its viscosity and allowing a more intimate mixing of the components. Unfortunately, the SCLSM analysis of the composites revealed that the use of the solvent-assisted premix did not improve the dispersion of the filler (**Figure 6.46**). In fact, the solvent assisted premixed composites shown no significant differences in the small and medium aggregate categories size, while the size of the large and outlier aggregates was statistically larger for the solvent assisted prepared composites. The distribution of the aggregates between the size categories was not affected by the manufacturing method of the composites; no relevant change in population was registered for any of the aggregate size categories. The premixing of the PPPE matrix with the MFC fillers using toluene as auxiliary solvent did not improve filler dispersion, but contributed to form larger aggregates in the composites.

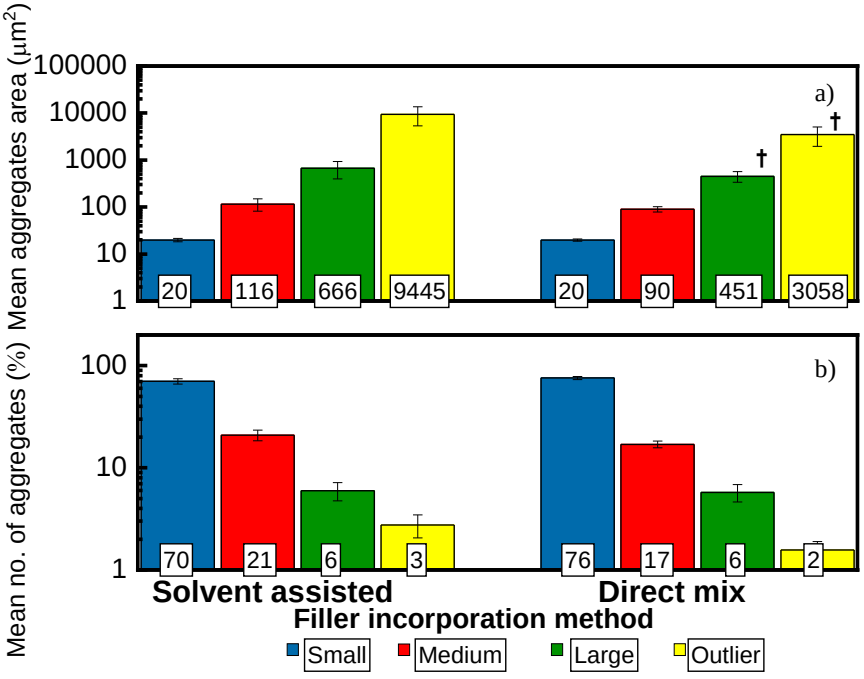

Figure 6.46 Comparison between a) the mean aggregate area for the composites obtained by direct mix of the filler and PPPE powder and composites obtained using the solvent assisted method. Error ± SE, and b) the mean number of aggregates for each composite sample. N = 3. † $p < 0.05$ compared to the solvent assisted prepared composite samples population of the same category. Error ± SE.

6.3.4.6 Effect of the MFC loading level

Increasing the filler loading from 1 to 20 wt.% increased the number and area of aggregates substantially but did not significantly affect their sizes: the area of the small aggregates hardly changes, but the area of the large ones increases by a factor of 3. (**Figure 6.47**). As already highlighted from the previous study on 1 wt.% and 15 wt.% tannic acid-octadecylamine-MFC reinforced composites, no significant difference was observed in the aggregate size distribution upon increasing the filler loading, indicating that the increased loading does not result in aggregation of the compatibilized filler particles.

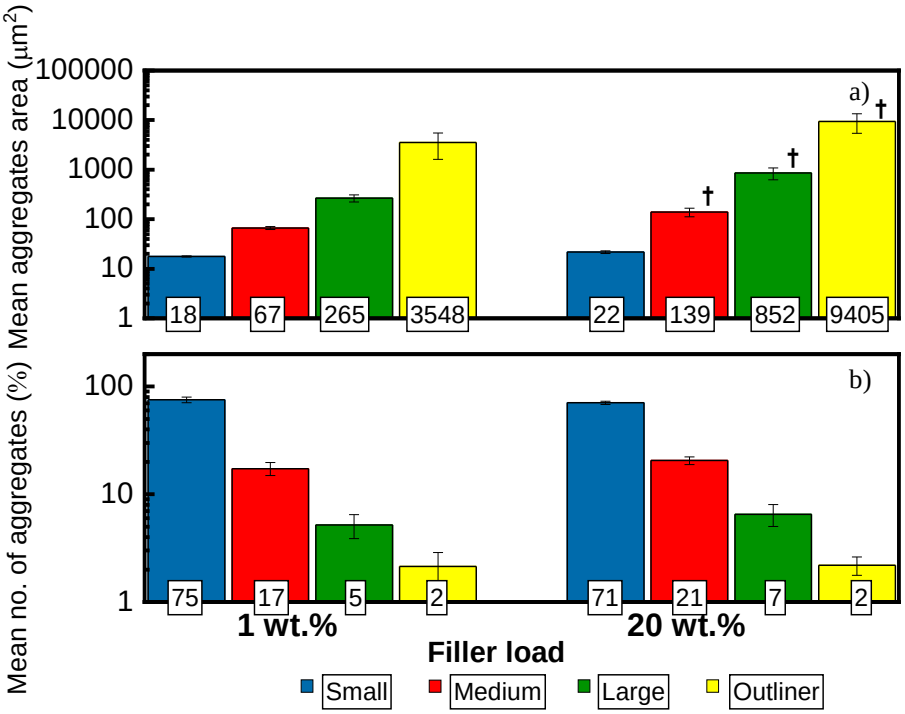

Figure 6.47 Comparison between a) the mean aggregate area for the composites at 1 wt.% filler loading and at 20 wt.% filler loading. Error ± SE, and b) the mean number of aggregates for each composite sample. N = 3. † $p < 0.05$ compared to the 1 wt.% reinforced composite samples population of the same category. Error ± SE.

6.4 Mechanical and impact properties of the compatibilized MFC reinforced composites

One of the main objectives of this research work was the production of MFC reinforced polyolefins using conventional thermoplastic manufacturing methods or easily industrially implementable approaches. To enhance the mechanical and impact properties of the composites, a good compatibility between filler and matrix, and a good level of filler dispersion was expected to be necessary requirements.

The most successful approach to the surface modification of the MFC was the water-based reaction of the fibrils with tannic acid and octadecylamine. This approach was also found to be the most effective at reinforcing the polyolefin matrix and achieving good filler dispersion. In the first part of this section, the mechanical properties of the neat PPPE matrix were compared with the composites obtained by reinforcement with the MAgPP, PVOH, PEO, and myristoyl chloride reacted MFC. The second part of this section is dedicated to a deeper investigation of the mechanical and impact properties of the composites reinforced with tannic acid-octadecyl amine compatibilized MFC, and a comparison with inorganic reinforced composites. In the last part, different filler production, drying and incorporation methods were compared to evaluate the effect of the filler and the manufacturing method of the composites on the final tensile and impact properties.

The tensile properties of the neat PPPE matrix and reinforced composites were obtained from an average of five tested specimens. Young's modulus of the samples was calculated at a maximum deformation of 0.2 %. The tensile data of the neat PPPE matrix, and MAgPP, PVOH, PEO, myristoyl chloride-MFC 1 wt.% reinforced composites are presented in **Table 6.4**.

Table 6.4 Tensile modulus of pure PPPE matrix and MFC reinforced composites.

Sample ID	**Young's Modulus (MPa)**
PPPE	900±20
MAgPP	1280±80
Myristoyl chloride	600±30
PVOH	150±10
PEO	900±20

The data in **Table 6.4** show that none of the reacted MFC fillers investigated contribute substantially to enhancing the Young's modulus of the neat PPPE matrix. In the following paragraph, the compatibilized fillers are presented separately, and the reasons for their poor performance is explained in further detail.

In the MAgPP compatibilized MFC the addition of this filler did improve the tensile properties of the neat matrix, but due to the large use of organic solvent involved in the preparation of this compatibilized form of MFC, and the consequent unsuitability of this chemical route to larger production, the composite reinforced with MAgPP-MFC were used as reference comparison.

The addition of the myristoyl chloride compatibilized MFC filler strongly affects and compromises the mechanical properties of the matrix. The filler itself proved to be thermally unstable under the processing conditions. The thermal degradation of the filler was believed to produce further reactive chemicals that damaged and compromised the polymeric structure. The degradation of both filler and matrix in the myristoyl chloride compatibilized MFC reinforced composites was attributed to the presence of residual pyridinium chloride salt, which was a residue from the catalyst and was assumed to be trapped in the filler even after several washes with an organic solvent. The removal of the pyridinium chloride salt from the compatibilized filler was challenging due to its polar nature, which has extremely low solubility in the organic solvents used as washing medium. Owing to the poor performance of the myristoyl chloride compatibilized MFC reinforced composites, and the technical difficulties related with the filler preparation route, no further characterizations were performed on the filler or on the composites prepared using this methodology.

The addition of PVOH compatibilized MFC to the neat PPPE matrix results in a dramatic decrease in the tensile modulus of the specimens due to poor compatibilization. The poor compatibilizing effect of the PVOH between the cellulose fibrils and the matrix is clearly visible in **Figure 6.48**. This SEM image of the PVOH-MFC reinforced composites shows a cellulose fibre (in white) surrounded by a large void and indicates complete disconnection from the matrix. The poor mechanical performance of the PVOH-MFC reinforced composites indicated the unsuitability of this route in the production of MFC reinforced composites.

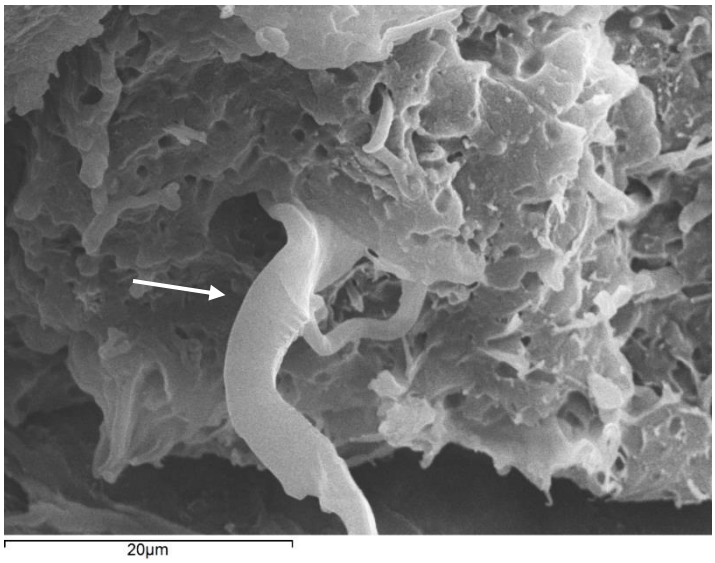

Figure 6.48 Typical fracture surface of a PVOH-MFC reinforced nanocomposite (in a PPPE matrix). The white fibrous structure is presumed to be a cellulose fibre (white arrow) surrounded by the PPPE matrix (×5000 magnification).

The addition of the PEO reacted MFC filler did not substantially modify the tensile properties of the neat matrix. SEM imaging of the PEO-MFC reinforced composites, however, revealed a good interaction between the cellulose fibrils and the matrix (**Figure 6.49**).

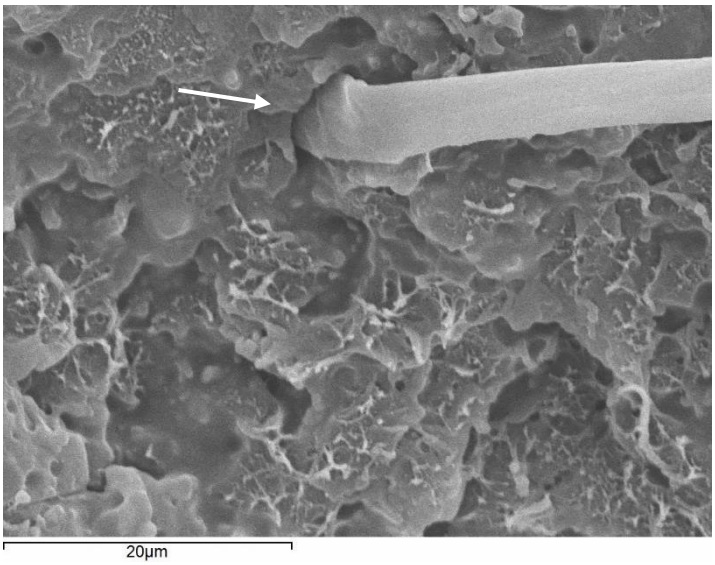

Figure 6.49 Typical fracture surface of a PEO-MFC reinforced nanocomposite (in a PPPE matrix). The white fibrous structure is a cellulose fibre (white arrow) surrounded by the PPPE matrix (×5000 magnification).

Unfortunately, the production of a suitable PEO compatibilized MFC filler involves the use of freeze-drying, which is a highly energy intensive filler production method. The product obtained from the surface reaction of MFC with PEO without the freeze-drying procedure was hard and impossible to grind to obtain a powder suitable for compounding (**Figure 6.50 a**). An SEM image of the freeze-dried PEO compatibilized MFC filler (**Figure 6.50 b**) indicated that the freeze-drying is an essential step in preventing the hornification of the PEO modified MFC filler. The necessity of the additional freeze-drying step in preparing the PEO-MFC filler strongly decreased the appeal of this technique. Furthermore, the impact on the tensile properties registered for the reinforced composites did not justify further investigation on this filler.

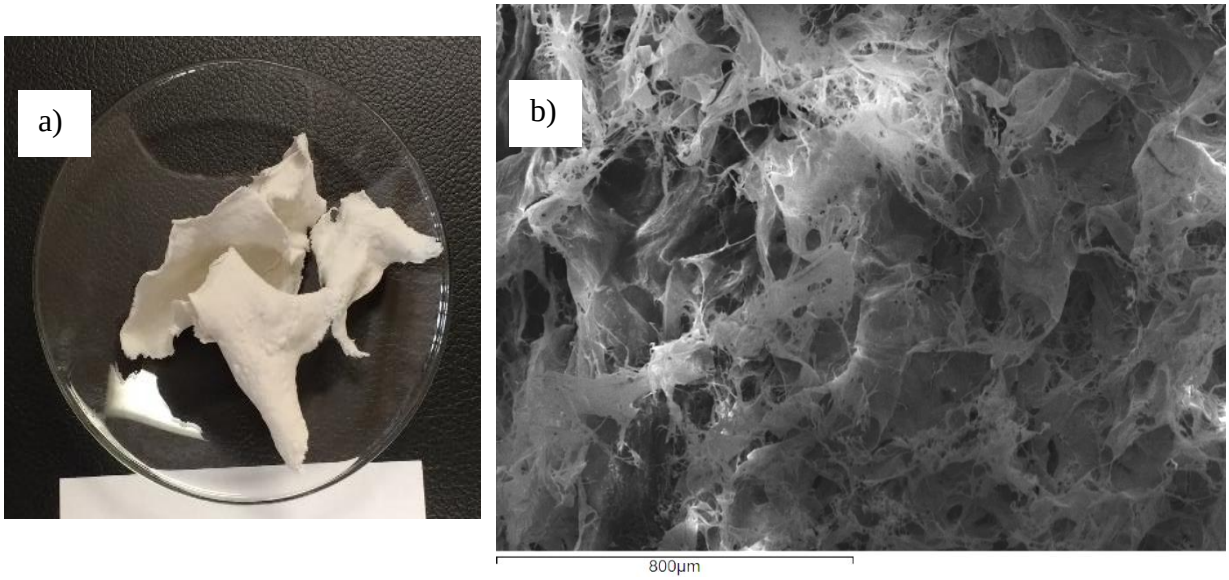

Figure 6.50 Air dried PEO compatibilized MFC. The filler product is difficult to grind and introduce in the polymer matrix a). ×150 SEM image of the freeze dried PEO compatibilized MFC filler. The freeze-drying procedure prevented the cellulose fibrils from collapsing and preserved the typical MFC networked structure.

6.5 Mechanical properties of the tannic acid alkyl amine compatibilized MFC reinforced composites

The tannic acid surface compatibilization of the MFC resulted in a thermostable and easily processable final product. The dry form of the modified MFC was, in fact, ground at room temperature to obtain a powder that was premixed with the neat matrix and compounded to obtain a set of composites at different filler loadings. Unlike the surface reactions previously described, this modification successfully increased the tensile properties of the neat matrix.

The mechanical and impact properties of the tannic acid-octadecylamine- MFC reinforced composites were evaluated against the neat PPPE matrix properties. These properties were compared with composites using inorganic reinforcements (talc and glass fibres), and properties obtained using the MAgPP-MFC reinforcement.

The use of the talc and glass fibres improved the modulus of the neat polymer and marginally impaired its impact properties. On the other hand, MAgPP and tannic acid-octadecylamine compatibilized MFC performed less well as reinforcements. Nevertheless, an increase in tensile properties of the MAgPP- and TA-C_{18}- MFC reinforced composites was registered at concentrations as low as 1 wt.%. The impact properties of the MFC reinforced composites were strongly compromised even at a 1 wt.% concentration. This is most likely due to the presence of large filler aggregates. The results of tensile and impact tests of 1 wt.% reinforced tannic acid-octadecylamine and reference filler composites are summarised in **Table 6.5**.

Table 6.5 Tensile and impact properties of pure matrix (PPPE) and 1 wt.% reinforced composites

	Modulus [GPa]					***Impact Energy [kJm^{-2}]***				
	PPPE	***+1% Talc***	***+1% GFs***	***+1% MFC MAgPP***	***+1% MFC TAC$_{18}$***	***PPPE***	***+1% Talc***	***+1% GFs***	***+1% MFC MAgPP***	***+1% MFC TAC$_{18}$***
Av	***1.098***	***1.440***	***1.204***	***1.235***	***1.120***	***76***	***61***	***43***	***25***	***55***
err	1.9×10^{-1}	2.5×10^{-1}	7.8×10^{-1}	1.9×10^{-1}	2.5×10^{-1}	3.0×10^{-1}	8.0×10^{-1}	4.0×10^{-1}	2.0×10^{-1}	6.0×10^{-1}
p	***-***	***1.79×10^{-7}***	***1×10^{-1}***	***5×10^{-4}***	***2.4×10^{-1}***	***-***	***9×10^{-2}***	***4×10^{-4}***	***5.9×10^{-6}***	***7.2×10^{-3}***

As the addition of the tannic acid-octadecylamine-MFC enhanced the tensile properties of the PPPE matrix, composites at loadings in the range between 0.5 and 15 wt. % were prepared to investigate this effect. The results are listed in **Table 6.6**.

The addition of the tannic acid-octadecylamine-MFC enhanced the tensile properties of the composite at all filler loadings. However, to obtain significant improvement in the modulus of the composites, a minimum of 2 wt.% of tannic acid-octadecylamine-MFC load is required ($p \leq 0.05$, **Table 6.6**). The reinforcement of the neat matrix with filler loading above 2 wt.% had a deep effect on the fracture properties of the composite produced. Owing to the presence of large visible aggregates, the impact resistance of the reinforced composites decreased at increasing filler loadings. The 0.5 wt.% reinforced composite samples showed an increased value of the impact energy compared with the neat matrix. The tensile properties were not significantly different from the neat matrix ($p = 0.4$). The increase in the filler concentration resulted in enhanced tensile properties, but also in a sharp decrease in the fracture toughness for all the tannic acid-octadecylamine-MFC reinforced composites.

Table 6.6 Tensile and impact properties of pure matrix (PPPE) and TA-octadecylamine-MFC (MFC-TA-C_{18}) reinforced composites at filler addition up to 15 wt.%

	Modulus [GPa]						
	PPPE	**+0.5%cMFC TAC$_{18}$**	**+1% MFC TAC$_{18}$**	**+2%MFC TAC$_{18}$**	**+5% MFC TAC$_{18}$**	**+10% MFC TAC$_{18}$**	**+15% MFC TAC$_{18}$**
Av	***1098***	***1.100***	***1.120***	***1.140***	***1.160***	***1.255***	***1.470***
err	18	2.6×10^{-1}	2.5×10^{-1}	1.8×10^{-1}	9×10^{-2}	1.9×10^{-1}	2.6×10^{-1}
P	**-**	4×10^{-1}	2×10^{-1}	5×10^{-2}	4×10^{-3}	2×10^{-5}	1×10^{-7}

	Impact Energy [kJm^{-2}]						
	PPPE	**+0.5%cMFC TAC$_{18}$**	**+1% MFC TAC$_{18}$**	**+2%MFC TAC$_{18}$**	**+5% MFC TAC$_{18}$**	**+10% MFC TAC$_{18}$**	**+15% MFC TAC$_{18}$**
Av	***76***	***101***	***55***	***51***	***28***	***26***	***25***
err	4	9	6	2	3	1	1
p	**-**	4×10^{-2}	7×10^{-3}	5×10^{-4}	5×10^{-5}	3×10^{-6}	8×10^{-7}

Figure 6.51 compared the modulus and fracture energy of the neat matrix and the inorganic and MFC reinforced composites. The inorganic fillers had the best combination of tensile and impact properties, and also at extremely low loadings (1 wt. %). Among the MFC reinforced composites, the 1 wt.% MAgPP-MFC reinforced composite gave the same properties as the 10 wt.% TA-octadecylamine-MFC reinforced sample ($p>0.05$). The 15 wt.% TA-octadecylamine-MFC reinforced composite had tensile properties comparable to the 1 wt.% talc reinforced composites ($p >0.05$), but the MFC reinforced sample had the lowest mechanical properties compare to its inorganic counterpart in term of fracture toughness; below the values obtained when adding 1 wt.% glass fibres.

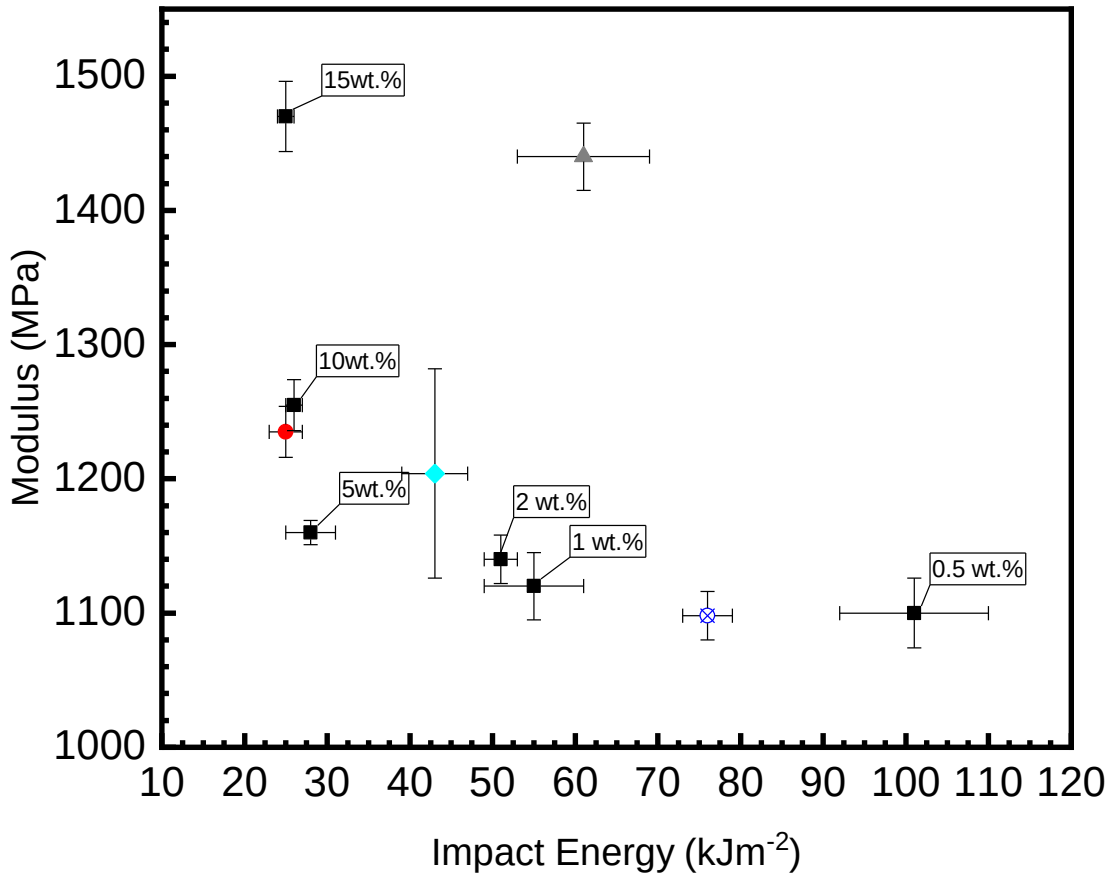

Figure 6.51 Tensile and impact property comparison of the neat PPPE matrix (blue crossed circle), 1 wt.% talc (grey triangle), 1 wt.% glass fibres (cyan diamond), 1 wt.% MAgPP-MFC (red dot), and 0.5 to 15 wt.% TA-octadecylamine-MFC reinforced composites (black squares).

The effectiveness of the tannic acid-octadecylamine-MFC as reinforcement in polyolefin composites only at a relatively high loading was attributed to the partial dispersion of the filler in the matrix. The presence of the large aggregates found in the MFC reinforced composite reduced the filler-matrix interphase and consequently decrease the stress transfer between the matrix and the cellulose fibrils. This led to an overall reduced effect of the MFC filler as a reinforcement. An important parameter to determine how much the filler agglomeration affected the real potential of cellulose fibrils as a reinforcement is the theoretical tensile modulus of the composites estimated through the 'Rule of Mixtures' according to the equation.

$$E_{\text{composite}} = \eta_0 \eta_1 E_{\text{fibril}} V_{\text{fibril}} + (1 - V_{\text{fibril}}) E_{\text{matrix}} \quad \textbf{(3)}$$

where $E_{\text{composite}}$ is the modulus of the composite, V_f is the volume fraction of the fibres (or fibrils) in the composite and E_{matrix} is the modulus of the matrix; η_l and η_0 are the fibre length and orientation efficiency factors: η_l is equal to 1 for long fibres, and η_0 is equal to $\frac{3}{8}$ for an in-plane random orientated network. The mechanical properties of a single cellulose fibril were evaluated using the Cox equation[292] for an in-plane random network of fibres through an independent experiment on MFC films. The tensile modulus of the sheets, E_{network}, was found to be approximately 3.5 GPa. The modulus for a single cellulose fibril can be calculated using the equation

$$E_{\text{fibril}} = \frac{8}{3} \times E_{\text{network}} \quad \textbf{(4)}$$

This gave an experimental value of E_{fibril} of 10 GPa. By comparison, the extrapolation of the moduli of the composites to 100 % filler content, using the fit obtained in **Figure 6.52**, gives an E_{network} modulus of 3.4 GPa, resulting in an effective value of E_{fibril} of 12.6 GPa.

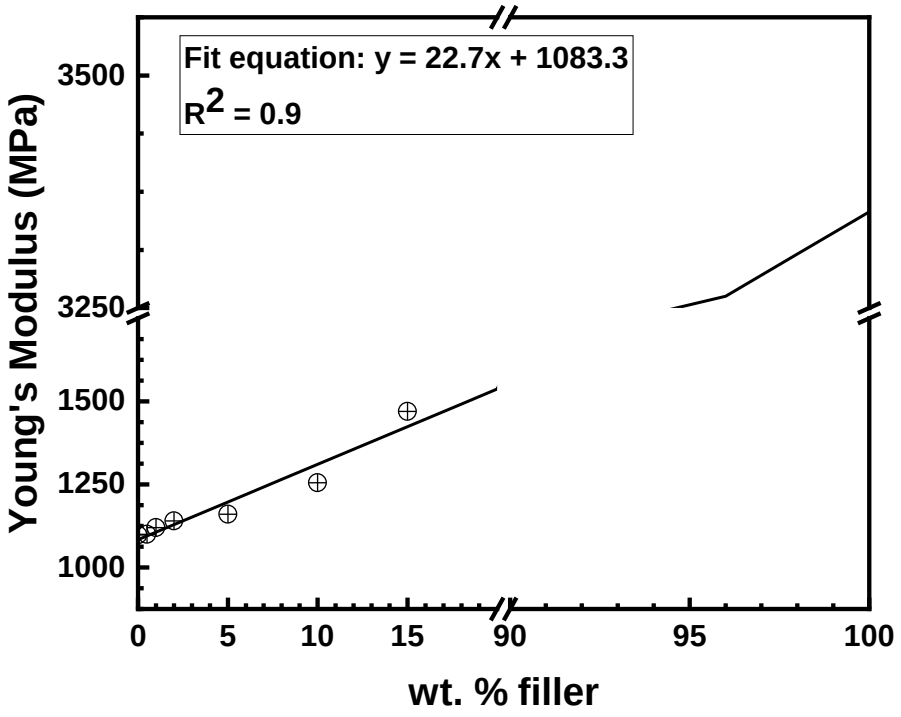

Figure 6.52 Experimental modulus data obtained from MFC-TA-C_{18} reinforced composites (dots). The solid line is a linear fit to these data, from which the fibril modulus E_{fibril} is estimated to be 12.6 GPa.

The relationship between the modulus of the composites and the volume fraction of the filler is approximately linear (**Figure 6.52**, R^2=0.94), in agreement with the rule of mixtures, from which an estimation the fibril modulus is found to be 12.6 GPa. The tensile data for the MFC reinforced composites showed a good adherence to the theoretical prediction made using the rule of mixtures for loads below 2 wt.%. For greater loadings, the real performance of the composites falls below the theoretical prediction. The described behaviour of highly reinforced composites was attributed to the incomplete dispersion of the cellulose fibrils: the presence of large aggregates most likely gave rise to an inefficient stress-transfer. To investigate further, the mechanical properties of a wider range of the samples prepared by different routes as described in **Figure 4.5** and **Table 6.6** were measured. The results of all of these measurements are listed in **Table 6.6** and plotted as impact strength vs. modulus in **Figure 6.53**.

The addition of MFC to the neat PPPE matrix increased the tensile modulus of all of the composites. However, the MFC surface treatment and the filler drying method is shown to have an effect on the fracture properties of the composites. The incorporation of never dried MFC fibrils in the PPPE matrix was found to be a less efficient method to prepare MFC reinforced composites.

In fact, the never dried MFC reinforced composites demonstrated tensile modulus increases greater than 50 %, but only for high filler loadings (20 wt.%). Untreated MFC and tannic acid-hexylamine fibrils had the lowest impact on tensile modulus accounting for modulus increases from a minimum of 0.8% (P1) up to a maximum of 57 % (P6). The tannic acid octadecylamine reacted MFC reinforced composites shown modulus increases of 38 and 57 % respectively for the 1 and 20 wt.% reinforced samples. These increases indicate a better stress transfer efficiency between the matrix and the compatibilized filler. The impact properties of the composites prepared using never dried fillers decreased sharply compared to the neat matrix. The impact energy decrease was evaluated to be greater than -40 % for all the specimens regardless of the MFC surface chemistry. It is worth noticing that the addition of untreated and tannic acid-hexylamine reacted MFC filler in the PPPE had a greater impact on the impact properties of the composites. This was due to the increased size of the aggregates found in them, as proven by SCLSM mapping.

The only form of the oven-dried MFC that can be efficiently used to produce reinforced composites is the tannic-acid octadecylamine, because the hornification that occurred in the hydrophilic forms of MFC (untreated and tannic acid-hexylamine reacted samples, P7-10), prevented the separation of the fibrils after drying and their dispersion in the polymer. The tannic acid octadecylamine-MFC reinforced composites were prepared by direct mixing and by solvent-assisted mixing. Despite being introduced to enhance the filler dispersion and assist in the development of a more complete filler-matrix stress transfer, the solvent assisted method proved to be detrimental in term of tensile and impact properties.

The addition of the tannic acid-octadecylamine-MFC filler increased the tensile modulus of the composites (P11-14), compared to the neat matrix, but no significative difference was found between the composites prepared by solvent-assisted or direct mixing. On the other hand, the solvent assisted mixing proved to be detrimental to the impact properties of the composites; the impact energy of the samples prepared by solvent-assisted mixing decreased by -46 and -72 % for the 1 and 20 wt.% loading respectively, compared to -30 and -44 % decreases for composites prepared by direct mixing.

The fillers produced by freeze-drying were all grindable at room temperature. This made the preparation of the composites reinforced using MFC with different surface treatments possible. It was also possible to do this by solvent-assisted or direct mixing.

It is worthwhile noting that none of the composites prepared by solvent-assisted mixing performed mechanically better than the composites prepared by direct mixing. The proposed explanation for this is that the lower viscosity makes it easier for the cellulose fibrils to segregate from the matrix even after having separate and surface treated them. All the composites prepared by solvent-assisted mixing exhibited decreases in the impact properties greater than -60 %. The highly loaded untreated MFC (P20) and tannic acid-hexylamine MFC (P22) samples resulted in a brittle composite, with impact properties below the instrument threshold. The composites obtained by direct mixing using the hydrophilic forms of MFC (untreated P15-16 and tannic acid-hexylamine-MFC P19-20) resulted in composites with marginally improved tensile properties but strongly compromised impact properties due to the inefficient dispersion of the polar fillers in the apolar matrix, and to the presence of large aggregates as demonstrated by SCLSM mapping.

The most efficient method to produce MFC reinforced composites with improved tensile properties was by the addition of the freeze-dried tannic acid-octadecylamine reacted MFC using a direct mixing approach. The composites obtained using the freeze-dried tannic acid-octadecylamine reacted MFC shown significant improvement in term of tensile modulus: +31 and +75 % for the 1 and 20 wt.% filler loadings respectively, while the impact properties decreased by -39 and 40 % respectively.

Table 6.7 Tensile and impact properties of the pure matrix (PPPE) and the composites produced. † $p < 0.05$ compared to PPPE properties. For the composites and filler preparation method characteristics please refer to Figure 4.5.

		wt.%	Sample ID		Modulus		errE	Modulus increase	Impact Energy		errIE	Impact Energy decrease	
		[%]	-		[GPa]		[GPa]	[%]	[kJ/m^2]		[kJ/m^2]	[%]	
			PPPE		1.108	±	1.6×10^{-2}	-	71.2	±	4.12	-	Direct mix
Never dried	Untreated	1	**P1**		1.117	±	2.9×10^{-2}	0.8	(†)39.7	±	3.29	-44.6	
		20	**P2**		(†)1.718	±	8.5×10^{-2}	55.0	<5				
	TA-C_6	1	**P3**		(†)1.276	±	4.5×10^{-2}	15.1	(†)35.4	±	2.65	-50.7	
		20	**P4**		(†)1.588	±	7.2×10^{-2}	43.3	(†)22.2	±	2.48	-69.1	
	TA-C_{18}	1	**P5**		(†)1.534	±	3.7×10^{-2}	38.4	(†)42.8	±	2.60	-40.3	
		20	**P6**		(†)1.742	±	4.6×10^{-2}	57.2	(†)22.6	±	4.41	-68.5	
Oven dried	Untreated/TA-C_6	N/A	~~**P7,8,9,10**~~			N/A							Direct mix
	TA-C_{18}	1	**P11**		(†)1.682	±	3.2×10^{-2}	51.8	(†)50.4	±	3.31	-29.7	
		20	**P12**		(†)1.848	±	3.3×10^{-2}	66.7	(†)40.1	±	4.78	-44.0	
		1	**P13**		(†)1.600	±	3.5×10^{-2}	44.2	(†)38.6	±	6.31	-46.1	Solvent assisted mix
		20	**P14**		(†)1.650	±	11.6×10^{-2}	48.9	(†)20.1	±	4.92	-72.0	
Freeze dried.	Untreated	1	**P15**		1.268	±	7.1×10^{-2}	14.4	(†)24.3	±	3.68	-66.2	Direct mix
		20	**P16**		(†)1.926	±	19.4×10^{-2}	73.8	(†)9.7	±	1.23	-86.5	
		1	**P17**		(†)1.384	±	5.5×10^{-2}	24.9	(†)25.1	±	3.85	-65.0	Solvent assisted mix
		20	**P18**		(†)1.458	±	2.8×10^{-2}	31.5	<5				
	TA-C_6	1	**P19**		(†)1.364	±	8.6×10^{-2}	23.1	(†)28.3	±	3.71	-60.6	Direct mix
		20	**P20**		(†)1.390	±	11.1×10^{-2}	25.4	<5				
		1	**P21**		(†)1.306	±	3.3×10^{-2}	17.8	(†)31.5	±	1.97	-56.1	Solvent assisted mix
		20	**P22**		(†)1.336	±	5.7×10^{-2}	20.5	<5				
	TA-C_{18}	1	**P23**		(†)1.458	±	10.2×10^{-2}	31.5	(†)36.5	±	2.43	-49.1	Direct mix
		20	**P24**		(†)1.938	±	7.8×10^{-2}	74.9	(†)43.1	±	4.60	-39.8	
		1	**P25**		(†)1.630	±	3.2×10^{-2}	47.1	(†)26.2	±	2.95	-63.5	Solvent assisted mix
		20	**P26**		(†)1.884	±	2.4×10^{-2}	70.0	(†)19.3	±	1.89	-73.1	

Figure 6.53 compares the modulus and fracture energy of the neat matrix and the inorganic and MFC reinforced composites. The composites reinforced using talc shown the best combination of tensile and impact properties at low and high filler loadings. However, the composite samples denoted P11 and 12 (1 and 20 wt.% oven dried tannic acid-octadecylamine MFC reinforced composites produced by direct mix), and P24 (20 wt.% freeze-dried tannic acid-octadecylamine MFC reinforced composites produced by direct mix) demonstrated properties comparable to the talc reinforced composites. The addition of MFC reinforcement proved to be an alternative to inorganic filler, but high filler loadings were required to obtain improved tensile properties. Increasing the filler loading, however, strongly impairs the impact properties of the composites. Most of the composites in fact demonstrated impact energies inferior to the composites produced by adding 1 wt.% glass fibres to the neat PPPE matrix.

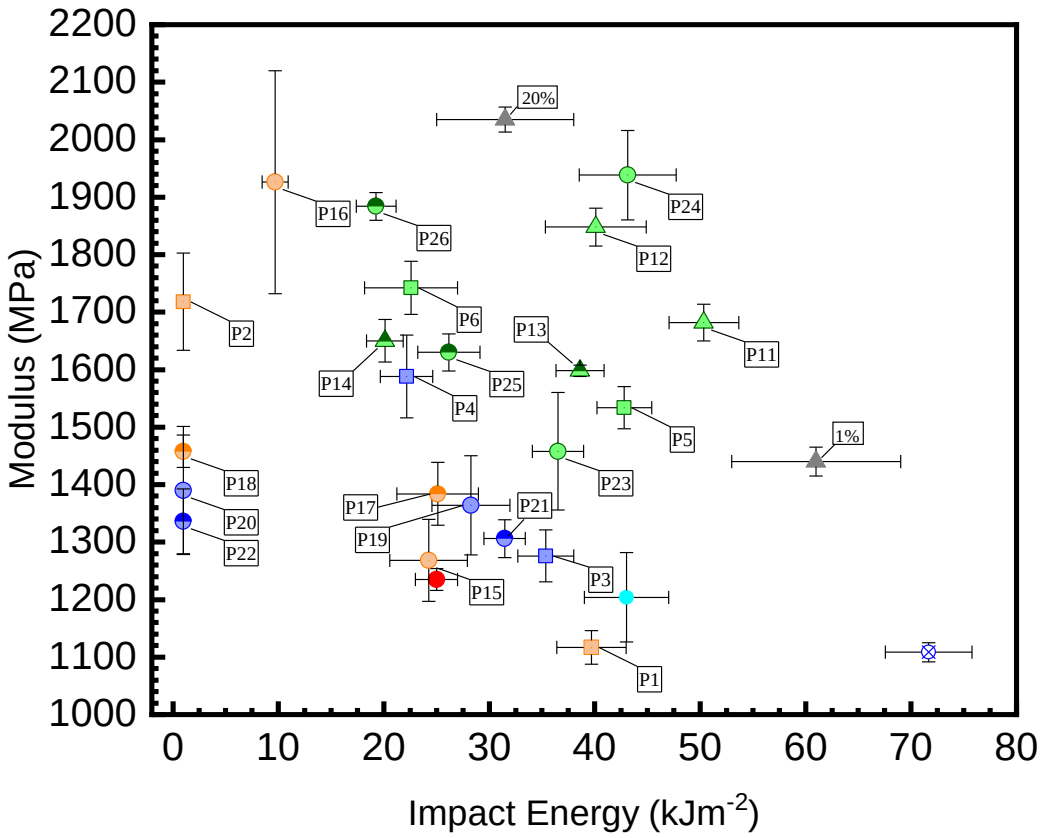

Figure 6.53 Tensile and impact property comparison of the neat PPPE matrix (blue crossed circle), talc (grey triangles), 1 wt.% glass fibres (cyan diamond), 1wt.% MAgPP-MFC (red dot) all used as references, and MFC reinforced composites -orange- untreated, -blue-TA-hexylamine reacted, -green- TA-octadecylamine reacted MFC; -squared- never dried, -triangles- oven dried, -circles- freeze dried; -monocromatic- direct mix, split symbol- toluene method.

In summary: SEM imaging of the MAgPP compatibilized MFC indicated the presence of aggregates of the compatibilizer on the surfaces of the cellulose fibrils. The aggregates were thought to be crystals of MAgPP as confirmed by XRD. Composites obtained using MAgPP compatibilized MFC indicated an enhanced tensile strength for a 1 wt.% filler reinforcement, and decreased impact properties, as would be expected from an incompletely dispersed reinforcement.

MAgPP compatibilized MFC reinforced composites were used as a reference for comparison with the water-based compatibilizations used, and in particular the mechanical performance of the composites produced from them. The water-based methods were based on the never-dried MFC slurry reacted with PVOH, PEO, and never dried, freeze-dried, oven-dried tannic-and tannic acid-primary amines respectively and against two conventional inorganic fillers - glass fibres (GFs) and talc.

The filler dispersion and filler aggregate distribution in the produced composites were critical parameters to be evaluated and were shown to have a major effect on the tensile and impact properties of the composites produced. To evaluate the filler dispersion in the composites, a series of analytical techniques were used. The methods used included EDX, TEM, and ToF-SIMS as qualitative techniques, while a more quantitative study was carried out using SCLSM mapping.

The EDX analysis revealed the presence of aggregates of ~100 μm for the 1wt.% MAgPP-MFC reinforced composites, while smaller aggregates were found for the 1 wt.% tannic acid-octadecylamine-MFC reinforced composites. The average aggregate size for the latter composites was estimated to be in the range 25-100 μm. The larger agglomerates were generally surrounded by smaller fragments. This finding indicated that a fraction of the compatibilized filler can be dispersed to a smaller scale. To verify that hypothesis, high magnification TEM was used on the 0.5 wt.% and 15 wt.% tannic-octadecylamine-MFC reinforced composites, but it didn't give conclusive results because the contrast was insufficient. The high magnification images of the composites were not conclusive but were found in agreement with the EDX analysis. However, due to the lack of specificity of the EDX analysis, the complex preparation process for TEM samples and the poor contrast obtained in the images, more suitable spectroscopic techniques were used.

ToF-SIMS allowed the reconstruction of 2D images of the tannic acid-hexylamine-MFC and tannic acid-octadecylamine-MFC reinforced composites.

The comparison of the ToF-SIMS images for these two different systems showed that while the MFC reacted with the short hexylamine, it was insufficient to disperse it homogeneously in the matrix. The octadecylamine treatment was successful in dispersing the filler to a much smaller scale, supporting the data obtained from EDX and TEM analysis.
ToF-SIMS analysis allowed a rapid and qualitative assessment of the filler dispersion in the composites. However, a detailed analysis of the filler aggregate size and distribution was carried out using SCLMS mapping, for which the findings were in accordance with those from ToF-SIMS. The modification of MFC with tannic acid and octadecylamine improved the filler dispersion within the apolar PPPE composite. This finding is supported by the polymer background intensity signal increase when the tannic acid-octadecylamine surface treatment was used, and a decrease in the observed aggregate area. Increasing the tannic acid-octadecylamine-MFC filler loading to 15 wt.% in the composite did not result in increased aggregate size. Therefore, the composite was not saturated below a tannic acid-octadecylamine-MFC loading of 15 wt.%.

A series of 1 and 20 wt.% loaded composites obtained using never dried, freeze-dried and oven dried MFC fillers and prepared by direct and solvent assisted mixing were compared to gain a better understanding of the filler dispersion and aggregate size using SCLSM mapping. The analysis confirmed that the tannic acid octadecylamine was efficient in enhancing the MFC filler dispersion for all drying methods. In fact, the composites containing tannic acid-octadecylamine-MFC presented significantly smaller aggregates, compared both to the unreacted MFC and to the tannic acid hexylamine treated reinforced samples. The final conclusion from the SCLSM filler aggregate analysis indicated that while the freeze-drying technique reduces the average dimension of the aggregates, no major advantage was obtained from the use of freeze-dried fillers in terms of dispersion.
The analysis also indicated that, contrary to the initial hypothesis, solvent assisted mixing did not enhance the MFC filler dispersion but contributed to the filler agglomeration and segregation. Therefore, the direct mixing remains the most suitable composite preparation method.
The filler loading had a neglectable impact on the filler aggregate size distribution, confirming that the MFC reinforced composites were not saturated at filler loadings up to 20 wt%.
The tensile and impact properties of all the produced samples were evaluated against the neat matrix.

While the myristoyl chloride, the PVOH and the PEO compatibilized MFC reinforced composites did not show any significant improvement over the neat matrix tensile properties, the MAgPP- and tannic acid-octadecylamine-MFC reinforced composite did show significant improvement in the stiffness of the composites. The reinforcement potential of tannic acid-octadecylamine-MFC was theoretically estimated using the 'Rule of Mixtures'. This analysis revealed a good agreement between the experimental results and the theory at low filler concentrations. However, at higher concentrations there was less agreement, probably indicating a less homogeneous dispersion of the filler in the matrix; this hypothesis was supported by the ToF-SIMS and SCLSM data.

The mechanical and impact properties of GFs, talc, MAgPP-MFC, and TA-octadecylamine-MFC reinforced composites were compared against the pure matrix. The data indicate that MFC based fillers perform less well than inorganic materials in enhancing the stiffness of the composites and the preservation of their impact properties. The filler dispersion data obtained from SCLSM cluster analysis correlates well with the stiffness increases registered for the composites, and with the sharp decrease in the impact properties of the MFC reinforced samples. The critical aggregate size calculated for the tannic acid-octadecylamine-MFC reinforced polyolefin composites is ≈37 nm which represents the critical aggregate size below which the composite will behave as a flawless structure. Because most of the aggregates found in the composite exceed this size, regardless of the filler loading, and because of the imperfect nature of the cellulose aggregates, the critical aggregate size analysis suggests that composites made with FiberLean MFC can never behave as flawless structures because the fibres and fibrils themselves are much larger than the critical size. Further work is necessary to achieve a better level of filler dispersion and fully exploit the FiberLean potential as a polyolefin reinforcement material.

6.6 Comparison of mechanical properties with theoretical models

Large filler aggregates were found in all the specimens regardless of the MFC surface treatment, the filler production method or the compounding method, as demonstrated by SCLSM analysis. The analysis of the aggregate size and distribution indicated that whilst the aggregate size is not dependent on the filler content, the number of aggregates found in the reinforced composites increases with it. Most aggregates had a viewable area between 11.0 and 30.3 μm^2 and were classified as small particles. The filler aggregation in PPPE composites is thought to marginally affect stiffness, but to strongly influence the impact resistance, which decreases sharply as aggregation increases.[114] In nanocomposites, the reinforcement carries the tensile load while the matrix transfers this load between the reinforcement particles.[346] To ensure the integrity of the composite structure, the reinforcement should be able to withstand large tensile stress without fracture, whilst the matrix should carry large shear stress without failure. The fracture resistance of a brittle solid is influenced by the flaw size according to Griffith criterion:

$$\sigma_r^f = \alpha E_r \Psi \quad \textbf{(5)}$$

$$\Psi = \sqrt{\frac{\gamma}{E_r h}} \quad \textbf{(6)}$$

where σ_r^f is fracture strength of the material (in this case aggregates of cellulose in the matrix), E_r is the theoretical modulus of the reinforcement, in this case, cellulose fibril, γ is the interfacial surface energy between the reinforcement and the matrix, and h is the thickness of the reinforcement. The parameter α depends on the crack geometry and can be considered approximately equal to $\sqrt{\pi}$. Below a defined reinforcement thickness (h^*) the fracture strength of a cracked reinforcement particle becomes identical to that of a flawless structure.[346] It is possible to estimate the critical aggregate length scale as:

$$h^* \approx \alpha^2 \frac{\gamma E_r}{\sigma_{th}^2} \quad \textbf{(7)}$$

The values considered for the calculation are γ=0.0339 J/m^2 calculated for the tannic acid-octadecylamine reacted cellophane film, E_r= 20 GPa and σ_{th} represents the theoretical tensile strength of cellulose fibrils and is equal to 240 MPa.[39,40,59] Using these values we estimate h* to be ≈ 37 nm. The dimension of the small aggregate found using the SCLSM analysis accounts for 11 μm^2 and thus a length of about 4 μm. The small aggregate found in the composites exceeds the critical aggregate length scale (0.037 μm) by several orders of magnitude. This indicates that the cellulose filler is not sufficiently dispersed to obtain its full potential as a reinforcement without compromising fracture toughness, as demonstrated by the recorded impact properties of the composites analysed.

7. Conclusions

The following chapter summarise and discuss the main finding of this research project. The results obtained were used to address the objective of this research work. The future work section highlights areas of future development and suggest future applications of the results obtained from the present research work.

In this research, the preparation and characterization of MFC reinforced polyolefin composites using traditional manufacturing methods was successfully achieved. Due to the presence of large filler aggregates in the composites, impact properties were strongly affected while tensile modulus was incremented only marginally. The requirements to produce good quality MFC-reinforced composites shaped the intermediate objectives of the present research work.

The intermediate aims of this research were

- ✓ the production of a hydrophobic and thermostable form of MFC, avoiding if possible the use of organic solvents and energetically demanding processes (*e.g*. freeze-drying);
- ✓ the production of homogeneously dispersed MFC-reinforced composites using conventional polyolefin manufacturing processes (*e.g.* compounding and injection moulding);
- ✓ to clarify the correlation between tensile modulus, impact energy and MFC filler dispersion in composites, using a sensible set of techniques to determine the size distribution of filler aggregates;
- ✓ to identify the most successful MFC-reinforced composite production route, combining the most suitable MFC surface chemistry, drying method, filler incorporation and compounding procedure.

The present research work was sponsored by FiberLean Technologies, a multinational company specialised in the production of Fiberlean^{TM}, a form of MFC produced using minerals as co-grinding media. The present study was aimed at developing an industrially applicable methodology to produce FiberLean^{TM} reinforced polyolefins at one of the company's production sites. The method selected was supposed to be efficient and easy to integrate into the current FiberLean production lines.

A series of organic solvents and water-based surface reaction methods were selected from the relevant literature on cellulose reinforced composites to investigate the production of hydrophobic thermostable forms of compatibilized MFC.

Myristoyl chloride compatibilized MFC was found to have an onset degradation temperature of <100°C, unsuitable for further processing. The MAgPP based MFC compatibilization was successful in producing a hydrophobic and thermally stable form of MFC filler. This approach was used to determine the dispersion of the reference filler, and the mechanical properties of a compatibilized MFC reinforced composite. Composites obtained using MAgPP compatibilized MFC were found to have an enhanced tensile strength for a 1 wt.% filler reinforcement, and decreased impact properties. Both PVOH and PEO compatibilized MFC fillers retained the original thermal stability of the untreated MFC, presenting degradation temperatures above the polymer processing temperature (≈ 200 °C), but the reinforced composites obtained using both modified fillers proved to perform poorly in terms of composite stiffness

The water-based reaction of tannic acid (TA) and primary aliphatic amines (water-soluble hexylamine and water insoluble octadecylamine) with never-dried MFC slurry was selected as the most effective and industrially applicable methodology to modify the hydrophilicity of the cellulose fibrils and enhance their dispersibility in the apolar polyolefin matrix. The results obtained using the tannic acid method were compared with two conventional inorganic fillers - glass fibres (GFs) and talc - and MFC treated using MAgPP, the method chosen from the literature which appeared to be the most reliable.

A first step in the production of these materials was the optimisation of the MFC:tannic acid:primary amine ratio. The MFC:tannic acid:primary amine ratio optimization was calculated for the octadecylamine reagent was found to be 10g-MFC dry fibrils:5g-tannic acid:5g-octadecylamine. This ratio was then used to prepare the TA-octadecylamine based MFC fillers. The reaction between ta and octadecylamine probably involves the formation of a Schiff base as a final product. FTIR spectroscopy indicated the presence of a strong absorption between 2800 and 3000 cm^{-1} and a small peak between 1400 and 1500 cm^{-1} in tannic acid-octadecylamine reacted MFC, related to the presence of covalently attached amines.

The crystallinity of the reinforced composites was recorded: the addition of MAgPP-MFC and tannic-octadecylamine-MFC (1 wt.%) only marginally changed the crystallinity of the pure matrix at the different concentrations. The additions of larger amounts of tannic acid-octadecylamine-MFC filler impact on the crystallinity of the composites, which reached a maximum value of 0.5 at a 0.5-5 wt.% tannic acid-octadecylamine-MFC filler addition.

The filler dispersion and filler aggregate distribution in the produced composites evaluate using EDX, TEM, and ToF-SIMS as qualitative techniques, while a more quantitative study was carried out using SCLSM mapping.

The EDX analysis revealed the presence of aggregates of ~100 µm for the 1wt.% MAgPP-MFC reinforced composites, while smaller aggregates were found for the 1 wt.% tannic acid-octadecylamine-MFC reinforced composites. The average aggregate size for the latter composites was estimated to be in the range 25-100 µm. The larger agglomerates were generally surrounded by smaller fragments. This finding indicated that a fraction of the compatibilized filler can be dispersed to a smaller scale. A detailed analysis of the filler aggregate size and distribution was carried out using SCLMS mapping, for which the findings were in accordance with those from ToF-SIMS. The modification of MFC with tannic acid and octadecylamine improved the filler dispersion within the apolar PPPE composite as proven by the decrease in the observed aggregate area.

A series of 1 and 20 wt.% loaded composites obtained using never dried, freeze-dried and oven dried MFC fillers and prepared by direct and solvent assisted mixing were compared to gain a better understanding of the filler dispersion and aggregate size using SCLSM mapping.

The analysis confirmed that the tannic acid octadecylamine was efficient in enhancing the MFC filler dispersion for all drying methods. The SCLSM filler aggregate analysis indicated that no major advantage was obtained from the use of freeze-dried fillers in terms of dispersion.

The analysis also indicated that, solvent assisted mixing did not enhance the MFC filler dispersion. The reinforcement potential of tannic acid-octadecylamine-MFC was theoretically estimated using the ‘Rule of Mixtures’.

The mechanical and impact properties of GFs, talc, MAgPP-MFC, and TA-octadecylamine-MFC reinforced composites indicate that MFC based fillers perform less well than inorganic materials in enhancing the stiffness of the composites. The critical aggregate size calculated for the tannic acid-octadecylamine-MFC reinforced polyolefin composites is ≈37 nm which represents the critical aggregate size below which the composite will behave as a flawless structure. Because most of the aggregates found in the composite exceed this size, regardless of the filler loading, and because of the imperfect nature of the cellulose aggregates, the critical aggregate size analysis suggests that composites made with FiberLean MFC can never behave as flawless structures because the fibres and fibrils themselves are much larger than the critical size. Further work is necessary to achieve a better level of filler dispersion and fully exploit the FiberLean potential as a polyolefin reinforcement material.

The main conclusions of this research work can be summarised as follow:

1. The water-based reaction of tannic acid and octadecylamine with MFC is a convenient method for the production of hydrophobic forms of MFC
2. The hydrophobisation of MFC is, however, a necessary but not a sufficient condition to ensure good dispersion of the compatibilized filler in the matrix
3. The presence of large aggregates in the composites was proven by a variety of spectroscopic and microscopic techniques, and it had a detrimental effect on the impact performance of the composites.
4. Commercial products containing cellulose fibres exceeding the calculated size limit of ≈37 nm have shown enhanced tensile and impact properties, indicating that is not necessary to disperse the MFC fibrils to the theoretical calculated size limit to obtain high performance composites reinforced with cellulose fibrils.

The main conclusion of this work leave, however, important unanswered questions that are presented in the future work section below.

7.1- Future work

The research work presented in this thesis identified an easy and water-based method based on tannic acid and octadecylamine to produce a hydrophobic form of MFC. This hydrophobic form of MFC can be dried either in a conventional vacuum oven or in a freeze drier. The final product is grindable at room temperature and premixed to a polymer powder and processed using conventional thermoplastic processing equipment.

The results obtained, however, have left some important questions unanswered:

1. Is the water-based tannic acid/primary amine reaction an effective method to produce hydrophobic MFC with tailorable characteristics suitable for the use with less apolar matrices (e.g. PLA)?
2. Is the aggregation of MFC fibrils inevitable, and is it caused by the peculiar branched structure of the product? Conversely, could a more aggressive production method enhance the filler dispersion and completely disaggregate the MFC?
3. What would be the effect of narrowing the size distribution of the MFC on its dispersion and aggregation and on the mechanical and impact properties of the composites?

To answer these important questions, a set of strategies were planned which are presented in the next paragraphs.

The hydrophobic powder form of cellulose produced in this study can be used as reinforcement for different thermoplastic matrices, a relevant example of which is polylactic acid (PLA).

PLA is aliphatic polyester commonly obtained from the α-hydroxy acid and is considered biodegradable and compostable. [404,405] PLA is a thermoplastic characterised by high strength and high tensile modulus; its main use is in industrial packaging and medical devices.[405]

PLA is commonly processed using standard processing equipment to produce moulded parts or fibres. Its stereochemical structure and its thermomechanical behaviour can be easily modified by polymerising a mixture with a controlled ration of L- or and D-isomers to obtain a high molecular weight amorphous or crystalline polymer.[406]

PLA degradation is due to the hydrolysis of the ester bond which can occur at room temperature without the need for catalysts. The degradation rate varies considerably according to the final product crystallinity, isomer ratio, temperature and humidity. [404]

The PLA matrix appears to be an excellent candidate in the production of biodegradable and environmentally friendly MFC reinforced composites.

PLA has a surface energy of 37.1 mNm^{-1}, a value that can allow a good dispersion of both tannic acid- hexylamine and -octadecylamine reacted MFC. The processing conditions of PLA are also compatible with the unreacted and compatibilized MFC as the PLA melting temperature is 175 °C and it undergoes thermal degradation above 200 °C, depending on temperature, low-molecular-weight impurities, and catalyst concentration in the product. [404,407,408]

The manufacture of PLA-MFC reinforced composites is not as straightforward as the production of reinforced polyolefins, because the PLA matrix is extremely sensitive to moisture[323,409] and has slow crystallisation kinetics. The addition of cellulose-based filler has been reported to influence both the crystallisation kinetics and the crystallinity fraction of the cellulose reinforced PLA based composites.

The crystallinity fraction and the size of the crystals have a significant effect on the mechanical properties of the composites. To enhance the impact property of the PLA based samples, annealing at 75 °C can follow the product manufacture to increase the crystal size and crystallinity fraction of the products.

Because of the peculiar melting and crystallization behaviour of the PLA matrix and its extreme sensitivity to moisture, the manufacturing conditions of the composites and the operational parameters must be carefully selected to obtain good filler dispersion, avoid PLA matrix degradation and allow the matrix to crystallize. The optimum conditions need careful planning.

To investigate the suitability of the tannic acid-primary amine treatment for PLA matrix, the tannic acid-MFC can be reacted with a series of amines of different chain lengths and functionalities. The influence of the matrix crystallinity can be investigated preparing a set of unfilled samples annealed at different time and the results can be used as a baseline for the PLA matrix properties at different crystallinity fractions.

The controlled mechanical deconstruction of the natural cellulose fibres leads to the production of different type of micro- and nano- celluloses having different properties ad possible application depending on their properties, most of which are strongly related to their production method. Mechanical defibrillation of pulp is the elective micro and nanocellulose production method. The mechanical processes on cellulose macroscopic fibres decrease the fibre diameter, increase the product specific area and the uniformity of the particle size distribution.

Those results are generally accompanied by the loss of critical cellulose structure related characteristic such as crystallinity and degree of fibrillation which in turn can have a profound effect on the product quality.[410] The tannic acid/amine procedure can be used to treat different nanocellulose products having a better defined morphology (e.g. those made in refiners and Masuko supermass colloiders, or by enzyme treatment followed by homogenisation). The mechanical and impact results can convey vital information on the influence of the cellulose reinforcement morphology on the processability and on the final properties of the composites. The ultimate test would be the use of TEMPO CNFs, because the fibrils produced by TEMPO-oxidation are not branched and have a very constant fibril diameter of only 4nm. Because of the TEMPO CNFs fibres width of 4nm, if no aggregation occurs, the compatibilized reinforcement produced would meet the critical aggregate size criterion.

To evaluate the effect of the production method on the filler distribution it would be ideal to design a set of experiments changing the compounding profile and increasing the shear mix and residence time of the product. To enhance the filler dispersion it would be also possible to prepare a batch system dispersing the compatibilized MFC filler into a low viscosity solvent/polymer mixture and then solvent cast the system to avoid shear induces filler-matrix separation.

Recently an increasing interest from both the academic and industrial environment was dedicated to the study of the kinetic changes induced in the physical structure properties of cellulosic pulps during fibrillation.[411] The understanding of the connection between the processing used and the characteristic of the produced can render possible to customize the defibrillation process to reach the best compromise among gain, improvement, and loss in cellulose properties while isolating the most suitable MFC for specific applications.

Despite the importance of this topic, however, the dispersion of highly refined cellulose-based reinforcement can be challenging and result in unsatisfactory mechanical and impact properties of the produced composites. Among the various method to enhance the cellulose fillers dispersion in polymeric matrices, the cellulose fibrils surface chemistry proved to be one of the most effective and customizable methods.

“Click”-chemistry principles attracted increasing attention from drug discovery to material sciences filed in both academia and industry. Click-chemistry is based on the use of robust reactions that have high tolerance toward water and oxygen, that have high yields at room temperature, avoiding multiple reactions and purification steps.

A relevant literature exists on the click-chemistry modification of polysaccharides, however only a little effort was dedicated to the modification of cellulose nanostructure using the click-chemistry principles. The introduction of reactive azide groups on the surface of cellulose nanofibrils by esterification with 1-azido-2,3-epoxy-propane in alkaline water/isopropanol-mixture at room temperature, and the successive reaction of the product with propargyl amine by the mean of the copper catalysed azide-alkyne cycloaddition was suggested as an aqueous medium based reaction for the functionalization of cellulose nanofibrils. The final product is a pH-responsive form of 1,2,3-triazole-4-methanamine decorate cellulose fibrils.[412]

Another interesting cellulose fibrils surface reaction is based on the use of an aqueous racemic lactic acid syrup as reactive solvent to achieve a stable and dispersed water suspension to the nanocellulosic product. The active solvent also participates to the esterification reaction producing an oligomer of polylactic acid grafted on the cellulose.

The system allows the *in-situ* solvent exchange from water to lactic acid without prior drying the cellulosic material. The final step consists in the esterification of the grafted cellulose with carboxylic acids or esters having a long hydrocarbon chain.[413]

Both the presented chemical route for the functionalisation of the cellulose fibrils surface present the advantage of being carried out in an aqueous environment under mild condition, however, further investigation is required to verify the suitability of any of the proposed methods.

References

1. Siro, I., Plackett, D., Siró, I. & Plackett, D. Microfibrillated cellulose and new nanocomposite materials: a review. *Cellulose* **17**, 459–494 (2010).

2. Sehaqui, H., Zhou, Q., Ikkala, O. & Berglund, L. A. Strong and tough cellulose nanopaper with high specific surface area and porosity. *Biomacromolecules* **12**, 3638–3644 (2011).

3. Svagan, A. J., Azizi Samir, M. A. S. & Berglund, L. A. Biomimetic Polysaccharide Nanocomposites of High Cellulose Content and High Toughness. *Biomacromolecules* **8**, 2556–2563 (2007).

4. Andresen, M. & Stenius, P. Water in oil Emulsions Stabilized by Hydrophobized Microfibrillated Cellulose. *J. Dispers. Sci. Technol.* **28**, 837–844 (2007).

5. Stenstad, P., Andresen, M., Tanem, B. S. & Stenius, P. Chemical surface modifications of microfibrillated cellulose. *Cellulose* **15**, 35–45 (2008).

6. Cheng, Q., Wang, S., Rials, T. G. & Lee, S.-H. Physical and mechanical properties of polyvinyl alcohol and polypropylene composite materials reinforced with fibril aggregates isolated from regenerated cellulose fiber. *Cellulose* **14**, 593–602 (2007).

7. Andresen, M., Stenstad, P., Møretrø, T., Langsrud, S., Syverud, K., Johansson, L-S., Nonleaching Antimicrobial Films Prepared from Surface-Modified Microfibrillated Cellulose. *Biomacromolecules* **8**, 2149–2155 (2007).

8. Aulin, C., Varga, I., Claesson, P. M., Wågberg, L. & Lindstrom, T. Buildup of Polyelectrolyte Multilayers of Polyethyleneimine and Microfibrillated Cellulose Studied by in Situ Dual-Polarization Interferometry and Quartz Crystal Microbalance with Dissipation Christian. *Langmuir* **24**, 2509–2518 (2008).

9. Henriksson, M. & Berglund, L. A. Structure and Properties of Cellulose Nanocomposite Films Containing Melamine Formaldehyde. *J. Appl. Polym. Sci.* **106**, (2007).

10. Henriksson, M., Henriksson, G., Berglund, L. A. A. & Lindstrom, T. An environmentally friendly method for enzyme-assisted preparation of microfibrillated cellulose (MFC) nanofibers M. *Eur. Polym. J.* **43**, 3434–3441 (2007).

11. Iwamoto, S., Nakagaito, A. N. & Yano, H. Nano-fibrillation of pulp fibers for the processing of transparent nanocomposites. *Appl. Phys. A Mater. Sci. Process.* **89**, 461–

466 (2007).

12. Werner, O., Persson, L., Nolte, M., Feryd, A. & Wagberga, L. Patterning of surfaces with nanosized cellulosic fibrils using microcontact printing. *Soft Matter* **4**, 1158–1160 (2008).

13. Syverud, K. & Stenius, P. Strength and barrier properties of MFC films. *Cellulose* **16**, 75 (2008).

14. Ahola, S., Salmi, J., Johansson, L. S., Laine, J. & Österberg, M. Model Films from Native Cellulose Nanofibrils. Preparation, Swelling, and Surface Interactions. *Biomacromolecules* **9**, 1273–1282 Model (2008).

15. Henriksson, M., Berglund, L. A., Isaksson, P., Lindström, T., Nishino, T. Cellulose Nanopaper Structures of High Toughness. *Biomacromolecules* **9**, 1579–1585 (2008).

16. Bhatnagar, A. & Sain, M. Processing of Cellulose Nanofiber-reinforced Composites. *J. Reinf. Plast. Compos.* **24**, 1259–1268 (2005).

17. Abe, K., Iwamoto, S. & Yano, H. Obtaining Cellulose Nanofibers with a Uniform Width of 15 nm from Wood. *Biomacromolecules* **8**, 3276–3278 (2007).

18. Ahola, S., Österberg, M. & Laine, J. Cellulose nanofibrils-adsorption with poly(amideamine) epichlorohydrin studied by QCM-D and application as a paper strength additive. *Cellulose* **15**, 303–314 (2008).

19. Pääkkö, M. Vapaavuori, J., Silvennoinen, R., Kosonen, H., Ankerfors, M., Lindström, T., Berglundc, L. A., Ikkala, O. Long and entangled native cellulose I nanofibers allow flexible aerogels and hierarchically porous templates for functionalities. *Soft Matter* **4**, 2492–2499 (2008).

20. Hult, E. L., Larsson, P. T. & Iversen, T. Cellulose fibril aggregation - An inherent property of kraft pulps. *Polymer*. **42**, 3309–3314 (2001).

21. Hult, E.-L., Tomas, L. P. & Tommy, I. A Comparative CP/MAS 13C-NMR Study of the Supermolecular Structure of Polysaccharides in Sulphite and Kraft Pulps. *Cellulose* **7**, 35–55 (2000).

22. Tommi, V., Sirkka, L. M., Tarja, T., Bo, H. & Tiina, L. Changes in fiber ultrastructure during various kraft pulping conditions evaluated by 13C CPMAS NMR spectroscopy. *Carbohydr. Polym.* **73**, 156–163 (2008).

23. Siqueira, G., Bras, J. & Dufresne, A. Cellulosic bionanocomposites: A review of preparation, properties and applications. *Polymers (Basel).* **2**, 728–765 (2010).

24. Andresen, M., Johansson, L. S., Tanem, B. S. & Stenius, P. Properties and characterization of hydrophobized microfibrillated cellulose. *Cellulose* **13**, 665–677 (2006).

25. Aulin, C., Gällstedt, M. & Lindström, T. Oxygen and oil barrier properties of microfibrillated cellulose films and coatings. *Cellulose* **17**, 559–574 (2010).

26. Fukuzumi, H., Saito, T., Iwata, T., Kumamoto, Y. & Isogai, A. Transparent and High Gas Barrier Films of Cellulose Nanofibers Prepared by TEMPO-Mediated Oxidation. *Biomacromolecules* **10**, 162–165 (2009).

27. Aulin, C., Netrval, J., Wagberg, L. & Lindström, T. Aerogels from nanofibrillated cellulose with tunable oleophobicity. *Soft Matter* **6**, 3298–3305 (2010).

28. Fischer, F., Rigacci, A., Pirard, R., Berthon-Fabry, S. & Achard, P. Cellulose-based aerogels. *Polymer.* **47**, 7636–7645 (2006).

29. Shah, J. & Brown, M. R. Towards electronic paper displays made from microbial cellulose. *Appl. Microbiol. Biotechnol.* **66**, 352–355 (2005).

30. Torvinen, K., Sievänen, J., Hjelt, T. & Hellén, E. Smooth and flexible filler-nanocellulose composite structure for printed electronics applications. *Cellulose* **19**, 821–829 (2012).

31. Nakagaito, A. N. & Yano, H. Novel high-strength biocomposites based on microfibrillated cellulose having nano-order-unit web-like network structure. *Appl. Phys. A Mater. Sci. Process.* **80**, 155–159 (2005).

32. Nakagaito, A. N. & Yano, H. Toughness enhancement of cellulose nanocomposites by alkali treatment of the reinforcing cellulose nanofibers. *Cellulose* **15**, 323–331 (2008).

33. Bruce, D. M., Hobson, R. N., Farrent, J. W. & Hepworth, D. G. High-performance composites from low-cost plant primary cell walls. *Compos. Part A Appl. Sci. Manuf.* **36**, 1486–1493 (2005).

34. Malainine, M. E., Mahrouz, M. & Dufresne, A. Thermoplastic nanocomposites based on cellulose microfibrils from Opuntia ficus-indica parenchyma cell. *Compos. Sci. Technol.* **65**, 1520–1526 (2005).

35. Dalmas, F., Cavaillí, J. Y., Gauthier, C., Chazeau, L. & Dendievel, R. Viscoelastic behavior and electrical properties of flexible nanofiber filled polymer nanocomposites. Influence of processing conditions. *Compos. Sci. Technol.* **67**, 829–839 (2007).

36. Aksoy, E. A., Akata, B., Bac, N. & Hasirci, N. Preparation and Characterization of Zeolite Beta–Polyurethane Composite Membranes. *Polym. Polym. Compos.* **5**, 3378–3387 (2006).

37. Auad, M. L., Contos, V. S., Nutt, S., Aranguren, M. I. & Marcovich, N. Characterization of nanocellulose- reinforced shape memory polyurethanes. *Polym. Int.* **57**, 651–659 (2007).

38. Hisaaki, T., Hisashi, H., Etsuko, Y. & Shunichi, H. Thermomechanical properties in a thin film of shape memory polymer of polyurethane series. *Smart Mater. Struct.* **5**, 483 (1996).

39. Zimmermann, T., Pöhler, E. & Geiger, T. Cellulose fibrils for polymer reinforcement. *Adv. Eng. Mater.* **6**, 754–761 (2004).

40. Leitner, J., Hinterstoisser, B., Wastyn, M., Keckes, J. & Gindl, W. Sugar beet cellulose nanofibril-reinforced composites. *Cellulose* **14**, 419–425 (2007).

41. Lu, J., Wang, T. & Drzal, L. T. Preparation and properties of microfibrillated cellulose polyvinyl alcohol composite materials. *Compos. Part A Appl. Sci. Manuf.* **39**, 738–746 (2008).

42. Avérous, L. Biodegradable Multiphase Systems Based on Plasticized Starch: A Review. *J. Macromol. Sci. Part C Polym. Rev.* **44**, 231–274 (2004).

43. Ma, X., Chang, P. R. & Yu, J. Properties of biodegradable thermoplastic starch/carboxymethyl cellulose and starch/microcrystalline cellulose composites. *Carbohydr. Polym.* **72**, 369–375 (2008).

44. Grande, C. J., Torres, F. G., Gomez, C. M., Troncoso, O. P. & Josep, C. Morphological Characterisation of Bacterial Cellulose-Starch Nanocomposites. *Polym. Polym. Compos.* **16**, 181–185 (2008).

45. Mondragán, M., Arroyo, K. & Romero-García, J. Biocomposites of thermoplastic starch with surfactant. *Carbohydr. Polym.* **74**, 201–208 (2008).

46. Sreekala, M. S., Goda, K. & Devi, P. V. Sorption characteristics of water, oil and diesel in cellulose nanofiber reinforced corn starch resin/ramie fabric composites. *Compos. Interfaces* **15**, 281–299 (2008).

47. Svagan, A. J., Hedenqvist, M. S. & Berglund, L. Reduced water vapour sorption in cellulose nanocomposites with starch matrix. *Compos. Sci. Technol.* **69**, 500–506 (2009).

48. Nordqvist, D. Idermark, J., Hedenqvist, M. S., Gällstedt, M., Ankerfors, M., Lindström, T., Enhancement of the wet properties of transparent chitosan - acetic acid - salt films using microfibrillated cellulose. *Biomacromolecules* **8**, 2398–2403 (2007).

49. Rodionova, G., Lenes, M., Eriksen, Ø. & Gregersen, Ø. Surface chemical modification of microfibrillated cellulose: improvement of barrier properties for packaging applications. *Cellulose* **18**, 127–134 (2011).

50. Spence, K. L., Venditti, R. A., Rojas, O. J., Habibi, Y. & Pawlak, J. J. The effect of chemical composition on microfibrillar cellulose films from wood pulps: water interactions and physical properties for packaging applications. *Cellulose* **17**, 835–848 (2010).

51. Eichhorn, S. J., Dufresne, A., Aranguren, M., Marcovich, N. E., Capadona, J. R., Rowan, S. J., Weder, C., Thielemans, W., Roman, M., Renneckar, S., Gindl, W., Veigel, S., Keckes, J., Yano, H., Abe, K., Nogi, M., Nakagaito, A. N., Mangalam, A., Simonsen, J., Benight, A. S., Bismarck, A., Berglund L. A., Peijs, T. Review: current international research into cellulose nanofibres and nanocomposites. *J. Mater. Sci.* **45**, 1–33 (2010).

52. Klemm, D., Kramer, F., Moritz, S., Lindström, T., Ankerfors, M., Gray, D., Dorris, A. Nanocelluloses: A new family of nature-based materials. *Angew. Chemie - Int. Ed.* **50**, 5438–5466 (2011).

53. Moon, R. J., Martini, A., Nairn, J. & Youngblood, J. Chem Soc Rev Cellulose nanomaterials review: structure , properties and nanocomposites. *Chem. Soc. Rev* **40**, 3941–3994 (2011).

54. Lavoine, N., Desloges, I., Dufresne, A. & Bras, J. Microfibrillated cellulose – Its barrier properties and applications in cellulosic materials: A review. *Carbohydr. Polym.* **90**, 735–764 (2012).

55. Hult, E.-L., Iotti, M. & Lenes, M. Efficient approach to high barrier packaging using microfibrillar cellulose and shellac. *Cellulose* **17**, 575–586 (2010).

56. Spence, K. L., Venditti, R. A., Rojas, O. J., Pawlak, J. J. & Hubbe, M. A. Water vapor barrier properties of coated and filled microfibrillated cellulose composite films. *BioResources* **6**, 4370–4388 (2011).

57. Hubbe, M. A., Ferrer, A., Tyagi, P., Yin, Y., Salas, C., Pal, L., Rojas, O. J. Nanocellulose in Thin Films, Coatings, and Plies for Packaging Applications: A Review. *Bioresour. Technol.* **12**, 2143–2233 (2017).

58. Missoum, K., Belgacem, M. N. & Bras, J. Nanofibrillated Cellulose Surface Modification: A Review. *Materials (Basel).* **6**, 1745–1766 (2013).

59. Zimmermann, T., Pöhler, E. & Schwaller, P. Mechanical and morphological properties of cellulose fibril reinforced nanocomposites. *Adv. Eng. Mater.* **7**, 1156–1161 (2005).

60. Herrick, F., Casebier, R., Hamilton, J. & Sandberg, K. Microfibrillated cellulose: morphology and accessibility. *J. Appl. Polym. Sci.* **37**, 797–813 (1983).

61. Spence, K. L., Venditti, R. A., Rojas, O. J., Habibi, Y. & Pawlak, J. J. A comparative study of energy consumption and physical properties of microfibrillated cellulose produced by different processing methods. *Cellulose* **18**, 1097–1111 (2011).

62. Klemm, D., Schumann, D., Kramer, F., Heßler, N., Hornung, M., Schmauder, H-P., Marsch, *S.* Nanocelluloses as Innovative Polymers in Research and Application. *Adv. Polym. Sci.* **205**, 49–96 (2006).

63. Ljungberg, N., Cavaillí, J. Y. & Heux, L. Nanocomposites of isotactic polypropylene reinforced with rod-like cellulose whiskers. *Polymer.* **47**, 6285–6292 (2006).

64. Meng, X.-Y., Ye, L., Zhang, X-G., Tang, P-M., Tang, J-H., Ji, X., Li, *Z-M.* Effects of expandable graphite and modified ammonium polyphosphate on the flame-retardant and mechanical properties of wood flour-polypropylene composites. *J Appl Polym Sci* **21**, 449–456 (2013).

65. Wambua, P., Ivens, J. & Verpoest, I. Natural fibres: Can they replace glass in fibre reinforced plastics? *Compos. Sci. Technol.* **63**, 1259–1264 (2003).

66. Peijs, T., Garkhail, S., Heijenrath, R., Van Den Oever, M. & Bos, H. Thermoplastic composites based on flax fibres and polypropylene: Influence of fibre length and fibre volume fraction on mechanical properties. *Macromol. Symp.* **127**, 193–203 (1998).

67. Sharma, A., Thakur, M., Bhattacharya, M., Mandal, T. & Goswami, S. Commercial application of cellulose nano-composites – A review. *Biotechnol. Reports* **21**, 1–15 (2019).

68. Nechyporchuk, O., Belgacem, M. N. & Bras, J. Production of cellulose nanofibrils: A review of recent advances. *Ind. Crops Prod.* **93**, 2–25 (2016).

69. Kim, J.-H., Shim, B. S., Kim, H. S., Lee, Y., Min, S-K., Jang, D., Abas, Z., Kim, J. Review of nanocellulose for sustainable future materials. *Int. J. Precis. Eng. Manuf. Technol.* **2**, 197–213 (2015).

70. Jonoobi, M., Oladi, R., Davoudpour, Y., Oksman, K. Different preparation methods and properties of nanostructured cellulose from various natural resources and residues: a review. *Cellulose* **22**, 935–969 (2015).

71. Feynman, R. P. There's (still) plenty of room at the bottom. *Appl. Therm. Eng.* **61**, 22–36 (1960).

72. Khalil, H. P. S. A., Davoudpoura, Y., Nazrul, M., Asniza, I., Mustaph, K., Sudesh, R., Jawaid, M. Production and modification of nanofibrillated cellulose using various mechanical processes: A review. *Carbohydr. Polym.* **99**, 649–665 (2014).

73. Pöllänen, M., Suvanto, M. & Pakkanen, T. T. Cellulose reinforced high density polyethylene composites - Morphology, Mechanical and thermal expansion properties. *Compos. Sci. Technol.* **76**, 21–28 (2013).

74. Duchemin, B. J. C., Newman, R. H. & Staiger, M. P. Structure-property relationship of all-cellulose composites. *Compos. Sci. Technol.* **69**, 1225–1230 (2009).

75. Spoljaric, S., Genovese, A. & Shanks, R. A. Polypropylene-microcrystalline cellulose composites with enhanced compatibility and properties. *Compos. Part A Appl. Sci. Manuf.* **40**, 791–799 (2009).

76. Miao, C. & Hamad, W. Y. Cellulose reinforced polymer composites and nanocomposites: A critical review. *Cellulose* **20**, 2221–2262 (2013).

77. Lee, K.-Y., Aitomäki, y., Berglund, l. A., Oksman, A., Bismarck, A. On the use of nanocellulose as reinforcement in polymer matrix composites. *Compos. Sci. Technol. J.* **105**, 15–27 (2014).

78. Khalil, H. P., Bhat, A. H. & Yusra, A. F. I. Green composites from sustainable cellulose nanofibrils: A review. *Carbohydr. Polym.* **87**, 963–979 (2012).

79. Maya, J. J. & Sabu, T. Biofibres and biocomposites. *Carbohydr. Polym.* **71**, 343–364 (2008).

80. Rosenthal, J. A model for determining fiber reinforcement efficiencies and fiber orientation in polymer composites *Polymer Composites*. **13**, 462-466 (1992).

81. Mendieta, C. M., Vallejos, M. E., Felissia, F. E., Chinga-Carrasco, G. & Area, M. C. Review: Bio-polyethylene from Wood Wastes. *J. Polym. Environ.* (2019).

82. Kallmes, O. J. & Perez, M. A new theory for the load/elongation properties of paper. in *Consolidation of the paper web-Cambridge* 779–800 (1965).

83. Saheb, D. N., Jog, J. P., Nabi Saheb, D. & Jog, J. P. Natural Fiber Polymer Composites : A Review. *Adv. Polym. Technol.* **18**, 351–363 (1999).

84. Luo, X. & Zhu, J. Y. Effects of drying-induced fiber hornification on enzymatic saccharification of lignocelluloses. *Enzyme Microb. Technol.* **48**, 92–99 (2011).

85. Kato, K. L. & Cameron, R. E. A Review of the Relationship Between Thermally-Accelerated Ageing of Paper and Hornification. *Cellulose* **6**, 23–40 (1999).

86. Newman, R. H. Carbon-13 NMR evidence for cocrystallization of cellulose as a mechanism for hornification of bleached kraft pulp. *Cellulose* **11**, 45–52 (2004).

87. Klemm, D., Heublein, B., Fink, H. P. & Bohn, A. Cellulose: Fascinating biopolymer and sustainable raw material. *Angew. Chemie - Int. Ed.* **44**, 3358–3393 (2005).

88. Maya, J. J. & Rajesh, A. Recent Developments in Chemical Modification and Characterization of Natural Fiber-Reinforced Composites. *Polym. Polym. Compos.* **16**, 187–207 (2008).

89. Ioelovich, M. Cellulose As a Nanostructured Polymer: a short review. *BioResources* **3**, 1403–1418 (2008).

90. Pukanszky, B. & Fekete, E. Aggregation tendency of particulate fillers: determination and consequences. *Period. Polytech. Chem. Eng.* **42**, 167–187 (1998).

91. Pukánszky, B. & Móczó, J. Morphology and Properties of Particulate Filled Polymers. *Macromol. Symp.* **214**, 115–134 (2004).

92. Zuiderduin, W. C. J., Westzaan, C., Huetink, J. & Gaymans, R. J. J. Toughening of polypropylene with calcium carbonate particles. *Polymer.* **44**, 261–275 (2003).

93. Bataille, B., Ricard, R. & Sapieha, S. Effects of cellulose fibers in polypropylene composites. *Polym. Compos.* **10**, 103–108 (1989).

94. Hafrén, J., Zou, W. & Córdova, A. Heterogeneous 'organoclick' derivatization of polysaccharides. *Macromol. Rapid Commun.* **27**, 1362–1366 (2006).

95. Gruber, E. & Granzow, C. Preparing cationic pulp by graft copolymerisation: Synthesis and characterization. *Papier* **50**, (1996).

96. Heux, L., Chauve, G. & Bonini, C. Nonflocculating and chiral-nematic self-ordering of cellulose microcrystals suspensions in nonpolar solvents. *Langmuir* **16**, 8210–8212 (2000).

Bonini, C., Heux, L., Cavaillé, J. Y. Lindner, P., Dewhurst, C., TerechE, P., Rodlike cellulose whiskers coated with surfactant: A small-angle neutron scattering characterization. *Langmuir* **18**, 3311–3314 (2002).

98. Bulota, M., Kreitsmann, K., Hughes, M. & Paltakari, J. Acetylated microfibrillated cellulose as a toughening agent in poly(lactic acid). *J. Appl. Polym. Sci.* **126**, 449–458 (2012).

99. Siró, I., Plackett, D., Hedenqvist, M., Ankerfors, M. & Lindström, T. Highly Transparent Films from Carboxymethylated Microfibrillated Cellulose: The Effect of Multiple Homogenization Steps on Key Properties. *J. ofAppliedPolymer Sci.* **119**, 2652–2660 (2011).

100. Habibi, Y., Lucian, L. A. & Rojas, O. J. Cellulose nanocrystals: Chemistry, self-assembly, and applications. *Chem. Rev.* **110**, 3479–3500 (2010).

101. González, C. & LLorca, J. Mechanical behavior of unidirectional fiber-reinforced polymers under transverse compression: Microscopic mechanisms and modeling. *Compos. Sci. Technol.* **67**, 2795–2806 (2007).

102. Zadorecki, P. & Flodin, P. Surface modification of cellulose fibers. II. The effect of cellulose fiber treatment on the performance of cellulose–polyester composites. *J. Appl. Polym. Sci.* **30**, 3971–3983 (1985).

103. Espert, A., Vilaplana, F. & Karlsson, S. Comparison of water absorption in natural cellulosic fibres from wood and one-year crops in polypropylene composites and its influence on their mechanical properties. *Compos. Part A Appl. Sci. Manuf.* **35**, 1267–1276 (2004).

104. Pasquini, D., de Morais Teixeira, E., da Silva Curvelo, A. A., Belgacem, M. N. & Dufresne, A. Surface esterification of cellulose fibres: Processing and characterisation of low-density polyethylene/cellulose fibres composites. *Compos. Sci. Technol.* **68**, 193–201 (2008).

105. Lu, T., Liu, S., Jianga, M., Xua, X., Wanga, Y., Wanga, Z., Gou, J., Huic, D., Zhou, Z., Effects of modifications of bamboo cellulose fibers on the improved mechanical properties of cellulose reinforced poly(lactic acid) composites. *Compos. Part B Eng.* **62**, 191–197 (2014).

106. Ashori, A. & Nourbakhsh, A. Performance properties of microcrystalline cellulose as a reinforcing agent in wood plastic composites. *Compos. Part B Eng.* **41**, 578–581 (2010).

107. Lu, J., Askeland, P. & Drzal, L. T. Surface modification of microfibrillated cellulose for epoxy composite applications. *Polymer.* **49**, 1285–1296 (2008).

108. Gabr, M. H., Elrahman, M. A., Okubo, K. & Fujii, T. Effect of microfibrillated cellulose on mechanical properties of plain-woven CFRP reinforced epoxy. *Compos. Struct.* **92**, 1999–2006 (2010).

109. Kalaprasad, G., Joseph, K., Thomas, S. & Pavithran, C. Theoretical modelling of tensile properties of short sisal fibre-reinforced low-density polyethylene composites. *J. Mater. Sci.* **32**, 4261–4267 (1997).

110. Zhong, W., Li, F., Zhang, Z., Song, L. & Li, Z. Short fiber reinforced composites for fused deposition modeling. *Mater. Sci. Eng. A* **301**, 125–130 (2001).

111. Alberti, M. G., Enfedaque, A., Gálvez, J. C. & Reyes, E. Numerical modelling of the fracture of polyolefin fibre reinforced concrete by using a cohesive fracture approach. *Compos. Part B Eng.* **111**, 200–210 (2017).

112. Sobczak, L., Lang, R. W. & Haider, A. Polypropylene composites with natural fibers and wood – General mechanical property profiles. *Compos. Sci. Technol.* **72**, 550–557 (2012).

113. Joseph, K., Varghese, S., Kalaprasad, G., Prasannakumari, P. L., Koshy, P., Pavithran, C. Influence of interfacial adhesion on the mechanical properties and fracture behaviour of short sisal fibre reinforced polymer composites. *Eur. Polym. J.* **32**, 1243–1250 (1996).

114. Fekete, E., Molnár, S., Kim, G.-M., Michler, G. H. & Pukánszky, B. Aggregation, fracture initiation, and strength of PP/CaCO3 composites. *J. Macromol. Sci.* **38**, 885–899 (1999).

115. Hu, Z., Berry, M., Pelton, R. & Cranston, E. One-Pot Water-Based Hydrophobic Surface Modification of Cellulose Nanocrystals Using Plant Polyphenols. *Sustain. Chem. Eng.* **5**, 5018–5026 (2017).

116. Preston, R. D. The fine structure of sisal fibres. *Journal of the Textile Institute Transactions* **40**, 715–726 (1949).

117. Lin, N. & Dufresne, A. Nanocellulose in biomedicine: Current status and future prospect. *Eur. Polym. J.* **59**, 302–325 (2014).

118. Farid, K., Youssef, H., Philippe, L. & Philippe, D. Convection-assisted assembly of cellulose nanowhiskers embedded in an acrylic copolymer. *Nanoscale* **5**, 1082–1090 (2013).

119. Somerville, C. Cellulose synthesis in higher plants. *Annu Rev Cell Dev Biol* **22**, 53–78 (2006).

120. Habibi, Y. Key advances in the chemical modification of nanocelluloses. *Chem. Soc. Rev.* **43**, 1519–42 (2014).

121. Jarvis, M. Cellulose stacks up. *Nature* **426**, 611–612 (2003).

122. Williamson, R. E., Burn, J. E. & Hocart, C. H. Towards the mechanism of cellulose synthesis. *Trends Plant Sci.* **7**, 461–467 (2002).

123. Vincent, J. F. V. Survival of the cheapest. *Mater. Today* **5**, 28–41 (2002).

124. Park, S., Baker, J. O., Himmel, M. E., Parilla, P. A. & Johnson, D. K. Cellulose crystallinity index: measurement techniques and their impact on interpreting cellulase performance. *Biotechnol. Biofuels* **3**, 10 (2010).

125. Atalla, R. H. & Vanderhart, D. L. Native Cellulose: A Composite of Two Distinct Crystalline Forms. *Science (80-.).* **223**, 283–285 (1984).

126. Clowes, F. & Juniper, B. *Plant cells*. (Blackwell Scientific Publications, 1968).

127. Shen, D. K. & Gu, S. The mechanism for thermal decomposition of cellulose and its main products. *Bioresour. Technol.* **100**, 6496–6504 (2009).

128. Kim, U.-J., Eom, S. H. & Wada, M. Thermal decomposition of native cellulose: Influence on crystallite size. *Polym. Degrad. Stab.* **95**, 778–781 (2010).

129. Utracki, L. A. *Commercial Polymer Blends*. (Springer US, 1998).

130. Mülhaupt, R. Hermann Staudinger and the Origin of Macromolecular Chemistry. *Angew. Chemie Int. Ed.* **43**, 1054–1063 (2004).

131. Lee, J. H., Brown, R. M., Kuga, S., Shoda, S. & Kobayashi, S. Assembly of synthetic cellulose I. *Proc. Natl. Acad. Sci.* **91**, 7425 LP – 7429 (1994).

132. Qiu, K. & Netravali, A. N. A Review of Fabrication and Applications of Bacterial Cellulose Based Nanocomposites. *Polym. Rev.* **54**, 598–626 (2014).

133. Saito, T., Kimura, S., Nishiyama, Y. & Isogai, A. Cellulose nanofibers prepared by TEMPO-mediated oxidation of native cellulose. *Biomacromolecules* **8**, 2485–2491 (2007).

134. Lu, P. & Hsieh, Y.-L. Preparation and properties of cellulose nanocrystals: Rods, spheres, and network. *Carbohydr. Polym.* **82**, 329–336 (2010).

135. Bondeson, D., Mathew, A. & Oksman, K. Optimization of the isolation of nanocrystals from microcrystalline celluloseby acid hydrolysis. *Cellulose* **13**, 171 (2006).

136. Hubbe, M. A., Rojas, O. J., Lucian, L. A. & Sain, M. Cellulosic Nanocomposites: a Review. *BioResources* **3**, 929–980 (2008).

137. Turbak, A. F., Snyder, F. W., Sandberg, K. R. Suspensions Containing Microfibrillated Cellulose. *J. Appl. Polym. Sci. Appl. Polym. Symp.* **37**, 1–5 (1983).

138. Janardhnan, S. & Sain, M. M. Isolation of Cellulose Microfibrils – an Enzymatic Approach. *Cellul. Microfibril Isol. Bioresour.* **1**, 176–188 (2006).

139. Saito, T. & Isogai, A. Introduction of aldehyde groups on surfaces of native cellulose fibers by TEMPO-mediated oxidation. *Colloids Surfaces A Physicochem. Eng. Asp.* **289**, 219–225 (2006).

140. Saito, T. & Isogai, A. Wet strength improvement of TEMPO-oxidized cellulose sheets prepared with cationic polymers. *Ind. Eng. Chem. Res.* **46**, 773–780 (2007).

141. Saito, T., Nishiyama, Y., Putaux, J. L., Vignon, M. & Isogai, A. Homogeneous suspensions of individualized microfibrils from TEMPO-catalyzed oxidation of native cellulose. *Biomacromolecules* **7**, 1687–1691 (2006).

142. Saito, T., Hirota, M., Tamura, M., Kimura, S., Fukuzumi, H., Heux, L., Isogai, A. Individualization of nano-sized plant cellulose fibrils by direct surface carboxylation using TEMPO catalyst under neutral conditions. *Biomacromolecules* **10**, 1992–1996 (2009).

143. Iwamoto, S., Nakagaito, A. N., Yano, H. & Nogi, M. Optically transparent composites reinforced with plant fiber-based nanofibers. *Appl. Phys. A Mater. Sci. Process.* **81**, 1109–1112 (2005).

144. Reddy, N. & Yang, Y. Biofibers from agricultural byproducts for industrial applications. *Trends Biotechnol.* **23**, 22–27 (2005).

145. Dinand, E., Chanzy, E. & Vignon, M. R. Parenchymal cell cellulose from sugar beet pulp: preparation and properties. *Cellulose* **3**, 183–188 (1996).

146. Alemdar, A. & Sain, M. Isolation and characterization of nanofibers from agricultural residues - Wheat straw and soy hulls. *Bioresour. Technol.* **99**, 1664–1671 (2008).

147. Dufresne, A. & Cavaille, J. Mechanical Behavior of Sheets Prepared from Sugar Beet Cellulose Microfibrils. 1185–1194 (1997).

148. Dinand, E., Alalin, M., Chanzy, H., Vincent, I. & Vignon, M. Microfibrillated cellulose and process for making the same from vegetable pulps having primary walls, especially from sugar beet pulp. (1996).

149. Dinand, E., Chanzy, H. & Vignon, R. M. Suspensions of cellulose microfibrils from sugar beet pulp. *Food Hydrocoll.* **13**, 275–283 (1999).

150. Goussé, C., Chanzy, H., Cerrada, M. L. & Fleury, E. Surface silylation of cellulose microfibrils: Preparation and rheological properties. *Polymer.* **45**, 1569–1575 (2004).

151. Habibi, Y. & Vignon, M. R. Optimization of cellouronic acid synthesis by TEMPO-mediated oxidation of cellulose III from sugar beet pulp. *Cellulose* **15**, 177–185 (2008).

152. Dufresne, A. Cellulose Microfibrils from Potato Tuber Cells : Processing and Characterization of Starch – Cellulose Microfibril Composites. *Polymer.* **76**, 2080–2092 (2000).

153. Bhattacharya, D., Germinario, L. T. & Winter, W. T. Isolation, preparation and characterization of cellulose microfibers obtained from bagasse. *Carbohydr. Polym.* **73**, 371–377 (2008).

154. Morán, J. I., Alvarez, V. A., Cyras, V. P. & Vázquez, A. Extraction of cellulose and preparation of nanocellulose from sisal fibers. *Cellulose* **15**, 149–159 (2008).

155. Imai, T., Putaux, J. L. & Sugiyama, J. Geometric phase analysis of lattice images from algal cellulose microfibrils. *Polymer.* **44**, 1871–1879 (2003).

156. Habibi, Y., Mahrouz, M. & Vignon, M. R. Microfibrillated cellulose from the peel of prickly pear fruits. *Food Chem.* **115**, 423–429 (2009).

157. Zuluaga, R., Putaux, J. L., Restrepo, A., Mondragon, I. & Gañán, P. Cellulose microfibrils from banana farming residues: Isolation and characterization. *Cellulose* **14**, 585–592 (2007).

158. El-Saied, H., Basta, A. H. & Gobran, R. H. Research Progress in Friendly Environmental Technology for the Production of Cellulose Products (Bacterial Cellulose and Its Application). *Polym. Plast. Technol. Eng.* **43**, 797–820 (2004).

159. Brown, R. M. Bacterial cellulose: Its potential for new products of commerce. *Abstr. Pap. Am. Chem. Soc.* **227**, (2004).

160. Iguchi, M., Yamanaka, S. & Budhiono, A. Bacterial cellulose - a masterpiece of nature's arts. *J. Mater. Sci.* **35**, 261–270 (2000).

161. Brown, E. E., Laborie, M. G. & Box, P. O. Bioengineering Bacterial Cellulose / Poly (ethylene oxide) Nanocomposites. *Biomacromolecules* **8**, 3074–3081 (2007).

162. Czaja, W., Romanovicz, D. & Brown, R. M. Structural investigations of microbial cellulose produced in stationary and agitated culture. *Cellulose* **11**, 403–411 (2004).

163. Guhados, G., Wan, W. & Hutter, J. L. Measurement of the elastic modulus of single bacterial cellulose fibers using atomic force microscopy. *Langmuir* **21**, 6642–6646 (2005).

164. Mohanty, A. K., Misra, M. & Hinrichsen, G. Biofibres, biodegradable polymers and biocomposites: An overview. *Macromol. Mater. Eng.* **276**–**277**, 1–24 (2000).

165. Juntaro, J., Pommet, M., Mantalaris, A., Shaffer, M. & Bismarck, A. Nanocellulose enhanced interfaces in truly green unidirectional fibre reinforced composites. *Compos. Interfaces* **14**, 753–762 (2007).

166. Wan, W., Hutter, J., Millon, L. & Guhados, G. *Bacterial cellulose and its nanocomposites for biomedical applications.* (American Chemical Society, 2006).

167. Barud, H. S., Barrios, C., Ribeiro, S. J. Self-supported silver nanoparticles containing bacterial cellulose membranes. *Mater. Sci. Eng. C* **28**, 515–518 (2008).

168. Nogi, M., Handa, K., Nakagaito, A. N. & Yano, H. Optically transparent bionanofiber composites with low sensitivity to refractive index of the polymer matrix. *Appl. Phys. Lett.* **87**, 1–3 (2005).

169. Nogi, M., Ifuku s., Abe, K. Fiber-content dependency of the optical transparency and thermal expansion of bacterial nanofiber reinforced composites. *Appl. Phys. Lett.* **88**, (2006).

170. Yano, H. Optically transparent composites reinforced with networks of bacterial nanofibers. *Sustain. Humanosph.* 11 (2005).

171. Maeda, H., Nakajima, M., Hagiwara, T., Sawaguchi, T. & Yano, S. Bacterial cellulose/silica hybrid fabricated by mimicking biocomposites. *J. Mater. Sci.* **41**, 5646–5656 (2006).

172. Sanchavanakit, N., Sangrungraungroj, W., Phisalaphong, M., Growth of human keratinocytes and fibroblasts on bacterial cellulose film. *Biotechnol. Prog.* **22**, 1194–1199 (2006).

173. Ifuku, S., Nogi, M., Yano, H. Surface modification of bacterial cellulose nanofibers for property enhancement of optically transparent composites: Dependence on acetyl-group DS. *Biomacromolecules* **8**, 1973–1978 (2007).

174. Juntaro, J., Pommet, M., Bismarck, A. Creating hierarchical structures in renewable composites by attaching bacterial cellulose onto sisal fibers. *Adv. Mater.* **20**, 3122–3126 (2008).

175. Shoda, M. & Sugano, Y. Recent advances in bacterial cellulose production. *Biotechnol. Bioprocess Eng.* **10**, 1–8 (2005).

176. Eriksen, O., Syverud, K. & Gregersen, O. The use of microfibrillated cellulose produced from kraft pulp as strength enhancer in TMP paper. *Nord. Pulp Pap. Res. J.* **23**, 299–304 (2008).

177. Pääkkö, M., Ankerfors, m., Kosonen, H., Nykänen, A., Laine, j., Larsson P. T., Ikkala, O., Lindström, T. Enzymatic hydrolysis combined with mechanical shearing and high-pressure homogenization for nanoscale cellulose fibrils and strong gels. *Biomacromolecules* **8**, 1934–1941 (2007).

178. Svagan, A. J., Samir, M. A. S. A. & Berglund, L. A. Biomimetic foams of high mechanical performance based on nanostructured cell walls reinforced by native cellulose nanofibrils. *Adv. Mater.* **20**, 1263–1269 (2008).

179. Ankerfors, M. & Lindstrom, T. On the manufacture and use of nanocellulose. 9th International. in *9th International Conference on Wood & Biofiber Plastic Composites* 21–23 (2007).

180. Wang, B. & Sain, M. Isolation of nanofibers from soybean source and their reinforcing capability on synthetic polymers. *Compos. Sci. Technol.* **67**, 2521–2527 (2007).

181. Wang, B. & Sain, M. Dispersion of soybean stock-based nanofiber in a plastic matrix. *Polym. Int.* **56**, 538–554 (2007).

182. Wang, B. & Sain, M. The effect of chemically coated nanofiber reinforcement on biopolymer based nanocomposites. *BioResources* **2**, 371–388 (2007).

183. Wang, B., Sain, M. & Oksman, K. Study of structural morphology of hemp fiber from the micro to the nanoscale. *Appl. Compos. Mater.* **14**, 89–103 (2007).

184. Henriksson, G., Nutt, A., Henrikson, H., Patterson, G. Endoglucanase 28 (Cel12A), a new Phanerochaete chrysosporium cellulase. *Eur. J. Biochem.* **259**, 88–95 (1999).

185. Henriksson, G., Christiernin, M. & Agnemo, R. Monocomponent endoglucanase treatment increases the reactivity of softwood sulphite dissolving pulp. *J. Ind. Microbiol. Biotechnol.* **32**, 211–214 (2005).

186. Berghem, E. R. & Pettersson, L. G. Mechanism of enzymatic cellulose degradation—purification of a cellulolytic enzyme from trichoderma-viride active on highly ordered cellulose. *Eur J Biochem* **37**, 21–30 (1973).

187. López-Rubio, A., Lagaron, J. M., Lindström, T., Hedemqvist, M. S. Enhanced film forming and film properties of amylopectin using micro-fibrillated cellulose. *Carbohydr. Polym.* **68**, 718–727 (2007).

188. Liimatainen, H., Visanko, M., Sirvio, J., Hormi, O. & Niinimaki, J. Sulfonated cellulose nanofibrils obtained from wood pulp through regioselective oxidative bisulfite pre-treatment. *Cellulose* **20**, 741–749 (2013).

189. Sirvió, J. A., Kolehmainen. A., Liimatainen, H., Hormi, O. E. O. Strong, self-standing oxygen barrier films from nanocelluloses modified with regioselective oxidative treatments. *ACS Appl. Mater. Interfaces* **6**, 14384–14390 (2014).

190. Cai, X., Riedl, B. & Ait-Kadi, A. Effect of surface-grafted ionic groups on the performance of cellulose-fiber-reinforced thermoplastic composites. *J. Polym. Sci. Part B Polym. Phys.* **41**, 2022–2032 (2003).

191. Abbott, A. P., Bell, T. J., Handa, S. & Stoddart, B. Cationic functionalisation of cellulose using a choline based ionic liquid analogue. *Green Chem.* **8**, 784–786 (2006).

192. Song, Y., Sun, Y., Zhang, X., Zhou, J. & Zhang, L. Homogeneous quaternization of cellulose in NaOH/Urea aqueous solutions as gene carriers. *Biomacromolecules* **9**, 2259–2264 (2008).

193. Aulin, C., Johansson, E., Wågberg, L. & Lindström, T. Self-organized films from cellulose i nanofibrils using the layer-by-layer technique. *Biomacromolecules* **11**, 872–882 (2010).

194. Liimatainen, H., Suopajarvi, T., Sirvio, J., Hormi, O. & Niinimaki, J. Fabrication of cationic cellulosic nanofibrils through aqueous quaternization pretreatment and their use in colloid aggregation. *Carbohydr. Polym.* **103**, 187–192 (2014).

195. Olszewska, A., Eronen, P., Johansson, L-S., Laine, J., Lindström, T., Österberg, M. The behaviour of cationic NanoFibrillar Cellulose in aqueous media. *Cellulose* **18**, 1213–1226 (2011).

196. Ho, T. T. T., Zimmermann, T., Hauert, R. & Caseri, W. Preparation and characterization of cationic nanofibrillated cellulose from etherification and high-shear disintegration processes. *Cellulose* **18**, 1391–1406 (2011).

197. Saini, S., Yücel Falco, Ç., Belgacem, M. N. & Bras, J. Surface cationized cellulose nanofibrils for the production of contact active antimicrobial surfaces. *Carbohydr. Polym.* **135**, 239–247 (2016).

198. Chaker, A. & Boufi, S. Cationic nanofibrillar cellulose with high antibacterial properties. *Carbohydr. Polym.* **131**, 224–232 (2015).

199. Hassan, M. L., Hassan, E. A. & Oksman, K. N. Effect of pretreatment of bagasse fibers on the properties of chitosan/microfibrillated cellulose nanocomposites. *J. Mater. Sci.* **46**, 1732–1740 (2011).

200. de Campos, A., Dufresne, A., Mattoso, H. C., Cassland, P., Sanadi, A. R. Obtaining nanofibers from curau and sugarcane bagasse fibers using enzymatic hydrolysis followed by sonication. *Cellulose* **20**, 1491–1500 (2013).

201. Nakagaito, A. N., Ikenaga, K. & Takagi, H. Cellulose nanofiber extraction from grass by a modified kitchen blender. *Mod. Phys. Lett. B* **29**, (2015).

202. Carrillo, C. A., Laine, J. & Rojas, O. J. Microemulsion systems for fiber deconstruction into cellulose nanofibrils. *ACS Appl. Mater. Interfaces* **6**, 22622–22627 (2014).

203. Sirviö, J. A., Visanko, M. & Liimatainen, H. Deep eutectic solvent system based on choline chloride-urea as a pre-treatment for nanofibrillation of wood cellulose. *Green Chem.* **17**, 3401–3406 (2015).

204. Saito, T. & Isogai, A. Ion-exchange behavior of carboxylate groups in fibrous cellulose oxidized by the TEMPO-mediated system. *Carbohydr. Polym.* **61**, 183–190 (2005).

205. Saito, T., Yanagisawa, M. & Isogai, A. TEMPO-mediated Oxidation of Native Cellulose: SEC–MALLS Analysis of Water-soluble and -Insoluble Fractions in the Oxidized Products. *Cellulose* **12**, 305–315 (2005).

206. Lasseuguette, E., Roux, D. & Nishiyama, Y. Rheological properties of microfibrillar suspension of TEMPO-oxidized pulp. *Cellulose* **15**, 425–433 (2008).

207. Nakagaito, A. N. & Yano, H. The effect of morphological changes from pulp fiber towards nano-scale fibrillated cellulose on the mechanical properties of high-strength plant fiber based composites. *Appl. Phys. A Mater. Sci. Process.* **78**, 547–552 (2004).

208. Kose, R., Mitani, I., Kasai, W. & Kondo, T. 'Nanocellulose' as a single nanofiber prepared from pellicle secreted by gluconacetobacter xylinus using aqueous counter collision. *Biomacromolecules* **12**, 716–720 (2011).

209. Kondo, T., Kose, R., Naito, H. & Kasai, W. Aqueous counter collision using paired water jets as a novel means of preparing bio-nanofibers. *Carbohydr. Polym.* **112**, 284–290 (2014).

210. Taniguchi, T. & Okamura, K. New films produced from microfibrillated natural fibres. *Polym. Int.* **47**, 291–294 (1998).

211. Uetani, K. & Yano, H. Nanofibrillation of wood pulp using a high- speed blender. *Biomacromolecules* **12**, 348–353 (2011).

212. Jiang, F. & Hsieh, Y. Lo. Chemically and mechanically isolated nanocellulose and their self-assembled structures. *Carbohydr. Polym.* **95**, 32–40 (2013).

213. Chaker, A., Alila, S., Mutjé, P., Vilar, M. R. & Boufi, S. Key role of the hemicellulose content and the cell morphology on the nanofibrillation effectiveness of cellulose pulps. *Cellulose* **20**, 2863–2875 (2013).

214. Zhang, L., Tsuzuki, T. & Wang, X. Preparation of cellulose nanofiber from softwood pulp by ball milling. *Cellulose* **22**, 1729–1741 (2015).

215. Kekäläinen, K., Liimatainen, H., Biale, F. & Niinimäki, J. Nanofibrillation of TEMPO-oxidized bleached hardwood kraft cellulose at high solids content. *Int. J. Biol. Chem. Physics, Technol. Wood* **69**, 1077–1088 (2015).

216. Wang, S. & Cheng, Q. A novel process to isolate fibrils from cellulose fibers by high-intensity ultrasonication, part 1: process optimization. *J. Appl. Polym. Sci.* **113**, 1270–1275 (2009).

217. Kaboorani, A., Riedl, B. & Blanchet, P. Ultrasonication technique: A method for dispersing nanoclay in wood adhesives. *J. Nanomater.* **2013**, (2013).

218. Cheng, Q., Wang, S. & Rials, T. G. Poly(vinyl alcohol) nanocomposites reinforced with cellulose fibrils isolated by high intensity ultrasonication. *Compos. Part A Appl. Sci. Manuf.* **40**, 218–224 (2009).

219. Chen, W., Yu, H., Liu, Y., Hai, Y. Individualization of cellulose nanofibers from wood using high-intensity ultrasonication combined with chemical pretreatments. *Carbohydr. Polym.* **83**, 1804–1811 (2011).

220. Johnson, R. K., Zink-Sharp, A., Renneckar, S. H. & Glasser, W. G. A new bio-based nanocomposite: Fibrillated TEMPO-oxidized celluloses in hydroxypropylcellulose matrix. *Cellulose* **16**, 227–238 (2009).

221. Zhou, Y. M., Fu, S. Y., Zheng, L. M. & Zhan, H. Y. Effect of nanocellulose isolation techniques on the formation of reinforced poly(vinyl alcohol) nanocomposite films. *Express Polym. Lett.* **6**, 794–804 (2012).

222. Saito, T., Kuramae, R., Wohlert, J., Berglund, L. & Isogai, A. An Ultrastrong Nano fibrillar Biomaterial: The Strength of Single Cellulose Nano fibrils Revealed via Sonication-Induced Fragmentation. *Biomacromolecules* **14**, 248–253 (2013).

223. Chakraborty, A., Sain, M., Kortschot, M. & Cutler, S. Dispersion of Wood Microfibers in a Matrix of Thermoplastic Starch and Starch–Polylactic Acid Blend. *J Biobased Mater Bioenergy* **1**, 71–77 (2007).

224. Fernández-Bolaños, J., Rodríguez, R., Guillén, R., Jiménez, A. Steam-explosion of olive stones: Hemicellulose solubilization and enhancement of enzymatic hydrolysis of cellulose. *Bioresour. Technol.* **79**, 53–61 (2001).

225. Sun, X. F., Xu, F., Sun, R. C., Fowler, P. & Baird, M. S. Characteristics of degraded cellulose obtained from steam-exploded wheat straw. *Carbohydr. Res.* **340**, 97–106 (2005).

226. Cherian, B. M., Lopes Leão, A., Kottaisamy, M., Isolation of nanocellulose from pineapple leaf fibres by steam explosion. *Carbohydr. Polym.* **81**, 720–725 (2010).

227. Deepa, B., Abraham, E., Cherian, M. B., de Souza, S. F., Kottaisamy, M. Structure, morphology and thermal characteristics of banana nano fibers obtained by steam explosion. *Bioresour. Technol.* **102**, 1988–1997 (2011).

228. Kaushik, A. & Singh, M. Isolation and characterization of cellulose nanofibrils from wheat straw using steam explosion coupled with high shear homogenization. *Carbohydr. Res.* **346**, 76–85 (2011).

229. Manhas, N., Balasubramanian, K., Prajith, P., Rule, P. & Nimje, S. PCL/PVA nanoencapsulated reinforcing fillers of steam exploded/autoclaved cellulose nanofibrils for tissue engineering applications. *RSC Adv.* **5**, 23999–24008 (2015).

230. Phipps, J. S. Engineering minerals for performance applications: an industrial perspective. *Clay Miner.* **49**, 1–16 (2014).

231. Ho, T. T. T., Abe, K., Zimmermann, T. & Yano, H. Nanofibrillation of pulp fibers by twin-screw extrusion. *Cellulose* **22**, 421–433 (2015).

232. Suzuki, K., Okumura, H., Kitagawa, K., Sato, S., Norio, A., Yano, H. Development of continuous process enabling nanofibrillation of pulp and melt compounding. *Cellulose* **20**, 201–210 (2013).

233. Cobut, A., Sehaqui, H. & Berglund, L. A. Cellulose Nanocomposites by Melt Compounding of TEMPO-Treated Wood Fibers in Thermoplastic Starch Matrix. *Bioresources.com* **9**, 3276–3289 (2014).

234. Saarikoski, E., Saarinen, T., Salmela, J. & Seppälä, J. Flocculated flow of microfibrillated cellulose water suspensions: an imaging approach for characterisation of rheological behaviour. *Cellulose* **19**, 647–659 (2012).

235. Nechyporchuk, O., Belgacem, M. N. & Pignon, F. Rheological properties of micro-/nanofibrillated cellulose suspensions: Wall-slip and shear banding phenomena. *Carbohydr. Polym.* **112**, 432–439 (2014).

236. Agoda-Tandjawa, G., Durand, S., Doubriel, J-L. Rheological characterization of microfibrillated cellulose suspensions after freezing. *Carbohydr. Polym.* **80**, 677–686 (2010).

237. Nakagaito, A. N. & Yano, H. The effect of fiber content on the mechanical and thermal expansion properties of biocomposites based on microfibrillated cellulose. *Cellulose* **15**, 555–559 (2008).

238. Ozgur Seydibeyoglu, M. & Oksman, K. Novel nanocomposites based on polyurethane and micro fibrillated cellulose. *Compos. Sci. Technol.* **68**, 908–914 (2008).

239. Fernandes Diniz, J. M. B., Gil, M. H. & Castro, J. A. A. M. Hornification-its origin and interpretation in wood pulps. *Wood Sci. Technol.* **37**, 489–494 (2004).

240. Quiávy, N., Deroanne, C., Paquot, M., Devaux, J. Influence of homogenization and drying on the thermal stability of microfibrillated cellulose. *Polym. Degrad. Stab.* **95**, 306–314 (2010).

241. Peng, Y., Gardner, D. J. & Han, Y. Drying cellulose nanofibrils: In search of a suitable method. *Cellulose* **19**, 91–102 (2012).

242. Syverud, K., Chinga-Carrasco, G., Toledo, J. & Toledo, P. G. A comparative study of Eucalyptus and Pinus radiata pulp fibres as raw materials for production of cellulose nanofibrils. *Carbohydr. Polym.* **84**, 1033–1038 (2011).

243. Butchosa, N. & Zhou, Q. Water redispersible cellulose nanofibrils adsorbed with carboxymethyl cellulose. *Cellulose* **21**, 4349–4358 (2014).

244. Saito, T., Uematsu, T., Kimura, S., Enomae, T. & Isogai, A. Self-aligned integration of native cellulose nanofibrils towards producing diverse bulk materials. *Soft Matter* **7**, 8804 (2011).

245. Abe, K. & Yano, H. Formation of hydrogels from cellulose nanofibers. *Carbohydr. Polym.* **85**, 733–737 (2011).

246. Abe, K. & Yano, H. Cellulose nanofiber-based hydrogels with high mechanical strength. *Cellulose* **19**, 1907–1912 (2012).

247. Dong, H., Snyder, J. F., Williams, K. S. & Andzelm, J. W. Cation-induced hydrogels of cellulose nanofibrils with tunable moduli. *Biomacromolecules* **14**, 3338–3345 (2013).

248. Dong, H., Snyder, J. F., Tran, D. T. & Leadore, J. L. Hydrogel, aerogel and film of cellulose nanofibrils functionalized with silver nanoparticles. *Carbohydr. Polym.* **95**, 760–767 (2013).

249. Sehaqui, H., Salajková, M., Zhou, Q. & Berglund, L. a. Mechanical performance tailoring of tough ultra-high porosity foams prepared from cellulose I nanofiber suspensions. *Soft Matter* **6**, 1824 (2010).

250. Chen, W., Yu, H., Li, Q., Liu, Y. & Li, J. Ultralight and highly flexible aerogels with long cellulose I nanofibers. *Soft Matter* **7**, 10360–10368 (2011).

251. Sehaqui, H., Zhou, Q. & Berglund, L. High-porosity aerogels of high specific surface area prepared from nanofibrillated cellulose (NFC). *Compos. Sci. Technol.* **71**, 1593–1599 (2011).

252. Fumagalli, M., Ouhab, D., Boisseau, S. M. & Heux, L. Versatile gas-phase reactions for surface to bulk esterification of cellulose microfibrils aerogels. *Biomacromolecules* **14**, 3246–3255 (2013).

253. Wan, C., Lu, Y., Sun, Q., Li, J.Ultralight and hydrophobic nanofibrillated cellulose aerogels from coconut shell with ultrastrong adsorption properties. *J. Appl. Polym. Sci.* **132**, 1–7 (2015).

254. Blanco, A., Monte, M.c., Merayo, N., Negro, C. Nanocellulose for Industrial Use: Cellulose Nanofibers (CNF), Cellulose Nanocrystals (CNC), and Bacterial Cellulose (BC). in *Handbook of Nanomaterials for Industrial Applications* (ed. Hussain, C. M.) 74–126 (Elsevier, 2018).

255. Dufresne, A., Thomas, S. & Pothan, L. A. *Review of Nanocellulosic Products and Their Applications*. (John Wiley & Sons, Inc, 2013).

256. Zou, X., Tan, X., Berry, R. & Godbout, J. D. L. Flexible, iridescent nanocrystalline cellulose film, and method for preparation. (2016).

257. Heiskanen, I. & Backfolk, K. Composition comprising microfibrillated cellulose and a processes for the production of a composite. (2016).

258. Aspler, J. S., Zou, X., Laleg, M., Manfred, T. & Greon, J. Print quality on thin coating of cellulose nanocrystals. (2017).

259. Bardet, R. & Bras, J. Cellulose Nanofibers and Their Use in Paper Industry. in *Handbook of Green Materials* **Volume 5**, 207–232 (World Scientific, 2013).

260. Boluk, Y. & Zhao, L. Aircrafr ant-icing fluid formulated with nanocrystalline cellulose. (2012).

261. Sanchez-Garcia, M. D., Gimenez, E. & Lagaron, J. M. Novel PET Nanocomposites of Interest in Food Packaging Applications and Comparative Barrier Performance With Biopolyester Nanocomposites. *J. Plast. Film Sheeting* **23**, 133–148 (2007).

262. Sanchez-Garcia, M. D. & Lagaron, J. M. On the use of plant cellulose nanowhiskers to enhance the barrier properties of polylactic acid. *Cellulose* **17**, 987–1004 (2010).

263. Avrous, L., Fringant, C. & Moro, L. Starch-Based Biodegradable Materials Suitable for Thermoforming Packaging. *Starch - Stärke* **53**, 368–371 (2001).

264. Bendahou, A., Kaddami, H. & Dufresne, A. Investigation on the effect of cellulosic nanoparticles' morphology on the properties of natural rubber based nanocomposites. *Eur. Polym. J.* **46**, 609–620 (2010).

265. Suryanegara, L., Nakagaito, A. N. & Yano, H. The effect of crystallization of PLA on the thermal and mechanical properties of microfibrillated cellulose-reinforced PLA composites. *Compos. Sci. Technol.* **69**, 1187–1192 (2009).

266. Nakagaito, A. N., Fujimura, A., Sakai, T., Hama, Y. & Yano, H. Production of microfibrillated cellulose (MFC)-reinforced polylactic acid (PLA) nanocomposites from sheets obtained by a papermaking-like process. *Compos. Sci. Technol.* **69**, 1293–1297 (2009).

267. Iwatake, A., Nogi, M. & Yano, H. Cellulose nanofiber-reinforced polylactic acid. *Compos. Sci. Technol.* **68**, 2103–2106 (2008).

268. Weng, Z., Su, Y., Du, J., Cheng, H-M. Graphene–Cellulose Paper Flexible Supercapacitors. *Adv. Energy Mater.* **1**, 917–922 (2011).

269. Park, J. S., Kim, T. & Kim, W. S. Conductive Cellulose Composites with Low Percolation Threshold for 3D Printed Electronics. *Sci. Rep.* **7**, 3246 (2017).

270. Nogi, M. & Yano, H. Transparent nanocomposites based on cellulose produced by bacteria offer potential innovation in the electronics device industry. *Adv. Mater.* **20**, 1849–1852 (2008).

271. Zhao, H., Kwak, J. H., Arery, W., Holladay, J. E. Studying cellulose fiber structure by SEM, XRD, NMR and acid hydrolysis. *Carbohydr. Polym.* **68**, 235–241 (2007).

272. Abe, K. & Yano, H. Comparison of the characteristics of cellulose microfibril aggregates of wood, rice straw and potato tuber. *Cellulose* **16**, 1017–1023 (2009).

273. Duchesne, I., Hult, E., Molin, U., Iversen, T., Lennholm, H. The influence of hemicellulose on fibril aggregation of kraft pulp fibres as revealed by FE-SEM and CP/MAS 13C-NMR. *Cellulose* **8**, 103–111 (2001).

274. Baker, A. A., Helbert, W., Sugiyama, J. & Miles, M. J. Surface structure of native cellulose microcrystals by AFM. *Appl. Phys. A* **66**, 559–563 (1998).

275. Crawshaw, J., Bras, W., Mant, G. R. & Cameron, R. E. Simultaneous SAXS and WAXS investigations of changes in native cellulose fiber microstructure on swelling in aqueous sodium hydroxide. *J. Appl. Polym. Sci.* **83**, 1209–1218 (2002).

276. Bootten, T. J., Harris, P. J., Melton, L. D. & Newman, R. H. WAXS and 13C NMR study of Gluconoacetobacter xylinus cellulose in composites with tamarind xyloglucan. *Carbohydr. Res.* **343**, 221–229 (2008).

277. Leppänen, K., Andersson, S., Knaapila, M., Serimaa, R. Structure of cellulose and microcrystalline cellulose from various wood species, cotton and flax studied by X-ray scattering. *Cellulose* **16**, 999–1015 (2009).

278. Pastorova, I., Botto, R. E., Arisz, P. W. & Boon, J. J. Cellulose char structure: a combined analytical Py-GC-MS, FTIR, and NMR study. *Carbohydr. Res.* **262**, 27–47 (1994).

279. Wickholm, K., Larsson, P. T. & Iversen, T. Assignment of non-crystalline forms in cellulose I by CP/MAS ^{13}C NMR spectroscopy. *Carbohydr. Res.* **312**, 123–129 (1998).

280. Hult, E. L., Larsson, P. T. & Iversen, T. Comparative CP/MAS 13C-NMR study of cellulose structure in spruce wood and kraft pulp. *Cellulose* **7**, 35–55 (2000).

281. Hult, E. L., Iversen, T. & Sugiyama, J. Characterization of the supermolecular structure of cellulose in wood pulp fibres. *Cellulose* **10**, 103–110 (2003).

282. Zhang, H., Tong, M., Shao, H. & Xuechao, H. Comparison of the Structures and Properties of Lyocell Fibers from High Hemicellulose Pulp and High a-Cellulose Pulp. *Polym. Polym. Compos.* **107**, 632–641 (2008).

283. Iwamoto, S., Abe, K. & Yano, H. The effect of hemicelluloses on wood pulp nanofibrillation and nanofiber network characteristics. *Biomacromolecules* **9**, 1022–1026 (2008).

284. Zhang, H. & Tong, M. Influence of Hemicelluloses on the Structure and Properties of Lyocell Fibers. *Polym. Eng. Sci.* 702–706 (2007).

285. Aulin, C., Ahola, S., Josefsson, P., Nishino, T., Hirose, Y., Österberg, M., Wågberg, L. Nanoscale cellulose films with different crystallinities and mesostructures - Their surface properties and interaction with water. *Langmuir* **25**, 7675–7685 (2009).

286. Yano, H. & Nakahara, S. Bio-composites produced from plant microfiber bundles with a nanometer unit web-like network. *J. Mater. Sci.* **39**, 1635–1638 (2004).

287. Hoeger, I. C., Nair, S. S., Deng, Y., Rojas, O. J., Zhu, J. Y. Mechanical deconstruction of lignocellulose cell walls and their enzymatic saccharification. *Cellulose* **20**, 807–818 (2013).

288. Besbes, I., Vilar, M. R. & Boufi, S. Nanofibrillated cellulose from Alfa, Eucalyptus and Pine fibres: Preparation, characteristics and reinforcing potential. *Carbohydr. Polym.* **86**, 1198–1206 (2011).

289. Benhamou, K., Dufresne, A., Magnin, A., Mortha, G. & Kaddami, H. Control of size and viscoelastic properties of nanofibrillated cellulose from palm tree by varying the TEMPO-mediated oxidation time. *Carbohydr. Polym.* **99**, 74–83 (2014).

290. Qing, Y., Sabo, R., Zhu, J. Y., Cai, Z., Wu, Y. A comparative study of cellulose nanofibrils disintegrated via multiple processing approaches. *Carbohydr. Polym.* **97**, 226–234 (2013).

291. Liimatainen, H., Visanko, M., Sirvio, J. A., Hormi, O. E. O. & Niinimaki, J. Enhancement of the nanofibrillation of wood cellulose through sequential periodate-chlorite oxidation. *Biomacromolecules* **13**, 1592–1597 (2012).

292. Cox, H. L. The elasticity and strength of paper and other fibrous materials. *Br. J. Appl. Phys.* **3**, 72–79 (1952).

293. Schulgasser, K. & Page, D. H. The influence of tranverse fibre properties on the in-plane elastic behaviour of paper. *Compos. Sci. Technol.* **32**, 279–292 (1988).

294. Fukuzumi, H., Saito, T., Iwata, T., Kumamoto, Y. & Isogai, A. Transparent and High Gas Barrier Films of Cellulose Nanofibers Prepared by TEMPO-Mediated Oxidation Transparent and High Gas Barrier Films of Cellulose Nanofibers Prepared by TEMPO-Mediated Oxidation. *Biomacromolecules* **10**, 162–165 (2009).

295. Nogi, M., Iwamoto, S., Nakagaito, A. N. & Yano, H. Optically Transparent Nanofiber Paper. *Adv. Mater.* **21**, 1595–1598 (2009).

296. Nogi, M. & Yano, H. Optically transparent nanofiber sheets by deposition of transparent materials: A concept for a roll-to-roll processing. *Appl. Phys. Lett.* **94**, 35–38 (2009).

297. Plackett, D., Andersen, T. L., Pedersen, W. B. & Nielsen, L. Biodegradable composites based on L-polylactide and jute fibres. *Compos. Sci. Technol.* **63**, 1287–1296 (2003).

298. Oksman, K., Mathew, A. P., Bondeson, D. & Kvien, I. Manufacturing process of cellulose whiskers/polylactic acid nanocomposites. *Compos. Sci. Technol.* **66**, 2776–2784 (2006).

299. Petersson, L., Kvien, I. & Oksman, K. Structure and thermal properties of poly(lactic acid)/cellulose whiskers nanocomposite materials. *Compos. Sci. Technol.* **67**, 2535–2544 (2007).

300. Akbari, Z., Ghomashchi, T. & Moghadam, S. Improvement in Food Packaging Industry with Biobased Nanocomposites. *Int. J. Food Eng.* **3**, 1–26 (2007).

301. Rhim, J.-W. & Perry, K. W. Natural biopolymer-based nanocomposite films for packaging applications. *Crit. Rev. Food Sci. Nutr.* **47**, 411–33 (2007).

302. Bledzki, A. K. & Gassan, J. Composites reinforced with cellulose based fibres. *Prog. Polym. Sci.* **24**, 221–274 (1999).

303. Eichhorn, S. J., Dufrence, A., Herrefe-Franco, P. J., Escamilla, G. C., Hughes, M., Rials, T. G., Wild, P. M. Current international research into cellulosic fibres and composites. *J. Mater. Sci.* **36**, 2107–2131 (2001).

304. Dufresne, A. & Vignon, M. R. Improvement of Starch Film Performances Using Cellulose Microfibrils. *Macromolecules* **31**, 2693–2696 (1998).

305. Tserki, V., Matzinos, P., Zafeiropoulos, N. E. & Panayiotou, C. Development of biodegradable composites with treated and compatibilized lignocellulosic fibers. *J. Appl. Polym. Sci.* **100**, 4703–4710 (2006).

306. Sanchez-Garcia, M. D., Gimenez, E. & Lagaron, J. M. Morphology and barrier properties of solvent cast composites of thermoplastic biopolymers and purified cellulose fibers. *Carbohydr. Polym.* **71**, 235–244 (2008).

307. Nishino, T. & Arimoto, N. All-cellulose composite prepared by selective dissolving of fiber surface. *Biomacromolecules* **8**, 2712–2716 (2007).

308. Hassan, C. & Peppas, N. Structure and Applications of Poly(vinyl alcohol) Hydrogels Produced by Conventional Crosslinking or by Freezing/Thawing Methods. *Polym Nanocomposites* **153**, 37–65 (2011).

309. Paradossi, G., Cavalieri, F., Chiessi, E., Spagnoli, C. & Cowman, M. K. Poly(vinyl alcohol) as versatile biomaterial for potential biomedical applications. *J. Mater. Sci. Mater. Med.* **14**, 687–691 (2003).

310. Ding, B., Kimura, E., Sato, T., Fujita, S. & Shiratori, S. Fabrication of blend biodegradable nanofibrous nonwoven mats via multi-jet electrospinning. *Polymer.* **45**, 1895–1902 (2004).

311. Ma, X., Chang, P. R., Yu, J. & Wang, N. Preparation and properties of biodegradable poly(propylene carbonate)/thermoplastic dried starch composites. *Carbohydr. Polym.* **71**, 229–234 (2008).

312. Ma, X. & Yu, J. Formamide as the plasticizer for thermoplastic starch. *J. Appl. Polym. Sci.* **93**, 1769–1773 (2004).

313. Wang, N., Yu, J., Chang, P. R. & Ma, X. Influence of formamide and water on the properties of thermoplastic starch/poly(lactic acid) blends. *Carbohydr. Polym.* **71**, 109–118 (2008).

314. Alemdar, A. & Sain, M. Biocomposites from wheat straw nanofibers: Morphology, thermal and mechanical properties. *Compos. Sci. Technol.* **68**, 557–565 (2008).

315. Kaczmarek, H., Bajer, K., Gałka, P. & Kotnowska, B. Photodegradation studies of novel biodegradable blends based on poly(ethylene oxide) and pectin. *Polym. Degrad. Stab.* **92**, 2058–2069 (2007).

316. Crini, G. & Badot, P. M. Application of chitosan, a natural aminopolysaccharide, for dye removal from aqueous solutions by adsorption processes using batch studies: A review of recent literature. *Prog. Polym. Sci.* **33**, 399–447 (2008).

317. Chenite, A., Buschmann, M., Wang, D., Chaput, C. & Kandani, N. Rheological characterisation of thermogelling chitosan / glycerol-phosphate solutions. *Carbohydr. Polym.* **46**, 39–47 (2001).

318. Gällstedt, M. & Hedenqvist, M. S. Packaging-related mechanical and barrier properties of pulp-fiber-chitosan sheets. *Carbohydr. Polym.* **63**, 46–53 (2006).

319. Hosokawa, J., Nishiyama, M., Yoshihara, K., Kubo, T. & Terabe, A. Reaction between chitosan and cellulose on biodegradable composite film formation. *Ind. Eng. Chem. Res.* **30**, 788–792 (1991).

320. Hosokawa, J., Nishiyama, M., Yoshihara, K. & Kubo, T. Biodegradable Film Derived from Chitosan and Homogenized Cellulose. *Ind. Eng. Chem. Res.* **29**, 800–805 (1990).

321. Chen, R. H., Lin, W. C. & Lin, J. H. Effects of pH, ionic strength, and type of anion on the rheological properties of chitosan solutions. *Acta Polym.* **45**, 41–46 (1994).

322. Plackett, D. V., Holm, V. K., Johansen, P., Södergård, A., Verstichel, S. Characterization of L-potylactide and L-polylactide-polycaprolactone co-polymer films for use in cheese-packaging applications. *Packag. Technol. Sci.* **19**, 1–24 (2006).

323. Mathew, A. P., Oksman, K. & Sain, M. Mechanical properties of biodegradable composites from poly lactic acid (PLA) and microcrystalline cellulose (MCC). *J. Appl. Polym. Sci.* **97**, 2014–2025 (2005).

324. Ren, J., Zichao, L. & Tianbin, R. Mechanical and Thermal Properties of poly(lactic Acid)/Starch/Montmorillonite Biodegradable Bleds. *Polym. Polym. Compos.* **15**, 633–639 (2007).

325. Baiardo, M., Frisori, G., Scandola, M., Lips, D., Ruffieux, K., Wintermantel, E. Thermal and Mechanical Properties of Plasticized Poly(L-lactic acid). *J Appl Polym Sci* **90**, 1731–1738 (2003).

326. Huda, M. S., Drzal, L. T., Mohanty, A. K. & Misra, M. Effect of fiber surface-treatments on the properties of laminated biocomposites from poly(lactic acid) (PLA) and kenaf fibers. *Compos. Sci. Technol.* **68**, 424–432 (2008).

327. Huda, M. S., Drzal, L. T., Mohanty, A. K. & Misra, M. Chopped glass and recycled newspaper as reinforcement fibers in injection molded poly(lactic acid) (PLA) composites: A comparative study. *Compos. Sci. Technol.* **66**, 1813–1824 (2006).

328. Tsuji, H. & Fukui, I. Enhanced thermal stability of poly(lactide)s in the melt by enantiomeric polymer blending. *Polymer.* **44**, 2891–2896 (2003).

329. Park, J. W. & Im, S. S. Miscibility and morphology in blends of poly(L-lactic acid) and poly(vinyl acetate-co-vinyl alcohol). *Polymer.* **44**, 4341–4354 (2003).

330. Ljungberg, N. & Wesslán, B. The effects of plasticizers on the dynamic mechanical and thermal properties of poly(lactic acid). *J. Appl. Polym. Sci.* **86**, 1227–1234 (2002).

331. Mehta, R., Kumar, V., Bhunia, H. & Upadhyay, S. N. Synthesis of Poly(Lactic Acid): A Review. *J. Macromol. Sci. Part C Polym. Rev.* **45**, 325–349 (2005).

332. Gupta, A. P. & Kumar, V. New emerging trends in synthetic biodegradable polymers - Polylactide: A critique. *Eur. Polym. J.* **43**, 4053–4074 (2007).

333. Okubo, K. & Fujii, T. Improvement of interfacial adhesion in bamboo polymer composite enhanced with microfibrillated cellulose. *Polym. Compos. Biocomposites* **3**, 317–329 (2013).

334. Petersson, L. & Oksman, K. Biopolymer based nanocomposites: Comparing layered silicates and microcrystalline cellulose as nanoreinforcement. *Compos. Sci. Technol.* **66**, 2187–2196 (2006).

335. Gross, R. A. & Kalra, B. Biodegradable Polymers for the Environment. **297**, 803–808 (2002).

336. Nair, L. S. & Laurencin, C. T. Biodegradable polymers as biomaterials. *Prog. Polym. Sci.* **32**, 762–798 (2007).

337. Gunatillake, P., Mayadunne, R. & Adhikari, R. Recent developments in biodegradable synthetic polymers. *Biotechnol. Annu. Rev.* **12**, 301–347 (2006).

338. Siqueira, G., Bras, J. & Dufresne, A. Cellulose whiskers versus microfibrils: Influence of the nature of the nanoparticle and its surface functionalization on the thermal and mechanical properties of nanocomposites. *Biomacromolecules* **10**, 425–432 (2009).

339. Favier, V., Chanzy, H. & Cavaille, J.-Y. Y. Polymer Nanocomposites Reinforced by Cellulose Whiskers. *Macromolecules* **28**, 6365–6367 (1995).

340. Halpin, J. C. & Kardos, J. L. Moduli of crystalline polymers employing composite theory. *J. Appl. Phys.* **43**, 2235–2241 (1972).

341. Ouali, N., Cavaille, J. & Peres, J. Elastic, viscoelastic and plastic behavior of multiphase polymer blends. *Plast. Rubbers Compos. Process. Appl.* **16**, 55–60 (1991).

342. Ljungberg, N., Bonini, C., Bortolussi, F., Heux, L. New nanocomposite materials reinforced with cellulose whiskers in atactic polypropylene: Effect of surface and dispersion characteristics. *Biomacromolecules* **6**, 2732–2739 (2005).

343. Takayanagi, M., Uemura, S. & Minami, S. Application of equivalent model method to dynamic rheo-optical properties of crystalline polymer. *J. Polym. Sci. Part C Polym. Symp.* **5**, 113–122 (1964).

344. Angle, M. N. & Dufresne, A. Plasticized Starch / Tunicin Whiskers Nanocomposite Materials. 2. Mechanical Behavior. **15**, 2921–2931 (2001).

345. Gao, H., Ji, B., Jager, I. L., Arzt, E. & Fratzl, P. Materials become insensitive to flaws at nanoscale: Lessons from nature. *PNAS* **100**, 5597–5600 (2003).

346. Jager, I. & Fratzl, P. Mineralized Collagen Fibrils: A Mechanical Model with a Staggered Arrangement of Mineral Particles. *Byophysic J.* **79**, 1737–1746 (2000).

347. Nishino, T., Matsuda, I. & Hirao, K. All-cellulose composite. *Macromolecules* **37**, 7683–7687 (2004).

348. Nogi, M., Abe, K. Property enhancement of optically transparent bionanofiber composites by acetylation. *Appl. Phys. Lett.* **89**, 87–90 (2006).

349. Wu, J., Zhang, J., He, J., Ren, Q., Guo, M. Homogeneous acetylation of cellulose in a new ionic liquid. *Biomacromolecules* **5**, 266–268 (2004).

350. Matias, M. C., De La Orden, M. U., Gonzalez Sánchez, C. & Martinez Urreaga, J. Comparative spectroscopic study of the modification of cellulosic materials with different coupling agents. *J. Appl. Polym. Sci.* **75**, 256–266 (2000).

351. La Mantia, F. P. & Morreale, M. Green composites: A brief review. *Compos. Part A Appl. Sci. Manuf.* **42**, 579–588 (2011).

352. Trejo-O'reilly, J.-A., Cavaille, J.-Y., Belgacem, N. & Gandini, A. Surface Energy and Wettability of Modified Cellulosic Fibres for Use in Composite Materials. *J. Adhes.* **67**, 359–374 (1998).

353. Li, Q. & Matuana, L. M. Effectiveness of Maleated and Acrylic Acid-Functionalized Polyolefin Coupling Agents for HDPE-Wood-Flour Composites. *J. Thermoplast. Compos. Mater.* **16**, 551–564 (2003).

354. Jeon, Y., Lowell, A. V. & Gross, R. Studies of Starch Esterification: Reactions with Alkenylsuccinates in Aqueous Slurry Systems. *Starch - Stärke* **51**, 90–93 (1999).

355. Yoshida, Y., Heux, L. & Isogai, A. Heterogeneous reaction between cellulose and alkyl ketene dimer under solvent-free conditions. *Cellulose* **19**, 1667–1676 (2012).

356. Takihara, T., Yoshida, Y. & Isogai, A. Reactions between cellulose diacetate and alkenylsuccinic anhydrides and characterization of the reaction products. *Cellulose* **14**, 357–366 (2007).

357. Teramoto, Y. & Nishio, Y. Cellulose diacetate-graft-poly(lactic acid)s: Synthesis of wide-ranging compositions and their thermal and mechanical properties. *Polymer.* **44**, 2701–2709 (2003).

358. Garnier, G., Wright, J., Godbout, L. & Yu, L. Wetting mechanism of alkyl ketene dimers on cellulose films. *Colloids Surfaces A Physicochem. Eng. Asp.* **145**, 153–165 (1998).

359. Moigne, N. Le, Longerey, M., Taulemesse, J.-M., Bénézet, J.-C. & Bergeret, A. Study of the interface in natural fibres reinforced poly(lactic acid) biocomposites modified by optimized organosilane treatments. *Ind. Crops Prod.* **52**, 481–494 (2014).

360. Lin, W., Hu, X., Yang, W., Li, Y. Hydrophobic Modification of Nanocellulose via a Two-Step Silanation Method. *Polymers* **10**, (2018).

361. Alonso, E., Pothan, L. A., Ferreira, A. & Cordeiro, N. Surface modification of banana fibers using organosilanes: an IGC insight. *Cellulose* **26**, 3643–3654 (2019).

362. Bel-Hassen, R., Boufi, S., Salon, M.-C. B., Abdelmouleh, M. & Belgacem, M. N. Adsorption of silane onto cellulose fibers. II. The effect of pH on silane hydrolysis, condensation, and adsorption behavior. *J. Appl. Polym. Sci.* **108**, 1958–1968 (2008).

363. Suegama, P. H., de Melo, H. G., Benedetti, A. V & Aoki, I. V. Influence of cerium (IV) ions on the mechanism of organosilane polymerization and on the improvement of its barrier properties. *Electrochim. Acta* **54**, 2655–2662 (2009).

364. Kawasum, M., Hasegawa, N., Kato, M., Usuki, A. & Okada, A. Preparation and Mechanical Properties of Polypropylene-Clay Hybrids. *Macromolecules* **30**, 6333–6338 (1997).

365. Larsson, P. T., Wickholm, K. & Iversen, T. A CP / MAS 13C NMR investigation of molecular ordering in celluloses. *Carbohydr. Res.* **302**, 19–25 (1997).

366. Sekkar, V., Gopalakrishnan, S. & Ambika Devi, K. Studies on allophanate-urethane networks based on hydroxyl terminated polybutadiene: Effect of isocyanate type on the network characteristics. *Eur. Polym. J.* **39**, 1281–1290 (2003).

367. Goussé, C., Chanzy, H., Excoffier, G., Soubeyrand, L. & Fleury, E. Stable suspensions of partially silylated cellulose whiskers dispersed in organic solvents. *Polymer.* **43**, 2645–2651 (2002).

368. Thomas, H., Heine, E. & Wollseifen, R. Nanofibers from natural and inorganic polymers via electrospinning. *Int Nonwovens J* **14**, 12–18 (2005).

369. Araki, J., Wada, M. & Kuga, S. Steric stabilization of a cellulose microcrystal suspension by poly(ethylene glycol) grafting. *Langmuir* **17**, 21–27 (2001).

370. Sclavons, M., Laurent, M., Devaux, J. & Carlier, V. Maleic anhydride-grafted polypropylene : FTIR study of a model polymer grafted by ene-reaction. **46**, 8062–8067 (2005).

371. Gauthier, R., Joly, C., Coupas, A. C., Gauthier, H. & Escoubes, M. Interfaces in polyolefin/cellulosic fiber composites: Chemical coupling, morphology, correlation with adhesion and aging in moisture. *Polym. Compos.* **19**, 287–300 (1998).

372. Kazayawoko, M., Balatinecz, J. J. & Woodhams, R. T. Diffuse reflectance Fourier transform infrared spectra of wood fibers treated with maleated polypropylenes. *J. Appl. Polym. Sci.* **66**, 1163–1173 (1997).

373. Bledzki, A. K., Reihmane, S. & Gassan, J. Properties and modification methods for vegetable fibers for natural fiber composites. *J. Appl. Polym. Sci.* **59**, 1329–1336 (1996).

374. Takase, S. & Shiraishi, N. Studies on composites from wood and polypropylenes. II. *J. Appl. Polym. Sci.* **37**, 645–659 (1989).

375. Maldas, D. & Kokta, B. V. Role of Coupling Agents on the Performance of Woodflour-Filled Polypropylene Composite. *Int. J. Polym. Mater. Polym. Biomater. Vol. 27, 1994 - Issue 1-2* **27**, 77–88 (1994).

376. Qiu, W., Endo, T. & Hirotsu, T. Interfacial interaction, morphology, and tensile properties of a composite of highly crystalline cellulose and maleated polypropylene. *J. Appl. Polym. Sci.* **102**, 3830–3841 (2006).

377. Sealey, J. E., Samaranayake, G., Todd, J. G. & Glasser, W. G. Novel cellulose derivatives: Preparation and thermal analysis of waxy esters of cellulose. *J. Polym. Sci. Part B-Polymer Phys.* **34**, 1613–1620 (1996).

378. Mark, H. F., Bikales, N. M., Overberger, C. G., Menges, G. & Wiley-VCH. *Encyclopedia of Polymer Science and Engineering, Vol. 3: Cellular Materials to Composites*. (1985).

379. Champetier, G. & Monnerie, L. *Introduction la Chimie Macromolculaire*. (1969).

380. Chauvelon, G., Gergaud, N., Lourdin, D., Krausz, P. Esterification of cellulose-enriched agricultural by-products and characterization of mechanical properties of cellulosic films. *Carbohydr. Polym.* **42**, 385–392 (2000).

381. Kloser, E. & Gray, D. G. Surface grafting of cellulose nanocrystals with poly(ethylene oxide) in aqueous media. *Langmuir* **26**, 13450–13456 (2010).

382. Qiu, K. & Netravali, A. N. Fabrication and characterization of biodegradable composites based on microfibrillated cellulose and polyvinyl alcohol. *Compos. Sci. Technol.* **72**, 1588–1594 (2012).

383. Stevens, E. *Green plastics: an introduction to the new science of biodegradable plastics.* (Princeton University Press, 2002).

384. Wang, J., Gao, C., Zhang, Y. & Wan, Y. Preparation and in vitro characterization of BC/PVA hydrogel composite for its potential use as artificial cornea biomaterial. *Mater. Sci. Eng. C* **30**, 214–218 (2010).

385. Millon, L. E., Oates, C. J. & Wan, W. Compression properties of polyvinyl alcohol-bacterial cellulose nanocomposite. *J. Biomed. Mater. Res. - Part B Appl. Biomater.* **90 B**, 922–929 (2009).

386. Gindl-Altmutter, W., Obersriebnig, M., Veigel, S. & Liebner, F. Compatibility between cellulose and hydrophobic polymer provided by microfibrillated lignocellulose. *ChemSusChem* **8**, 87–91 (2015).

387. Lee, H., Dellatore, S. M., Miller, W. M. & Messersmith, P. B. P. B. Mussel-Inspired Surface Chemistry for Multifunctional Coatings. *Science (80-.).* **318**, 426–431 (2007).

388. Ejima, H., Richardsin, J., Su, g. K. One-Step Assembly of Coordination. *Science (80-.).* **341**, 154–157 (2013).

389. Sileika, T. S., Barrett, D. G., Zhang, R., Lau, K. H. A. & Messersmith, P. B. Colorless multifunctional coatings inspired by polyphenols found in tea, chocolate, and wine. *Angewandte Chemie - International Edition* **52**, 10766–10770 (2013).

390. Hu, Z., Marway, H., Kasem, H., Pelton, R. & Cranston, E. Dried and Redispersible Cellulose Nanocrystal Pickering Emulsions. *ACS Macro Lett.* **5**, 185–189 (2016).

391. Tang, H. R., Covington, A. D. & Hancock, R. A. Structure-Activity Relationships in the Hydrophobic Interactions of Polyphenols with Cellulose and Collagen. *Biopolymers* **70**, 403–413 (2003).

392. Machatova, Z., Barbieriková, Z., Poliak, P., Jančovičová, V., Lukeš, V., Brezová, V., Study of natural anthraquinone colorants by EPR and UV/vis spectroscopy. *Dye. Pigment.* **132**, 79–93 (2016).

393. Van den Oever, M. J. A., Bos, L. H. & Kemenade, M. J. J. M. Influence of the Physical Structure of Flax Fibres on theMechanical Properties of Flax Fibre Reinforced Polypropylene Composites. *Appl. Compos. Mater.* **7**, 387–402 (2000).

394. Owens, D. K., Nemours, E. I. P. De & Film, S. Estimation of the Surface Free Energy of Polymers D. *juurnal Appl. Polym. Sci.* **13**, 1741–1747 (1969).

395. Kvien, I., Tanem, B. S. & Oksman, K. Characterization of Cellulose Whiskers and Their Nanocomposites by Atomic Force and Electron Microscopy. *Biomacromolecules* **6**, 3160–3165 (2005).

396. Quillin, D. T., Caulfield, D. F. & Koutsky, J. A. Crystallinity in the polypropylene/cellulose system. I. Nucleation and crystalline morphology. *J. Appl. Polym. Sci.* **50**, 1187–1194 (1993).

397. Gray, D. G. Transcrystallization of polypropylene at cellulose nanocrystal surfaces. *Cellulose* **15**, 297–301 (2008).

398. Felix, J. M. & Gatenholm, P. Effect of transcrystalline morphology on interfacial adhesion in cellulose/polypropylene composites. *J. Mater. Sci.* **29**, 3043–3049 (1994).

399. French, A. D. & Santiago Cintrón, M. Cellulose polymorphy, crystallite size, and the Segal Crystallinity Index. *Cellulose* **20**, 583–588 (2013).

400. Garvey, C. J., Parker, I. H. & Simon, G. P. On the interpretation of X-ray diffraction powder patterns in terms of the nanostructure of cellulose I fibres. *Macromolecular Chemistry and Physics* **206**, 1568–1575 (2005).

401. Rabiej, S. Determination of the crystallinity of polymer blends by an X-ray-diffraction method. *European Polymer Journal* **29**, 625–633 (1993).

402. Monasse, B. & Haudin, J. M. Growth transition and morphology change in polypropylene. *Colloid Polym. Sci.* **263**, 822–831 (1985).

403. Johns, M. A., Lewandowska, A. E. & Eichhorn, S. J. Rapid Determination of the Distribution of Cellulose Nanomaterial Aggregates in Composites Enabled by Multi-Channel Spectral Confocal Microscopy. *Microsc. Microanal.* **25**, 682–689 (2019).

404. Hartmann, M. H. High Molecular Weight Polylactic Acid Polymers -Biopolymers from Renewable Resources. in (ed. Kaplan, D. L.) 367–411 (Springer Berlin Heidelberg, 1998).

405. Garlotta, D. A Literature Review of Poly(Lactic Acid). *Springer* **9**, 63–84 (2002).

406. Conn, R. E., Kolstad, J. J., Dixler, D. S., Pariza, M. W. Safety assessment of polylactide (PLA) for use as a food-contact polymer. *Food Chem. Toxicol.* **33**, 273–283 (1995).

407. Jamshidi, K., Hyon, S.-H. & Ikada, Y. Thermal characterization of polylactides. *Polymer*. **29**, 2229–2234 (1988).

408. Spinu, M., Jackson, C., Keating, M. Y. & Gardner, K. H. Material Design in Poly(Lactic Acid) Systems: Block Copolymers, Star Homo- and Copolymers, and Stereocomplexes. *J. Macromol. Sci. Part A* **33**, 1497–1530 (1996).

409. Ying, Z., Wu, D., Wang, Z., Xie, W., Qui, Y., Wei, X. Rheological and mechanical properties of polylactide nanocomposites reinforced with the cellulose nanofibers with various surface treatments. *Cellulose* **25**, 3955–3971 (2018).

410. Ang, S., Haritos, V. & Batchelor, W. Effect of refining and homogenization on nanocellulose fiber development, sheet strength and energy consumption. *Cellulose* **26**, 4767–4786 (2019).

411. Berto, G. L. & Arantes, V. International Journal of Biological Macromolecules Kinetic changes in cellulose properties during de fi brillation into micro fi brillated cellulose and cellulose nano fi brils by ultra-re fi ning. **127**, 637–648 (2019).

412. Pahimanolis, N. & Hippi, U. Surface functionalization of nanofibrillated cellulose using click-chemistry approach in aqueous media. *cellulose* **18**, 1201–1212 (2011).

413. Yoo, Y. & Youngblood, J. P. Green One-Pot Synthesis of Surface Hydrophobized Cellulose Nanocrystals in Aqueous Medium. *ACS Sustain. Chem. Eng.* **4**, 3927–3938 (2016).

Cellulose (2019) 26:9645–9659
https://doi.org/10.1007/s10570-019-02756-8

ORIGINAL RESEARCH

The effect of the dispersion of microfibrillated cellulose on the mechanical properties of melt-compounded polypropylene–polyethylene copolymer

Caterina Palange · Marcus A. Johns · David J. Scurr · Jonathan S. Phipps · Stephen J. Eichhorn

Received: 28 June 2019 / Accepted: 12 September 2019 / Published online: 27 September 2019

Abstract Microfibrillated cellulose (MFC) is a highly expanded, high surface area networked form of cellulose-based reinforcement. Due to the poor compatibility of cellulose with most common apolar thermoplastic matrices, the production of cellulose-reinforced composites in industry is currently limited to polar materials. In this study, a facile water-based chemistry, based on the reaction of MFC with tannic acid and subsequent functionalisation with an alkyl amine, is used to render the surface of the MFC fibrils hydrophobic and enhance the dispersion of the cellulose-based filler into an apolar thermoplastic matrix. The level of dispersion of the compatibilized MFC reinforced composites was evaluated using Time of Flight Secondary Ion Mass Spectrometry and multi-channel Spectral Confocal Laser Scanning Microscopy. The agglomeration of cellulosic filler within the composites was reduced by functionalising the surface of the MFC fibrils with tannic acid and octadecylamine. The resulting composites exhibited an increase in modulus at a high cellulose content. Despite the dispersion of a large portion of the functionalised filler, the presence of some remaining aggregates affected the impact properties of the composites produced.

Keywords Microfibrillated cellulose · Composites · Mechanical properties

Electronic supplementary material The online version of this article (https://doi.org/10.1007/s10570-019-02756-8) contains supplementary material, which is available to authorized users.

C. Palange · J. S. Phipps
FiberLean Technologies Ltd., Par Moor Centre, Par Moor Rd, Par PL24 2SQ, UK

C. Palange · M. A. Johns · S. J. Eichhorn (✉)
School of Civil, Aerospace, and Mechanical Engineering, Bristol Composites Institute (ACCIS), University Walk, University of Bristol, Bristol BS8 1TR, UK
e-mail: s.j.eichhorn@bristol.ac.uk

D. J. Scurr
School of Pharmacy, University of Nottingham, Boots Science Building, Nottingham NG7 2RD, UK

Introduction

Cellulose-based nanofillers have the potential to increase the mechanical performance of composites dramatically, even at extremely low concentrations (Duchemin et al. 2009; Spoljaric et al. 2009; Miao and Hamad 2013; Pöllänen et al. 2013; Lee et al. 2014). The production of composites based on cellulose fillers and polyolefins has also been the target of much recent research (Peijs et al. 1998; Wambua et al. 2003; Ljungberg et al. 2006; Guo et al. 2013). Nanomaterials are defined as a class of materials having at least one dimension less than 100 nm (Siro et al. 2010). Nanofillers, one form of nanomaterials, are generally characterised by an extremely high surface to volume

ratio, which generates an extended filler-matrix interfacial area (Siro et al. 2010; Sehaqui et al. 2011). Using an appropriate filler-matrix combination, it is possible to obtain reinforced nanocomposites in which the strong and extended interfacial area increases the mechanical properties of the matrix (Klemm et al. 2011; Missoum et al. 2013; Khalil et al. 2014).

Microfibrillated cellulose (MFC) is characterized by a fibrillar network morphology and a highly expanded interfacial area alongside attractive mechanical properties (calculated Young's modulus of $\approx$ 20 GPa (network) and strength of $\approx$ 240 MPa) (Zimmermann et al. 2004, 2005; Leitner et al. 2007), low production cost, renewability and wide availability (Herrick et al. 1983; Klemm et al. 2006; Henriksson and Berglund 2007; Iwamoto et al. 2007; Siro et al. 2010; Spence et al. 2011). These characteristics render MFC an interesting nano-reinforcement. The structure and characteristics of MFC are dependent on the source of the raw material and on the fibrillation process. The MFC used in this study was produced at FiberLean Technologies Ltd.; it is uncharged, due to the mechanical production method used, and hydrophilic due to the presence of the hydroxyl groups on the surface of the fibrils. Polyolefins represent a large portion of the polymer market with a global annual production of 135 million tonnes (Woodhams et al. 1984; Malkapuram et al. 2008), and have a well-established industrial production route, from synthesis up to the final product conveyance. The products obtained from polyolefins are durable, chemically stable, have low melting temperatures and viscosities and excellent processability. The efficient production of MFC-reinforced polyolefins represents an important step in the establishment of naturally derived composites. Unfortunately, an industrial method to produce MFC-reinforced composites using the normal polyolefin manufacturing process has not yet been developed. The main issue to solve with these composites is the incompatibility of untreated cellulose fillers with hydrophobic polymer matrices. This incompatibility leads to a weak filler-matrix interface, and thereby poorly performing composites. Cellulosic fillers also possess a strong tendency to agglomerate, thereby minimising the surface exposed to the unfavourable environment represented by the apolar matrix.

Chemical surface modification (Gruber and Granzow 1996; Heux et al. 2000; Bonini et al. 2002; Hafrén et al. 2006) can substitute the hydroxyl groups on the surface of MFC fibrils. This decreases surface energy (Klemm et al. 2005; Maya and Rajesh 2008; Maya and Sabu 2008), potentially improving the mixing and dispersion of the filler and preventing aggregation (Habibi et al. 2010). Chemical treatments on the surface of MFC fibrils can be divided into those based on organic solvents and water-based systems. Organic solvent-based techniques are impractical due to the large volume of chemicals required to treat small amounts of MFC (Kazayawoko et al. 1997; Matias et al. 2000). Nevertheless, the functionalisation of cellulose with maleic anhydride grafted polypropylene (MAgPP) in an organic solvent has proven to be efficient in producing individualized hydrophobic cellulose fibrils which can be readily and homogeneously dispersed in polyolefin matrices (Takase and Shiraishi 1989; Maldas and Kokta 1994; Bledzki et al. 1996; Gauthier et al. 1998; Sclavons et al. 2005; Qiu et al. 2006). The polyphenol tannic acid (TA) has also been demonstrated to functionalise the surface of MFC fibrils under alkaline conditions at room temperature (Lee et al. 2007; Ejima et al. 2013; Sileika et al. 2013). The hydrophilic product obtained can further react with primary amines (Lee et al. 2007; Ejima et al. 2013; Sileika et al. 2013; Hu et al. 2017). In this study the primary amines used are the short chain hexylamine ($C_6H_{13}NH_2$) and the hydrophobic long chain octadecylamine ($C_{18}H_{37}NH_2$), which form stable covalent bonds with the MFC-TA complex. The material obtained using the short chain hexylamine and the material obtained from the reaction with octadecylamine were filtered and oven dried. The resultant dry form is easy to grind at room temperature to obtain a powder. This can then be processed alongside polyolefins in a classical compounder to obtain MFC reinforced nanocomposites (see Supplementary Information, Figs. 1S and 2S). The long aliphatic tail (C_{18}) of the octadecylamine renders the cellulose fibrils hydrophobic, and thereby supports the efficient dispersion of the reacted MFC in the composites. On the other hand the hexylamine short aliphatic tail (C_6) confers to the TA-MFC compound a less marked hydrophobic character, insufficient to obtain a good dispersion of the filler. This approach is favourable over other chemical treatment methods since it uses natural products for the modification of the cellulose, moving away from commonly used organic solvent approaches.

In the present work a set of tannic acid-hexylamine treated MFC (MFC-TA-C_6) reinforced composites are used as a comparison to tannic acid-octadecylamine treated MFC (MFC-TA-C_{18}) reinforced composites, and the dispersion of the reinforcing phase characterised using both ToF–SIMS and Spectral Confocal Laser Scanning Microscopy (SCLSM). The hypothesis is that this approach can better disperse the MFC within a hydrophobic resin, improving mechanical properties, and removing aggregates.

Materials

MFC slurry having a water content of 95 wt% was produced by FiberLean by the mechanical grinding of softwood bleached Kraft pine pulp. The poly(propylene)-poly(ethylene) compolymer (PPPE) matrix material (with a melting temperature of 170 °C) was purchased from LyondellBasell (Rotterdam, Netherlands). Pure non-porous cellulose film was received from the Fraunhofer-Institut für Angewandte Polymerforschung (Geiselbergstr). The following chemicals and reagents were purchased from Sigma Aldrich (Dorset, UK): Tannic acid (TA) powder, octadecylamine ($C_{18}H_{37}NH_2$) powder technical grade 90%, hexylamine ($C_6H_{13}NH_2$) 99%, 4-(2-hydroxyethyl)-1-piperazineethanesulfonic acid (HEPES) powder $> 99.5\%$, polypropylene-graft-maleic anhydride (MAgPP—average Mw $\sim$ 9100 and Mn $\sim$ 3900 by GPC), maleic anhydride 8–10 wt%, acetone $\geq$ 99.9% ($\rho = 0.79$ g cm^{-3}) and anhydrous toluene, 99.8% ($\rho = 0.87$ g cm^{-3}). Xylene, 99% ($\rho = 0.88$ g cm^{-3}) and sodium hydroxide reagent grade were supplied by Fisher Scientific (Leicestershire, UK).

Experimental methods

Solvent swap

40 g of MFC slurry at 5 wt% of cellulose in water, containing 2 g of cellulose fibrils, was filtered and resuspended in 100 mL of acetone. The suspension was magnetically stirred for 10 min at 500 rpm and then filtered under vacuum on a glass filter before re-suspending in acetone; this procedure was repeated 3 times. The filtered material was then re-suspended in 100 mL of toluene. The washing procedure was repeated 3 times with toluene. The solvent-exchanged material was filtered, recovered and further processed.

MAgPP surface reaction

The solvent-swapped, filtered MFC sample (2 g of MFC) was re-suspended in 100 mL of xylene and washed, as previously described, 2 times; the suspension was filtered and the filtercake was re-suspended in 160 mL of xylene in a round-bottomed, three-necked flask and heated up to 160 °C. The suspension was kept at 160 °C (boiling point of xylene) and refluxed, under magnetic stirring at 500 rpm, for 10 min to eliminate residual water. 0.2 g of MAgPP was added through a separate funnel and the system was refluxed under magnetic stirring at 500 rpm for 1 h. The final solid product was filtered on a glass filter with a Venturi vacuum system, weighed and kept in a vacuum oven at 60 °C overnight.

Tannic acid-octadecylamine and tannic acid-hexylamine surface reaction

100 g of MFC slurry at 1 wt% of cellulose was diluted to a final volume of 500 mL with distilled water; 2.5 g of HEPES was added to the suspension and the pH was adjusted to 8 with sodium hydroxide. 0.5 g of tannic acid (TA) was added to the suspension and kept under magnetic agitation at 500 rpm overnight at room temperature. 0.5 g of octadecylamine (melting point 50 °C) was suspended in 50 mL of water at 70 °C by magnetic stirring the suspension at 500 rpm. The suspension was added to the MFC-TA reacted suspension and kept under magnetic stirring at 200 rpm for 3 h at room temperature. The product was filtered on a paper filter (Whatman^{TM}541-hardened ashless) under vacuum. The recovered material was resuspended in 100 mL of acetone, filtered under vacuum, recovered and kept in a fume cupboard to dry. The dried product was weighed and then passed through a laboratory grinder. The same procedure was followed to produce MFC samples functionalised with hexylamine in place of octadecylamine, replacing 0.5 g (0.002 mol) of octadecylamine with 0.2 g (0.002 mol) of hexylamine. The same procedure used to prepare the octadecylamine reacted MFC was used to prepare hydrophobic non-porous cellulose films, substituting

100 g of MFC slurry at 1 wt% of cellulose with 1 g of non-porous cellulose film cut in strips of 1.5 cm width. After the reaction the strips were recovered, washed in an acetone bath and left to dry in a fume cupboard.

Preparation of nanocomposites

Compounding

Composites were prepared in a ZSK Mc^{18} counter rotating twin screw extruder (Coperion) with a specific torque of 18 Nm cm^{-3}, maximum screw speed of 1200 min^{-1}, and screw inner diameter ratio (D_o/D_i) of 1.55 (8.2 mm screw diameter) using filler concentrations of 0.5, 1, 2, 3, 4, 5, 10, 15 and 20 wt%. Specimens reinforced with 1 wt% polymerised TA were prepared using the powder obtained by the grinding of tannic acid powder (average particle diameter $\sim$ 30 μm) polymerised under alkali conditions overnight, to mimic the MFC-TA reaction. The samples were compounded at 210 °C at a 2 kg h^{-1} feed rate and 200 rpm. The obtained composite pellets were recovered for further processing.

Preparation of specimens for testing

Specimens for tensile and impact tests were injection moulded using an Arburg 221 M machine, in accordance with ASTM D4761-13 and ASTM D 882. The specimens produced were Type I of ASTM D 882.

Contact angle and free surface energy

Contact angles of pure non-porous cellulose and TA-octadecylamine reacted non-porous cellulose films were measured using a Fibrodat 68-96 DAT Dynamic Absorption Tester (Testing Machines, Inc.). Sheets of untreated MFC, TA-C_6 and TA-C_{18} treated MFC were obtained by the filtration of the MFC suspension using a standard handsheet former followed by pressing of the filtercake into a sheet and drying according to TAPPI procedure T205; untreated MFC sheets were also cut into strips for tensile modulus measurements. Contact angles on these were measured using the same instrument. De-ionized water was used as a probe liquid. The free surface energy of the pure and TA-octadecylamine reacted non-porous cellulose films and of MFC and TA-C_6 and TA-C_{18} treated MFC sheets were evaluated using the Fibrodat tester with water as the polar probe liquid and bromonaphthalene (BN) as the apolar probe liquid. The contact angle and free surface energy for the MFC films are reported in Supplementary Information. To minimize experimental errors, the values were measured at five random locations for each sample, and an average reported.

Energy-dispersive X-ray spectroscopy (EDX) imaging

A JEOL IT300 Scanning Electron Microscopy (SEM) operated at 2 keV and a working distance of 15 mm was used to image TA-C_{18} treated MFC reinforced composites. The samples were carbon coated and analysed using Energy-Dispersive X-ray spectroscopy (EDX) imaging.

Time of Flight Secondary Ion Mass Spectroscopy (ToF-SIMS) mapping

ToF-SIMS images were acquired at Nottingham University using a ToF-SIMS IV instrument (ION-TOF GmbH, Münster, Germany) equipped with a bismuth liquid metal ion gun and a single-stage reflectron analyser. Operating conditions utilized Bi^{3+} ions with a primary energy of 25 kV and a pulsed target current of approximately 1.0 pA. Low-energy electrons (20 eV) were used to compensate for surface charging caused by the positively charged primary ion beam on the insulating surfaces. Individual spots were analysed by rastering areas of 500 × 500 μm at a resolution of 256 × 256 pixels. The total primary ion beam dose for each analysed area was kept below 1×10^{12} ions cm^{-2}, ensuring static conditions.

Multi-channel spectral confocal laser scanning microscopy (SCLSM) mapping

Composite samples were cryo-microtomed into slices of 20 μm thickness cut from the central part of a dumbbell having dimensions of 10 × 4 mm (length × width). Slices were placed between a glass slide and a coverslip to flatten the surface. Spectral *z*-stack images (800 × 800 μm) were generated using a Zeiss LSM 880 confocal microscope (405 nm diode laser, 5.0% power, Plan-Apochromat 10 ×/0.45 M27 objective, MBS-405 filter, 32 channels:

λ = 411–695 nm). The maximum distance between stack slices was $\sim$ 2 μm.

Image processing

Image stacks generated using spectral confocal microscopy were processed in Fiji software. The *z*-projection function (projection type: standard deviation) was used to flatten image stacks into single images. After thresholding, images were analysed to determine the observed aggregate areas. Aggregates at the edge of the images were excluded, as were aggregates smaller than 11 μm^2, i.e. less than four pixels, as these could not be visually identified.

Aggregate analysis

Aggregate distribution was subdivided into four categories: small, medium, large and outliers. Rather than set these categories between fixed area values, the maximum and minimum values for each category were determined using the box plots themselves. A box plot was constructed using the entire data set, and the values at which data would be classified as an upper, or lower, outlier determined. The box plot was then regenerated using the outlier values as the maximum and minimum for the data range and new outlier values calculated. This process was repeated until the range of values fell between the upper and lower outlier values. This determined the aggregates that fell into the small category for each sample. To determine the medium category range, the process was repeated excluding all values in the small category. The process was repeated excluding values in the small and medium categories to define the large category range. All values that fell out of these ranges were classified as outliers. Due to the skew present in the data sets, the calculated lower outlier values were always less than the initial lower data values for all samples. To compare the aggregate populations, the boundaries for the four size categories were set as the boundaries determined for the 1 wt% MFC-TA-C_{18} composite sample using the above technique.

Statistical analysis

For the comparison of the composite mean aggregate areas and aggregate population analysis, a one-way analysis of variance (ANOVA) test was used to determine the statistical differences between two or more samples, assuming equal variance, with Tukey HSD posthoc correction. A confidence interval of 0.95 was used.

Mechanical and impact tests

Mechanical tests were conducted using a tensile testing machine (Instron 3367). The maximum load and the crosshead speed used were 30 kN and 10 mm min^{-1}. The tests were performed in accordance with ASTM D4761-13 and ASTM D 882. The impact tests were conducted using an impact testing machine (Instron-CEAST 9340-Drop Tower Impact System) at room temperature. The tests were performed according to ISO-179 2.

Results and discussion

Contact angle and free surface energy

The contact angles and the free surface energies of the pure matrix (PPPE), untreated and TA–C_{18} reacted non-porous cellulose films are provided in Table 1. The values of contact angle and free surface energy for porous MFC films are reported in Table 1S in Supplementary Information. The values were calculated from five different sampling points on the same specimen to minimize the errors. The free surface energy was evaluated using water and bromonaphthalene (BN) and applying the Owens, Wendt, Rabel and Kaelble method according to the equation

$$\sigma_{sl} = \sigma_s + \sigma_l - 2\left[(\sigma_{sw}\sigma_{lw})^{\frac{1}{2}} + (\sigma_{sd}\sigma_{ld})^{\frac{1}{2}}\right]. \quad (1)$$

combined with Young's equation

$$\sigma_s = \sigma_{sl} + \sigma_l \cos\theta \quad (2)$$

where σ_{sl} is the solid–liquid interfacial tension, σ_s is the solid–air surface tension and σ_l is the liquid–air surface tension, σ_{sw} is the polar component of the solid-air surface tension, σ_{lw} is the polar component of the liquid–air surface tension, σ_{sd} is the dispersed component of the solid-air surface tension, σ_{ld} is the dispersed component of the liquid–air surface tension, and θ is the measured contact angle. The Owens, Wendt, Rabel and Kaelble method relies on the data collected for at least two liquids, one polar and one

Table 1 Free surface energy, polar and apolar contribution, water and BN contact angle of PPPE, untreated non-porous cellulose, and TA-C_{18} reacted non-porous cellulose films

	Free surface energy (mN m^{-1})	Polar contribution (mN m^{-1})	Dispersive contribution (mN m^{-1})	Contact angle (°)	
				Water	BN
PPPE	37.6 ± 0.2	3.6 ± 0.1	33.9 ± 0.1	83 ± 1	41 ± 1
Non-porous cellulose	70.1 ± 0.1	36.1 ± 0.1	34.6 ± 0.1	21 ± 1	45.1 ± 0.7
Non-porous cellulose TAC_{18}	33.9 ± 0.1	1.2 ± 0.1	32.8 ± 0.1	93 ± 1	44 ± 0.5

apolar. From the two sets of contact angle data it is possible to write a system of two equations which is solved by the geometrical mean method giving a value for the solid-air surface tension ($\sigma_{s.}$)

The TA-C_{18} surface treatment of the non-porous cellulose film increases the sample water contact angle from 21° to 93° and decreases the free surface energy of the samples from 70.1 to 33.9 mN m^{-1} respectively. The non-porous cellulose films were used as a model system because the porous nature of MFC films made it impossible to obtain reliable values for the contact angle and free surface energy. Nevertheless, the measured water contact angle of MFC varies from 44° for the untreated sample to 121° for the TA-C_{18} surface reacted MFC film.

The contact angle data for both non-porous cellulose and MFC shows that the surface modification of cellulose by the reaction with TA and octadecylamine decreases the surface energy of the cellulose substantially, and thus should improve its dispersibility in apolar polymers. The contact angle of MAgPP reacted MFC was not measured as it was impossible to form a coherent sheet. The time evolution of the polar and apolar contact angle with water and BN probe on the different supports (Fig. 3S and 4S) can be found in Supplementary Information.

EDX imaging of MFC reinforced composites

The composites obtained by reinforcing the neat matrix with 1 wt% MAgPP-MFC and 0.5 wt%, 1 wt% and 15 wt% MFC-TA-C_{18} were investigated using EDX imaging. EDX analysis of the transverse surface of the composites was used to investigate the filler dispersion. MAgPP reacted MFC was used as a reference to determine the level of dispersion using a solvent based cellulose surface chemistry.

A typical aggregate of MAgPP-MFC is reported in Fig. 1; the dimension of this aggregate was evaluated to be ∼ 100 μm in length. Similar aggregates were found within the MFC-TA-C_{18} reinforced samples (Fig. 2).

EDX spectroscopic evidence suggests that there is an incomplete dispersion of the MFC, resulting in the formation of aggregates. Aggregates in samples containing MAgPP treated MFC are typically different sizes from those in samples containing TA-C_{18} treated MFC. The presence of small aggregates (10 μm or below) and a semi-continuous background is noted. This latter result suggests that a fraction of the filler can be dispersed in the matrix at a much smaller scale compared to the size of the large visible aggregates. Unfortunately, EDX cannot fully discriminate the signal from cellulose since the presence of the oxygen from the background could be related to contamination of the specimens.

ToF-SIMS chemical mapping

It is difficult to identify cellulose unequivocally using EDX, which is also a demanding technique in terms of sample preparation. For those reasons, ToF-SIMS and SCLSM were also used to evaluate the dispersion of the filler. ToF-SIMS analysis was used to produce 2D maps of the distribution of cellulose within the composites. In the analysis, characteristic secondary ion peaks were assigned to the matrix (fragment $C_5H_9^+$ at 69.1 m/z) and to the cellulose (fragment $C_{14}H_{23}O_5^+$ at 270.3 m/z). Figures 3 and 4 indicate the relative m/z and normalised ion intensities of the characteristic peaks selected as references. Aggregates

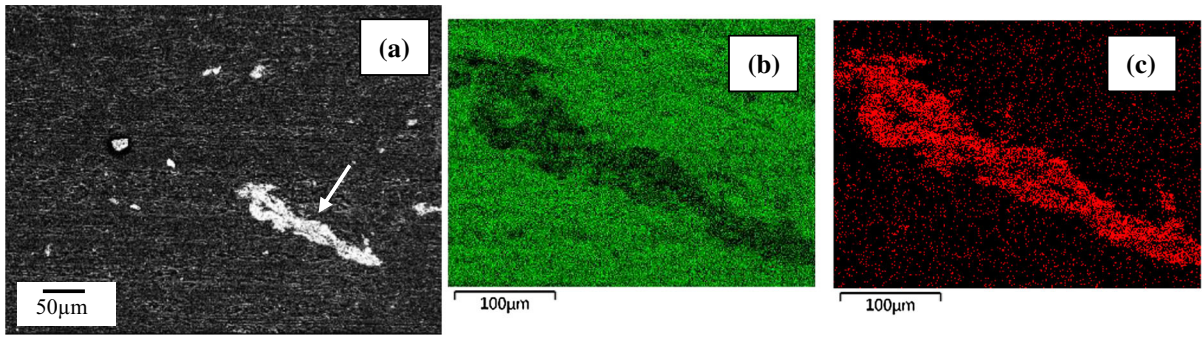

Fig. 1 Typical Back-scattered Electron EBSD and energy-dispersive X-ray spectroscopy (EDX) images of 1 wt% MAgPP-MFC reinforced composites. From left to right: **a** grayscale image of a large agglomerate (identified with an arrow); **b** back-scattered image of the large agglomerate where carbon is identified with a green colour; **c** back-scattered image of the agglomerate, where oxygen is identified in red

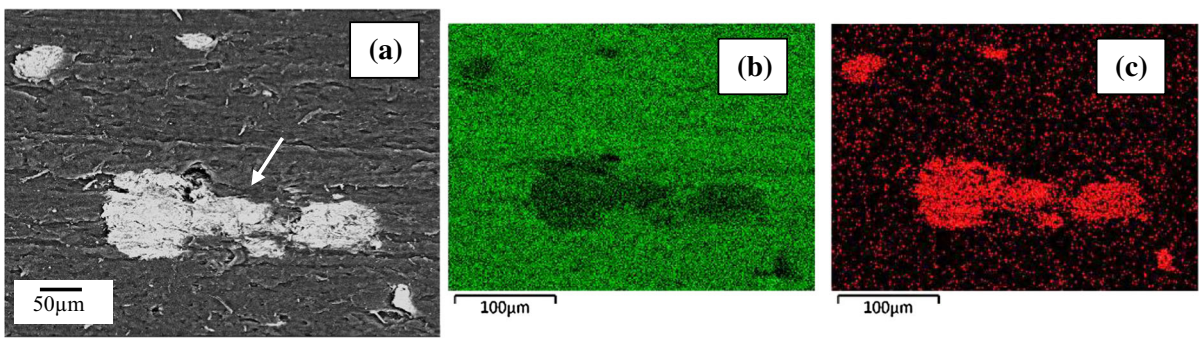

Fig. 2 Typical Back-scattered Electron EBSD and energy-dispersive X-ray spectroscopy (EDX) images of 1% MFC-TA-C_{18} reinforced composites. From left to right: **a** grayscale image of a large agglomerate (identified with an arrow); **b** back-scattered image of the large agglomerate where carbon is identified with a green colour; **c** back-scattered image of the agglomerate, where oxygen is identified in red

in the composites containing 5 wt% of MFC-TA-C_6 were very large and easy to identify, and so were assumed to be comprised mostly of cellulose and used to verify the peak assignment (Fig. 5). Hexylamine is a water-soluble amine which should react with tannic acid in the same way as octadecylamine; however, its chain length appears insufficient to disperse the cellulose in the polymer matrix. Large MFC aggregates can been seen in the composites (Fig. 1S). In the 2D reconstruction of the reference system, the cellulose signal located at 270 m/z, identified by a blue colour, is very distinctive from the signal from the matrix (in red; Fig. 5b). This shows that the ToF-SIMS mapping has successfully resolved the cellulose filler from the matrix. ToF-SIMS 2D analysis was used to obtain the map for a 5 wt% MFC-TA-C_{18} reinforced composites sample; the area selected did not exhibit aggregates of large dimensions (Fig. 6a). The 2D reconstructed map (Fig. 6b) indicated a more homogeneous dispersion of the hydrophobic filler.

SCLSM spectra

Previous research has confirmed that SCLSM can be used to identify cellulose aggregates in composite materials without the need for a fluorescent dye (Johns et al. 2019). Here we confirmed the autofluorescence of microfibrillated cellulose (MFC), tannic acid (TA) and the MFC-TA-C_{18} filler in composites. This ensured that the CLSM images of the composite samples enabled identification of the aggregates (Fig. 7), for all composites. Aggregates observed in the 1 wt% MFC and 1 wt% MFC-TA-C_{18} composites had similar spectra, whilst the 1 wt% TA aggregates

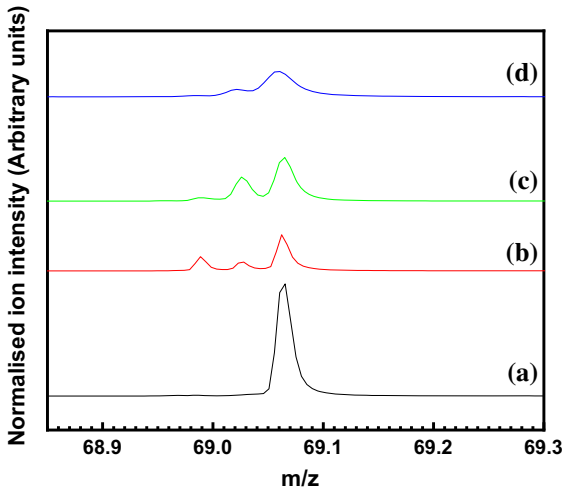

Fig. 3 Typical ToF-SIMS mass spectra magnification of peaks corresponding to the polymer matrix (fragment $C_5H_9^+$ at 69.1 m/z); (**a**), pure tannic acid (**b**), untreated MFC (**c**), and MFC-TA-C_{18} (**d**) samples

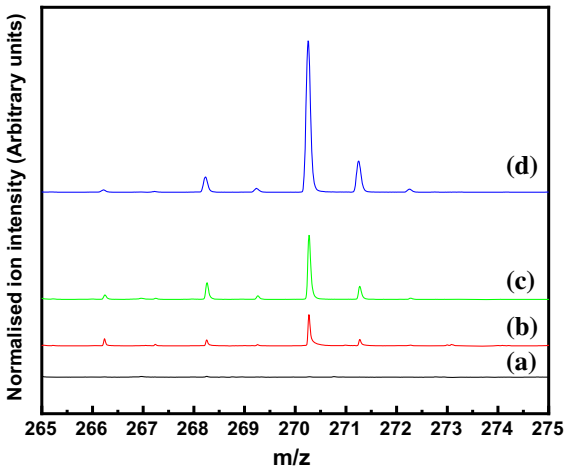

Fig. 4 ToF-SIMS mass spectra magnification of the peaks corresponding to cellulose (fragment $C_{14}H_{23}O_5^+$ at 270.3 m/z); (**a**), pure tannic acid (**b**), untreated MFC (**c**), and MFC-TA-C_{18} (**d**) samples

were less intense (Fig. 8a), in line with spectra from the raw materials (Fig. 8b).

The background spectra for the composites all contain a clearly defined matrix peak and a contribution from the composite material (Fig. 8b). The 1 wt% MFC-TA-C_{18} sample background appears to have a honeycomb-like structure (Fig. 7c and Fig. 5S). The origin of this structure is unclear and requires further investigation. It is presumed that the 15 wt% MFC-TA-C_{18} composite has a similar structure, but the increase in intensity obscures this. In addition, this sample (Fig. 7d) exhibits a uniform background fluorescence, which we assume is the dispersion of non-aggregated cellulose, although we do not have definitive evidence for this.

Aggregate size and distribution obtained by SCLSM

The modification of MFC with TA-C_{18} results in a significant increase in the number of aggregates observed, and a decrease in the mean area of the observed aggregates compared with those in the 1 wt% MFC and 1 wt% TA composites (Fig. 9). This suggests that the modification improves the distribution of material throughout the polymer composite. As expected, an increase in the MFC-TA-C_{18} loading results in an increase in the number of aggregates observed but has no effect on the mean aggregate area observed.

Division of the aggregate areas into small, medium and large categories confirms the differences in distribution between composite samples (Fig. 10). Whilst the 1 wt% and 15 wt% MFC-TA-C_{18} samples are similar, the 1 wt% MFC aggregates are much larger; for example, both the median and mean values for the large aggregates are an order of magnitude greater than those for the MFC-TA-C_{18} samples. The fact that the 1 wt% TA, 1 wt% MFC-TA-C_{18} and 15 wt% MFC-TA-C_{18} samples have no lower bound for the small category suggests that there are aggregates present that are smaller than the minimum viewable area ($\sim$ 11 μm^2). It is also worth noting that, whilst there appear to be many outlier values for the 15 wt% MFC-TA-C_{18} sample, they consist of less than 1% of the total number of aggregates observed, and they fall within the same range as the MFC aggregates.

By setting the 1 wt% MFC-TA-C_{18} composite as the control for defining the aggregate area categories, it is possible to compare the population distribution across the samples (Fig. 11). Under these boundary conditions, the distribution of aggregates for the 1 wt% MFC composite is quite even; 31 $\pm$ 4% of aggregates fall into the small category, whilst 17 $\pm$ 5% are classified as outliers. The TA aggregates are significantly skewed towards the small category; 61% of aggregates fall into this category. There is,

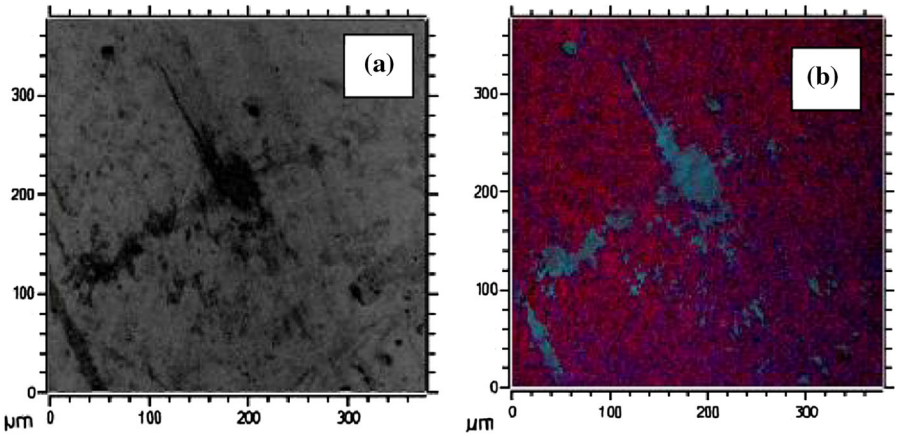

Fig. 5 Typical ToF-SIMS images of the MFC-TA-C_6 reinforced composite used verify the peak assignment. **a** Optical image of the sample (grayscale), with a large agglomerate of cellulose reinforcement visible in the centre of the sample and **b** a 2D reconstruction of the composite system using the assigned peaks: the red colour indicates the matrix and the blue colour indicates the presence of cellulose

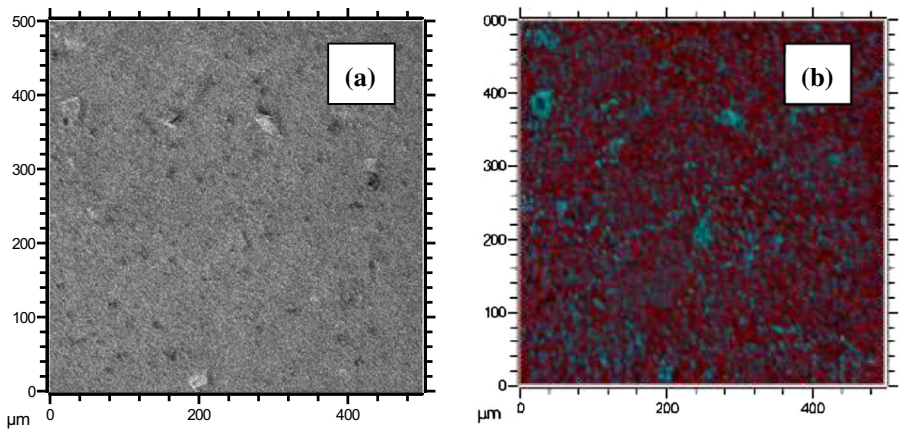

Fig. 6 Typical ToF-SIMS images of the MFC-TA-C_{18} reinforced composite. The grayscale image **a** represents the optical image of the sample—no large cellulose agglomerates are visible in the sample; **b** is a 2D reconstruction of the composite system: the red colour indicates the matrix and the blue colour indicates the presence of cellulose

however, no significant difference between the MFC and TA aggregates for the other three categories. This analysis also confirms that the modification of MFC with TA-C_{18} significantly improves the distribution of the material within the matrix. Over 85% of the aggregates fall into the small category for both 1 and 15 wt% MFC-TA-C_{18} composites, with less than 3% of the aggregates falling into the large and outlier categories combined. This results in composites that are significantly different to the 1 wt% MFC sample across all categories and are also significantly different to the 1 wt% TA composite in the small and medium categories. Importantly, no significant difference is observed in the population distribution between the 1 wt% and 15 wt% MFC-TA-C_{18} composites, indicating that the increased loading does not result in aggregation of the MFC-TA-C_{18} particles.

Mechanical and impact properties of composites

The mechanical properties of pure PPPE matrix and MFC-TA-C_{18} reinforced composites were obtained from the average of five tested specimens. Young's modulus was calculated from the slope of the stress–strain curve between 0 and 0.2% strain.

Figure 12 presents tensile and impact properties of the neat matrix and composites reinforced with 0.5 wt% up to 15 wt% of MFC-TA-C_{18}. The addition

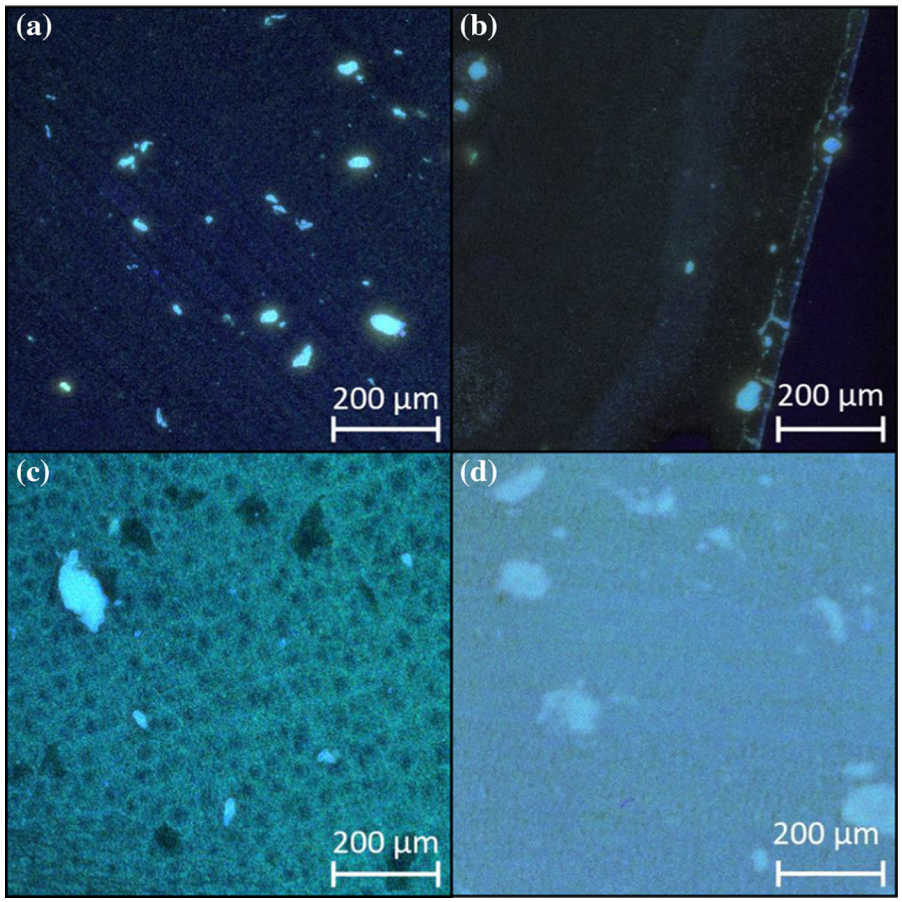

Fig. 7 Typical SCLSM images of **a** 1 wt% MFC, **b** 1 wt% TA, the visible fibre-like structure is a cutting mark, **c** 1 wt% MFC-TA-C_{18}, and **d** 15 wt% MFC-TA-C_{18} composites. The images are flattened from 3D stacks using the standard deviation z-project function in Fiji software

of reinforcement up to 2 wt% did not significantly enhance the tensile modulus of the composites. This increase in the reinforcing phase did however have an impact on the fracture energy of the specimens. Further increase in the filler concentration results in enhanced tensile properties but in a rapid decrease in the impact properties of the composites. Fracture energy increases from $\sim$ 76 kJ m^{-2} (pure PPPE) to $\sim$ 101 kJ m^{-2} at 1% MFC content (see Fig. 12 and Supplementary Information, Table 2S). This then progressively decreases at higher fractions of MFC, which is thought to be due to the presence of aggregates in the sample.

Large filler aggregates were found in the specimens with low and high filler contents, as demonstrated by SCLSM. The analysis of the aggregate size and distribution indicated that, whilst the aggregate size is not dependent on the filler content, the number of aggregates found in the reinforced composites increases with it. Most aggregates had a viewable area between 11 and 30 μm^2 and were classified as small particles. The filler aggregation in PPPE composites is thought to affect stiffness only marginally, but to strongly influence the impact resistance, which decreases sharply as aggregation increases (Fekete et al. 1999). In nanocomposites the reinforcement carries the tensile load while the matrix transfers this load between the reinforcement particles (Jager and Fratzl 2000). To ensure the integrity of the composite structure, the reinforcement should be able to withstand large tensile stress without fracture, whilst the matrix should carry a large shear stress without failure. The fracture resistance of a brittle solid is influenced by the flaw size according to the Griffith criterion

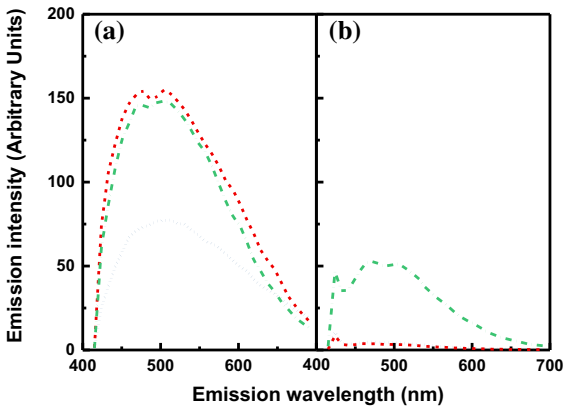

Fig. 8 Typical emission spectra of **a** aggregates and **b** the background for 1 wt% MFC (dashed red line), 1 wt% TA (dotted blue line), and 1 wt% MFC-TA-C_{18} (dash-dot green line). Note that the aggregates for 1 wt% MFC and 1 wt% MFC-TA-C_{18} have similar intensities, whilst 1 wt% TA is less intense. Note also that the 1 wt% MFC-TA-C_{18} background spectrum is more intense than the other two spectra and consists of signals from both the PPPE matrix and MFC-TA-C_{18}

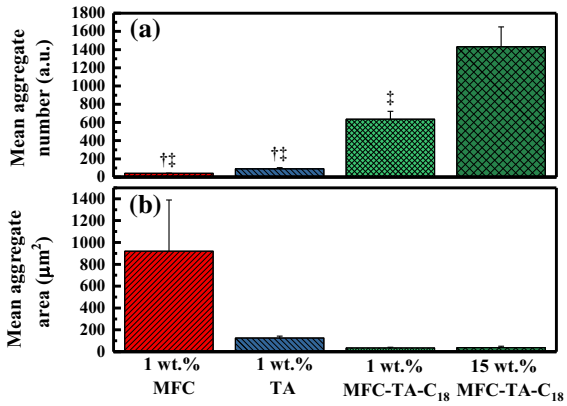

Fig. 9 **a** Mean number of aggregates for each composite sample. N = 3. † $p < 0.05$ compared to 1 wt% MFC-TA-C_{18}; ‡ $p < 0.05$ compared to 15 wt% MFC-TA-C_{18}. Error ± SE; **b** mean aggregate area for each composite sample. No statistical difference was observed between samples. N = 3, n ≥ 35. Error ± SE. a.u. = arbitrary units

$$\sigma_r^f = \alpha E_r \Psi \tag{3}$$

$$\Psi = \sqrt{\frac{\gamma}{E_r h}} \tag{4}$$

where σ_r^f is fracture strength of the material (in this case an aggregate of cellulose in a matrix), E_r is the theoretical modulus of the reinforcement, in this case a cellulose fibril, γ is the interfacial surface energy

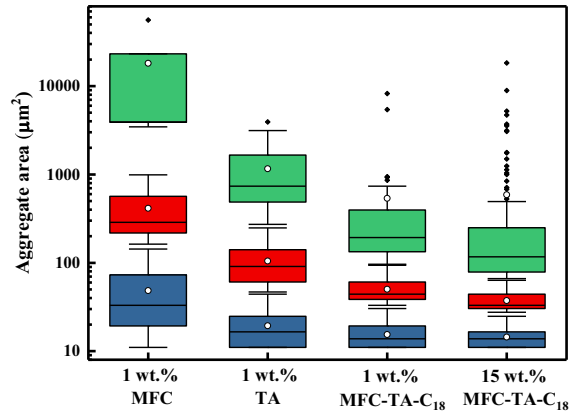

Fig. 10 Box plot comparing distribution of aggregates between samples obtained using spectral confocal microscopy. Aggregates are divided into four categories: small (blue boxes), medium (red boxes with light spot scattering), large (green boxes with medium spot scattering), and outliers (black diamonds). The mean values for each category are represented by white circles. Aggregates < 11 μm² ignored for analysis. n > 120

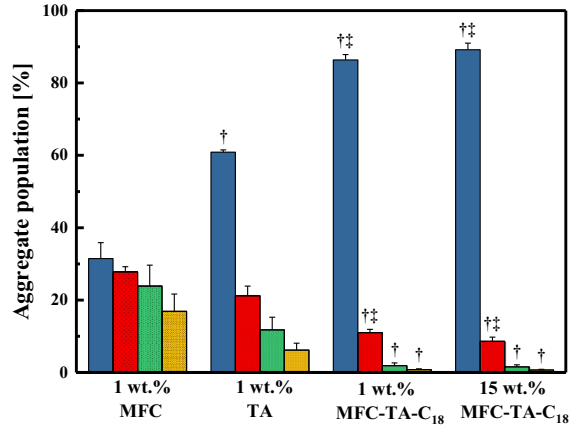

Fig. 11 Aggregate populations for various composites obtained via SCLSM. Aggregate categories, as defined by ranges determined for 1 wt% MFC-TA-C_{18}: small (blue bars, 11.0 ≥ X ≤ 30.3 μm²), medium (red bars with light spot scattering, 30.3 > X ≤ 93.8 μm²), large (green bars with medium spot scattering, 93.8 > X ≤ 385.3 μm²), and outliers (yellow bars with heavy spot scattering, X > 385.3 μm²). For all categories N = 3. †$p < 0.05$ compared to 1 wt% MFC in the respective category; ‡$p < 0.05$ compared to 1 wt% TA in the respective category. Error ± SE

between the reinforcement and the matrix, and h is the thickness of the reinforcement. The parameter α depends on the crack geometry and can be considered approximately equal to $\sqrt{\pi}$. Below a defined reinforcement thickness (h^*) the fracture strength of a

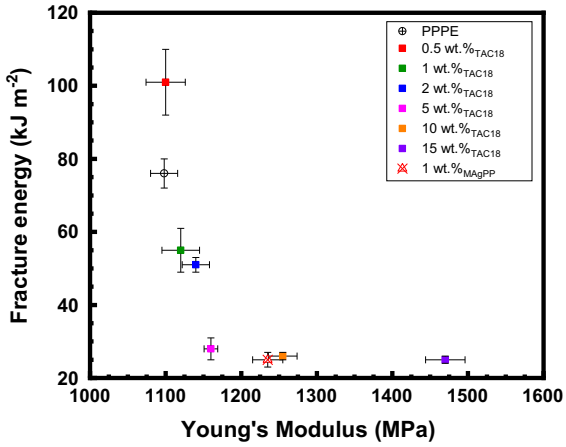

Fig. 12 Young's modulus and fracture energy of pure matrix (PPPE), 1 wt% MFC-MAgPP reinforced composites, and MFC-TA-C_{18} reinforced composites at filler loadings from 0.5 up to 15 wt%. These data, along with tensile strength (at yield and break), fracture energy and strain to failure, are available in Table 2S in the supplementary information section

cracked reinforcement particle becomes identical to that of a flawless structure (Jager and Fratzl 2000). It is possible to estimate the critical aggregate length scale as

$$h^* \approx \alpha^2 \frac{\gamma E_r}{\sigma_{th}^2} \tag{5}$$

The values considered for the calculation are $\gamma = 0.0339$ J/m^2 calculated for the tannic acid-octadecylamine reacted MFC film, $E_r = 20$ GPa and σ_{th} represents the theoretical tensile strength of cellulose fibrils and is equal to 240 MPa (Zimmermann et al. 2004, 2005; Leitner et al. 2007). Using these values we estimate h^* to be $\approx$ 37 nm. The dimension of the small aggregate found using the SCLSM analysis accounts for 11 μm^2 and thus a length of about 2 μm, assuming a circular geometry to the aggregates. The small aggregates found in the composites exceed the critical aggregate length scale (0.037 μm) by several orders of magnitude. This indicates that the cellulose filler is not sufficiently dispersed to obtain its full potential as a reinforcement without compromising fracture toughness.

The presence of aggregates also reduces the area of the filler matrix interface, limiting the effectiveness of MFC as reinforcement. Using the modulus of the composite as the measure, the potential of MFC as a reinforcement for the PPPE matrix was estimated using the 'Rule of Mixtures', which is expressed by the equation

$$E_{\text{composite}} = \eta_0 \eta_1 E_{\text{fibril}} V_{\text{fibril}} + (1 - V_{\text{fibril}}) E_{\text{matrix}} \tag{6}$$

where $E_{\text{composite}}$ is the modulus of the composite, V_{fibril} is the volume fraction of the fibres (or fibrils) in the composite and E_{matrix} is the modulus of the matrix; η_l and η_0 are the fibre length and orientation efficiency factors: η_l is equal to 1 for long fibres, and η_0 is equal to 3/8 for an in-plane random orientated network. The mechanical properties of a single cellulose fibril were evaluated using the Cox equation (Cox 1952) for an in plane random network of fibres, using an experiment in which sheets of pure MFC were made, cut into strips, and their tensile moduli were measured. The tensile modulus of the sheets, E_{network}, was found to be approximately 3.5 GPa. The modulus for a single cellulose fibril can be calculated using the equation

$$E_{\text{fibril}} = \frac{8}{3} \times E_{\text{network}} \tag{7}$$

This gave an experimental value of E_{fibril} of 10 GPa. By comparison, the extrapolation of the moduli of the composites to 100% filler content, using the fit obtained in Fig. 13, gives an E_{network} modulus of 3.4 GPa, resulting in an effective value of E_{fibril} of 12.6 GPa.

The relationship between the modulus of the composites and the volume fraction of the filler is approximately linear (Fig. 13, $R^2 = 0.9$), in agreement

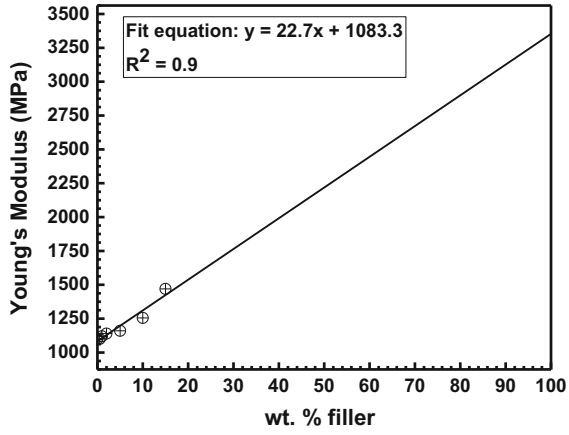

Fig. 13 Experimental Young's modulus data obtained from MFC-TA-C_{18} reinforced composites (dots). Solid line is a linear fit to these data, from which the fibril modulus E_{fibril} is estimated to be 12.6 GPa

with the rule of mixtures. A better dispersion of the cellulosic filler should be achieved before it becomes possible to obtain enhanced tensile and impact properties in the MFC reinforced composites, and reinforcement above a relatively low volume fraction.

Conclusions

In this study, a hydrophobic form of MFC was obtained by reacting an undried MFC slurry with tannic acid and octadecylamine. Sheets made from the product (MFC-TA-C_{18}) were shown to have a low free surface energy, which favours the dispersion of the MFC in apolar polymers. Composites of MFC-TA-C_{18} in PPPE had higher modulus than the pure PPPE polymer when the loading of the MFC-TA-C_{18} was greater than 2 wt%. Despite the effective dispersion of a large portion of the MFC-TA-C_{18} filler, the presence of some remaining aggregates impaired the mechanical performance of the composites, especially their impact properties, which were compromised at reinforcement loadings greater than 1 wt%.

Filler dispersion in the composites plays a central role in the effectiveness of the reinforcement. In this study, spectroscopic and confocal microscopy techniques were utilised to determine the level of dispersion in the produced specimens. EDX images of composites reinforced with MFC-TA-C_{18} and MAgPP-MFC revealed the presence of large (up to 100 μm) and small aggregates in the composites. Due to the lack of selectivity of the EDX technique towards cellulose, it was impossible to determine whether the cellulose signal in the background was due to the presence of cellulose or to other contaminants.

ToF-SIMS imaging and SCLSM techniques were also used to determine the filler dispersion and agglomerate size in the reinforced composites. ToF-SIMS analysis produced a 2D map of the 5 wt% MFC-TA-C_{18} reinforced composites. ToF-SIMS results indicated that, despite the presence of large aggregates, a significant proportion of the surface-treated cellulose fibrils were dispersed at a much smaller scale. SCLSM findings are in accordance with ToF-SIMS: the modification of MFC with TA-C_{18} improved the filler dispersion within the apolar PPPE composite. This finding is supported by the polymer background intensity signal increase when TA-C_{18} surface treatment was used and a decrease in the observed aggregate area. Increasing the MFC-TA-C_{18} loading to 15 wt% in the composite does not result in increased aggregation. Therefore, the composite is not saturated below a MFC-TA-C_{18} loading of 15 wt%. The filler dispersion data obtained from SCLSM cluster analysis correlates well with the stiffness increases registered for the composites and with the sharp decrease in the impact properties. The critical aggregate size calculated for the MFC-TA-C_{18} reinforced polyolefin system is about 37 nm. Because most of the aggregates found in the composite were greater than this value, regardless of the filler loading, and because of the imperfect nature of the cellulose aggregates, the real potential of the surface treated MFC reinforcement was not fully achieved. Further work is necessary to achieve a better level of filler dispersion and fully exploit the MFC potential as polyolefin reinforcement.

Acknowledgments This work was funded by the Engineering and Physical Sciences Research Council (Grant No. EP/L015 102/1) the Industrial Doctorate Centre (IDC) in Composites Manufacture.

References

Bledzki AK, Reihmane S, Gassan J (1996) Properties and modification methods for vegetable fibers for natural fiber composites. J Appl Polym Sci 59:1329–1336

Bonini C, Heux L, Cavaillé JY et al (2002) Rodlike cellulose whiskers coated with surfactant: a small-angle neutron scattering characterization. Langmuir 18:3311–3314

Cox HL (1952) The elasticity and strength of paper and other fibrous materials. Br J Appl Phys 3:72–79

Duchemin BJC, Newman RH, Staiger MP (2009) Structure-property relationship of all-cellulose composites. Compos Sci Technol 69:1225–1230

Ejima H, Richardson JJ, Liang K et al (2013) One-step assembly of coordination. Science 341:154–157

Fekete E, Molnár S, Kim G-M et al (1999) Aggregation, fracture initiation, and strength of PP/CaCO3 composites. J Macromol Sci 38:885–899

Gauthier R, Joly C, Coupas AC et al (1998) Interfaces in polyolefin/cellulosic fiber composites: chemical coupling,

morphology, correlation with adhesion and aging in moisture. Polym Compos 19:287–300
Gruber E, Granzow C (1996) Preparing cationic pulp by graft copolymerisation. 1. Synthesis and characterization. Papier 50:293
Guo C, Zhou L, Lv J (2013) Effects of expandable graphite and modified ammonium polyphosphate on the flame-retardant and mechanical properties of wood flour-polypropylene composites. Polym Polym Compos 21:449–456
Habibi Y, Lucia LA, Rojas OJ (2010) Cellulose nanocrystals: chemistry, self-assembly, and applications. Chem Rev 110:3479–3500
Hafrén J, Zou W, Córdova A (2006) Heterogeneous "organoclick" derivatization of polysaccharides. Macromol Rapid Commun 27:1362–1366
Henriksson M, Berglund LA (2007) Structure and properties of cellulose nanocomposite films containing melamine formaldehyde. J Appl Polym Sci 106:449–456
Herrick F, Casebier R, Hamilton J, Sandberg K (1983) Microfibrillated cellulose: morphology and accessibility. J Appl Polym Sci 37:797–813
Heux L, Chauve G, Bonini C (2000) Nonflocculating and chiral-nematic self-ordering of cellulose microcrystals suspensions in nonpolar solvents. Langmuir 16:8210–8212
Hu Z, Berry M, Pelton R, Cranston E (2017) One-pot water-based hydrophobic surface modification of cellulose nanocrystals using plant polyphenols. Sustain Chem Eng 5:5018–5026
Iwamoto S, Nakagaito ANNN, Yano H (2007) Nano-fibrillation of pulp fibers for the processing of transparent nanocomposites. Appl Phys A Mater Sci Process 89:461–466
Jager I, Fratzl P (2000) Mineralized collagen fibrils: a mechanical model with a staggered arrangement of mineral particles. Byophys J 79:1737–1746
Johns MA, Lewandowska A, Eichhorn SJ (2019) Rapid determination of the distribution of cellulose nanomaterial aggregates in composites enabled by multi-channel spectral confocal microscopy. Microsc Microanal 25:682–689
Kazayawoko M, Balatinecz JJ, Woodhams RT (1997) Diffuse reflectance Fourier transform infrared spectra of wood fibers treated with maleated polypropylenes. J Appl Polym Sci 66:1163–1173
Khalil HPSA, Davoudpour Y, Islam MN et al (2014) Production and modification of nanofibrillated cellulose using various mechanical processes: a review. Carbohydr Polym 99:649–665
Klemm D, Heublein B, Fink HP, Bohn A (2005) Cellulose: fascinating biopolymer and sustainable raw material. Angew Chem Int Ed 44:3358–3393
Klemm D, Schumann D, Kramer F et al (2006) Nanocelluloses as innovative polymers in research and application. Adv Polym Sci 205:49–96
Klemm D, Kramer F, Moritz S et al (2011) Nanocelluloses: a new family of nature-based materials. Angew Chem Int Ed 50:5438–5466
Lee H, Dellatore SM, Miller WM, Messersmith PBPB (2007) Mussel-inspired surface chemistry for multifunctional coatings. Science 318:426–431
Lee K-Y, Aitomäki Y, Berglund LA et al (2014) On the use of nanocellulose as reinforcement in polymer matrix composites. Compos Sci Technol J 105:15–27
Leitner J, Hinterstoisser B, Wastyn M et al (2007) Sugar beet cellulose nanofibril-reinforced composites. Cellulose 14:419–425
Ljungberg N, Cavaillí JY, Heux L (2006) Nanocomposites of isotactic polypropylene reinforced with rod-like cellulose whiskers. Polymer (Guildf) 47:6285–6292
Maldas D, Kokta BV (1994) Role of coupling agents on the performance of woodflour-filled polypropylene composite. Int J Polym Mater Polym Biomater 27(1–2):77–88
Malkapuram R, Kumar V, Singh Negi Y, Negi YS (2008) Recent development in natural fiber reinforced polypropylene composites. J Reinf Plast Compos 28:1169–1189
Matias MC, De La Orden MU, Gonzalez Sánchez C, Martinez Urreaga J (2000) Comparative spectroscopic study of the modification of cellulosic materials with different coupling agents. J Appl Polym Sci 75:256–266
Maya JJ, Rajesh A (2008) Recent developments in chemical modification and characterization of natural fiber-reinforced composites. Polym Polym Compos 16:187–207
Maya JJ, Sabu T (2008) Biofibres and biocomposites. Carbohydr Polym 71:343–364
Miao C, Hamad WY (2013) Cellulose reinforced polymer composites and nanocomposites: a critical review. Cellulose 20:2221–2262
Missoum K, Belgacem MN, Bras J (2013) Nanofibrillated cellulose surface modification: a review. Materials (Basel) 6:1745–1766
Peijs T, Garkhail S, Heijenrath R et al (1998) Thermoplastic composites based on flax fibres and polypropylene: influence of fibre length and fibre volume fraction on mechanical properties. Macromol Symp 127:193–203
Pöllänen M, Suvanto M, Pakkanen TT (2013) Cellulose reinforced high density polyethylene composites—morphology, mechanical and thermal expansion properties. Compos Sci Technol 76:21–28
Qiu W, Endo T, Hirotsu T (2006) Interfacial interaction, morphology, and tensile properties of a composite of highly crystalline cellulose and maleated polypropylene. J Appl Polym Sci 102:3830–3841
Sclavons M, Laurent M, Devaux J, Carlier V (2005) Maleic anhydride-grafted polypropylene: FTIR study of a model polymer grafted by ene-reaction. Polymer 46:8062–8067
Sehaqui H, Zhou Q, Ikkala O, Berglund LA (2011) Strong and tough cellulose nanopaper with high specific surface area and porosity. Biomacromolecules 12:3638–3644
Sileika TS, Barrett DG, Zhang R et al (2013) Colorless multifunctional coatings inspired by polyphenols found in tea, chocolate, and wine. Angew Chem Int Ed 52:10766–10770
Siro I, Plackett D, Siró I, Plackett D (2010) Microfibrillated cellulose and new nanocomposite materials: a review. Cellulose 17:459–494
Spence KL, Venditti RA, Rojas OJ et al (2011) A comparative study of energy consumption and physical properties of microfibrillated cellulose produced by different processing methods. Cellulose 18:1097–1111
Spoljaric S, Genovese A, Shanks RA (2009) Polypropylene-microcrystalline cellulose composites with enhanced compatibility and properties. Compos Part A Appl Sci Manuf 40:791–799

Takase S, Shiraishi N (1989) Studies on composites from wood and polypropylenes. II. J Appl Polym Sci 37:645–659

Wambua P, Ivens J, Verpoest I (2003) Natural fibres: can they replace glass in fibre reinforced plastics? Compos Sci Technol 63:1259–1264

Woodhams RT, Thomas G, Rodgers DK (1984) Wood fibers as reinforcing fillers for polyolefins. Polym Eng Sci 24:1166–1171

Zimmermann T, Pöhler E, Geiger T (2004) Cellulose fibrils for polymer reinforcement. Adv Eng Mater 6:754–761

Zimmermann T, Pöhler E, Schwaller P (2005) Mechanical and morphological properties of cellulose fibril reinforced nanocomposites. Adv Eng Mater 7:1156–1161